GENERAL ELECTRIC CO CINCINNATI OHIO AIRCRAFT ENGINE GROUP F/G 20/1 GE CORE ENGINE NOISE INVESTIGATION - LOW EMISSION ENGINES.(U) FEB 77 R K MATTA, G T SANDUSKY, V L DOYLE DOT-FA75WA-3688 FAA/RD-77/4 NL AD-A048 590 UNCLASSIFIED 195 ADA048 590

12

Report No. FAA - RD - 77 - 4

GE CORE ENGINE NOISE INVESTIGATION -LOW EMISSION ENGINES

R.K. Matta G.T. Sandusky V.L. Doyle

AIRCRAFT ENGINE GROUP GENERAL ELECTRIC COMPANY CINCINNATI, OHIO 45215



February 1977 Final Report

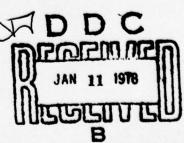
Document is available to the public through the National Technical Information Service,
Springfield, Virginia 22151.

Prepared for

U.S. DEPARTMENT OF TRANSPORTATION FEDERAL AVIATION ADMINISTRATION

Systems Research & Development Service DD C
Washington, D.C. 20590





NOTICE

This document is disseminated under the sponsorship of the Department of Transportation in the interest of information exchange. The United States Government assumes no liability for its contents or use thereof.

This program was directed towards elements of combiturbine tone interaction with jet stream turbulence Combustor (Core) Noise - Investigations were conducted source strength, spectrum shape, and farfield direct model tests to evaluate the effects of exhaust nozal frequency noise. A full-scale combustor rig test wariables of combustor noise at the source. Two endings from the scale model tests and add to the The relationship between combustor source noise and trends identified for advanced low emissions combustor. Turbine Noise - Studies were made of the attenuation stream blade rows, the broadband noise generation of for turbine tone/jet stream interaction. This inclustage configurations, along with a unique data acquitor define the effect of the pertinent aero-acoustic jet stream turbulence. The results of these investigations were used to inderived under the Core Engine Noise Control Program diction techniques were used to predict the noise current and advanced to the stream of the core engine to the core to the control program diction techniques were used to predict the noise current and advanced to the current and the	3. Recipient's Catalog No. Becort Date Feb 77	Code
Title and Subtitle GE CORE ENGINE NOISE INVESTIGATION - LOW EMISSION E R.K. MATTA, G.T./SANDUSKY V.L./DOYLE 9. Performing Organization Name and Address General Electric Company Aircraft Engine Group Cincinnati, Ohio 45215 12. Sponsoring Agency Name and Address U.S. Department of Transportation Federal Aviation Administration Systems Research and Development Service Washington, D.C. 20590 15. Supplementary Notes Related Documents: Core Engine and III. 16. Actact This program was directed towards elements of combuturbine tone interaction with jet stream turbulence Combustor (Core) Noise - Investigations were conducted to the service of	GINES Feb 77	Code
GE CORE ENGINE NOISE INVESTIGATION - LOW EMISSION E Author(s) R.K. MATTA, G.T./SANDUSKY V.L./DOYLE 8. Performing Organization Name and Address General Electric Company Aircraft Engine Group Cincinnati, Ohio 45215 12. Sponsoring Agency Name and Address U.S. Department of Transportation Federal Aviation Administration Systems Research and Development Service Washington, D.C. 20590 15. Supplementary Notes Related Documents: Core Engine and III. 16. Advance This program was directed towards elements of combuturbine tone interaction with jet stream turbulence Combustor (Core) Noise - Investigations were conduct source strength, spectrum shape, and farfield direct model tests to evaluate the effects of exhaust nozifrequency noise. A full-scale combustor rig test wariables of combustor noise at the source. Two er findings from the scale model tests and add to the The relationship between combustor source noise and trends identified for advanced low emissions combus Turbine Noise - Studies were made of the attenuatic stream blade rows, the broadband noise generation of the turbine tone/jet stream interaction. This inclustage configurations, along with a unique data acquito define the effect of the pertinent aero-acoustic jet stream turbulence. The results of these investigations were used to inderived under the Core Engine Noise Control Program diction techniques were used to predict the noise of turbofan engines representative of current and advanced turbof	GINES Feb 77	Code
R. MATTA, G.T. SANDUSKY V.L. DOYLE 8. Performing Organization Name and Address General Electric Company Aircraft Engine Group Cincinnati, Ohio 45215 12. Sponsoring Agency Name and Address U.S. Department of Transportation Federal Aviation Administration Systems Research and Development Service Washington, D.C. 20590 15. Supplementary Notes Related Documents: Core Engine and III. 16. Advant This program was directed towards elements of combuturbine tone interaction with jet stream turbulence Combustor (Core) Noise - Investigations were conduct source strength, spectrum shape, and farfield direct model tests to evaluate the effects of exhaust noza frequency noise. A full-scale combustor rig test of variables of combustor noise at the source. Two findings from the scale model tests and add to the The relationship between combustor source noise and trends identified for advanced low emissions combus Turbine Noise - Studies were made of the attenuatic stream blade rows, the broadband noise generation of for turbine tone/jet stream interaction. This inclustage configurations, along with a unique data acqu to define the effect of the pertinent aero-acoustic jet stream turbulence. The results of these investigations were used to in derived under the Core Engine Noise Control Program diction techniques were used to predict the noise of turbofan engines representative of current and advantables.	GINES -	Code
9. Performing Organization Name and Address General Electric Company Aircraft Engine Group Cincinnati, Ohio 45215 12. Sponsoring Agency Name and Address U.S. Department of Transportation Federal Aviation Administration Systems Research and Development Service Washington, D.C. 20590 15. Supplementary Notes Related Documents: Core Engine and III. 16. Advisct This program was directed towards elements of combuturbine tone interaction with jet stream turbulence Combustor (Core) Noise - Investigations were conducted source strength, spectrum shape, and farfield directed model tests to evaluate the effects of exhaust noze frequency noise. A full-scale combustor rig test warriables of combustor noise at the source. Two endings from the scale model tests and add to the The relationship between combustor source noise and trends identified for advanced low emissions combuster and identified for advanced low emissions combuster turbine Noise - Studies were made of the attenuation for turbine tone/jet stream interaction. This incistage configurations, along with a unique data acquito define the effect of the pertinent aero-acoustic jet stream turbulence. The results of these investigations were used to it derived under the Core Engine Noise Control Program diction techniques were used to predict the noise of turbofan engines representative of current and advanced turbofan engines representative of current and ad	A COLUMN CONTRACTOR	
9. Performing Organization Name and Address General Electric Company Aircraft Engine Group Cincinnati, Ohio 45215 12. Sponsoring Agency Name and Address U.S. Department of Transportation Federal Aviation Administration Systems Research and Development Service Washington, D.C. 20590 15. Supplementary Notes Related Documents: Core Engine and III. 16. Advisct This program was directed towards elements of combuturbine tone interaction with jet stream turbulence Combustor (Core) Noise - Investigations were conducted source strength, spectrum shape, and farfield directed model tests to evaluate the effects of exhaust noze frequency noise. A full-scale combustor rig test warriables of combustor noise at the source. Two endings from the scale model tests and add to the The relationship between combustor source noise and trends identified for advanced low emissions combuster and identified for advanced low emissions combuster turbine Noise - Studies were made of the attenuation for turbine tone/jet stream interaction. This incistage configurations, along with a unique data acquito define the effect of the pertinent aero-acoustic jet stream turbulence. The results of these investigations were used to it derived under the Core Engine Noise Control Program diction techniques were used to predict the noise of turbofan engines representative of current and advanced turbofan engines representative of current and ad	1/2/3870	7
9. Performing Organization Name and Address General Electric Company Aircraft Engine Group Cincinnati, Ohio 45215 12. Sponsoring Agency Name and Address U.S. Department of Transportation Federal Aviation Administration Systems Research and Development Service Washington, D.C. 20590 15. Supplementary Notes Related Documents: Core Engine and III. 16. Actact This program was directed towards elements of combuturbine tone interaction with jet stream turbulence Combustor (Core) Noise - Investigations were conduct source strength, spectrum shape, and farfield direct model tests to evaluate the effects of exhaust nozo frequency noise. A full-scale combustor rigitest wariables of combustor noise at the source. Two er findings from the scale model tests and add to the The relationship between combustor source noise and trends identified for advanced low emissions combustor Turbine Noise - Studies were made of the attenuation for turbine tone/jet stream interaction. This incl stream blade rows, the broadband noise generation of for turbine tone/jet stream interaction. This incl stream blade rows, the broadband noise generation of for turbine tone/jet stream interaction. This incl stream blade rows, the broadband noise generation of the results of these investigations were used to define the effect of the pertinent aero-acoustic jet stream turbulence. The results of these investigations were used to in derived under the Core Engine Noise Control Program diction techniques were used to predict the noise of turbofan engines representative of current and advanced turbofan engin	b. Performing Organization	Repeat No.
General Electric Company Aircraft Engine Group Cincinnati, Ohio 45215 12. Sponsoring Agency Name and Address U.S. Department of Transportation Federal Aviation Administration Systems Research and Development Service Washington, D.C. 20590 15. Supplementary Notes Related Documents: Core Engine and III. 16. Advact This program was directed towards elements of combuturbine tone interaction with jet stream turbulence Combustor (Core) Noise - Investigations were conducted source strength, spectrum shape, and farfield direct model tests to evaluate the effects of exhaust noza frequency noise. A full-scale combustor rig test wariables of combustor noise at the source. Two endindings from the scale model tests and add to the The relationship between combustor source noise and trends identified for advanced low emissions combustor turbine Noise - Studies were made of the attenuatic stream blade rows, the broadband noise generation for turbine tone/jet stream interaction. This inclustage configurations, along with a unique data acque to define the effect of the pertinent aero-acoustic jet stream turbulence. The results of these investigations were used to it derived under the Core Engine Noise Control Program diction techniques were used to predict the noise of turbofan engines representative of current and advanced turbofan engines representative of curre	10. Work Unit No.	
Aircraft Engine Group Cincinnati, Ohio 45215 12. Sponsoring Agency Name and Address U.S. Department of Transportation Federal Aviation Administration Systems Research and Development Service Washington, D.C. 20590 15. Supplementary Notes Related Documents: Core Engine and III. 16. Acat This program was directed towards elements of combit turbine tone interaction with jet stream turbulence Combustor (Core) Noise - Investigations were conduct source strength, spectrum shape, and farfield direct model tests to evaluate the effects of exhaust noze frequency noise. A full-scale combustor rig test wariables of combustor noise at the source. Two end findings from the scale model tests and add to the The relationship between combustor source noise and trends identified for advanced low emissions combustor trubine Noise - Studies were made of the attenuation stream blade rows, the broadband noise generation of for turbine tone/jet stream interaction. This inclustage configurations, along with a unique data acquity to define the effect of the pertinent aero-acoustic jet stream turbulence. The results of these investigations were used to inderived under the Core Engine Noise Control Program diction techniques were used to predict the noise of turbofan engines representative of current and advantage of turbofan engines representative of current and advantage turbofan engine engine engine engine engine	1 1 1 1 1 1 1 1 1 1 1 1 1 1 1 1 1 1 1	
Cincinnati, Ohio 45215 12. Sponsoring Agency Name and Address U.S. Department of Transportation Federal Aviation Administration Systems Research and Development Service Washington, D.C. 20590 15. Supplementary Notes Related Documents: Core Engine and III. 16. Advance This program was directed towards elements of combiturbine tone interaction with jet stream turbulence Combustor (Core) Noise - Investigations were conducted source strength, spectrum shape, and farfield direct model tests to evaluate the effects of exhaust nozation frequency noise. A full-scale combustor rig test wariables of combustor noise at the source. Two effindings from the scale model tests and add to the The relationship between combustor source noise and trends identified for advanced low emissions combustive and the stream blade rows, the broadband noise generation for turbine tone/jet stream interaction. This inclustage configurations, along with a unique data acquito define the effect of the pertinent aero-acoustic jet stream turbulence. The results of these investigations were used to inderived under the Core Engine Noise Control Program diction techniques were used to predict the noise of turbofan engines representative of current and advanced turbofan engine	N. Contract or Grant No.	./
U.S. Department of Transportation Federal Aviation Administration Systems Research and Development Service Washington, D.C. 20590 15. Supplementary Notes Related Documents: Core Engine and III. 16. August This program was directed towards elements of combit turbine tone interaction with jet stream turbulence Combustor (Core) Noise - Investigations were conducted source strength, spectrum shape, and farfield direct model tests to evaluate the effects of exhaust noze frequency noise. A full-scale combustor rig test wariables of combustor noise at the source. Two enders from the scale model tests and add to the The relationship between combustor source noise and trends identified for advanced low emissions combustor. Turbine Noise - Studies were made of the attenuatic stream blade rows, the broadband noise generation for turbine tone/jet stream interaction. This inclustage configurations, along with a unique data acquite to define the effect of the pertinent aero-acoustic jet stream turbulence. The results of these investigations were used to inderived under the Core Engine Noise Control Program diction techniques were used to predict the noise of turbofan engines representative of current and advance turbofan engines representative engines engines engi	DOT-FA75WA-3688	N Sured
U.S. Department of Transportation Federal Aviation Administration Systems Research and Development Service Washington, D.C. 20590 15. Supplementary Notes Related Documents: Core Engine and III. 16. Auract This program was directed towards elements of combit turbine tone interaction with jet stream turbulence Combustor (Core) Noise - Investigations were conducted source strength, spectrum shape, and farfield direct model tests to evaluate the effects of exhaust noze frequency noise. A full-scale combustor rig test wariables of combustor noise at the source. Two enderings from the scale model tests and add to the The relationship between combustor source noise and trends identified for advanced low emissions combustor. Turbine Noise - Studies were made of the attenuatic stream blade rows, the broadband noise generation for turbine tone/jet stream interaction. This inclustage configurations, along with a unique data acquite to define the effect of the pertinent aero-acoustic jet stream turbulence. The results of these investigations were used to inderived under the Core Engine Noise Control Program diction techniques were used to predict the noise of turbofan engines representative of current and advantage of the service of turbofan engines representative of current and advantage of the service of turbofan engines representative of current and advantage of the service of turbofan engines representative of current and advantage of the service of turbofan engines representative of current and advantage of the service of turbofan engines representative of current and advantage of the service of turbofan engines representative of current and advantage of the service of turbofan engines representative of current and advantage of the service of turbofan engines representative of current and advantage of the service of turbofan engines representative of current and advantage of the service of turbofan engines representative of current and advantage of the service of turbofan engines representative of current and ad	G Final rept.	
Systems Research and Development Service Washington, D.C. 20590 Related Documents: Core Engine and III. Related Documents: Core Engine Noise Control Program diction techniques were used to current and advanced low engines representative of current and advanced low engines representative represent	Jun 75 Dec	76
Related Documents: Core Engine and III. This program was directed towards elements of combuturbine tone interaction with jet stream turbulence. Combustor (Core) Noise - Investigations were conducted source strength, spectrum shape, and farfield direct model tests to evaluate the effects of exhaust nozal frequency noise. A full-scale combustor rig test wariables of combustor noise at the source. Two enders of the relationship between combustor source noise and trends identified for advanced low emissions combustors. Turbine Noise - Studies were made of the attenuation stream blade rows, the broadband noise generation of for turbine tone/jet stream interaction. This inclustage configurations, along with a unique data acquity to define the effect of the pertinent aero-acoustic jet stream turbulence. The results of these investigations were used to inderived under the Core Engine Noise Control Program diction techniques were used to predict the noise of turbofan engines representative of current and advanced to the stream of the control program diction techniques were used to predict the noise of turbofan engines representative of current and advanced to the current and the current and the current and the current a	6-14. Sponsoring Agency Gods	-
This program was directed towards elements of combiturbine tone interaction with jet stream turbulence Combustor (Core) Noise - Investigations were conducted source strength, spectrum shape, and farfield direct model tests to evaluate the effects of exhaust nozal frequency noise. A full-scale combustor rig test wariables of combustor noise at the source. Two endings from the scale model tests and add to the The relationship between combustor source noise and trends identified for advanced low emissions combustor. Turbine Noise - Studies were made of the attenuation stream blade rows, the broadband noise generation of for turbine tone/jet stream interaction. This inclustage configurations, along with a unique data acquito define the effect of the pertinent aero-acoustic jet stream turbulence. The results of these investigations were used to inderived under the Core Engine Noise Control Program diction techniques were used to predict the noise curbofan engines representative of current and advanced to the service of the predict the noise current and advanced to the service of current service of current and the service of current an		
This program was directed towards elements of combuturbine tone interaction with jet stream turbulence Combustor (Core) Noise - Investigations were conducted source strength, spectrum shape, and farfield direct model tests to evaluate the effects of exhaust nozal frequency noise. A full-scale combustor rig test wariables of combustor noise at the source. Two endings from the scale model tests and add to the The relationship between combustor source noise and trends identified for advanced low emissions combustor. Turbine Noise - Studies were made of the attenuation stream blade rows, the broadband noise generation for turbine tone/jet stream interaction. This inclustage configurations, along with a unique data acquito define the effect of the pertinent aero-acoustic jet stream turbulence. The results of these investigations were used to inderived under the Core Engine Noise Control Program diction techniques were used to predict the noise current and advanced to the service of current and the service of current and	loise Control Program; FAA-RD-74-1	
This program was directed towards elements of combuturbine tone interaction with jet stream turbulence Combustor (Core) Noise - Investigations were conducted source strength, spectrum shape, and farfield direct model tests to evaluate the effects of exhaust nozal frequency noise. A full-scale combustor rig test wariables of combustor noise at the source. Two endings from the scale model tests and add to the The relationship between combustor source noise and trends identified for advanced low emissions combustor. Turbine Noise - Studies were made of the attenuation stream blade rows, the broadband noise generation of for turbine tone/jet stream interaction. This inclustage configurations, along with a unique data acquito define the effect of the pertinent aero-acoustic jet stream turbulence. The results of these investigations were used to inderived under the Core Engine Noise Control Program diction techniques were used to predict the noise of turbofan engines representative of current and advanced turbofan engines representative of current and advanced to the service of the predict the noise of turbofan engines representative of current and advanced turbofan engines representative engines representative engines representative engines repr		125-1, 11
source strength, spectrum shape, and farfield direct model tests to evaluate the effects of exhaust nozal frequency noise. A full-scale combustor rig test wariables of combustor noise at the source. Two endings from the scale model tests and add to the The relationship between combustor source noise and trends identified for advanced low emissions combustor. Turbine Noise - Studies were made of the attenuation stream blade rows, the broadband noise generation for turbine tone/jet stream interaction. This inclustage configurations, along with a unique data acquito define the effect of the pertinent aero-acoustic jet stream turbulence. The results of these investigations were used to inderived under the Core Engine Noise Control Program diction techniques were used to predict the noise of turbofan engines representative of current and advanced to the second of the second of the core and the second of the control program diction techniques were used to predict the noise of turbofan engines representative of current and advanced to the second of the second of the current and advanced to the second of the se		125-1, 11
stream blade rows, the broadband noise generation for turbine tone/jet stream interaction. This inclusing configurations, along with a unique data acquired to define the effect of the pertinent aero-acoustic jet stream turbulence. The results of these investigations were used to inderived under the Core Engine Noise Control Program diction techniques were used to predict the noise of turbofan engines representative of current and advantage of the program of the core of the program of the core of the predict the noise of turbofan engines representative of current and advantage of the predict of the predict the noise of turbofan engines representative of current and advantage of the predict of the predict the noise of the predict the noise of the predict of the predict the noise of the predict of the predict the noise of the predict the noise of the predict of the predict the noise of the predict the noise of the predict of the predict the noise of the no	otor and turbine noise; the latter	includir
derived under the Core Engine Noise Control Program diction techniques were used to predict the noise of turbofan engines representative of current and adva	etor and turbine noise; the latter sed to determine the variables affectivity. This investigation include e geometry on radiation patterns on a used to identify the controlling gine tests were run to validate the overall data base of core noise meremissions was studied and qualitate	includir ecting ed scale of low & e
7. Key Words (Suggested by Author(s)) 18. Di	etor and turbine noise; the latter ded to determine the variables affectivity. This investigation include e geometry on radiation patterns of us used to identify the controlling the tests were run to validate the overall data base of core noise meanissions was studied and qualitations. To of high frequency turbine noise to turbines, and the controlling pained a turbine rig test in single assition system. Scale model tests	including ed scale of low ge asurement tive by down-rameters and multiwere use
7. Key Words (Suggested by Author(s)) 18. Di	ed to determine the variables affectivity. This investigation includes ageometry on radiation patterns on the second of the seco	including ed scale of low ge asurement tive by down-rameters and multiwere usering by hniques oved pre-
	ed to determine the variables affectivity. This investigation includes ageometry on radiation patterns on the second of the seco	including ed scale of low ge asurement tive by down-rameters and multiwere usering by hniques oved pre-
Core Engine Noise, Turbofan Engine Noise, Aircraft Noise Control, Low Noise Technology,	ed to determine the variables affectivity. This investigation includes ageometry on radiation patterns on the second of the seco	including ed scale of low ge asurement tive by down-rameters and multiwere usering by hniques oved pre-
Combustor Noise, Turbine Noise, Tone/Jet	etor and turbine noise; the latter ded to determine the variables affectivity. This investigation include e geometry on radiation patterns of the state of the st	including ed scale of low ge asurement tive by down-rameters and multiwere usering by hniques oved preh bypass
Stream Interaction, Noise/Emissions Relation- ships	etor and turbine noise; the latter ded to determine the variables affectivity. This investigation includes ageometry on radiation patterns as used to identify the controlling gine tests were run to validate the overall data base of core noise meremissions was studied and qualitations. The opening of the controlling parameters, and the controlling parameters on turbine rig test in single assition system. Scale model tests parameters on turbine tone scatter of the component prediction technology. The controlling of each source for high need technology.	including ecting ed scale of low ge asurement tive by down- rameters and multi were use ring by hniques oved pre- h bypass
9. Security Classif. (of this report) 20. Security Classif. (of this p	etor and turbine noise; the latter ded to determine the variables affectivity. This investigation includes ageometry on radiation patterns as used to identify the controlling fine tests were run to validate the overall data base of core noise meremissions was studied and qualitations. The option of high frequency turbine noise to turbines, and the controlling particular turbine rig test in single assistion system. Scale model tests parameters on turbine tone scatter or over the component prediction tech (FAA-RD-74-125, III). These improposed technology.	including ecting ed scale of low ge asurement tive by down- rameters and multi were use ring by hniques oved pre- h bypass
Unclassified Unclassified	etor and turbine noise; the latter ded to determine the variables affectivity. This investigation includes ageometry on radiation patterns of suspending the controlling time tests were run to validate the overall data base of core noise meremissions was studied and qualitations. The of high frequency turbine noise of turbines, and the controlling parameters, and the controlling parameters on turbine rig test in single sistion system. Scale model tests parameters on turbine tone scatter of the component prediction technology. The open statement of the controlling parameters on turbine tone scatter of the component prediction technology.	including ecting ed scale of low ge asurement tive by down- rameters and multi were use ring by hniques oved pre- h bypass

* For sale by the National Technical Information Service, Springfield, Virginia 22151

403 468 sur

METRIC CONVERSION FACTORS

	l ar	41231 /a.,7	333		linn		
ie Measuras]	Hitt				1	99
raises from Metri	Methoty by LENGTH	ASU28	2.5 2.5 2.5 2.5 3.5 4.5 5.5 5.5 5.5 5.5 5.5 5.5 5.5 5.5 5	0.03 2.2 1.1 VOLUME	82228 E	TEMPERATURE (exect) 3/5 (thes	***
Approximate Conversions from Metric Measures		0.000mm	Section (10,000 or			Colous Insperdies	****
]	111	ננת	.7.	177	ا بر	* \$ + \$
1,1,1,1	lalalala	Libilibilit	ւեւեւեւեւեւ	Jalatalatal	ahahahaha	Lililidi	11/11/11/
10	1.	' I, '	l. ' l.	' l• '	l. '	,	1 1
	1	11.	37732	•2-	,	,	' '
Mosseres]	, ,	eques certimotes of a second o	ement seems		cubic maters and a second control maters and a second control maters and a second control materials and a second control mat	terriporateure to the see hills their. Publ. 286, to the see hills their. Publ. 286, to the see hills their see hill see h
erzione to Metric Mossures	:	12. Comments CO 1. Co	1	1 1		Colsius	1 4
Approximate Conversions to Metric Messures	:	1	1			EMPERATURE (exact) 5.75 cubic meters Color cubic meters 5.75 (after Colores	32) 32) Onversions and more details 5, 50 Cetalog No. Cl 3,10.2

PREFACE

This Final Report describes work performed by the General Electric Company, Aircraft Engine Group, for the Department of Transportation, Federal Aviation Administration, on the GE Core Engine Noise Investigation Program - Low Emission Engines (DOT-FA75WA-3688). The Program sought to develop and further core engine noise technology in the areas of combustor noise, turbine noise, and turbine tone interaction with the exhaust jet flows.

The work effort was performed in four phases as follows:

- Phase I GE Low Emissions Combustor Tests.

 Conduct full-scale component and engine combustor tests, utilizing low emission designs, including provisions in the component tests to obtain acoustic data at higher than ambient discharge pressures; conduct model tests to define the effect of core nozzle exit geometry on low frequency noise directivity; define relationships between emissions and noise where possible.
- Phase II Turbine Tone/Jet Interaction Tests.

 Investigate the effects of jet velocities, tone frequency, relative location of fan/core exhaust planes, and turbulence properties on turbine tone modulation by coannular jet streams.
- Phase III Turbine Noise Investigation.

 Conduct acoustic tests of a low pressure turbine in single and multi-stage configurations to determine turbine tone attenuation by downstream stages, and the broadband noise generation.
- Phase IV Noise Prediction Update.

 Update and expand the prediction methods developed under Contract DOT-FA72WA-3023.

This report is complementary to the five volume final report for DOT-FA72WA-3023:

- Volume I Identification of Component Noise Sources (FAA-RD-74-125, I).
- Volume II Identification of Noise Generation and Suppression Mechanisms (FAA-RD-74-125, II).
- Volume III Prediction Methods (FAA-RD-125, III).

Volume III
Supplement I - Extension of Prediction Methods. (FAA-RD-74-125, III-I)

Volume II
Supplement I - Extension to Identification of Noise Generation and Suppression Mechanisms. (FAA-RD-74-125, II-I)

SUMMARY

This program was directed towards elements of combustor and turbine noise; the latter including turbine tone interaction with jet stream turbulence. The overall objectives were:

- Extend understanding of combustor noise in terms of power generated and directional characteristics
- Provide quantitative data for the prediction of turbine tone/ jet interaction noise
- Establish the level of turbine tone attenuation by downstream turbine stages and broadband noise generation
- Where possible, establish noise/emission relationships
- Update the core engine noise prediction developed under contract DOT-FA72WA-3023

To accomplish these objectives, model, component and engine tests were conducted as indentified below. The results of these tests and those available in open literature were utilized to refine and improve the existing prediction method. Finally, a systems study was conducted to provide an example of how the results of this program and DOT-FA72WA-3023 may be exploited to gain fuller understanding of the problem of aircraft noise generation and control.

Combustor (Core) Noise

Four tests were conducted:

- (i) Full-scale component test of the best Experimental Clean Combustor configuration at high back pressures in order to independently define the relationship between the pertinent cycle parameters and noise generation.
- (ii) Model tests of a dual flow arrangement with simulated combustor noise generation in the core to evaluate the effect of different core nozzle exhaust geometry on the farfield directivity.
- (iii) Two engine tests, one a turbofan and the other a turboshaft, both incorporating designs for reduced combustor emissions, in order to obtain "clean" combustor noise data.

In addition, relationships between noise and emissions were studied, in particular to assess the impact of various emission reduction techniques being employed on advanced combustors on the noise generated by these combustors.

The high density component test demonstrated that a velocity term was fundamental to the combustion noise generation process, along with the inlet

pressure and temperature, and temperature rise. The spectrum shape obtained at the combustor exhaust was in agreement with that obtained by the prediction method, however, the peak was shifted to higher frequencies (630 to 1000 Hz). The difference could be attributed to the facility internal geometry, transmission through the turbine or exhaust nazzle, or to the low emission design. Only an engine test could resolve the problem.

The dual flow model tests suggest that core nozzles, incorporating high radius ratio plugs, could have a small beneficial effect on core noise. An 18-lobe mixer on the core produced the lowest farfield levels for model frequencies above 800 Hz by about 5 to 7 dB in the forward quadrant and 2 to 4 dB in the aft quadrant. The effect was attributed to the reduced characteristic dimension (as a ratio of the incident sound wavelength). The benefit achieved was independent of the velocity or velocity ratio, suggesting that the results obtained should be applicable to a range of engine cycles. The directivity characteristics of the various configurations appear to be a function of the frequency but largely independent of the velocity ratio. The lower frequencies exhibited a directivity pattern peaking near the jet axis; the peak moved to 120° with increase in frequency, which is indicative of combined control by convection and refraction.

The turbofan (CFM56) engine test utilized both internal and farfield acoustic measurements. The internal data were acquired with a special low frequency sound-separation probe, which was successfully used to extract the acoustic levels from the combined turbulence and sound signal. The probe data was also utilized to obtain that part of the signal coherent with the farfield. The sound-separated spectra were in essential agreement with the prediction spectrum. The duct sound power levels were 5 to 6 dB above the farfield levels, a large part of the difference being attributed to a nozzle transmission loss. The loss mechanism was modeled, and an analytical prediction defined. The directivity provided by the fartield coherence data supported the model directivity results in that the same frequency dependence was obtained.

The turboshaft (T700) engine test data, which consisted of farfield high and low microphone data, provided further validation of the core noise prediction method. The spectra and power levels were in essential agreement with prediction. The aft quadrant levels matched the prediction method directivity, but no determination could be obtained in the front quadrant due to contamination by water-brake noise.

Emissions data were correlated using parameters similar to those for noise generation, and it was found that the lean-burn emission reduction techniques currently being utilized to reduce nitrogen oxides could result in increased noise generation due to larger flow velocities through the primary combustion zone. The engine data correlations indicate that emission indices would experience relatively larger variations than would combustor noise with change in cycle conditions.

The high density component test results were used to develop a prediction method for combustor noise at the source. The same correlation was found to collapse farfield data from ambient back pressure component tests, thereby demonstrating that in-duct near-field measurements are representative of the noise radiated to the farfield by combustors. For an engine operating line, the source correlation was shown to be similar to the grouping used for engine data correlations by General Electric. However, before the source noise correlation can be used to predict engine noise, the transmission loss due to turbine blade rows and the exhaust nozzle must be entered separately. Analytical modeling of both mechanisms suggests significant effects.

General Electric component and engine data were used to evaluate other engine core noise prediction methods available in open literature and no adequate collapse could be achieved. It has been demonstrated on the other hand, that the prediction method of FA72WA-3023 derived from General Electric data would also collapse data acquired by Garrett AiResearch, the Boeing Company, and NASA-Lewis Research Center. This prediction method was updated to accommodate the directivity frequency dependence indicated by the model and engine tests.

Turbine Noise

Two test series were conducted:

- (i) Turbine tests utilizing a three stage low pressure rig in a single stage and a multi-stage configuration in order to determine the turbine noise attenuation by downstream blade rows, and the broadband noise generation.
- (ii) Model tests of a dual flow arrangement with simulated turbine tone generation in the core in order to enhance the understanding of turbine tone/jet stream interaction. A secondary objective was to determine the directivity of high frequency tones for coannular flows.

The turbine tests showed that there was a very large insertion loss associated with turbine blade rows applying both to broadband and discrete frequency sound. The loss for tones was correlated with aerodynamic and acoustic parameters and was found to be controlled largely by the wheel speed, and to involve the tone frequency and tip mach number. The work extraction and incidence angle were found to be secondary parameters.

The turbine broadband noise levels were extracted using the soundseparation technique developed by General Electric. The single and three stage configuration spectra were found to be quite different; the former exhibiting a pronounced peak at the blade passing frequency location for operating conditions near design point. At far off-design conditions, the spectrum flattened out due to shift of energy towards the second harmonic of the tone. These trends are similar to those noted for engine data in FA72WA-3023. The overall power levels for the broadband noise were found to correlate with the pressure ratio and either the relative velocity into the rotor or tip speed.

The dual flow model tests indicated that both shear layers participate in the scattering process. It was found that a turbulence eddy size approaching the incident tone wavelength was essential to the onset of this mechanism, and the dependence on the tone frequency was explicitly extracted for frequencies beyond this point. The absolute distance, rather than a multiple of fan diameter, between fan and core exhaust planes was found to be the important dimension. Increasing the turbulence level through vortex generators significantly increased the scattering, but only over a limited range of frequencies, velocities and farfield angles.

A configuration with the fan shroud extended half a fan diameter aft of the core exhaust plane produced the least amount of discernible haystacking. It also resulted in a directivity shift towards the side-line, in the form of a second lobe near 90°. The other configurations gave "conventional" turbine tone directivity shapes, with a single peak at 120°.

The turbine noise methods were updated to incorporate the significant results. It is interesting to observe that the attenuation due to downstream blade rows can more than compensate for the additional noise sources associated with the downstream stages. Consequently, even while additional stages increase the work output, the net noise radiated can decrease, as was demonstrated during the turbine tests.

Systems Study

The prediction methods developed in the Core Engine programs were exercised in a systems study to establish the component and engine noise levels for current and future cycles of interest. The magnitude of the major sources was presented in the form of bar charts providing the PNL at the max forward and aft angles, along with the EPNL for an aircraft system incorporating the engine under consideration. The value of such bar charts is in helping determine the optimal application of source reduction and suppression, and in accurately assessing the impact of component design changes and cycle variations on the systems noise.

The systems study indicated that turbine noise was a significant factor for both current and advanced engines, particularly for CTOL aircraft. There was an obvious need for precise prediction of turbine noise levels for present engines for the reasons explained in the preceding paragraph. Advanced engines, such as envisaged in the Energy Efficient Engine program, would require about 5 PNdB turbine source noise suppression.

The knowledge of the relative levels of combustor and jet noise allows a realistic determination of relative velocity effects on jet noise. It was

found that combustor noise was not a problem for current cycles because the jet and fan noise levels are fairly high. However, the study showed that it would be a problem for other engine cycles where jet noise levels are depressed, such as for STOL and turboshaft engines with quiet rotors. Duct burners could also present a combustor noise problem due to lack of turbine attenuation due to excitation of duct resonances.

The impact of the increased combustor noise associated with low emission combustors on the engine levels was found to be very small for current cycles. However, this factor must be kept in mind for future applications.

Finally, significant benefits derived from the program and recommendations for future work are discussed. The principal recommendations based on present and future systems requirements are for:

- Turbine source noise control work
- Completion of the elemental investigation of core engine noise in which source, transmission, radiation and propagation effects are considered separately. The latter would include inflight effects.

Table of Contents

Section			Page
	Pref	ace	iii
	Summ		v
	Nome	nclature	хi
1.0	Intr	oduction	1
2.0	Comb	ustor Noise	2
	2.2	Background Internal Density/Parametric Tests	2 2
	2.3 2.4 2.5 2.6	Tests	29 64 121 139
3.0	Turb	ine Noise	173
	3.1 3.2	Background Turbine Tone Attenuation and	173
	3.3	Broadband Noise Turbine Tone/Jet Stream Inter-	178
	3 /	action Tests Prediction Update	225 263
4.0			
		ems Study	287
5.0	Conc	lusions and Recommendations	301
Referen	ices		304
Appendi	x A	Internal Density Combustor Test Data	307
Appendi	х В	Low Frequency Noise Directivity Data	311
Appendi	x C	Turbine Noise Test Data	342
Appendi	x D	Turbine Tone/Jet Stream Interaction Data	349

NOMENCLATURE

A area AR exhaust nozzle area ratio (fan/core) nozzle radius a number of blades blade passing frequency BPF bypass ratio (fan/core) BPR jet shear layer thickness Ъ c_p coefficient of specific heat at constant pressure acoustic velocity C,c D diameter DI directivity index extra ground attenuation EGA EPNL effective perceived noise level f frequency f/a fuel-air ratio incident tone frequency fpeak spectrum peak frequency gravitational constant H enthalpy Hf heating value of fuel incidence angle 1 J mechanical equivalent of heat K constant wave number, $2\pi/\lambda = \omega/c$ k distance between fan and core exhaust planes L 2 chord turbulence eddy size Mach number, V/c M haystack slope m N speed in rpm Nf fan speed

NOMENCLATURE (continued)

```
OAPWL
                overall sound power level
OASPL
                overall sound pressure level
P
                total pressure
PR
                pressure ratio
PNL
                perceived noise level
PWL
                acoustic power level
                static pressure
p
                stoichiometric heat of combustion
q<sub>o</sub>P
R
                gas constant
                Reynolds number
Re
SL
                sideline
SPL
                sound pressure level
                axial spacing between blade rows
T
                total temperature
TL
                transmission loss
                blade-to-blade pitch
t
U
                blade physical speed
                volume
v<sub>()</sub>
                velocity
                gas velocity relative to rotor
                exhaust velocity ratio (fan/core),
VR
                weight flow rate
W
Z
                axial distance downstream of nozzle exit plane
                ratio of specific heats
Y
                difference or attenuation
Δ
δ
                drop in tone narrowband SPL due to haystacking
                ratio of flight to fan jet velocity
5
Θ
                angle from inlet
                wave length
                3.14159
                density
```

NOMENCLATURE (concluded)

ρς	-	acoustic impedance
ф	•	equivalence ratio: actual to stoichiometric fuel-air ratio
ψ	-	angle from jet axis
ω	-	circular frequency, 2πf
Subscr	ipts	
core	-	nominal value of core jet parameter
fan	-	nominal value of fan jet parameter
max	-	maximum value

P - pitch-line value

Ref - value at reference conditions, reference parameter

stage - value for given stage

mean value

T - tip value

mean

t - value for turbulent eddies

o - reference or ambient

18 - conditions at fan nozzle exit plane

3 - conditions entering combustor

conditions at combustor exit

5 - conditions at turbine exit

8 - conditions at core nozzle exit plane

SECTION 1.0

INTRODUCTION

The development of the high bypass turbofan engine has resulted in substantial reduction in the noise produced in the vicinity of airports. The current fleet of wide-body jets meets FAA regulation FAR-36 (1969) but considerable work remains to be accomplished in order to further improve community acceptance.

The quiet fan installations associated with turbofan engines such as the CF6, JT9D, and RB211 focused attention on the core engine noise components. Contract DOT-FA72WA-3023, Core Engine Noise Control Program, was oriented directly toward advancing the acoustic technology consistent with current and future noise abatement objectives. A basic understanding of the relationships between core engine noise generation and reduction mechanisms and the engine design was sought so that the technology developed would be applicable to a wide variety of engine types varying over a broad range of geometric and aerodynamic characteristics. The work utilized and built upon the considerable amount of General Electric experience and acoustic data accumulated in the development of a wide range of engine systems. The existing data permitted the identification and ranking of the significant core engine noise sources. A balanced theoretical and experimental program was then carried out on the most critical sources of noise in an engine core. Combining the above studies with the results of data correlations for various engine systems provided:

- A core engine noise prediction base for future technology aircraft engines.
- An improved understanding of the source mechanisms and an evaluation of the effectiveness of source noise reduction approaches.

Although the prediction methods developed during that effort represented the then current state-of-the art, several important extensions of that work were identified. Those extensions fell into two categories:

- 1. Efforts to increase the range of applicability of the methods.
- 2. Efforts to verify trends previously observed or predicted.

The current work addresses these two areas in a multi-faceted, integrated program for turbine and combustor (core) noise. The elements of the turbine noise investigation include broadband noise generation, the attenuation of turbine tones by downstream blade rows, and the phenomenon of scattering of discrete frequency noise by jet stream turbulence. The elements of the combustor noise investigation include parametric study of the significant variables, the effect of nozzle geometry and velocities on low frequency noise directivity, advanced engine tests, and emissions/noise relationships.

SECTION 2.0

COMBUSTOR NOISE

2.1 BACKGROUND

Studies of advanced aircraft propulsion systems indicate that combustor noise is a potential contributor to overall system noise. This is especially true for propulsion systems employing advanced acoustic treatment and mixed flow exhaust systems for jet noise reduction. The initial Core Engine Noise Control Program (Reference 1) made significant gains towards the understanding of combustor noise by providing a data base which could be used for development of a prediction technique. Although the prediction methods developed during that effort represented state-of-the art technology, four areas were identified which confirm and expand upon the work done under the earlier program:

- 1. A parametric study of an advanced low emission combustor to independently, define the relationship of various cycle parameters identified in Reference 1, to combustor noise generation.
- A model test to evaluate the effect of exhaust nozzle geometry on farfield radiation of low frequency noise. This study was suggested by the analysis of engine data conducted under Contract DOT-FA72WA-3023.
- The acquisition of data on advanced turboshaft and turbofan engines featuring reduced emission combustors to extend the data base.
- 4. A study of the relationship between noise and emissions. This aspect of the program is significant in view of the ever increasing concern over environmental impact of the jet aircraft fleet. In particular, it is vital to assess the impact on noise of various emission reduction techniques being employed on advanced combustors which will be used in future generation aircraft power-plants.

2.2 INTERNAL DENSITY/PARAMETRIC TESTS

2.2.1 Objectives

The objective was to independently establish the dependence of the combustor noise on the pertinent performance parameters - inlet temperature, inlet pressure, flow rate, and temperature rise. Such a trend is obviously impossible to determine from engine tests, even if it were assumed that clean data could be acquired for the combustor noise levels.

Outdoor component tests run during DOT-FA72WA-3023 indicated approximately a third power dependency of combustor noise on the flow velocity. However, since the combustor exhausted directly to the atmosphere, the inlet pressure could not be varied independently. Also, there was some uncertainty whether the combustion process at the ambient conditions was representative of that occuring in engines, where the inlet density is much higher. A secondary objective then was to establish the validity of atmospheric tests for combustor noise generation.

Finally, since the measurements were to be made internally with wave-guide probes, a comparison with farfield noise data would demonstrate the adequacy (or inadequacy) of using internal measurements to represent the sound radiated to the farfield. If the comparison was favorable, then the NASA Experimental Clean Combustor data (all acquired with probes) could be used to study noise/emission relationships (see Section 2.5).

2.2.2 Test Description

Combustor noise measurements were taken in a full-scale annular high pressure combustor test rig. The rig was capable of testing combustors over an inlet pressure range of 2.3 to 9.6 atmospheres and inlet temperature range of 600° R to 1500° R. A cross section of the rig is shown in Figure 2.2-1. Upstream of the combustor were straightening screens to insure uniform flow into the combustor. Aerodynamic instrumentation was located downstream of the combustor. Air was supplied from five radial compressors and was preheated to desired inlet test conditions by an indirect heater located upstream of the combustor.

The double annular combustor used for this test was the final (full scale) configuration of the Experimental Clean Combustor Program (Reference 2). A schematic of the combustor, designated D13, is shown in Figure 2.2-2 and some design parameters in Table 2.2-1. The D13 double annular combustor consisted of two annular rows of swirlers separated by a flame shield. The air swirlers consisted of primary air swirl venturi castings with a counter-rotating concentric secondary air swirler. This configuration used simplex fuel nozzles, with no air shroud, located in the center of each air swirler. Figure 2.2-3 shows some details of the D13.

Data were measured at two axial planes in the combustor test rig. Plane 3.0 was upstream of the combustor and represented the plane of the compressor discharge in an engine. Plane 3.9 was the exit plane of the combustor. Figure 2.2-4 shows a schematic of the set-up. Aerodynamic instrumentation at planes 3.0 and 3.9 measured total pressures and temperatures

Acoustic wave guide probes were used to measure the combustor noise. A semi-infinite or pc termination was used to eliminate the possibility of standing waves in the probe. The upstream probe is shown schematically in Figure 2.2-5. The downstream probe was similar to the upstream probe, except that it was water cooled. This probe is shown in Figure 2.2-6.

Both probes were calibrated for dynamic pressure losses in a probe calibration facility. The measured losses were within 1dB of the predicted probe losses using the Iberall method. The 1/3-octave band probe attenuation corrections for both probes are listed in Table 2.2-2.

Pressure transducers (Kulites) were used instead of microphones due to the extreme heat surrounding the test rig. Low noise amplifiers were used to amplify the output signal prior to recording the data on an FM tape recorder. Figure 2.2-7 shows a schematic of the electrical set-up.

The test matrix (Table 2.2-3) was selected so that the air flow rate, inlet temperature and inlet pressure were varied independently in order to determine their effect on the sound power level. Earlier experience had already shown (Reference 3) that the sound power level is a function of the fuel-air ratio, or the temperature rise, to the first power. Therefore, only sufficient variations in fuel-air ratio were performed to verify these trends.

2.2.3 Test Results

Data were acquired for the test matrix shown in Table 2.7-3, except for point number 3, where a steady state could not be maintained. The 1/3-octave band sound pressure levels from 31.5 to 10,000 Hz, and the calculated overall level for each point are listed in Appendix A. The measured aerodynamic data and the emissions levels of CO, HC and NO $_{\rm X}$ can be found in Table 2.2-4.

2.2.4 Data Analysis

Some typical spectral shapes are shown in Figures 2.2-8 and 2.2-9. Typically, the downstream probe spectrum started with an aerodynamic perturbation peak at 31 and 63 Hz, because of its placement in a high turbulence area, moving to a major sound peak between 630 and 1000 Hz. Sometimes, a secondary peak occurred near 4000 Hz for this probe. However, the upstream probe rarely displayed the low frequency aerodynamic peak, which was only to be expected. Surprisingly, though, the secondary peak near 4000 Hz was not evident in the upstream spectra, which suggests that only the major hump between 630 and 1000 Hz represents true sound. Early measurements in this rig (Reference 4) showed a large increase in the levels when the flame was lit, as opposed to no-flame points, thereby providing further validation that these were the true sound levels.

The shape of the major hump agrees closely with the spectrum shape found for engine related core noise except the peak frequency occurred between 630 and 1000 Hz, rather than at 400 Hz (Reference 1). Figure 2.2-10 shows a comparison of the measured data and the spectral shape used for engine predictions. This difference in peak frequency may be attributable to the effect of turbine and exhaust nozzle attenuation or to the physical termination differences between the rig and actual engines.

The OAPWL was calculated for each test point using the following relationship to account for flow Mach number, specific impedance and area (Reference 1):

OAPWL = OASPL + 10 $\log(1+M)^2 + 10 \log\left[\frac{p_o}{p}\sqrt{\frac{t}{t_o}}\right] + 10 \log A$; dB re: 10^{-13} watts (2.2-1)

where A is the annular exit area in square feet, p and t are the static pressure and temperature, the subscript o denoting standard day conditions, and M the Mach number.

It is desirable to use readily available engine cycle parameters for predicting combustor noise for aircraft engines. Such parameters include combustor inlet total temperature and pressure, weight flow, and temperature rise across the combustor. The test data were input to a linear multiple regression computer program, assuming the variables to be T_3 , P_3 , T_4 , and T_5 . The result was

OAPWL = 93 + 10 log
$$[\dot{w}(T_4 - T_3)\sqrt{T_3}]$$
; dB re: 10^{-13} watts (2.2-2)

where $\mathring{\mathbf{w}}$ is the combustor air flow in lb/sec, (T_4-T_3) is the temperature rise in $^\circ$ R and T_3 is the combustor inlet temperature in $^\circ$ R. However, the parametric trends indicated by plotting the noise variation with the individual changes in pressure, temperature, and weight flow were very different, as is shown in Figures 2.2-11, -12, and -13 respectively:

Parametric OAPWL
$$\approx 10 \log \left[\frac{T_3^2}{P_3^1.5} \dot{w}_3^3\right]$$
 at constant (T_4-T_3)

The fact that the functional relationships were found to be different, depending on whether the observed individual parametric trends or a multiple regression analysis was used suggests that the relationship is over-specified by this choice of parameters and that one of these quantities is not truly independent. The multiple correlation analysis assumes independent variables are supplied.

The weight flow rate term includes a density and a velocity specification. Since the inlet temperature and pressure also influence the density, it would be logical to replace $\hat{\mathbf{w}}$ by a reference velocity $(\mathbf{v}_{\text{Ref}})$. It appears that this substitution is the key to the problem as now the multiple regression analysis and the parametric trends yield the same functional relationships.

The multiple regression analysis gives the following fit with a standard deviation (σ) of 1.1 dB:

OAPWL =
$$10 \log[P_3^{1.53}T_3^{-1.41}V_{ref}^{3.46}(T_4 - T_3)^{0.75}] + 84 dB;$$
 (2.2-3)

where
$$V_{Ref} = \frac{\dot{W}_3}{\rho_3 A_{Ref}}$$
, $A_{Ref} = 4.01 \text{ ft}^2 (.373 \text{ m}^2)$

Rounding off the exponents, this yields, as is shown in Figure 2.2-14, a σ of 1.2 dB:

OAPWL = 10 log
$$[(P_3/T_3)^{1.5}$$
 $V_{Ref}^{3.5}$ $(T_4 - T_3)] + 79.4 dB; (2.2-4a)$
re: 10^{-13} Watts

or, in terms of the inlet density (ρ_3) :

OAPWL = 10
$$\log[\rho_3^{1.5} V_{Ref}^{3.5} (T_4 - T_3)] + constant$$
 (2.2-4b)

The parametric results give exactly the same trends as equation (2.2-4a). For example, the exponent on the velocity term is given by Figure 2.2-15. Since P_3 and T_3 were held constant for each pair of points, the parameter varied was really V_{Ref} . Alternately, in order to use all the D13 data, normalizing for P_3 and T_3 , the exponent on V_{Ref} is given by the slope in Figure 2.2-14, which is approximately 3.5.

The parametric variations of T₃ and P₃ were conducted at constant \hat{w} . However, since V_{Ref} varied along with either T₃ or P₃, it is first necessary to normalize for V_{Ref} to determine the correct exponents on T₃ and P₃. This is shown in Figures 2.2-16 and -17. The desired exponents are given by the slopes of the paired points and indicate the dependence is roughly P₃^{1.5} and T_{-1.5}. This exercise illustrates that the correct flow rate term required in a combustor noise correlation is the velocity, not the weight flow. A separate size correction is needed to proceed from the D13 correlation to other combustors. The conventional correction is an area term, and it is logical to add the reference area (A_{ref}), which gives:

OAPWL = 10
$$\log[\rho_3^{1.5} A_{Ref} V_{Ref}^{3.5} (T_4 - T_3)]$$
 or
OAPWL = 10 $\log[\dot{W} V_{Ref}^{2} (T_4 - \frac{T}{3}) (\rho_3^{1/2} V_{Ref}^{1/2})] + constant$ (2.2-5)

Hence, physically, the noise generated is proportional to the incoming kinetic energy, the potential energy added, and the square root of the inlet volumetric flow rate.

Equations (2.2-4 and 5) are in good agreement with component correlations published recently by other researchers. For example, based on both analytical modeling and combustor results, Strahle and Shivshankara (Reference 5) concluded that:

OAPWL =
$$10 \log \left[\frac{P_3}{T_3^{0.5}} \right] \left(D^2 \right) v^{2.3 + 2.7} \left(T_4 - T_3 \right)$$
 (2.2-6)

2.2.5 Summary and Conclusions

The significant results of the acoustic data analysis may be summarized as follows:

- A velocity term is more fundamental to the combustion noise generaration process than is the weight flow. The parametric tests show
 that the sound power generated is proportional to the inlet density
 to the 1.5 power, the reference velocity to the 3.5 power, and the
 temperature rise to the first power for the D13 Double Annular
 Combustor. When a size correction is included, the sound power is
 seen to be a function of the incoming kinetic energy, the potential
 energy addition by the fuel, and the square root of the volumetric
 flow rate.
- The spectrum shape observed is in good agreement with the shapes indicated by engine data, however, the peak is shifted to higher frequencies (630 to 1000 Hz instead of 400 Hz). The difference could be due to the transmission through turbine blade rows or the core nozzle, but is more likely due to the physical differences between this combustor and engines including the internal geometry and exit plenum conditions.

Table 2.2-1 Geometric Design Parameters, Double-Annular Combustor

		Outer Annulus	Inner Annulus	Overal1
Dome Height (1)	in. (cm)	2.24 (5.69)	2.10 (5.33)	4.47 (11.35)
Burning Length	in. (cm)	2.00 (5.08) (2)	2.00 (5.08) (2)	11.95 (30.35)
Fuel Injector Spacing	in. (cm)	3.04 (7.73)	2.50 (6.34)	
Area ⁽¹⁾	in. ² (cm ²)	203.2 (1311)	159.3 (1028)	373.4 (2409)
Volume	in. 3 (cm ³)	399.2 (6541) ⁽²⁾	311.0 (5097)	3355.8 (54,991)

⁽¹⁾ at trailing edge of centerbody

⁽²⁾ from flameshields to trailing edge of centerbody

Table 2.2-2 Tabulation of Waveguide Probe Attenuation

Frequency	Upstream Waveguide Probe	Downstream Water-Cooled Waveguide Probe
31.5	0.30	2.0
40	0.34	2.1
50	0.38	2.1
63	0.43	2.1
80	0.48	2.2
100	0.54	2.3
125	0.60	2.3
160	0.68	2.4
200	0.76	2.5
250	0.85	2.6
315	0.96	2.7
400	1.07	2.9
500	1.20	3.0
630	1.35	3.2
800	1.51	3.4
1000	1.70	3.6
1250	1.91	3.9
1600	2.14	4.3
2000	2.40	4.8
2500	2.69	5.3
3150	3.02	6.0
4000	3.39	6.7
5000	3.80	7.3
6300	4.27	8.3
8000	4.79	9.2
10000	5.37	10.3

Table 2.2-3 CENIP Test Matrix

Rdg.	Test Point	w 1b/sec	P ₃	°R ^T 3	f/a
764	1	20.0	35	1000	.024
765	2	20.0	35	1470	.024
-	3	20.0	35	1470	.012
766	4	20.0	42	1470	.024
767	5	24.3	42	1470	.024
763	6	40.0	57	1000	.024
762	7	40.0	70	1000	.024
753	8	40.0	70	1470	.012
752	9	40.0	70	1470	.024
751	10	33.0	70	1470	.024
754	11	40.0	85	1470	.024
761	12	80.0	115	680	.024
759	13	80.0	115	1000	.024
760	14	65.8	115	1000	.024
757	15	80.0	140	1000	.024
758	16	90.0	140	1000	.024
755	17	80.0	140	1470	.024
756	18	80.0	140	1470	.012

Table 2.2-4 Double Annular Combustor Aerodynamic Data

Rdg. Point Pt. Pt.<				A 4			1bm/sec	1 bm/hr		°R		1bm/1000 1bm	00 1bm(f	(fuel)	(1)0	D(2)
1 2.37 2.28 2.26 .0237 20.2 1724 999 2468 540 66.90 16.20 1.59 162.7 2 2.38 2.25 2.22 .0238 20.0 1720 1469 2904 538 6.64 0.29 4.39 152.4 4 2.87 2.76 2.74 .0238 20.3 1737 1474 2972 538 6.64 0.29 4.39 152.6 0.17 4.93 152.6 5 2.86 2.71 2.67 .0249 40.6 3499 999 2491 540 66.0 177 4.93 157.1 157.1 157.1 4.01 40.1 3481 997 2520 544 61.0 10.30 1.77 1175.3 1471 2522 544 157.1 157.1 157.1 157.1 157.1 157.1 157.1 157.1 157.1 157.1 157.1 157.1 157.1 157.1 157.1 <td< td=""><td>Rdg.</td><td>Point</td><td>P_T3</td><td>Ps3</td><td>P_{T3.9}</td><td>f/a</td><td>W(air)</td><td>W(fuel)</td><td>T T3</td><td>T_T3.9</td><td>Tfuel</td><td>8</td><td>НС</td><td></td><td>dB OASPL</td><td>dB OASPL</td></td<>	Rdg.	Point	P _T 3	Ps3	P _{T3.9}	f/a	W(air)	W(fuel)	T T3	T _T 3.9	Tfuel	8	НС		dB OASPL	dB OASPL
2 2.38 2.25 2.24 0.29 1724 994 2406 538 6.64 0.29 1521 1720 1469 2904 538 6.64 0.29 1531 1474 2926 538 6.64 0.29 4.39 1521 1474 2926 538 5.02 0.17 4.93 1521 4.39 1476 2926 536 5.02 0.17 4.93 1521 4.75 4.57 4.50 0.024 40.6 3499 999 2491 540 61.00 10.30 1.77 157.4 7 4.75 4.57 4.50 0.0241 40.1 3481 997 2520 544 39.20 1.77 157.4 8 4.75 4.51 4.46 0.0243 40.1 3505 1469 2929 549 39.20 310 1.77 157.4 9 4.75 4.54 0.0243 40.1 3505 1469 2929 540 <	764	-	2 37	2 28	2.26	75.00	20.2	1727.	000	37.69	67.0	00 33	00 31			
4 2.87 2.76 2.74 .0238 20.3 1737 1474 2972 538 3.68 0.17 6.07 153.11 5 2.86 2.71 2.67 .0240 24.3 2103 1476 2920 536 5.02 0.17 4.93 154.0 6 3.89 3.66 3.62 .0239 40.6 3499 999 2491 540 61.00 10.30 1.77 157.4 7 4.75 4.57 4.50 .0241 40.1 3481 997 2520 544 39.20 3.10 2.66 157.1 8 4.75 4.51 4.45 .0122 39.9 1753 1471 2234 540 72.70 2.20 5.24 155.3 9 4.76 4.51 4.04.1 3505 1469 2929 538 3.05 1.65 157.1 10 4.75 4.51 4.024 32.8 1471 2925	765	7	2.38	2.25	2.22	.0238	20.0	1720	1469	2904	538	6.64	0.29	4.39	152.4	151.0
5 2.86 2.71 2.67 .0240 24.3 2103 1476 2920 536 5.02 0.17 4.93 154.0 6 3.89 3.66 3.62 .0239 40.6 3499 999 2491 540 61.00 10.30 1.77 157.4 7 4.75 4.57 4.50 .0241 40.1 3481 997 2520 544 39.20 3.10 2.66 157.1 8 4.75 4.51 4.45 .0122 39.9 1753 1471 2234 540 72.70 2.20 5.24 155.5 9 4.75 4.51 4.04 35.5 1471 2925 540 72.70 2.20 5.24 155.5 10 4.75 4.56 .0242 32.8 1471 2925 540 74.50 49.7 158.9 11 5.79 5.56 5.54 .0242 33.9 35.3 164.1 52.	992	4	2.87	2.76	2.74	.0238	20.3	1737	1474	2972	538	3.68	0.17	6.07	153.1	151.2
6 3.89 3.66 3.62 .0239 40.6 3499 999 2491 540 61.00 10.30 1.77 157.4 7 4.75 4.57 4.50 .0241 40.1 3481 997 2520 544 39.20 3.10 2.66 157.1 8 4.75 4.51 4.45 .0122 39.9 1753 1471 2234 540 72.70 2.20 5.24 155.5 9 4.75 4.51 4.46 .0243 40.1 3505 1469 2929 538 3.05 0 6.62 158.9 10 4.75 4.56 .0243 40.1 3503 1473 3962 540 74.50 49.7 158.8 11 5.79 5.56 5.54 .0243 39.9 3503 1471 240 2.40 0 158.8 164.1 12 7.84 7.53 6.0240 80.5 6949 999 <td>191</td> <td>2</td> <td>2.86</td> <td>2.71</td> <td>2.67</td> <td>.0240</td> <td>24.3</td> <td>2103</td> <td>1476</td> <td>2920</td> <td>536</td> <td>5.02</td> <td>0.17</td> <td>4.93</td> <td>154.0</td> <td>152.7</td>	191	2	2.86	2.71	2.67	.0240	24.3	2103	1476	2920	536	5.02	0.17	4.93	154.0	152.7
7 4.75 4.57 4.50 .0241 40.1 3481 997 2520 544 39.20 3.10 2.66 157.11 8 4.75 4.51 4.45 .0122 39.9 1753 1471 2234 540 72.70 2.20 5.24 155.5 9 4.76 4.51 4.46 .0243 40.1 3505 1469 2929 538 3.05 0 6.62 158.9 10 4.76 4.56 4.54 .0242 32.8 2848 1471 2925 540 2.41 0 6.62 158.9 10 4.75 4.56 4.54 .0242 32.8 2848 1471 2925 540 2.41 0 8.00 157.11 11 5.79 5.56 5.54 .0243 39.9 3503 1473 3962 540 2.29 0.01 9.27 158.8 12 7.84 7.53 7.69	763	9	3.89	3.66	3.62	.0239	9.05	3499	666	2491	240	61.00	10,30	1.77	157.4	155.0
8 4.75 4.51 4.45 .0122 39.9 1753 1471 2234 540 72.70 2.20 5.24 155.5 9 4.76 4.51 4.46 .0243 40.1 3505 1469 2929 538 3.05 0 6.62 158.9 10 4.76 4.56 .0242 32.8 2848 1471 2925 540 2.41 0 6.62 158.9 10 4.75 4.56 .0242 32.8 2848 1473 3962 540 2.41 0 8.00 157.11 11 5.79 5.56 5.54 .0243 39.9 3503 1473 3962 540 2.29 0.01 9.27 158.8 12 7.84 7.53 7.49 .0240 80.5 6949 999 2517 542 40.60 3.03 16.1 16.1 13 7.88 7.55 7.51 7.50 60.4	762	7	4.75	4.57	4.50	.0241	40.1	3481	166	2520	544	39.20	3.10	2.66	157.1	154.6
9 4.76 4.51 4.46 .0243 40.1 3505 1469 2929 538 3.05 0 6.62 158.9 10 4.75 4.56 4.54 .0242 32.8 2848 1471 2925 540 2.41 0 8.00 157.1 11 5.79 5.56 5.54 .0243 39.9 3503 1473 3962 540 2.29 0.01 9.27 158.8 12 7.84 7.53 7.49 .0240 80.5 6936 1584 2169 544 74.50 49.70 1.82 164.1 13 7.87 7.42 7.36 .0240 80.2 6949 999 2517 542 40.60 3.03 2.63 165.6 14 7.68 7.55 7.51 .0240 80.2 6949 999 2517 542 40.60 3.03 165.6 15 9.51 9.14 9.10 .0243 <td>753</td> <td>∞</td> <td>4.75</td> <td>4.51</td> <td>4.45</td> <td>.0122</td> <td>39.9</td> <td>1753</td> <td>1471</td> <td>2234</td> <td>240</td> <td>72.70</td> <td>2.20</td> <td>5.24</td> <td>155.5</td> <td>154.3</td>	753	∞	4.75	4.51	4.45	.0122	39.9	1753	1471	2234	240	72.70	2.20	5.24	155.5	154.3
10 4,75 4,56 4,54 .0242 32.8 2848 1471 2925 540 2,41 0 8.00 157.11 11 5,79 5,56 5,54 .0243 39.9 3503 1473 3962 540 2.29 0.01 9.27 158.8 12 7,84 7,53 7,49 .0240 80.5 6936 1584 2169 544 74.50 49.70 1.82 164.1 13 7,87 7,42 7,36 .0240 80.2 6949 999 2517 542 40.60 3.03 2.63 165.6 14 7,68 7,55 7,51 .0240 80.2 6949 999 2517 542 40.60 3.03 2.63 165.6 15 9,51 9,14 9,10 .0240 80.6 7804 997 2515 542 23.00 1.04 3.65 165.8 16 9,52 8,97 8,9	752	6	4.76	4.51	97.4	.0243	40.1	3505	1469	2929	538	3.05	0	6.62	158.9	157.1
11 5.79 5.56 5.54 .0243 39.9 3503 1473 3962 540 2.29 0.01 9.27 158.8 12 7.84 7.53 7.49 .0240 80.5 6936 1584 2169 544 74.50 49.70 1.82 164.1 13 7.87 7.42 7.36 .0240 80.2 6949 999 2517 542 40.60 3.03 2.63 164.1 14 7.68 7.55 7.51 .0240 66.4 5730 1001 2522 544 28.30 1.52 3.42 163.4 15 9.51 9.10 .0240 66.4 5730 1001 2542 542 23.00 1.04 3.65 163.8 16 9.53 9.10 9.06 7804 997 2515 542 33.80 1.88 3.27 166.8 17 9.52 8.97 8.92 .0242 79.8 <td< td=""><td>751</td><td>10</td><td>4.75</td><td>4.56</td><td>4.54</td><td>,0242</td><td>32.8</td><td>2848</td><td>1471</td><td>2925</td><td>240</td><td>2.41</td><td>0</td><td>8.00</td><td>157.1</td><td>155.3</td></td<>	751	10	4.75	4.56	4.54	,0242	32.8	2848	1471	2925	240	2.41	0	8.00	157.1	155.3
12 7.84 7.53 7.49 .0240 80.5 6936 1584 2169 544 74.50 49.70 1.82 164.1 13 7.87 7.42 7.36 .0240 80.2 6949 999 2517 542 40.60 3.03 2.63 165.6 14 7.68 7.55 7.51 .0240 66.4 5730 1001 2522 544 28.30 1.52 3.42 163.4 15 9.51 9.14 9.10 .0243 79.6 6953 1001 2542 542 23.00 1.04 3.65 165.8 16 9.53 9.00 .0240 90.6 7804 997 2515 542 33.80 1.88 3.27 166.8 17 9.52 8.97 8.92 .0242 79.8 6960 1471 2229 542 55.90 1.84 7.55 163.6 18 9.56 9.02 8.97 <t< td=""><td>754</td><td>=</td><td>5.79</td><td>5.56</td><td>5.54</td><td>.0243</td><td>39.9</td><td>3503</td><td>1473</td><td>3962</td><td>240</td><td>2.29</td><td>0.01</td><td>9.27</td><td>158.8</td><td>157.3</td></t<>	754	=	5.79	5.56	5.54	.0243	39.9	3503	1473	3962	240	2.29	0.01	9.27	158.8	157.3
13 7.87 7.42 7.36 .0240 80.2 6949 999 2517 542 40.60 3.03 2.63 165.6 14 7.68 7.55 7.51 .0240 66.4 5730 1001 2522 544 28.30 1.52 3.42 163.4 15 9.51 9.10 .0243 79.6 6953 1001 2542 542 23.00 1.04 3.65 165.8 16 9.53 9.10 9.06 7804 997 2515 542 33.80 1.88 3.27 166.8 17 9.52 8.97 8.92 .0242 79.8 6960 1471 2929 542 1.26 0 9.63 165.1 18 9.56 9.02 8.97 .0121 80.0 3479 1471 2229 542 55.90 1.84 7.55 163.6	761	12	7.84	7.53	7.49	.0240	80.5	6936	1584	2169	244	74.50	49.70	1.82	164.1	160.3
14 7.68 7.55 7.51 .0240 66.4 5730 1001 2522 544 28.30 1.52 3.42 163.4 15 9.51 9.14 9.10 .0243 79.6 6953 1001 2542 542 23.00 1.04 3.65 165.8 16 9.53 9.10 9.06 7804 997 2515 542 33.80 1.88 3.27 166.8 17 9.52 8.97 8.92 .0242 79.8 6960 1471 2929 542 1.26 0 9.63 165.1 18 9.56 9.02 8.97 .0121 80.0 3479 1471 2229 542 55.90 1.84 7.55 163.6	759	13	7.87	7.42	7.36	.0240	80.2	6769	666	2517	545	40.60	3.03	2.63	165.6	163.3
15 9.51 9.14 9.10 .0243 79.6 6953 1001 2542 542 23.00 1.04 3.65 165.8 16 9.53 9.10 9.00 .0240 90.6 7804 997 2515 542 33.80 1.88 3.27 166.8 17 9.52 8.97 8.92 .0242 79.8 6960 1471 2929 542 1.26 0 9.63 165.1 18 9.56 9.02 8.97 .0121 80.0 3479 1471 2229 542 55.90 1.84 7.55 163.6	260	14	7.68	7.55	7.51	.0240	4.99	5730	1001	2522	544	28.30	1.52	3.42	163.4	160.7
16 9.53 9.10 9.00 .0240 90.6 7804 997 2515 542 33.80 1.88 3.27 166.8 17 9.52 8.97 8.92 .0242 79.8 6960 1471 2929 542 1.26 0 9.63 165.1 18 9.56 9.02 8.97 .0121 80.0 3479 1471 2229 542 55.90 1.84 7.55 163.6	757	15	9.51	9.14	9.10	.0243	9.62	6953	1001	2542	545	23.00	1.04	3.65	165.8	162.7
17 9.52 8.97 8.92 .0242 79.8 6960 1471 2929 542 1.26 0 9.63 165.1 18 9.56 9.02 8.97 .0121 80.0 3479 1471 2229 542 55.90 1.84 7.55 163.6	758	16	9.53	9.10	00.6	.0240	9.06	7804	266	2515	545	33.80	1.88	3.27	166.8	164.8
18 9.56 9.02 8.97 .0121 80.0 3479 1471 2229 542 55.90 1.84 7.55 163.6	755	17	9.52	8.97	8.92	.0242	8.62	0969	1471	2929	245	1.26	0	9.63	165.1	165.0
	756	18	9.56	9.05	8.97	.0121	0.08	3479	1471	2229	245	55.90	1.84	7.55	163.6	163.0

(1) Upstream of combustor (2) Downstream of combustor

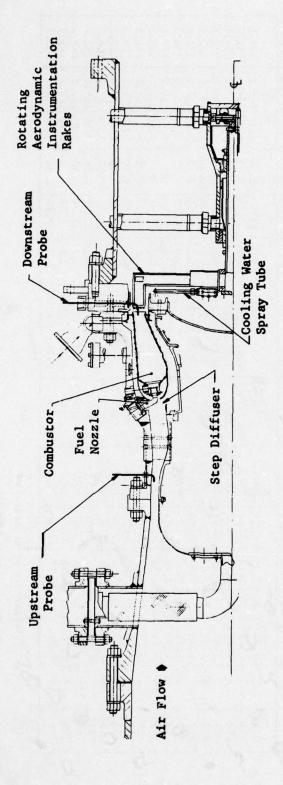


Figure 2.2-1 Cross-Section of Combustor Test Rig

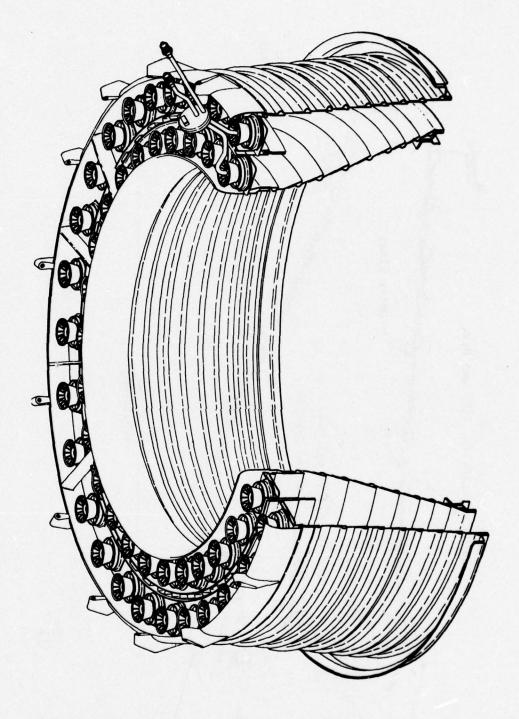


Figure 2.2-2 Double Annular Combustor

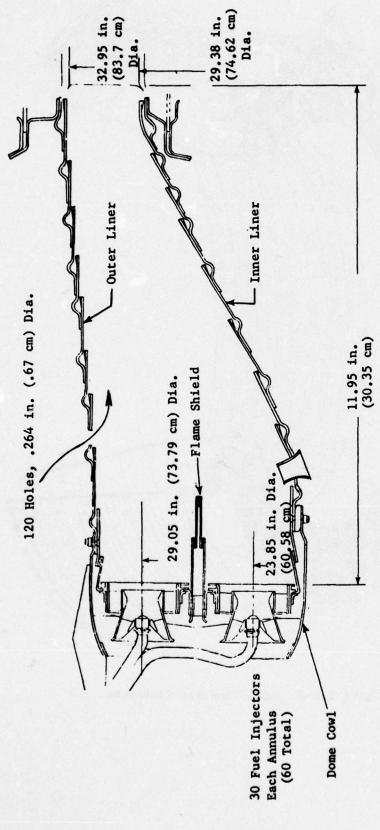


Figure 2.2-3 Cross-Section of Double Annular Combustor

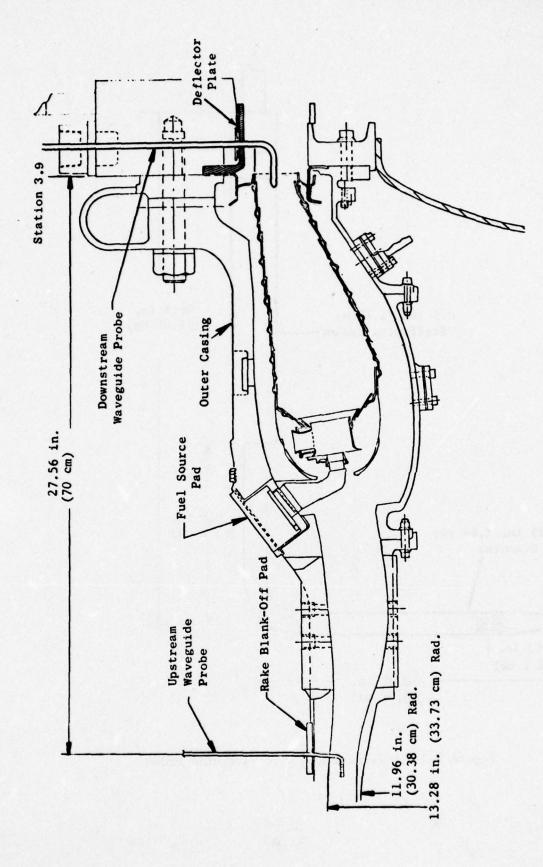


Figure 2.2-4 Cross-Section of Experimental Clean Combustor Test Rig Showing Acoustic Probe Locations

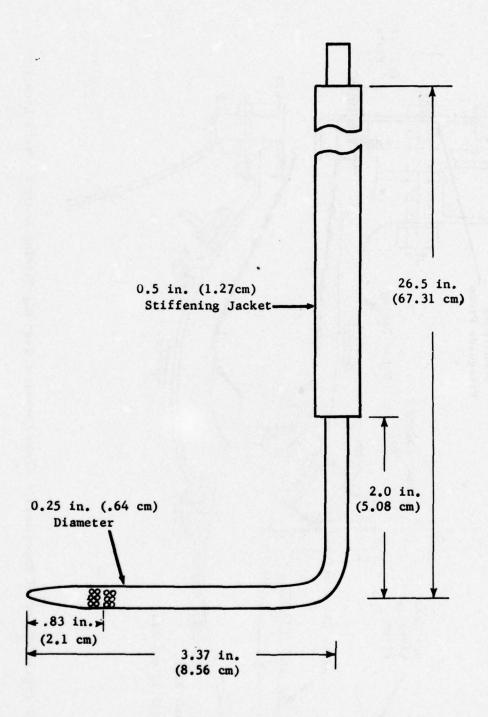


Figure 2.2-5 Upstream Acoustic Waveguide Probe

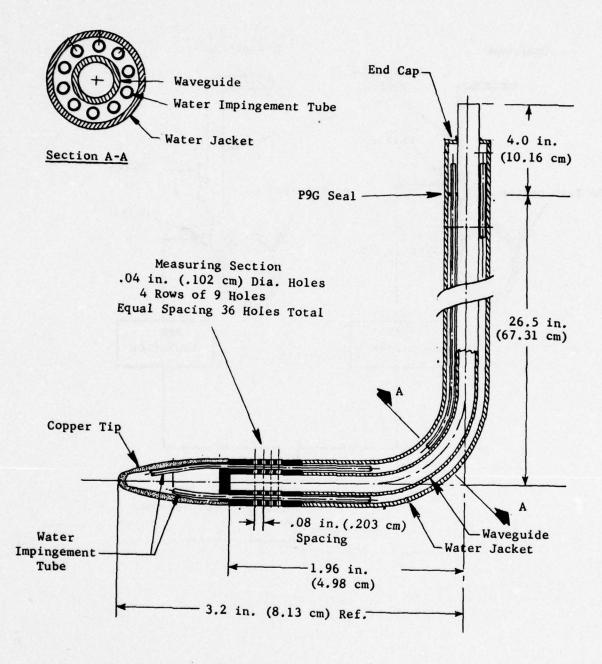


Figure 2.2-6 Cross-Section of Downstream, Water-Cooled Acoustic Waveguide Probe

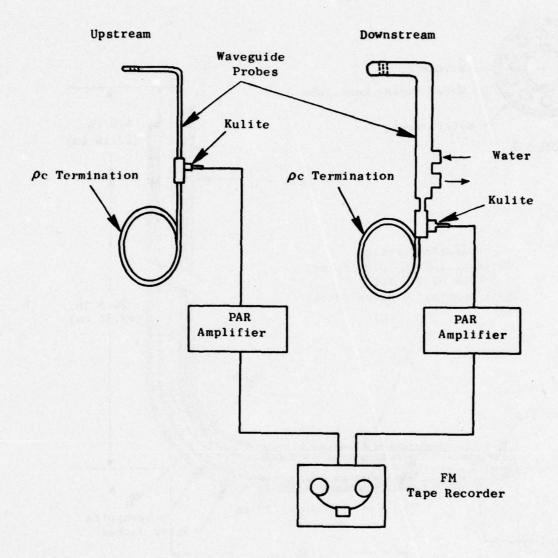
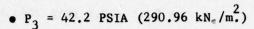


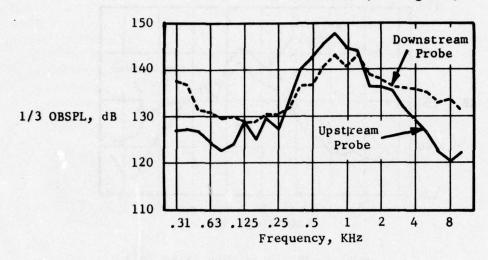
Figure 2.2-7 Acoustic Probe Data Acquisition System



•
$$T_3 = 1474^\circ R (819^\circ K)$$

•
$$f/a = 0.0238$$

•
$$\dot{\mathbf{w}} = 20.3 \text{ 1bm./sec. } (9.21 \text{ kg./s.})$$



•
$$P_3 = 42.0 \text{ PSIA } (289.58 \text{ kN./m}^2)$$

•
$$T_3 = 1476^\circ R (820^\circ K)$$

•
$$f/a = 0.0240$$

•
$$\dot{W} = 24.3 \text{ lbm./sec.} (11.0 \text{ kg./s.})$$

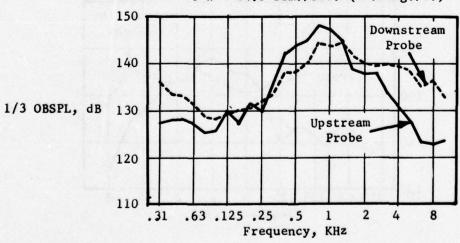


Figure 2.2-8 Typical Upstream and Downstream Acoustic Probe Measured Combustor Spectra for Low Air Flow Conditions

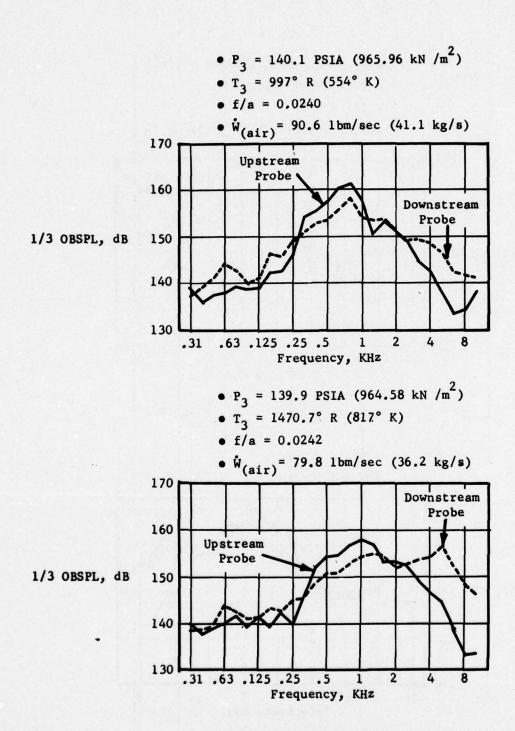


Figure 2.2-9 Typical Upstream and Downstream Acoustic Probe Measured Combustor Spectra for High Air Flow Conditions

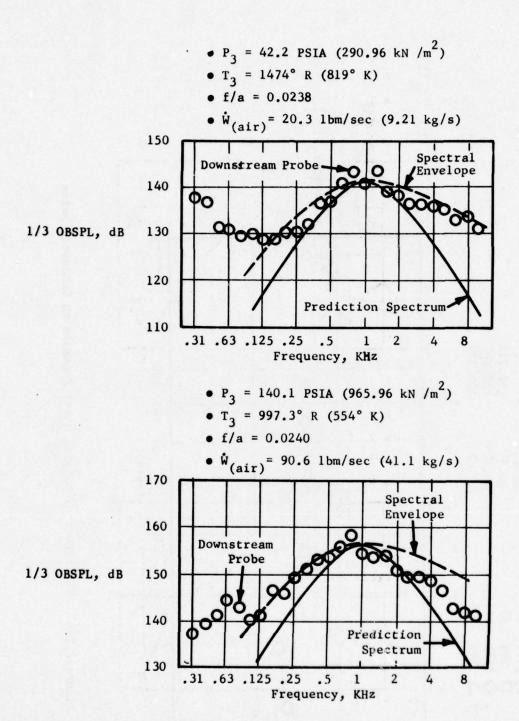


Figure 2.2-10 Comparison of Measured Spectrum to Prediction Spectrum for Low and High Air Flow Conditions

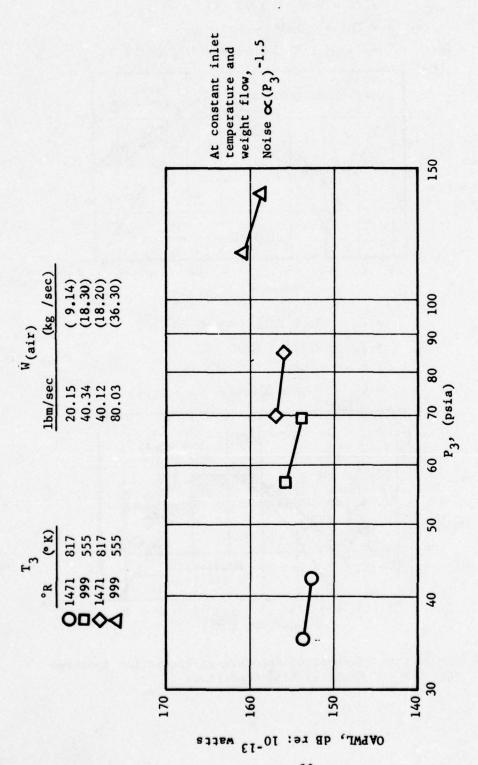


Figure 2.2-11 The Effect of Varying Inlet Pressure on Combustor Noise

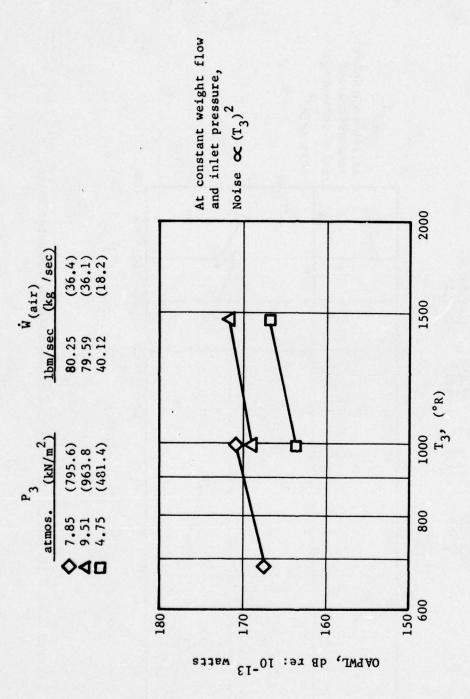


Figure 2.2-12 The Effect of Varying Inlet Temperature on Combustor Noise.

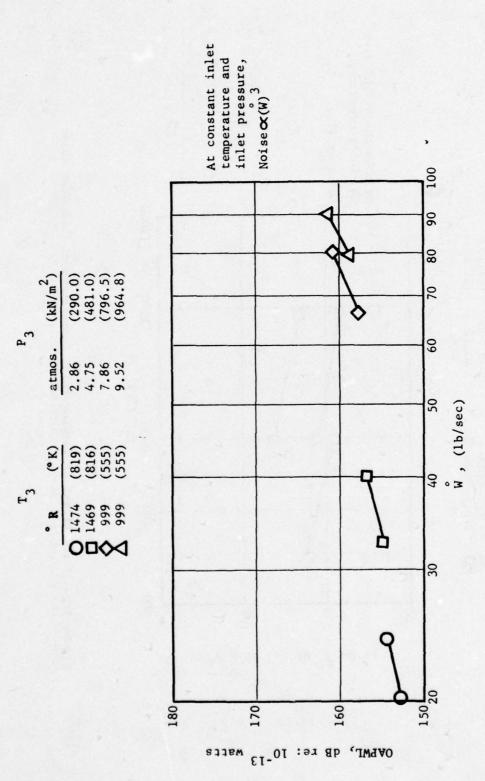


Figure 2.2-13 The Effect of Varying Air Flow Rate on Combustor Noise.

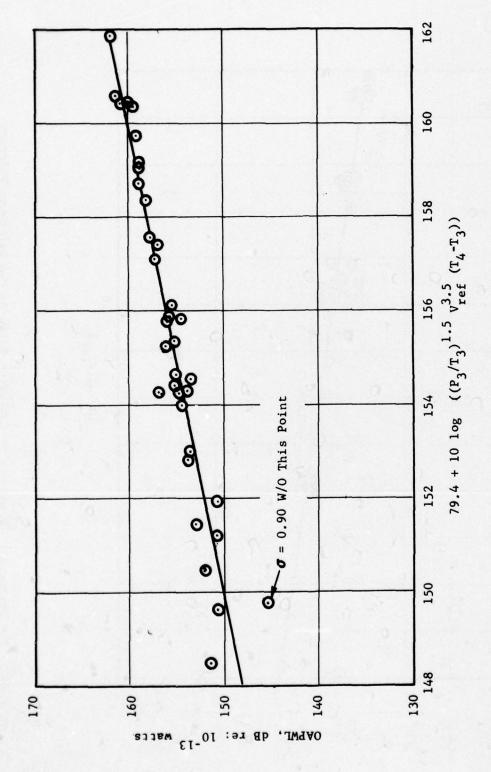
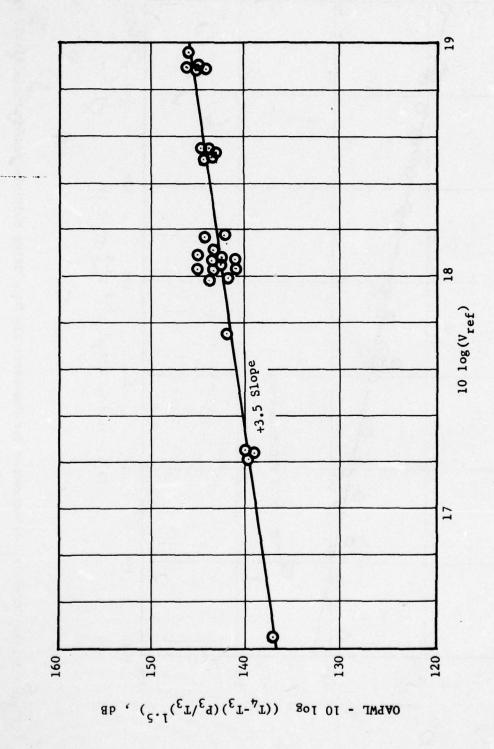


Figure 2.2-14 Correlation Parameter for Combustor Rig Data Using Multiple Regression Analysis Fit



, ...

Figure 2.2-15 The Parametric Dependence of Combustor Noise on the Reference Velocity

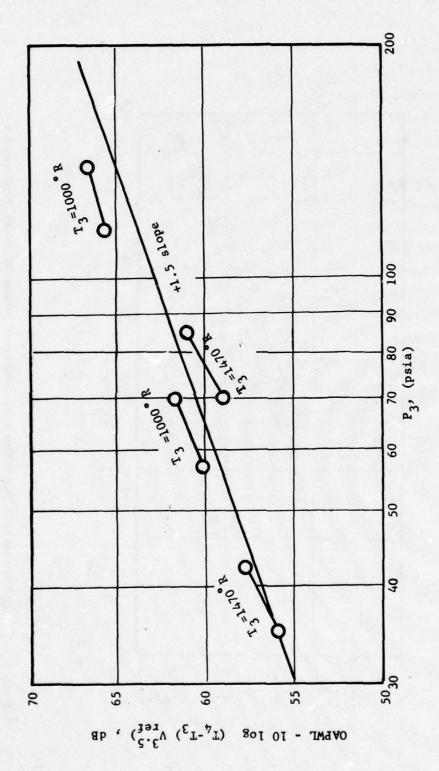


Figure 2.2-16 The Parametric Dependence of Combustor Noise on Inlet Pressure

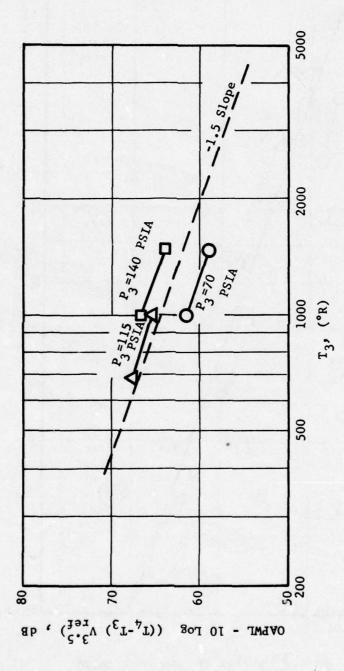


Figure 2.2-17 The Parametric Dependence of Combustor Noise on Inlet Temperature

2.3 LOW FREQUENCY NOISE DIRECTIVITY TESTS

2.3.1 Objectives

The primary objective of this task was to determine the impact of core exhaust nozzle geometry on low frequency farfield directivity. Five different nozzle configurations were evaluated; four separate flow and one mixed flow. Effects of nozzle geometry were also evaluated in terms of determining which configuration produced the lowest levels in the forward quadrant and the variation in farfield directivity with frequency.

2.3.2 Test Description

The tests were conducted at General Electric's Jet Engine Noise Outdoor Test Stand (JENOTS) facility located in Evendale, Ohio. JENOTS is a dual flow acoustic test facility, including an acoustically treated plenum (Figure 2.3-1), which absorbs upstream piping, valve, and combustor noise. The range of conditions under which the facility operates are:

	Minimum	Maximum
Bypass Ratio	0	15
Fan Temperature (°R)	ambient	ambient
Core Temperature (°R)	ambient	1600 (890° K)
Fan Pressure Ratio	1.05	3.5
Core Pressure Ratio	1.05	4.0
Fan Weight Flow (lb/sec)	0	30 (13.6 kg/sec)
Core Weight Flow (1b/sec)	0	30 (13.6 kg/sec)

A detailed description of the facility characteristics, including acoustic validation, can be found in Reference 1.

A total of five different nozzle configurations were tested under this phase of the program. These configurations are shown schematically in Figure 2.3-2. Configuration No. 1 has an internal centerbody core nozzle, while Configuration No. 2 has an external plug core nozzle. Configuration No. 3 is typical of exhaust systems for high bypass turbofans, e.g. CF6-50, as is Configuration No. 4, except that No. 4 has an extended core nozzle conical plug. Configuration No. 5 is an 18-lobe internal forced mixer typical of proposed exhaust systems for future high bypass turbofan engines. The basis for the separate flow nozzle configurations was to ensure a sufficient variation in plug geometry such that any effect on farfield low frequency noise directivity would be discernible. The configurations chosen represent the spectrum of core exhaust nozzles currently in use for high bypass turbofan engines and those proposed (i.e., mixer) for future use.

Figure 2.3-4 shows a typical test configuration set-up at the JENOTS test facility. The low frequency source was simulated by means of siren tones injected into the core stream just aft of the plenum chamber through a

one-inch (2.54 cm) tube. The tube entered the core section obliquely to maximize the termination area, thus reducing transmission loss at the interface (Figure 2.3-5). The siren itself was encased in an acoustically-treated case to prevent contamination of the farfield data. Siren tones from 125 to 1875 Hz, including fundamentals and harmonics, were generated at each power setting. The power level of the siren was monitored by a pressure transducer located just downstream of the siren tube exit port. The siren tone levels were in excess of 190 dB.

Each of the five configurations were tested at the nominal conditions listed in Table 2.3-1. These conditions encompassed the range of velocities encountered at approach and takeoff power settings for current and advanced high bypass turbofan engines such as the CF6, TF34, JT9D and CFM56.

The data acquisition system consisted of farfield microphones located on a 20-ft (6.lm) arc centered on the core nozzle exit plane. The microphones were flush mounted on the ground and located at 10° increments relative to the core nozzle centerline. Bruel and Kjaér No. 4133 microphones, 2615 cathode followers and 2801 power supplies were used for farfield measurements. The output level of the siren, used to generate the pure tones employed as the internal source for the directivity study, was monitored by a wall-mounted transducer located just downstream of the siren. A schematic of the farfield microphone system is shown in Figure 2.3-6. All data were recorded on an FM tape recorder for subsequent reduction.

2.3.3 Test Results

The farfield acoustic data were reduced on a narrowband basis using a one Hz bandwidth. This ensured that the tone levels could be read accurately, and any background broadband noise could be removed if necessary. After obtaining the farfield levels, the directivity indices for each tone and its harmonics were calculated.

The resultant farfield levels for each configuration and test condition are tabulated in Appendix B. Some typical results are shown in Figures 2.3-7 thru 2.3-16 for a range of power settings and frequencies.

2.3.4 Data Analysis

Comparison of Separate Flow Results

The separate flow test results, shown in Figures 2.3-7 through 2.3-16, indicate that Configurations No. 1 (internal centerbody) and No. 2 (external plug) tend to produce somewhat lower levels in the forward quadrant than the other two configurations. The data also show that these same configurations tend to have lower levels in the aft quadrant. This could be due to the fact that the high radius ratio plug designs for Configurations No. 1 and No. 2 yield very small passage heights, which offer increased impedance to the

transmission of low frequencies. In fact at low frequencies, all of the models were operating in a range where "ka" is small, thus the length-to- λ ratio exerts a significant influence on the nozzle radiation characteristics for the no flow case (Reference 6). Due to the significant amount of data scatter and limited number of data points, it is not possible to quantitatively assess the differences between the high radius ratio plugs and the other two configurations.

A second result is that the directivity pattern for any given frequency appears to be largely independent of velocity ratio ($V_{\rm fan}/V_{\rm core}$). Figures 2.3-17 through 2.3-19 show the directivity patterns for the average of Configurations 1-4 as a function of velocity ratio for three different source frequencies. This is significant since the only remaining variable affecting the low frequency directivity are nozzle geometry and frequency. Figure 2.3-19 also shows the field shape derived from engine test data (Reference 1) is in excellent agreement with the scale-model data for a source frequency of 1250 Hz.

Figures 2.3-7 through 2.6-16 also indicate a significant change in field shape with increasing source frequency. The lower frequencies appear to have a skewed directivity with the peak angle occurring at 150° to the inlet, similar to that seen for jet noise. As the source frequency increases, the peak angle shifts toward 120° to the inlet, and the field shape looks similar to that seen for core noise measured on engines. This shift in directivity may be attributable to the balance between convection and refraction effects caused by the jet stream; for example, see Reference 7. The results obtained here are consistent with those found by Bilwakesh (Reference 7) where the lower frequencies were controlled by convection effects and the higher frequencies showed the influence of refraction effects with the peak noise angle shifting away from the jet axis. The data indicate this shift begins to occur at frequencies between 400 and 625 Hz on a scale-model basis. Assuming a linear scale factor of 4:1, this would correspond to 100-200 Hz on a fullscale engine. This result is substantiated by the component rig data obtained under the Core Engine Noise Control Program, as shown in Figures 2.3-20 - 2.3-21. On a non-dimensional basis, the directivity shift occurs between ka = 1.2 to 1.8, based on the fan nozzle radius or 0.4 to 0.7 based on the core nozzle radius, where k is the wave number.

Comparison of Separate Flow and Mixed Flow

Figures 2.3-22 through 2.3-30 show a comparison of the separate and mixed flow test results for several power settings and source frequencies. At high power settings the mixer produced lower absolute tone levels than the separate flow configurations at 400, 800, and 1875 Hz. The tone levels at 125 Hz were comparable to the separate flow configurations, while at 1250 Hz the mixer levels were higher. In general, the mixer did tend to reduce the tone levels in both the forward and aft quadrants and shift the peak angle toward the jet axis with some evidence of a secondary peak at 90 to 100°. The reduction observed for the mixer configuration is attributed to the reduced character-

istic dimension at the core nozzle exit due to the mixer elements. Similar attenuation of low frequency noise is indicated for multi-element nozzle configurations used on a J85 engine (Reference 8). The results were representative of those observed at the other power settings with the reduction achieved by the mixer being limited to the higher frequencies (> 800 Hz). Overall, the mixer nozzle produced a 5-7 dB reduction in tone levels in the forward quadrant and a 2-4 dB reduction in the aft quadrant, depending upon the frequency.

2.3.5 Results and Conclusions

The significant results of this task are summarized below:

- 1. The high radius ratio core nozzles appear to reduce forward and aft propagation of low frequency noise by a small amount.
- The directivity characteristics of the various configurations tested appear to be largely independent of velocity ratio.
- 3. The farfield directivity pattern at all power settings appears to be frequency dependent with lower frequencies (ka <1.2) exhibiting a skewed pattern peaking at 150° to the inlet axis and higher frequencies (ka >1.8) having a pattern closely resembling measured core engine directivities peaking at 120° to the inlet. Here 'a' is the fan nozzle radius.
- 4. The change in directivity pattern with frequency is probably due to a shift in control from convection to refraction effects.
- 5. The 18-lobe mixer produced lower farfield tone levels at most frequencies and power settings, especially in the forward quadrant (5-7 dB).

These results tend to support the conclusion that high radius ratio plug core nozzles are more beneficial from a core noise standpoint than low radius ratio plugs. Further, the benefit achievable is independent of velocity and velocity ratio, suggesting that the results shown here should be generally applicable to a range of engine cycles. The agreement found between the model data, at higher frequencies, and the engine directivity reinforces the validity of the field shape currently used for predicting core engine noise. Results, however, do show that for very low frequencies the field shape changes significantly, with a marked shift in the peak angle towards the jet axis.

Table 2.3-1 Low Frequency Core Noise Directivity
Test Matrix

Frequency Survey: Siren Fundamentals of 125, 400, and 625 Hz, plus Harmonics.

T_{core} = 1400°R (778°K); T_{fan} = ambient

Core V	Core velocity			Velocity ratio	ratio		
ft/sec m/sec	m/sec	0	9.	.65	.75	.85	.85 1.0
200	152.4						×
800	243.9				×	×	
1100	335.3			×	×		
1500	457.3		×				

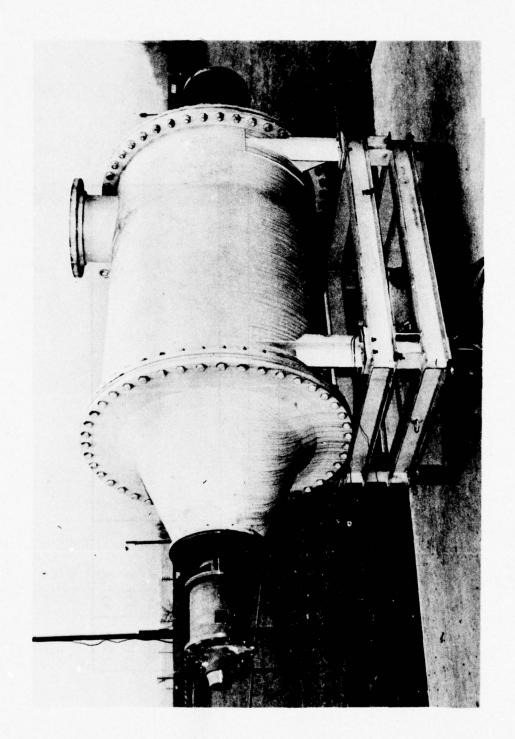


Figure 2.3-1 JENOTS Treated Plenum Chamber for Coannular Facility

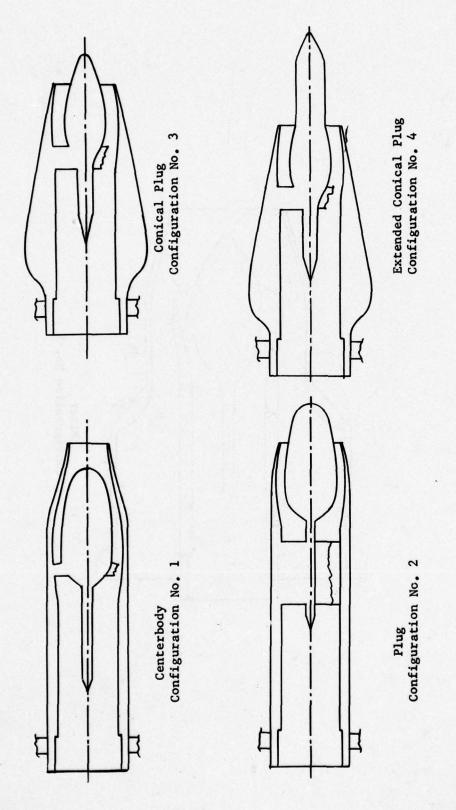


Figure 2.3-2 Schematics of Core Exhaust Geometry Variation for Separate Flow Configurations

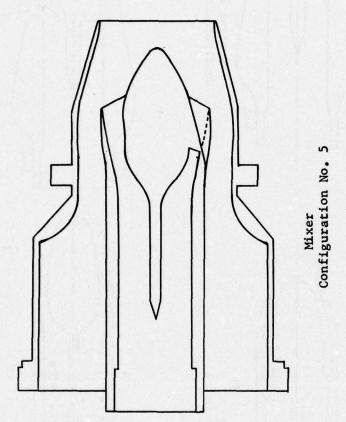


Figure 2,3-3 Schematic of Mixed Flow Configuration

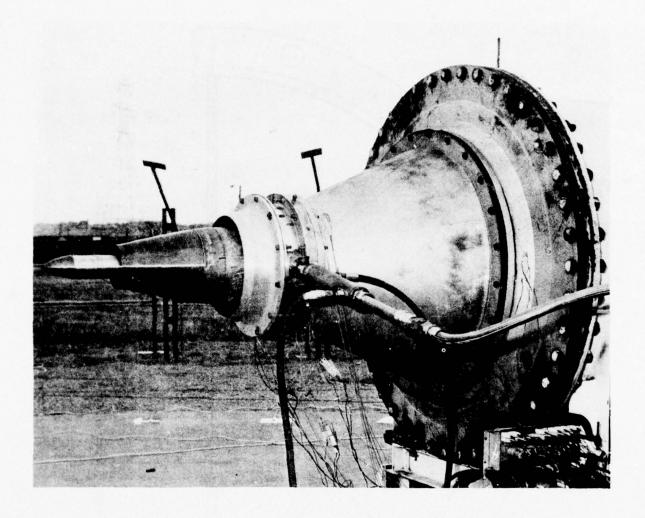


Figure 2.3-4 Typical Nozzle Configuration on JENOTS Acoustic Test Facility

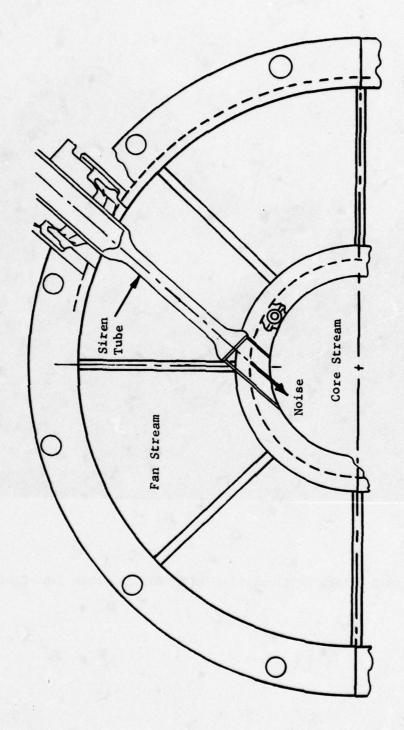
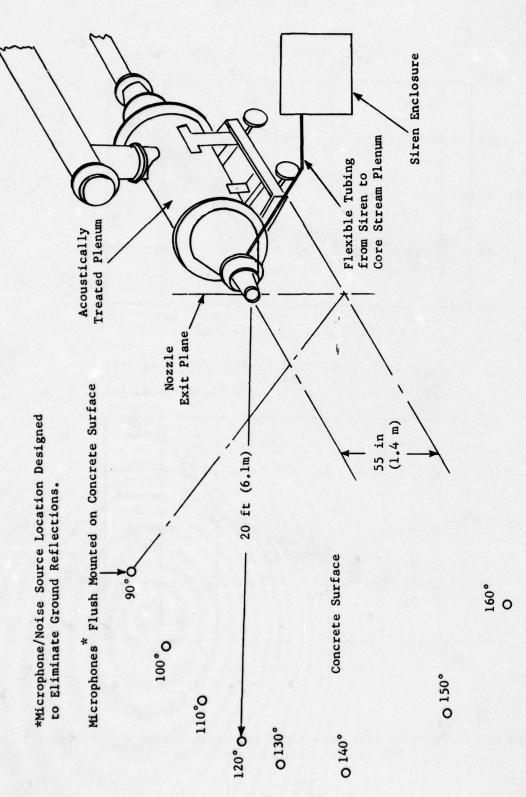
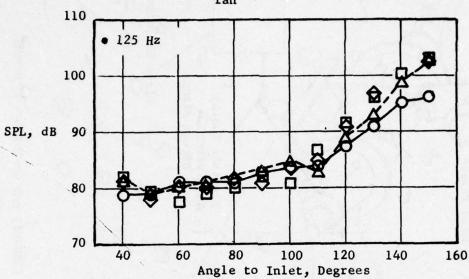


Figure 2.3-5 Siren Noise Source Installation



Schematic of Jet Noise Outdoor Test Stand (JENOTS) set up for Low Frequency Core Noise Directivity Test Figure 2.3-6

- 20 ft Arc (6.1 m)
- $V_{core} = 1486 \text{ ft/sec}$ (452.9 m/s)
- $V_{fan} = 901 \text{ ft/sec}$ (274.6 m/s)



- O Config. 1/Pt. 191
- ☐ Config. 3/Pt. 191
- △ Config. 2/Pt. 191
- ♦ Config. 4/Pt. 191

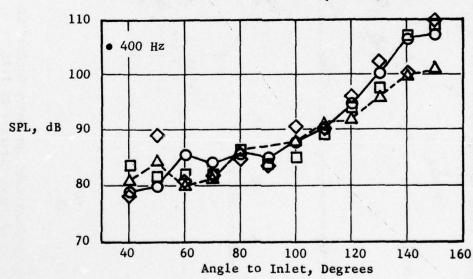


Figure 2.3-7 Separate Flow Core Noise Directivities at $V_{core} = 1486$, $V_{fan} = 901$ ft /sec for 125 and 400 Hz

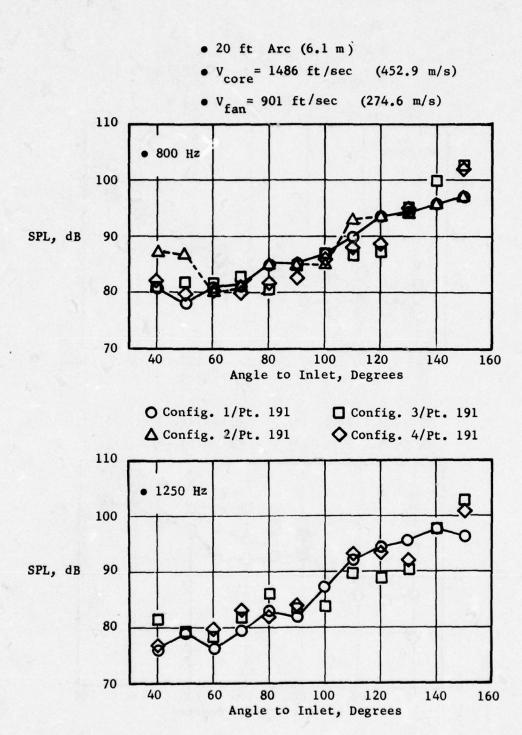


Figure 2.3-8 Separate Flow Core Noise Directivities at $V_{core} = 1486$, $V_{fan} = 901$ ft /sec for 800 and 1250 Hz

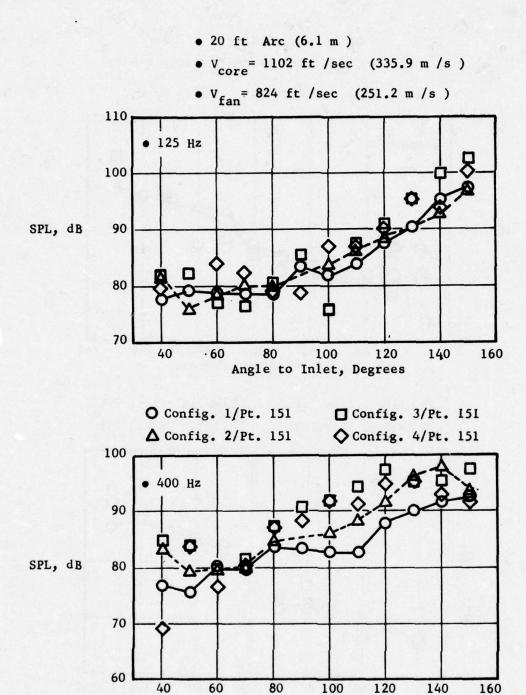


Figure 2.3-9 Separate Flow Core Noise Directivities at $V_{core} = 1102$, $V_{fan} = 824$ ft /sec for 125 and 400 Hz

Angle to Inlet, Degrees

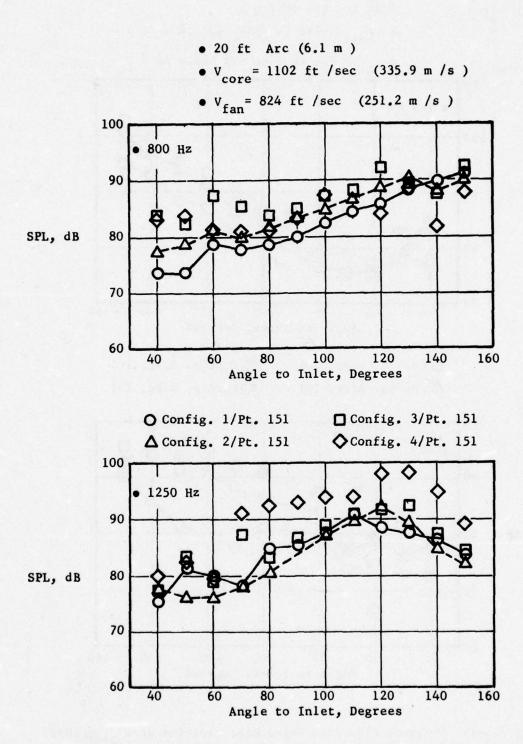
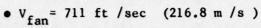
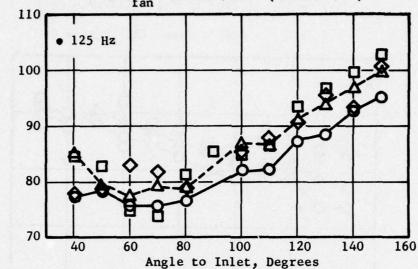


Figure 2.3-10 Separate Flow Core Noise Directivities at V core 1102, V = 824 ft /sec for 800 and 1250 Hz

- 20 ft Arc (6.1 m)
- V_{core} = 1095 ft /sec (333.8 m/s)





O Config. 1/Pt. 141

SPL, dB

- ☐ Config. 3/Pt. 141
- △ Config. 2/Pt. 141
- ♦ Config. 4/Pt. 141

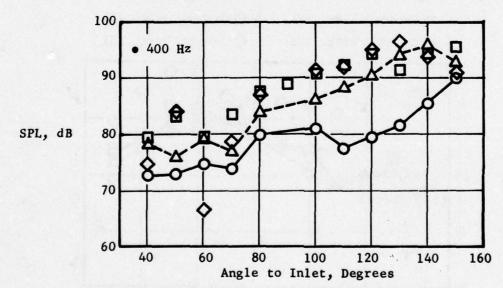


Figure 2.3-11 Separate Flow Core Noise Directivities at V_{core} = 1095, V_{fan} = 711 ft /sec for 125 and 400Hz

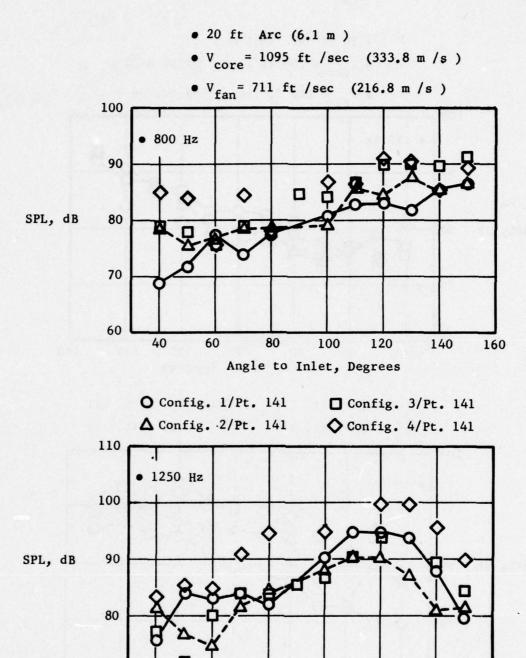


Figure 2.3-12 Separate Flow Core Noise Directivities at $V_{core} = 1095$, $V_{fan} = 711$ ft /sec for 800 and 1250 Hz

Angle to Inlet, Degrees

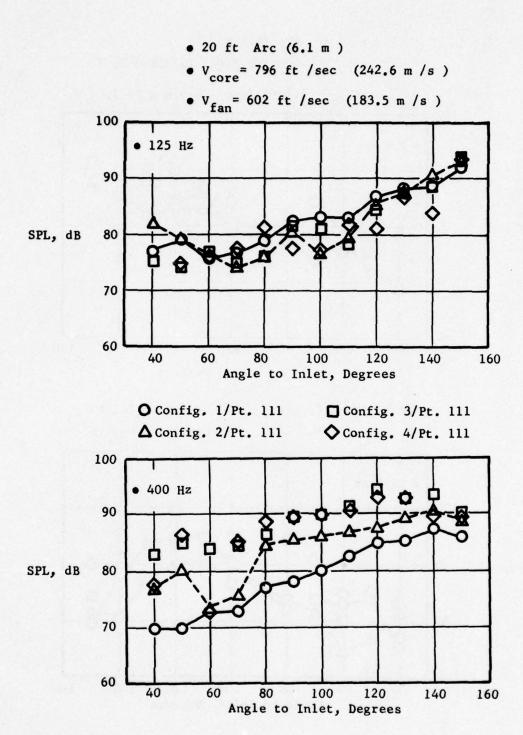


Figure 2.3-13 Separate Flow Core Noise Directivities at $V_{core} = 796$, $V_{fan} = 602$ ft /sec for 125 and 400 Hz

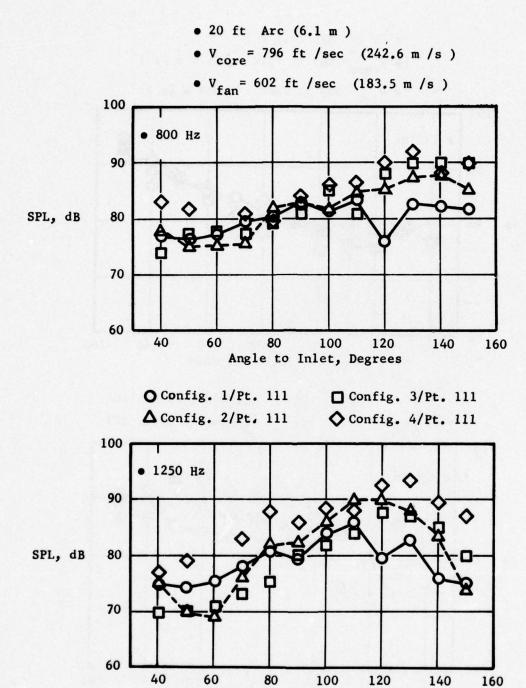


Figure 2.3-14 Separate Flow Core Noise Directivities at $V_{core} = 796$, $V_{fan} = 602$ ft /sec for 800 and 1250 Hz

Angle to Inlet, Degrees

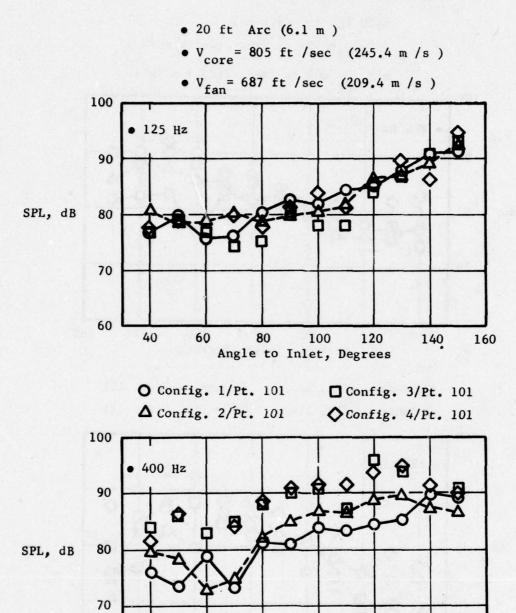


Figure 2.3-15 Separate Flow Core Noise Directivities at V_{core} =805, V_{fan} = 687 ft /sec for 125 and 400 Hz

Angle to Inlet, Degrees

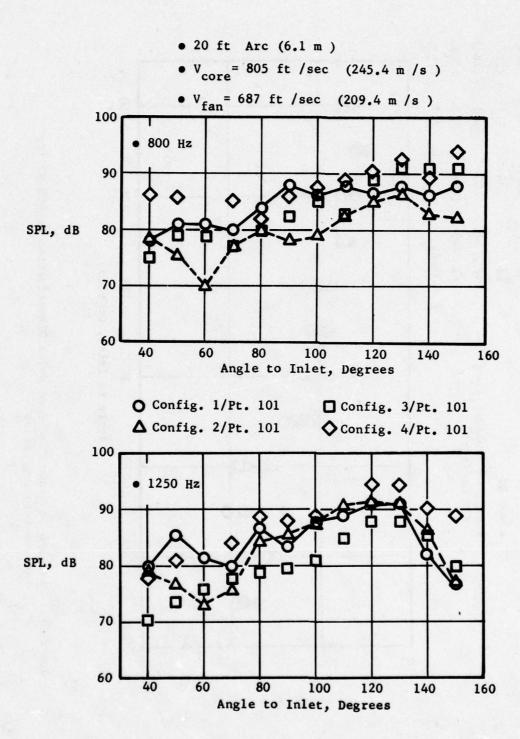


Figure 2.3-16 Separate Flow Core Noise Directivities at $V_{core} = 805$, $V_{fan} = 687$ ft /sec for 800 and 1250 Hz

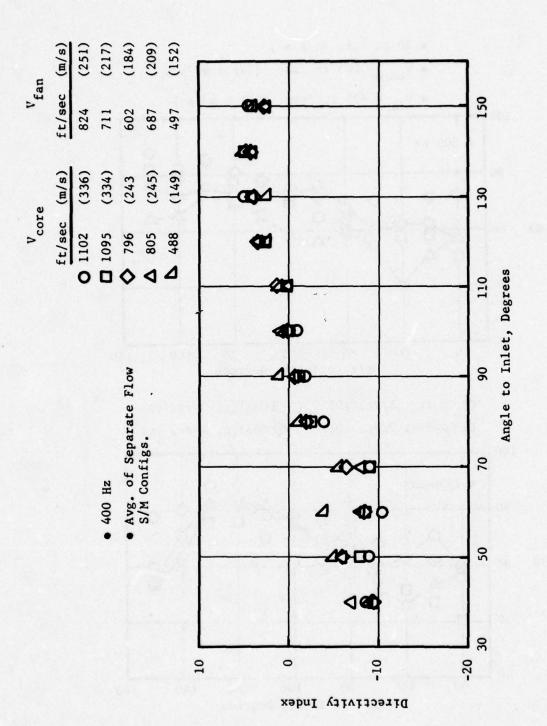
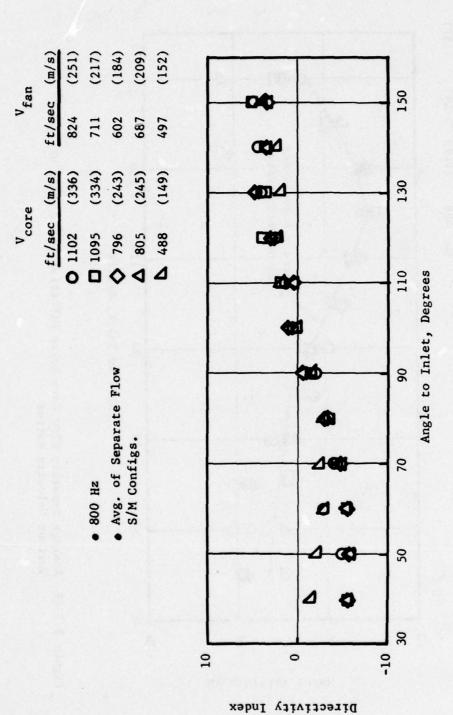


Figure 2.3-17 Average Separate Flow Core Noise Directivities at 400 Hz for Various Velocity Ratios



Average Separate Flow Core Noise Directivities at 800 Hz for Various Velocity Ratios Figure 2.3-18

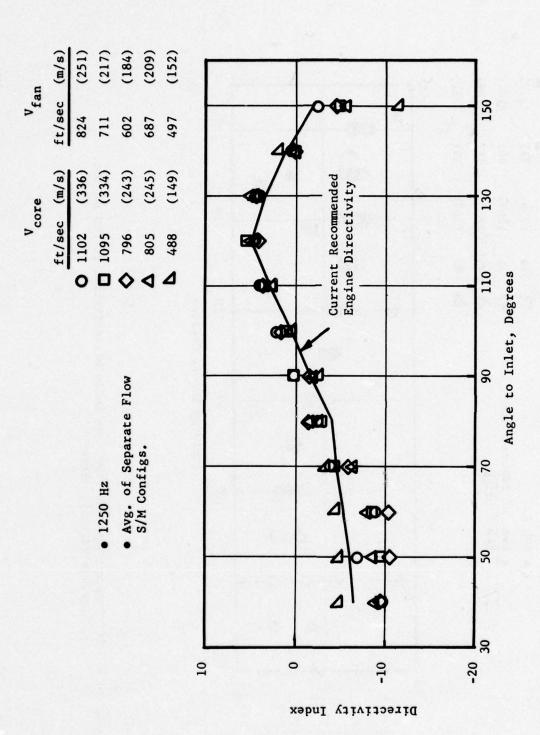
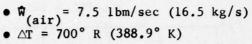
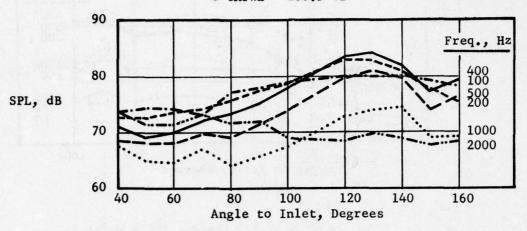
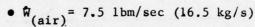


Figure 2.3-19 Average Separate Flow Core Noise Directivities at 1250 Hz for Various Velocity Ratios



•
$$\triangle T = 700^{\circ} R (388.9^{\circ} K)$$







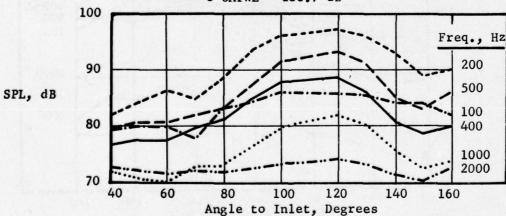
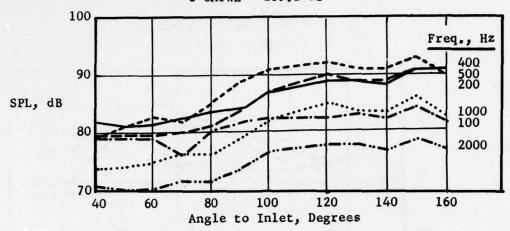


Figure 2.3-20 CF6 Combustor Directivities for Various Frequencies at AT of 700 and 1700° R

- $\hat{W}_{(air)} = 7.5 \text{ lbm/sec (16.5 kg/s)}$
- $\Delta T = 700^{\circ} R (388.9^{\circ} K)$
- OAPWL = 139.1 dB



- $\hat{W}_{(air)} = 7.5 \text{ lbm/sec } (16.5 \text{ kg/s})$
- $\triangle T = 1700^{\circ} R (944.4^{\circ} K)$
- OAPWL = 150.9 dB

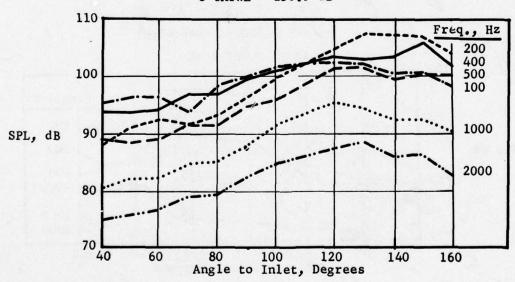


Figure 2.3-21 Advanced Technology Combustor Directivities for Various Frequencies at $\triangle T$ of 700 and 1700° R

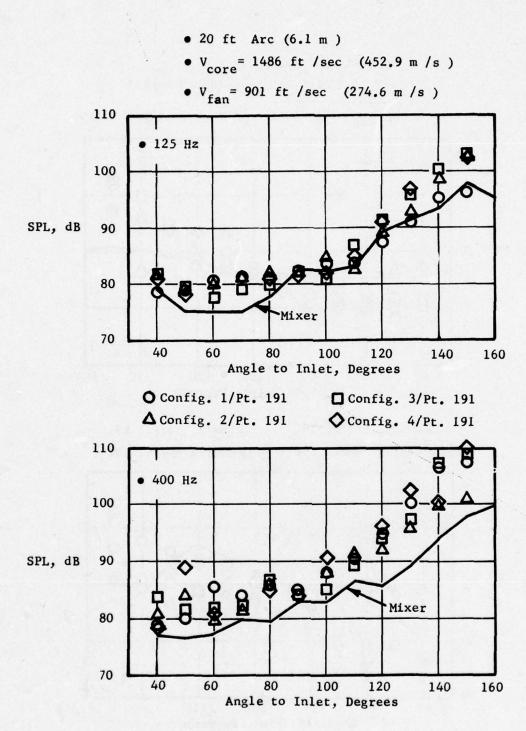


Figure 2.3-22 Mixed and Separate Flow Core Noise Directivity Comparison at $V_{\rm core}$ = 1486, $V_{\rm fan}$ = 901 ft /sec for 125 and 400 Hz

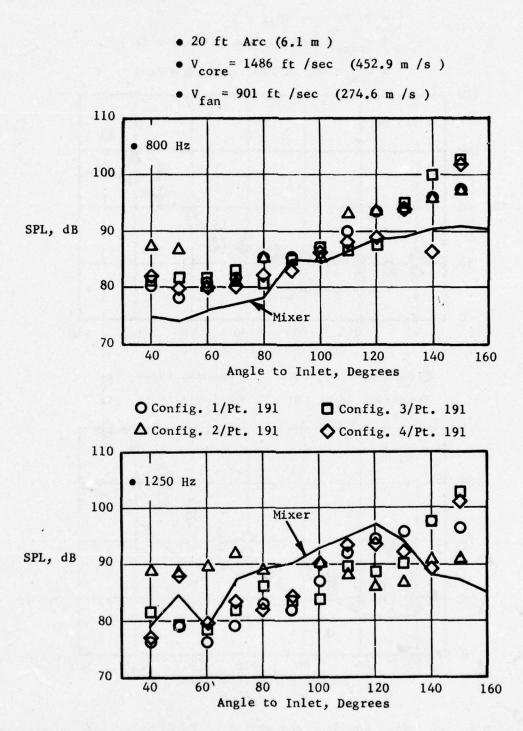
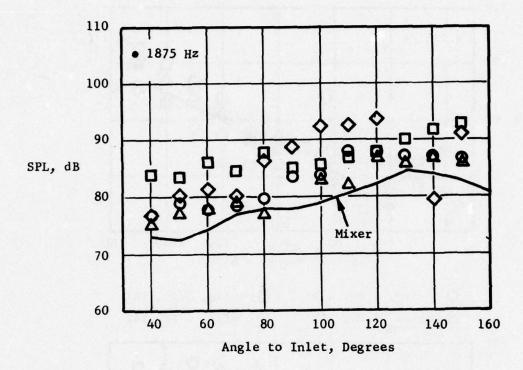


Figure 2.3-23 Mixed and Separate Flow Core Noise Directivity Comparison at $V_{core} = 1486$, $V_{fan} = 901$ ft /sec for 800 and 1250 Hz

- 20 ft Arc (6.1 m)
- V_{core} = 1486 ft /sec (452.9 m/s)
- V_{fan} = 901 ft /sec (274.6 m /s)



- O Config. 1/Pt. 191
- ☐ Config. 3/Pt. 191
- △ Config. 2/Pt. 191
- ♦ Config. 4/Pt. 191

Figure 2.3-24 Mixed and Separate Flow Core Noise Directivity Comparison at $V_{core} = 1486$, $V_{fan} = 901$ ft /sec for 1875 Hz

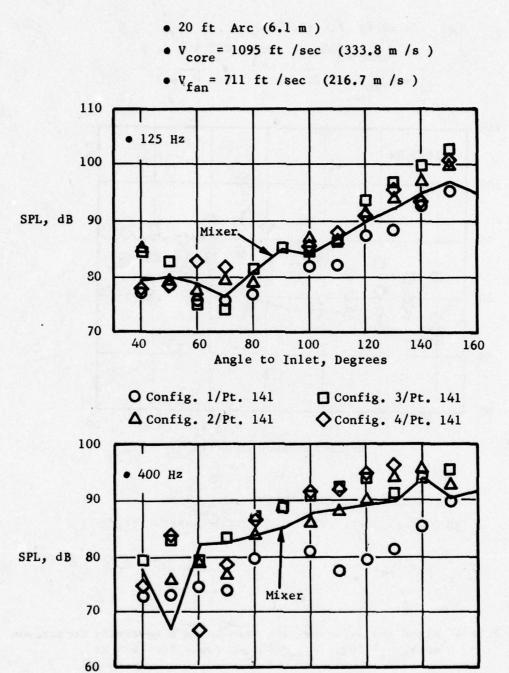
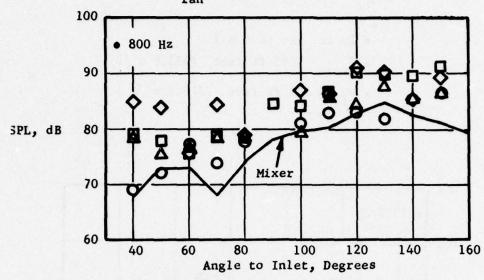


Figure 2.3-25 Mixed and Separate Flow Core Noise Directivity Comparison at $V_{core} = 1095$, $V_{fan} = 711$ ft /sec for 125 and 400 Hz

Angle to Inlet, Degrees

- 20 ft Arc (6.1 m)
 V_{core} = 1095 ft /sec (333.8 m/s)
- V_{fan} = 711 ft /sec (216.7 m /s)



- O Config. 1/Pt. 141
- ☐ Config. 3/Pt. 141
- △ Config. 2/Pt. 141
- ♦ Config. 4/Pt. 141

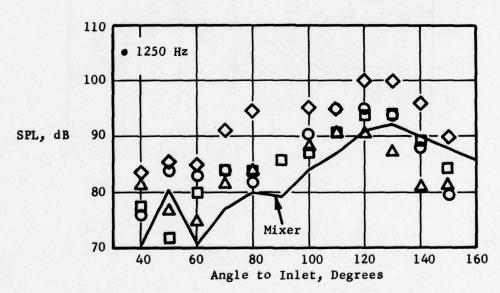
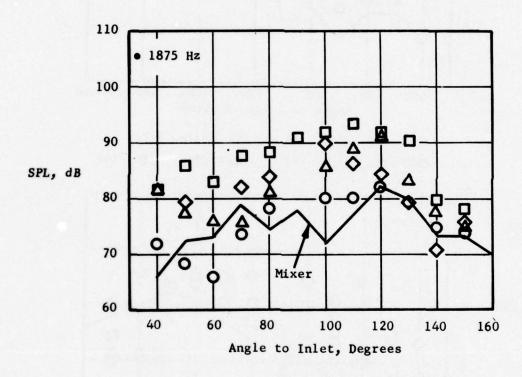


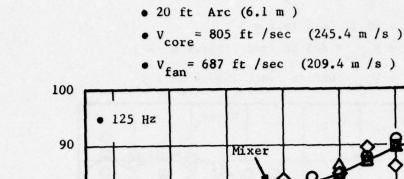
Figure 2.3-26 Mixed and Separate Flow Core Noise Directivity Comparison at V_{core} = 1095, V_{fan} = 711 ft /sec for 800 and 1250 Hz

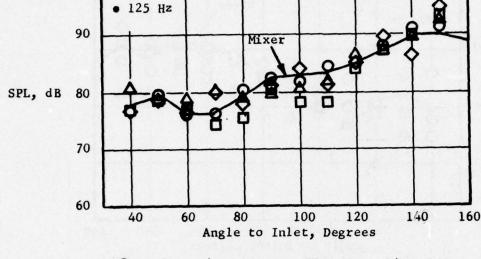
- 20 ft Arc (6.1 m)
- V_{core} = 1095 ft /sec (333.8 m /s)
- $V_{fan} = 711$ ft /sec (216.7 m /s)



- O Config. 1/Pt. 141
- ☐ Config. 3/Pt. 141
- △ Config. 2/Pt. 141
- ♦ Config. 4/Pt. 141

Figure 2.3-27 Mixed and Separate Flow Core Noise Directivity Comparison at $V_{core} = 1095$, $V_{fan} = 711$ ft /sec for 1875 Hz





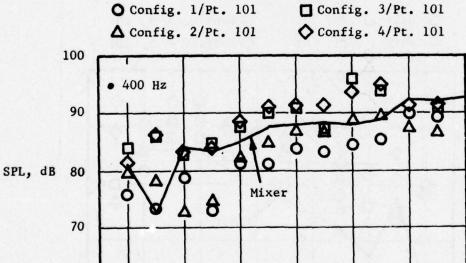


Figure 2.3-28 Mixed and Separate Flow Core Noise Directivity Comparison at $V_{core} = 805$, $V_{fan} = 687$ ft /sec for 125 and 400 Hz

Angle to Inlet, Degrees

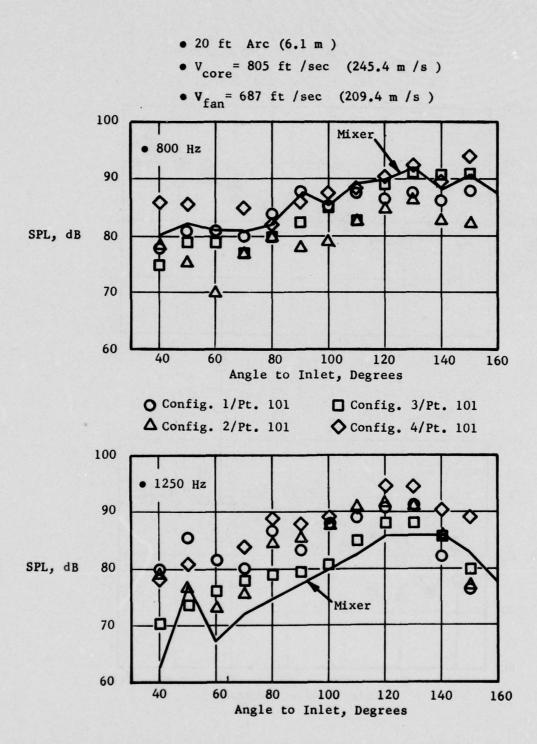
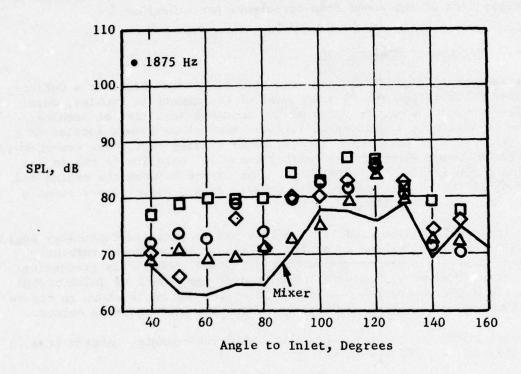


Figure 2.3-29 Mixed and Separate Flow Core Noise Directivity Comparison at v_{core} = 805, v_{fan} = 687 ft /sec for 800 and 1250 Hz

- 20 ft Arc (6.1 m)
- V_{core}= 805 ft /sec (245.4 m /s)
- V_{fan}= 687 ft /sec (209.4 m /s)



- O Config. 1/Pt. 101
- ☐ Config. 3/Pt. 101
- △ Config. 2/Pt. 101
- ♦ Config. 4/Pt. 101

Figure 2.3-30 Mixed and Separate Flow Core Noise Directivity Comparison at $V_{core}^{}$ = 805, $V_{fan}^{}$ = 687 ft /sec for 1875 Hz

2.4 ENGINE TESTS

2.4.1 Objectives

These data were acquired in order to enhance the data base used in the formulation of the combustor (core) noise prediction method for engines. In particular, the two engines selected (a turboshaft and a turbofan engine) provided information on combustors designed for lower emissions.

In order to determine the relationship between core and farfield low frequency noise levels, both internal and farfield instrumentation were used for the turbofan engine test. The internal instrumentation was designed to permit separation of the sound from turbulence perturbations.

2.4.2 Turboshaft Engine Test

The turboshaft engine test was conducted at General Electric's Outdoor Engine Test Facility located 90 miles west of Cincinnati in Peebles, Ohio. Figure 2.4-1 shows a panoramic view of the acoustic test site at Peebles. The acoustic test site consisted of farfield microphone towers located on a 150-ft (45.7 m) arc centered on the fan rotor leading edge. The towers were 40-ft (12.2m) above ground level located every 10° relative to the engine centerline which is 13-ft (3.96m) high. The ground between the engine and the microphone towers was covered with crushed rock. Figure 2.4-2 shows a schematic of the test facilty.

The turboshaft engine used for the test was an advanced technology engine utilizing a reduced emissions combustor and highly loaded power turbine. This engine featured a centrifugal compressor stage immediately preceding the combustor, thus providing some indication of the impact of inlet turbulence on the noise generation. A schematic of the engine is shown in Figure 2.4-3. A water brake system was used to absorb the power turbine output.

A total of ten test points were run, including repeats, ranging from 70 SHP (52.2KW) to 1300 SHP (969.4 KW).

Farfield acoustic data were recorded using the microphone set-up, described above, plus 2 additional microphones located 1-ft above the crushed rock surface at 110° and 120° to the inlet. These additional microphones were used to verify low frequency spectral shapes in the aft quadrant. The farfield measurements were made using B & K No. 4133 1/2" microphones, 2615 cathode followers, and 2801 power supplies. Data was recorded on a 28 channel FM tape recorder located in the engine control room. All engine performance data were also monitored in the control room.

Test Results

The farfield acoustic data were reduced on a 1/3-octave band basis and corrected to a standard (ISA) day. Figures 2.4-4 through 2.4-8 show 60° and 120° farfield spectra for each power setting, including the predicted core and jet noise. The jet noise is 20 dB below the measured data in all cases, indicating that it is not a contributing source. The predicted core noise levels are in excellent agreement with the measured data in the aft quadrant for frequencies between 100 and 630 Hz with the exception of ground idle. Below 100 Hz, the data is affected by a 60 Hz interference signal from the amplifiers. The data, however, include significant contributions from the waterbrake and rotating turbomachinery noise. The former was clearly audible in the forward quadrant, especially at low power settings. The latter was characterized by tonal peaks. Figures 2.4-9 and -10 show measured SPL's at 60° and 120° for several 1/3-octave band frequencies of interest plotted as a function of shaft horsepower. The 400 Hz levels at 120° varies, as predicted for combustor noise, over the entire speed range while at 60° the levels follow a different slope. The 125 Hz levels in the forward quadrant appear to be totally dominated by the waterbrake, as can be seen from the data trend in Figure 2.4-9. In the aft quadrant, however, the 125 Hz data indicate trends similar to the predicted values at all but the very lowest power setting. At higher frequencies (see Figure 2.4-10) the measured data trends indicate slightly different slopes than the predicted values, expecially at 2000 Hz.

The waterbrake noise appears to increase at a slower rate with engine power setting than does the combustor noise. Hence, the measured engine data in the vicinity of 400 Hz increasingly resembles combustor noise with increasing speed. Figures 2.4-11 through 2.4-19 show a comparison of measured and predicted core noise field shapes at 125, 400, and 630 Hz. These figures support the claim that the waterbrake influences the farfield levels, at low frequencies in the forward quadrant, because the measured field shape is not typical of that observed for core noise on other engines. On-site evaluation during the test indicated the waterbrake noise to clearly be audible at low power settings in the forward quadrant. Also the levels in the forward quadrant approach the predicted core noise levels as engine power setting increases. At 125 Hz, the engine data is higher than the prediction except at high power settings in the aft quadrant. This is due to the background noise of the waterbrake system dominating the forward quadrant as noted above. At 400 and 630 Hz, excellent agreement is obtained between measured and predicted levels in the aft quadrant. This good agreement on both a spectral and field shape basis, in the aft quadrant, supports the findings from the Core Engine Noise Control Program (DOT-FA72WA-3023).

Figures 2.4-20 and 2.4-21 show the low microphone data (mic height = 1-ft) compared to the standard 40-ft tower data. The low microphones were used to obtain low frequency spectrum shapes free of ground reflections. Unfortunately, there was a 60 Hz contamination signal which prevented obtaining a smooth spectrum down to 50 Hz. The low microphone data does, however, reconfirm the low frequency (100-400 Hz) spectrum shape of core noise.

Figure 2.4-22 shows the OAPWL calculated for this engine, at each power setting, compared to the engine correlation derived in Reference 8. These OAPWL's were calculated assuming a T64 spectrum shape and directivity pattern given in Reference 8 and fitting the spectrum shape to the measured engine level in the 400 Hz 1/3-octave band; as expected, there is excellent agreement with the previous data base on an OAPWL basis.

Results and Conclusions

The results of the testing on the turboshaft engine are summarized below:

- On a spectral basis the engine data were in essential agreement with the T64 spectrum shape recommended in the Core Engine Noise Control Program (DOT FA72WA-3023).
- The field shapes measured for the engine peak combustor noise frequencies in the aft quadrant were in good agreement with the prediction directivity. The front quadrant levels were contaminated by water-brake noise.
- 3. The calculated OAPWL's for the turboshaft engine correlated well with the procedure outlined in the referenced contract.

Relatively good agreement between this measured turboshaft engine data and the predicted levels on a directivity, spectral and OAPWL basis, supports the prediction method previously derived under DOT-FA72WA-3023 and provides a new set of data to be included in the core engine noise data base. The agreement on a PWL and spectral basis is notable considering the differences between this engine and those used to derive the prediction method; particularly the presence of a centrifugal compressor stage immediately preceding the combustor (impacts the turbulence entering the combustor), and the relatively high overall turbine pressure ratio (which determines the low frequency noise transmission).

2.4.3 Turbofan Engine Test

The turbofan engine test was conducted at SNECMA's (Societe' Nationale d'Etude et de Construction de Moteurs d'Aviation) outdoor acoustic test facility located in Istres, France. Figure 2.4-23 shows a view of the test facility with the engine mounted on the test stand. The acoustic test site consisted of farfield microphone towers located on a 201.7 ft (61.5m) arc centered on the core exhaust nozzle exit plane. The towers were 15.6 ft (4.75m) high, located every 5° relative to the engine centerline, which was 11.5 ft (3.5m) above the ground. In addition, there were two movable microphone systems mounted on trolleys which traversed a 197 ft (60m) arc at a speed of .86 ft/sec (.26 m/s). The height of these movable microphones was 11.5 ft (3.5m). The surface between the engine and the microphone was smooth concrete. Figure 2.4-24 shows a schematic of the test facility.

The engine was a separate flow configuration (Figure 2.4-25). Both the inlet and fan exhaust duct were lined with acoustic treatment. The core nozzle was untreated. This particular configuration was not chosen to ensure that the measured farfield core noise would be representative of a production engine with the fan noise suppressed.

The basic instrumentation setup is shown in Figure 2.4-24. A total of eight test points were run. Farfield acoustic data were as recorded at each test point. Acoustic probe data at five different immersions were also recorded at each test point with the exception of the lowest power setting where only three immersions were recorded. Figure 2.4-26 shows a schematic of the probe relative to the core nozzle and a tabulation of the different immersions which were chosen to provide five equal area measurements across the core exhaust. Table 2.4-1 contains the fan speeds and thrusts for this test.

The instrumentation used for this test consisted of farfield microphones and a water cooled acoustic sound separation probe located at the core nozzle exit plane.

Figure 2.4-24 shows the five farfield microphones used for this test. These microphones were located on a 213.2-ft (65m) arc at height of 0.79-inches (20 mm) to insure no ground reflection interference in the frequency range of interest. In addition, there were two other mocrophones located on a 201.7-ft (61.5m) arc at a height of 4.9-ft (1.5m). These microphones were used as a check on the low microphones.

The farfield microphone systems consisted of B&K No. 4133 1/2-inch microphones, 2615 cathode followers and 2801 power supplies. Data was recorded on a Bell and Howell 3360 AM tape recorder. The tape recorder and associated amplifiers were located in the acoustic instrumentation trailer, shown in Figure 2.4-24.

The water-cooled acoustic sound separation probe, which utilizes two Kulite (CQH 125 - 25D) pressure transducers located in the probe tip, was mounted parallel to the engine centerline with the sensing elements located just inside the core exhaust nozzle. Figure 2.4-26 provides a schematic of the probe mounting system relative to the engine. Figure 2.4-27 shows a photo of the probe and mounting stand in place on the test stand. The transducers were connected to two low noise amplifers (Princeton Applied Research No. 113) and the output from these amplifers was input to the amplifier/tape recorder system located in the acoustic instrumentation trailer. Figure 2.4-28 shows a schematic of the electrical hook-up and signal conditioning for the probe.

Data Analysis

The data analysis for this test consisted of two parts:

- 1. Analysis of the probe data using sound separation to distinguish between turbulence and sound.
- 2. Comparison of probe data and farfield levels.

Sound Separation Probe Test Results

The internal measurements for this test were made with a water-cooled sound separation probe. This unique piece of instrumentation was used to permit the true acoustic signal, at the core nozzle exit, to be separated from the overall measured signal which included turbulence pressure fluctuations as well as those due to the noise. Figure 2.4-29 shows a schematic of the environment surrounding the probe.

The sound separation technique utilizes two miniature pressure transducers, aligned axially, mounted on the side of the probe. A cross-correlation between the signals from sensor A and sensor B will provide a function with separate peaks for each of the components (sound, turbulence) of the signal due to the varying phase velocity associated with each. The slower moving turbulence provides the peak of the time delay corresponding to the convection velocity, while the sound travelling at the speed of sound plus the mean velocity of the flow, provides a peak at a much smaller time delay. In order to compute the overall level of the broadband components of the signals, use is made of the fact that the zero time delay value of the autocorrelation of any signal is equal to its mean square value. Since the sensors are close together and the time delays are small, the assumption that the mean square of each component of the signal is equal to the peak value of the cross correlation is valid. Therefore, solution of the simultaneous equations provides the overall sound level. The sound spectrum is separated from the total spectrum by iteration of the cross correlation function into time shifted autocorrelation functions. The Fourier transform of the sound autocorrelation will provide the sound spectrum.

The data taken during this test were reduced using a digital analyzer (Time Data TDA-53P). The results are presented in the form of the overall measured signal, in one-third octave band levels, with the corresponding separated acoustic signal. Typical results are shown in Figures 2.4-30 through 2.4-36 for one immersion at each speed point. Data at the lowest speed point was not reduced due to pure tone contamination.

The one-third octave band data was used to calculate the one-third octave band power spectra and OAPWL's for each test point. The PWL's were calculated using the probe corrections noted in Section 2.2.4. Similarly, the OAPWL is the logarithmic summation of the one third octave PWL's. Table 2.4-2 contains the power spectra and OAPWL's for the sound separated acoustic signal for each test point.

Figure 2.4-37 shows the PWL spectrum shape for each test point. It can be seen that the measured spectral shapes are very close to the recommended engine spectrum shape from Reference 10, with the peak frequency shifted to 315 Hz. The variations in the measured data could be due to changes in turbine attenuation or source characteristics with varying engine speed. This result reinforces the recommendation made in Reference 10, namely that the T64 (engine) spectrum provides the best fit for core noise, and that the broader spectral envelope is probably due to contamination of farfield data by jet and fan noise.

Figure 2.4-38 shows some typical one third octave band data at 500 and 1000 Hz plotted as a function of immersion for various engine power settings. The small variation in SPL across the duct indicates the radial mode content is not significant. Figure 2.4-39 shows the calculated OAPWL's plotted against the core engine noise correlation parameter from Reference 10. The measured probe power levels are 5-6 dB higher than the mean line. This is not unexpected since the probe levels do not include any of the losses associated with impedance change at the nozzle exit or propagation through the jet exhaust. It can be shown (Reference 9) that the loss through the exhaust nozzle may be approximated as:

TL = 10 log
$$\left(\frac{C8}{C_0}\right)^2$$
 = 10 log $\left(\frac{T8}{T_0}\right)$ (2.4-1)

A more rigorous loss prediction can be obtained by considering the problem in two parts: a transmission problem and a radiation problem (see Figure 2.4-40). The transmission problem models the effect of velocity, density and temperature changes induced by the exhaust nozzle. The radiation problem models the effect of radiation into open space. The Bekofske actuator disk analysis of low frequency noise transmission through turbine blade rows (Reference 3) lends itself to the transmission problem since, in the analysis, the low frequency sound does not actually recognize the blades, only the changes induced in flow conditions. The solution to the second problem is well known (see, for example, Reference 6) and the loss is given by (ka)² for circular nozzles, where k is the wave number and 'a' the radius. Combining the two solutions should give the transmission loss for sound transmission through a nozzle carrying a flow. As is shown in Section 2.6, this yields a transmission loss of

TL = 10 log
$$\left[1/4 \frac{\rho_0 C_0}{\rho_8 C_8} \left(\frac{C_8}{C_0} + \frac{\rho_8}{\rho_0} \right)^2 \right]$$
 (2.4-2)

since the radiation loss component is negligible ("ka" is very large). Over the operating range of this test, the resultant nozzle transmission loss is estimated to be 4-5 dB, thus bringing the measured probe levels more into line with the other engine data. Where this effect is included, the measured probe levels are in good agreement with the other data which are based on farfield measurements.

The farfield core noise spectra were extracted from the "directly measured" farfield spectra through coherence with the signal measured by the core probe. The resultant farfield spectrum is that part of the total farfield spectra attributable to the noise emanating from the core nozzle. Figures 2.4-41 thru 2.4-45 show some typical results using the probe levels at immersion number three as the "source signal". The variation in spectrum shape as a function of angle is typical for all power settings. This variation represents the same combination of convection and refraction effects due to the jets noted for the model tests (Section 2.3). Figures 2.4-46 through 2.4-48 show some farfield directivity patterns for various frequencies and power settings. The field shapes are clearly a function of frequency with lower frequencies (<250 Hz) exhibiting trends similar to jet noise. The higher frequencies (>400 Hz) show trends similar to that seen for core noise on other engines. Result 3 similar to these were seen for the low frequency directivity tests (Section 2.3). These data indicate that the exhaust plume has a significant effect on farfield core noise directivity. Since this test represents a small sample and the accuracy of the point-to-point coherence analysis used is not fully known as yet, the farfield coherence levels determined by this test cannot be used with high confidence. However, the trends, such as dependence of farfield directivity on frequency, are believed to be valid. More work needs to be done in the area of the spectral content before any changes to current prediction procedures can be recommended.

Results And Conclusions

The results of the turbofan engine test are summarized below:

- Power spectra measured at the core nozzle exit confirm the T64 engine spectrum shape for core noise.
- 2. Probe OAPWL's are 5-6 dB higher than the current engine core noise correlation, with most of the difference being accounted for by a nozzle transmission loss term.
- 3. The coherence analysis indicates a strong frequency dependence for farfield directivity; with low frequencies showing characteristics similar to jet noise and higher frequencies trends similar to those seen for core noise on other engines. These findings are substantiated by the nozzle directivity test results (Section 2.3).
- 4. The use of sound separation and coherence analysis has proved to be a useful diagnostic tool for accurately measuring core noise on a turbofan engine.

Table 2.4-1 Turbofan Engine Test Matrix

Fan Speed	Thrust		
(rpm)	(1bs)	(kN)	
2674	5600	24.91	
2944	7000	31.14	
3246	8800	39.14	
3744	12400	55.16	
4122	15900	70.73	
4406	19000	84.52	
4648	22000	97.86	

Table 2.4-2 Core Probe Power Levels

• PWL dB re: 10⁻¹³ watts

Frequency	Point No.							
(Hz)	72	73	74	75	76	77	78	
100	137.5	135.9	137.5	133.1	131.5	131.9	130.6	
125	139.9	139.1	141.6	135.5	133.8	132.1	131.7	
160	141.3	140.5	143.4	137.7	136.0	133.6	132.7	
200	142.3	142.9	144.8	139.2	136.7	135:0	133.4	
250	142.7	144.3	145.2	139.3	138.0	136.9	133.3	
315	141.1	143.2	145.3	139.1	136.9	134.4	133.7	
400	142.7	143.8	145.5	138.9	136.0	133.5	132.1	
500	141.6	144.2	146.4	137.7	134.0	132.8	132.4	
630	137.1	139.6	141.6	134.3	132.8	131.2	131.7	
800	135.2	137.9	138.2	133.3	132.1	130.5	130.5	
1000	133.2	136.1	138.5	130.3	129.9	128.7	128.4	
1250	132.4	136.3	139.0	127.3	128.4	127.3	126.4	
1600	129.7	134.3	136.5	126.9	126.9	124.6	124.6	
2000	127.6	132.9	135.9	125.0	125.4	122.2	122.3	
OAPWL	150.9	152.2	154.2	147.6	145.6	143.9	142.7	

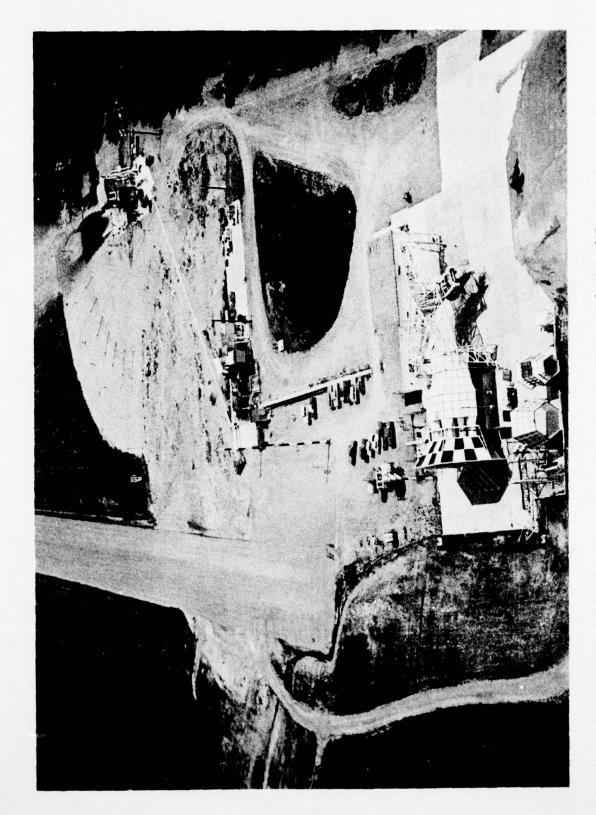


Figure 2.4-1 Aerial View of Peebles Sites IV A, B and D

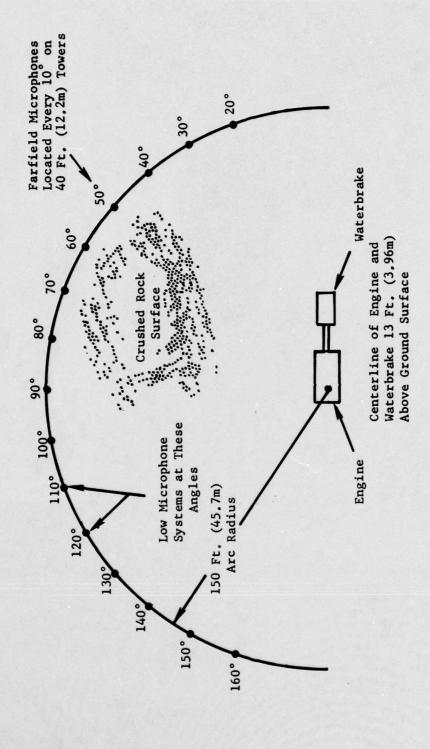


Figure 2.4-2 Schematic of Acoustic Sound Field at Peebles Site IV-D

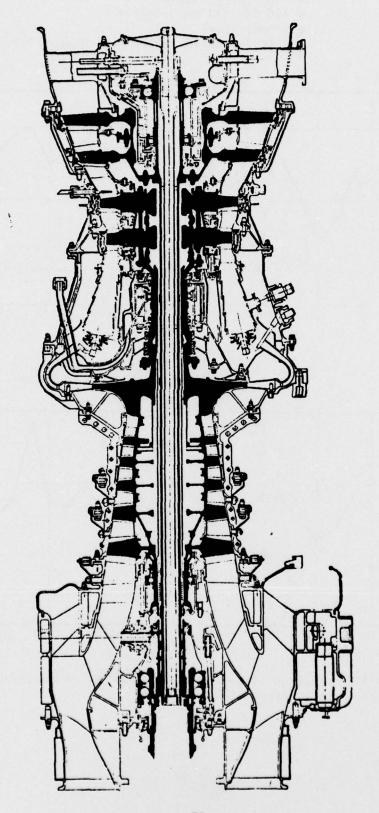


Figure 2.4-3 Schematic of Turboshaft Engine

- Turboshaft Engine
- 200 ft. (61 m) Sideline
- Ground Idle
- Peak Jet Noise Levels Less Than 45 dB

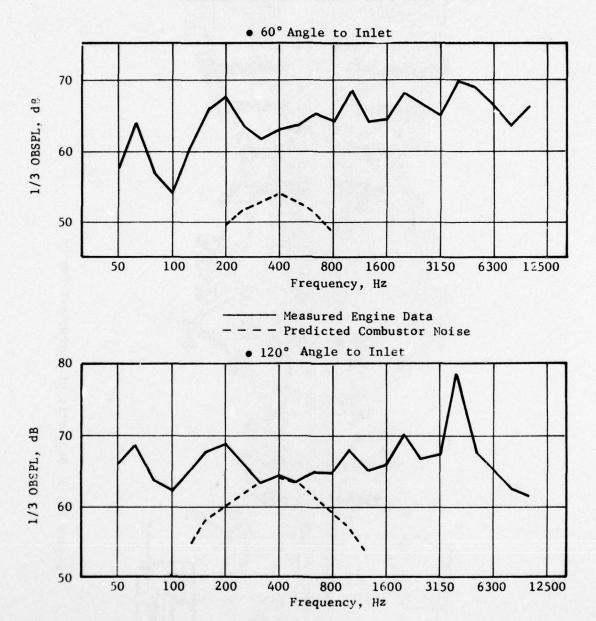
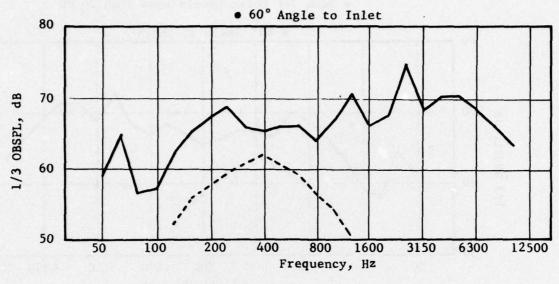


Figure 2.4-4 Comparison of Core Noise Prediction to Measured Engine Data at Ground Idle Speed.

- Turboshaft Engine
- 200 ft. (61 m) Sideline
- Flight Idle
- Peak Jet Noise Less Than 45 dB



---- Measured Engine Data
--- Predicted Combustor Noise

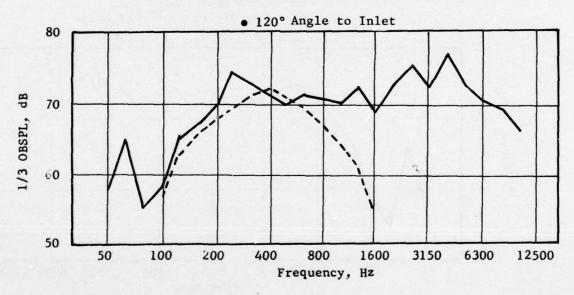
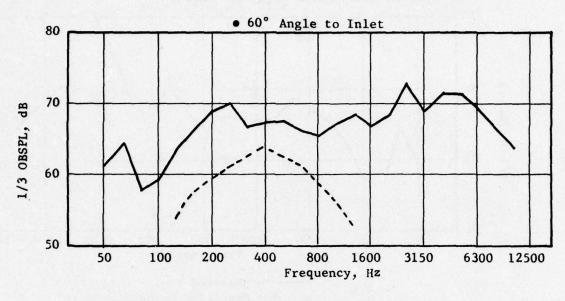


Figure 2.4-5 Comparison of Core Noise Prediction to Measured Engine
Data at Flight Idle Speed

- Turboshaft Engine
- 200 ft. (61 m) Sideline
- 650 Shaft Horsepower
- Peak Jet Noise Levels Less Than 50 dB



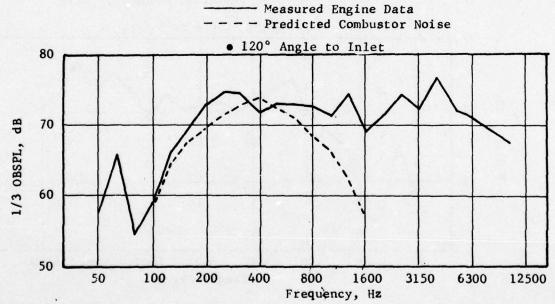


Figure 2.4-6 Comparison of Core Noise Prediction to Measured Engine Data at 650 SHP

- Turboshaft Engine
- 200 ft. (61 m) Sideline
- 930 Shaft Horsepower

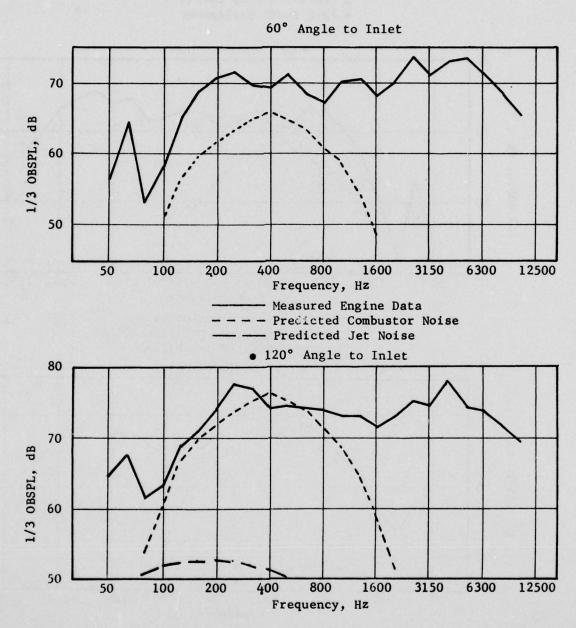


Figure 2.4-7 Comparison of Core Noise Prediction to Measured Engine Data at 930 SHP

- Turboshaft Engine 200 ft. (61 m) Sideline
- 1320 Shaft Horsepower

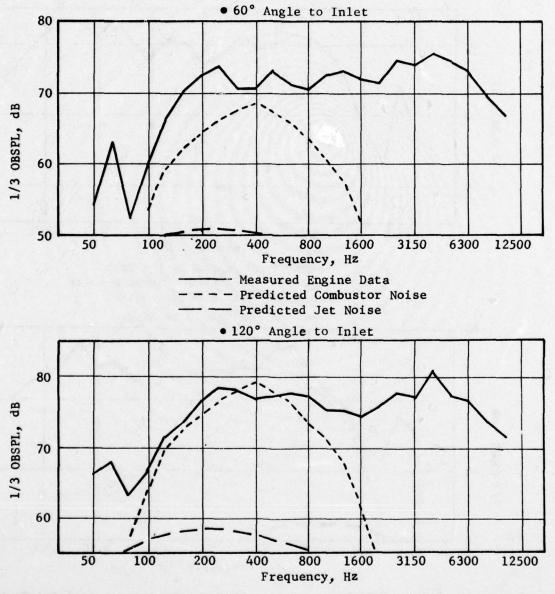
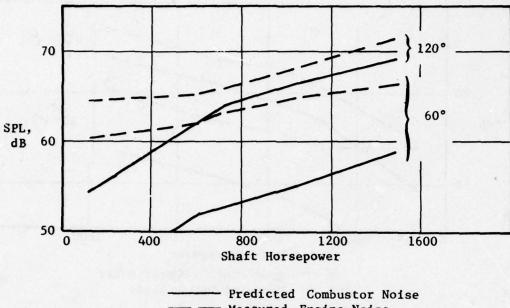
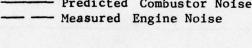


Figure 2.4-8 Comparison of Core Noise Prediction to Measured Engine Data at 1320 SHP

- Turboshaft Engine
- 200 ft. (61 m) Sideline
- 125 Hz





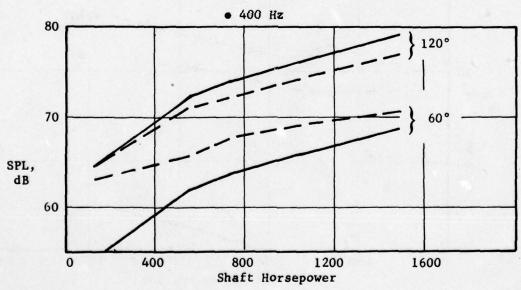
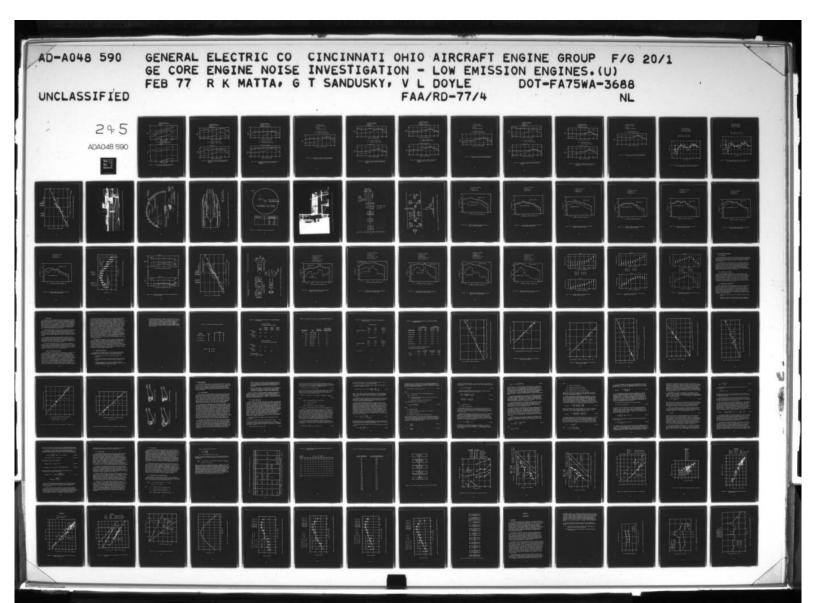


Figure 2.4-9 Variation of Farfield SPL's with Engine Power Setting at 125 and 400 Hz



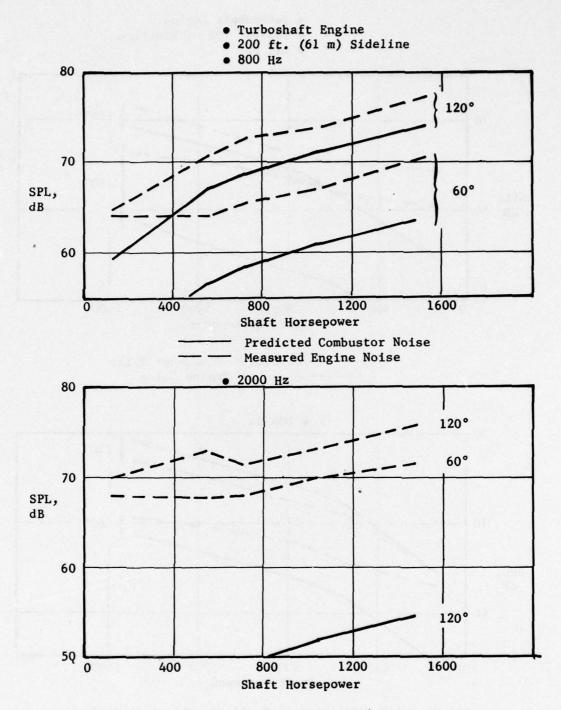
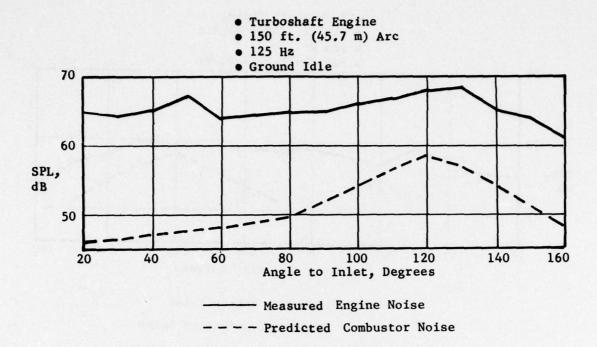


Figure 2.4-10 Variation of Farfield SPL's with Engine Power Setting at 800 and 1200 Hz.



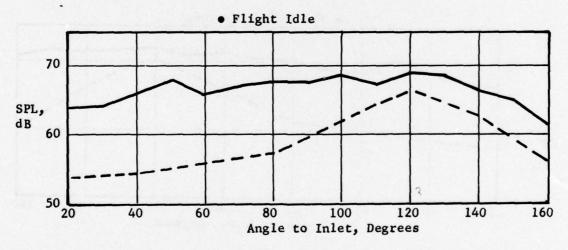
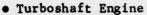
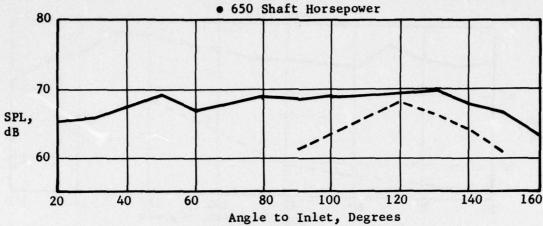


Figure 2.4-11 Predicted vs. Measured 125 Hz SPL Levels for Turboshaft Engine at Ground and Flight Idle Speeds



- 150 ft. (45.7 m) Arc
- 125 Hz



- Measured Engine Noise

- Predicted Combustor Noise

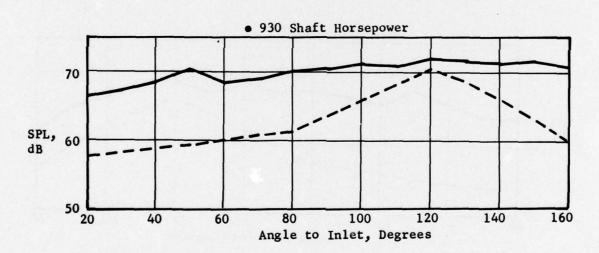
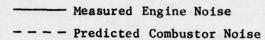


Figure 2.4-12 Predicted vs. Measured 125 Hz SPL Levels for Turboshaft Engine at 650 and 930 Shaft Horsepower

- Turboshaft Engine
- 150 ft. (45.7 m) Arc
- 125 Hz
- 1320 Shaft Horsepower



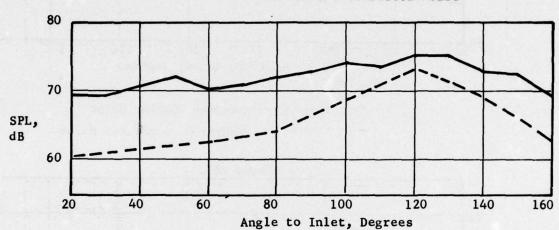
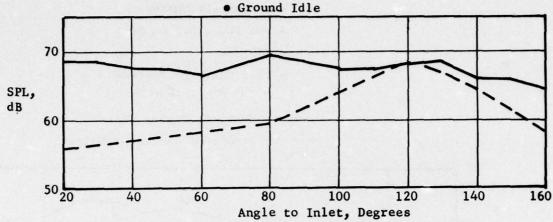


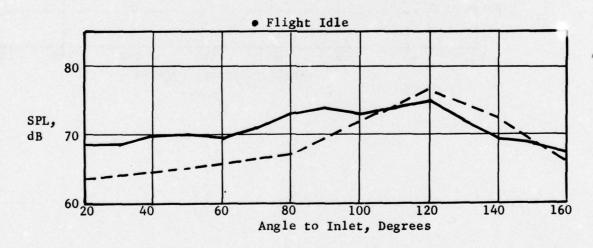
Figure 2.4-13 Predicted vs. Measured 125 Hz SPL Levels for Turboshaft Engine at 1320 Shaft Horsepower

- Turboshaft Engine
- 150 ft. (45.7 m) Arc
- 400 Hz

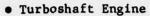


Measured Engine Noise

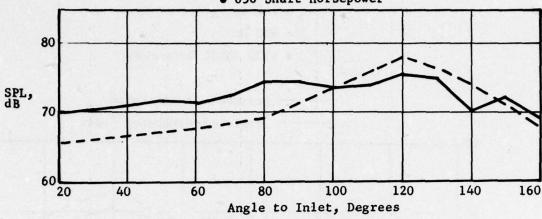
- Predicted Combustor Noise



Predicted vs. Measured 400 Hz SPL Levels for Figure 2.4-14 Turboshaft Engine at Ground and Flight Idle Speeds



- 150 ft. (45.7 m) Arc
- 400 Hz
- 650 Shaft Horsepower



Measured Engine Noise
Predicted Combustor Noise

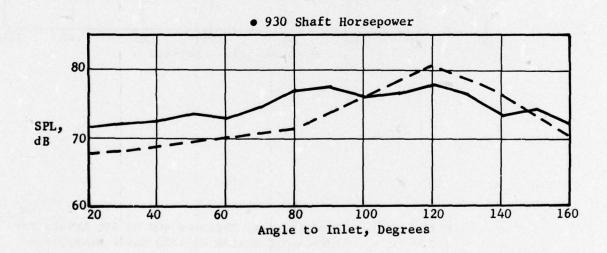


Figure 2.4-15 Predicted vs. Measured 400 Hz SPL Levels for Turboshaft Engine at 650 and 930 Shaft Horsepower

- Turboshaft Engine
- 150 ft. (45.7 m) Arc
- 400 Hz
- 1320 Shaft Horsepower

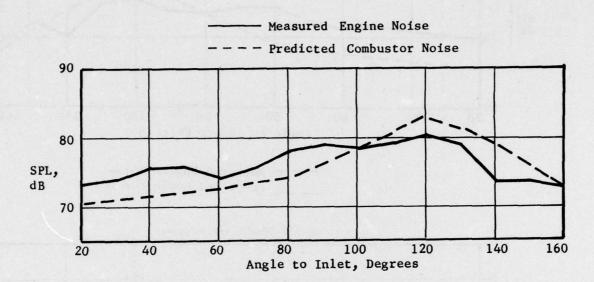
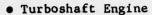
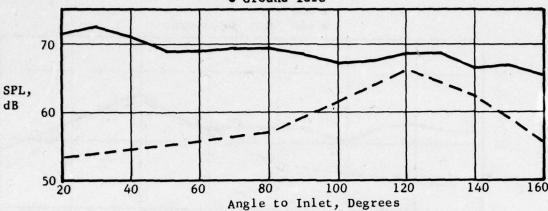


Figure 2.4-16 Predicted vs. Measured 400 Hz SPL Levels for Turboshaft Engine at 1320 Shaft Horsepower



- 150 ft. (45.7 m) Arc
- 630 Hz
- Ground Idle



----- Measured Engine Noise

--- Predicted Combustor Noise

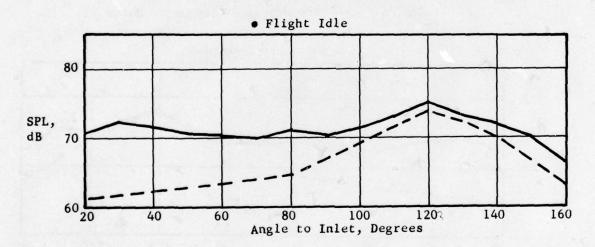
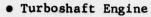
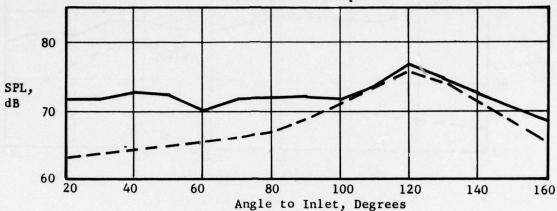


Figure 2.4-17 Predicted vs. Measured 630 Hz SPL Levels for Turboshaft Engine at Ground and Flight Idle Speeds



- 150 ft. (45.7 m) Arc
- 630 Hz
- 650 Shaft Horsepower



Measured Engine Noise

--- Predicted Combustor Noise

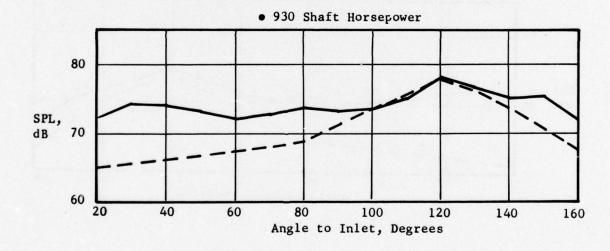


Figure 2.4-18 Predicted vs. Measured 630 Hz SPL Levels for Turboshaft Engine at 650 and 930 Shaft Horsepower

- Turboshaft Engine
- 150 ft. (45.7 m) Arc
- 630 Hz
- 1320 Shaft Horsepower

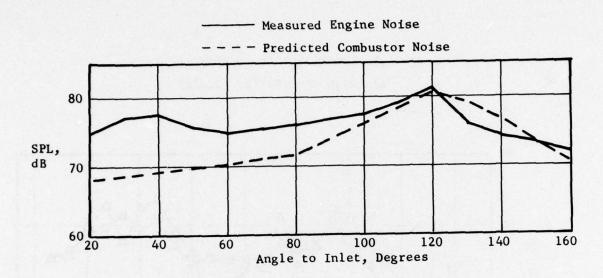


Figure 2.4-19 Predicted vs. Measured 630 Hz SPL Levels for Turboshaft Engine at 1320 Shaft Horsepower

- Turboshaft Engine
- 150 ft. (45.7m) Arc
- 110° Acoustic Angle
- 930 Shaft Horsepower

△- Low Mic, 1 Ft. (.31m)

O- High Mic, 40 Ft. (12.2m)

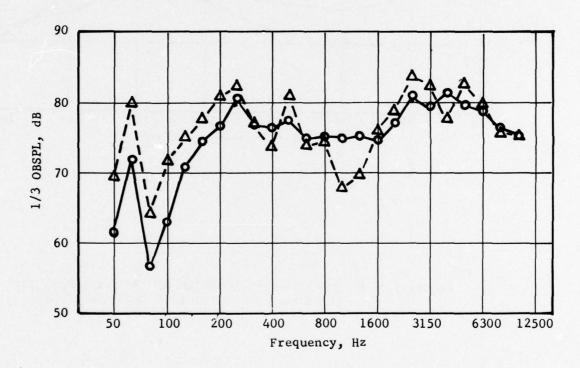


Figure 2.4-20 Low vs. High Microphone Data at 110° Acoustic Angle for Turboshaft Engine at 930 Shaft Horsepower

- Turboshaft Engine
- 150 ft. (45.7m) Arc
- 110° Acoustic Angle
- Ground Idle Speed

△ - Low Mic, 1 Ft. (.31m)

O - High Mic, 40 Ft. (45.7m)

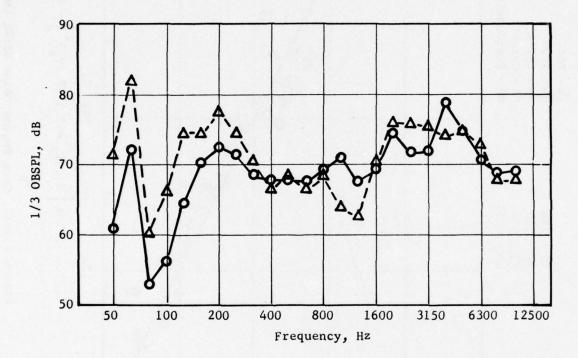


Figure 2.4-21 Low vs. High Microphone Data at 110° Acoustic Angle for Turboshaft Engine at Ground Idle Speed

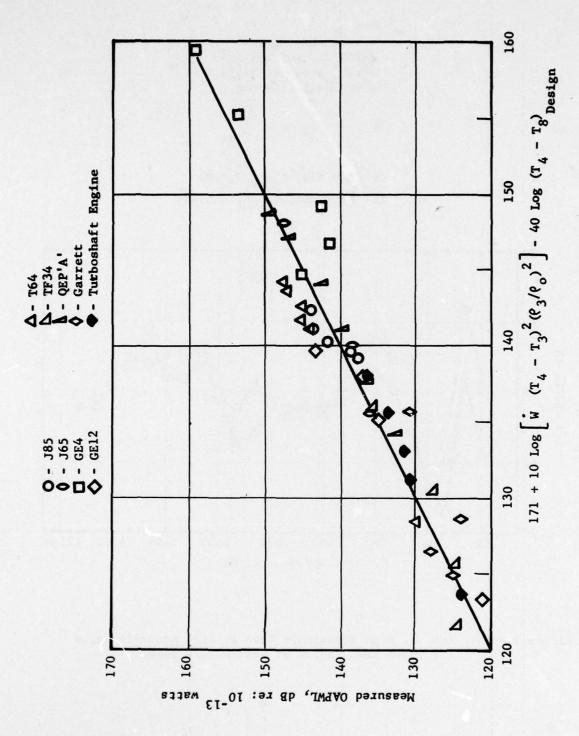


Figure 2.4-22 Core Engine Noise OAPWL Correlation

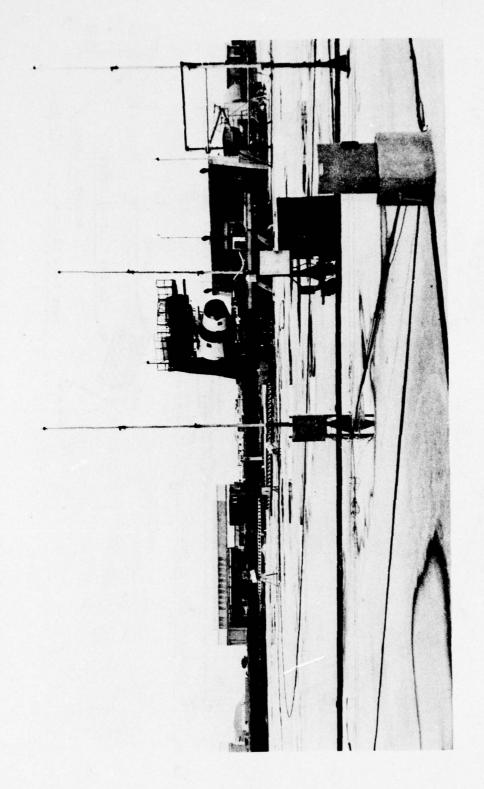


Figure 2.4-23 SNECMA Acoustic Test Site at Istres Showing Farfield Static and Mobile Mics

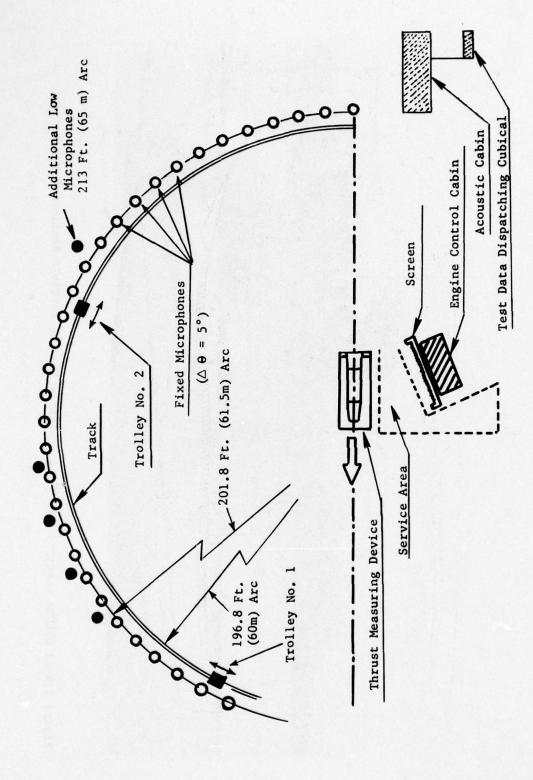
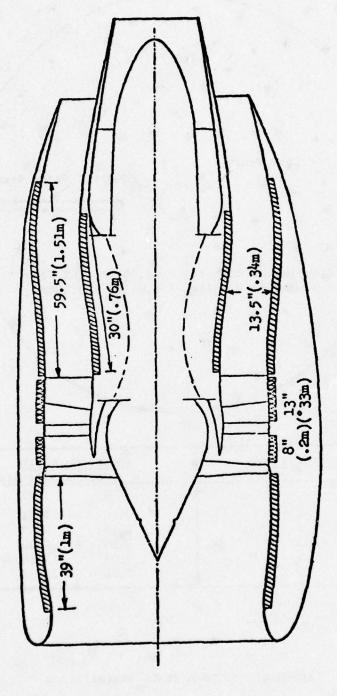
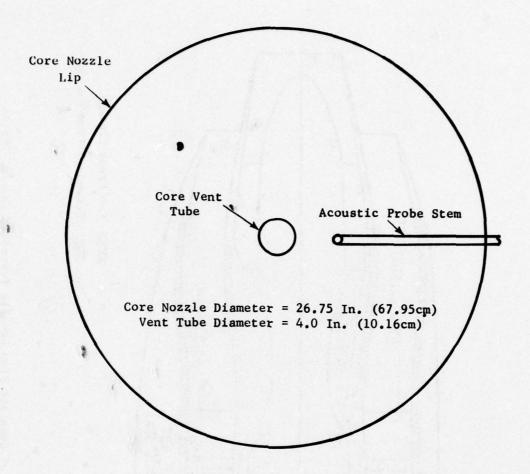


Figure 2.4-24 SNECMA Acoustic Test Site Located at Istres, France



XXXX Fan Frame Linings
77772 Secondary Flow Linings

Schematic of Separate Flow Nacelle Tested at Istres, France Figure 2.4-25



Immersion No.	Immersion Depth Re: Core Nozzle Lip		
	In.	(cm)	
1	0.75	1.91	
2	2.16	5.49	
3	3.86	9.80	
4	5.96	15.14	
5	9.26	23.52	

Figure 2.4-26 Schematic of Core Probe Installation

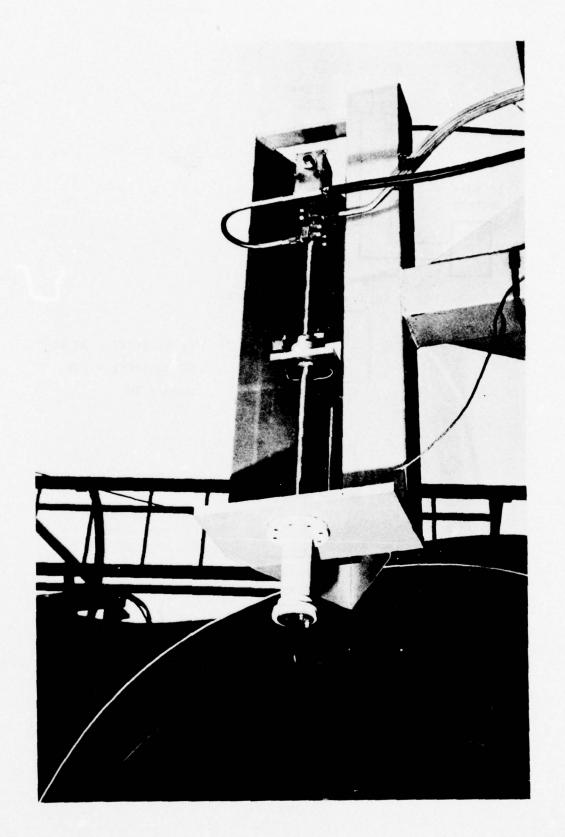


Figure 2.4-27 Sound Separation Probe Mounted on Stand at SNECMA Acoustic Test Facility

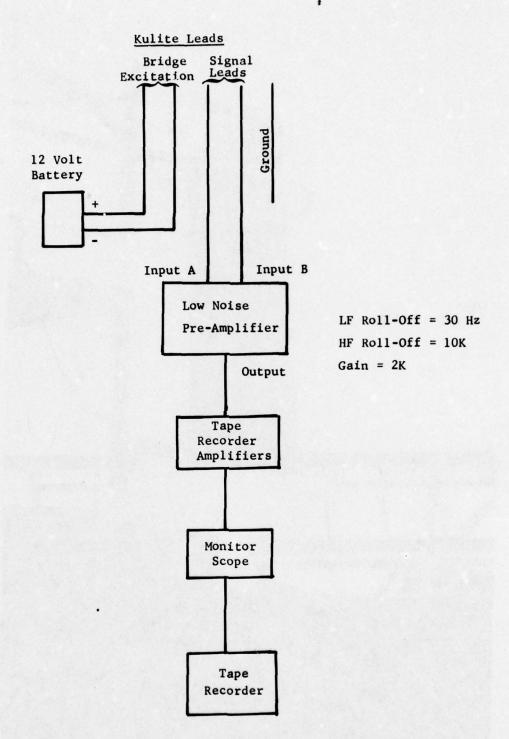
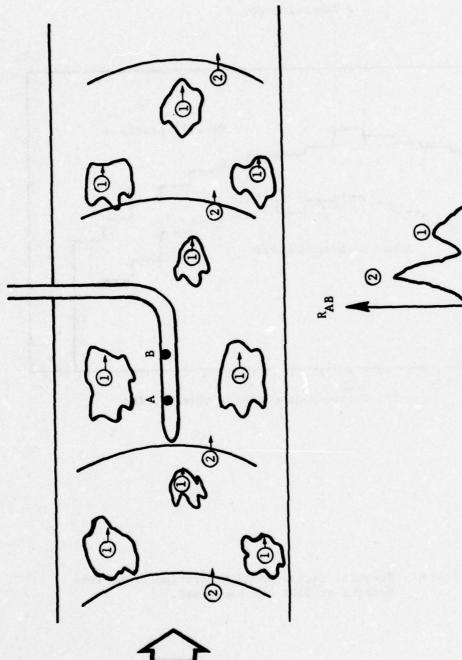
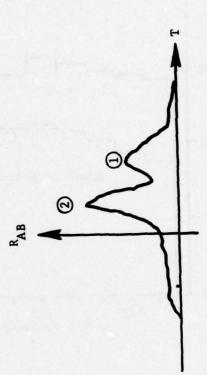


Figure 2.4-28 Instrumentation Schematic for Core Probe Test





Sound Separation Probe Concept Using Cross-Correlation Technique Figure 2.4-29

- Fan Speed = 2674 rpm
- Reading No. 78
- Immersion No. 3

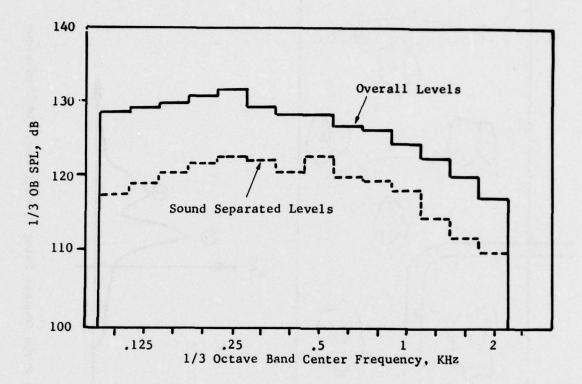


Figure 2.4-30 Turbofan Engine Sound Separation Probe Test. Results at 2674 RPM Fan Speed.

- Fan Speed = 2944 rpm
- Reading No. 77
- Immersion No. 3

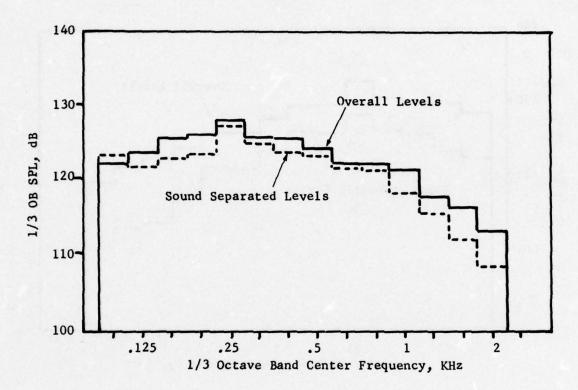


Figure 2.4-31 Turbofan Engine Sound Separation Probe Test Results at 2944 RPM Fan Speed

- Fan Speed = 3246 rpm
- Reading No. 76
- Immersion No. 3

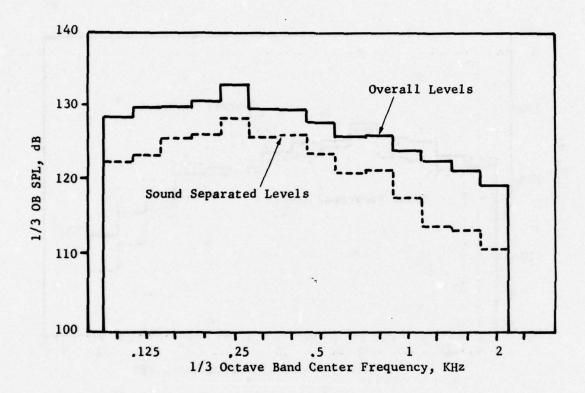


Figure 2.4-32 Turbofan Engine Sound Separation Probe Test Results at 3246 RPM Fan Speed

- Fan Speed = 3744 rpm
- Reading No. 75
- Immersion No. 3

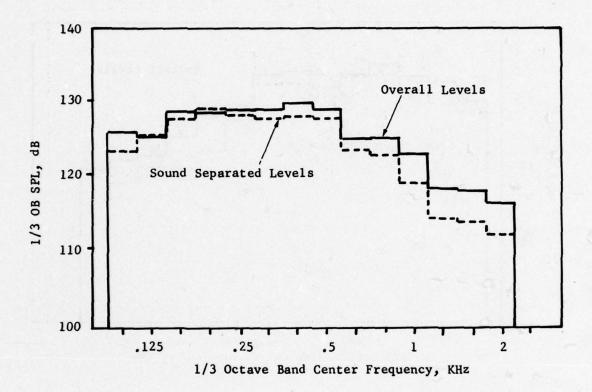


Figure 2.4-33 Turbofan Engine Sound Separation Probe Test Results at 3744 RPM Fan Speed

- Fan Speed = 4122 rpm
- Reading No. 72
- Immersion No. 3

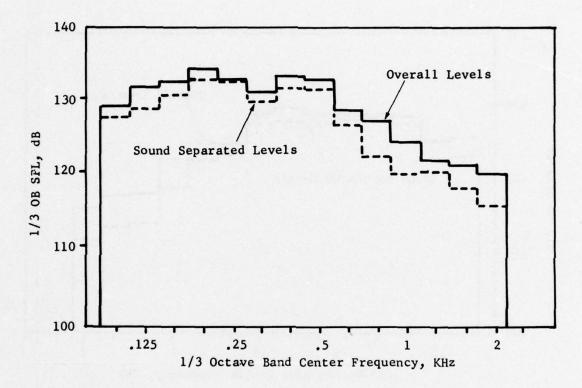


Figure 2.4-34 Turbofan Engine Sound Separation Probe Test Results at 4122 RPM Fan Speed

- Fan Speed = 4406 rpm
- Reading No. 73
- Immersion No. 3

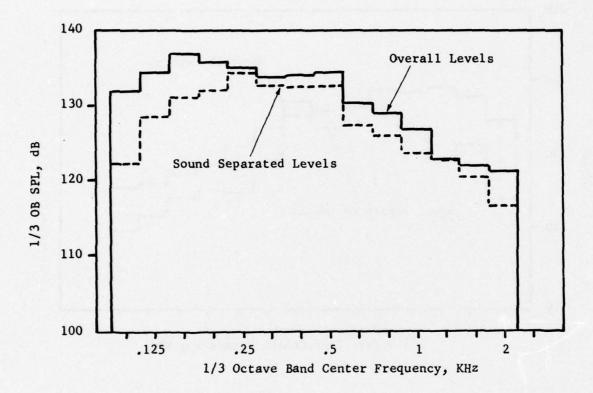


Figure 2.4-35 Turbofan Engine Sound Separation Probe Test Results at 4406 RPM Fan Speed

- Fan Speed = 4648 rpm
- Reading No. 74
- Immersion No. 3

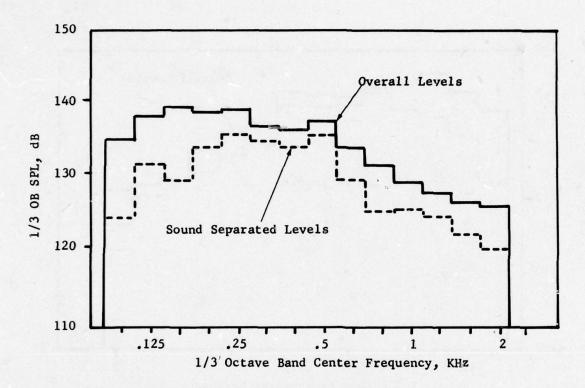


Figure 2.4-36 Turbofan Engine Sound Separation Probe Test Results at 4648 RPM Fan Speed

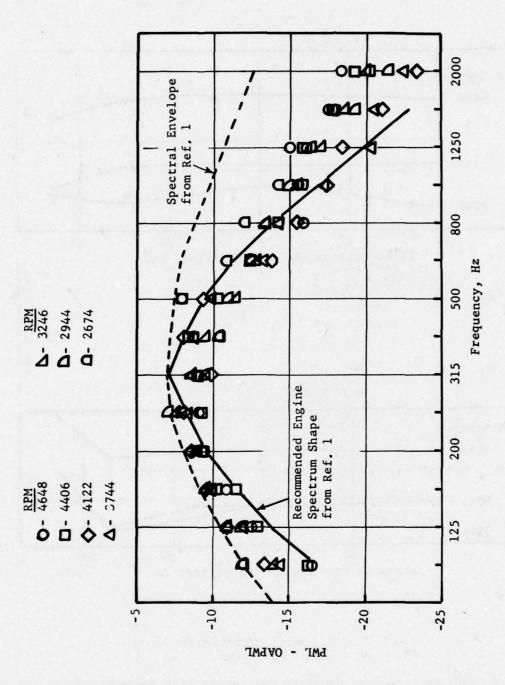


Figure 2.4-37 Turbofan Engine Probe Power Level Spectra

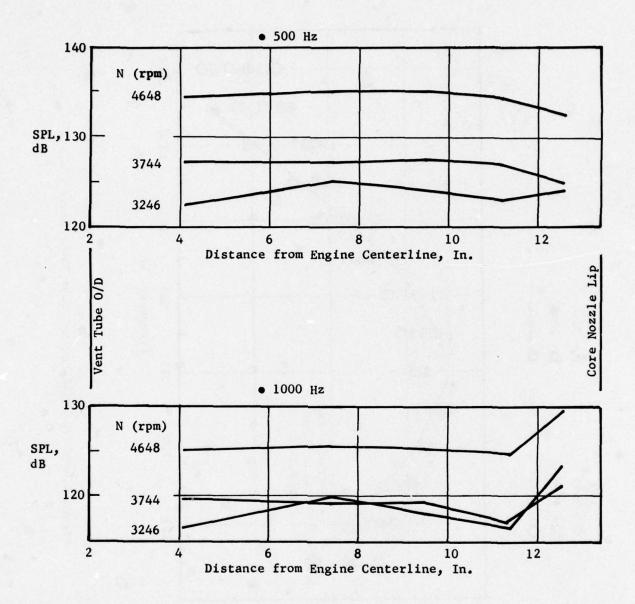


Figure 2.4-38 Variation of Measured SPL Levels with Immersion Depth at 500 and 1000 Hz.

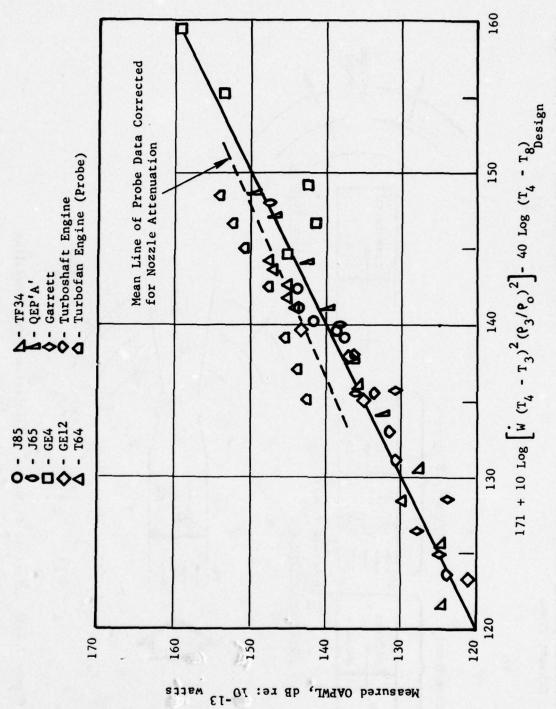


Figure 2.4-39 Core Engine Noise OAPWL Correlation

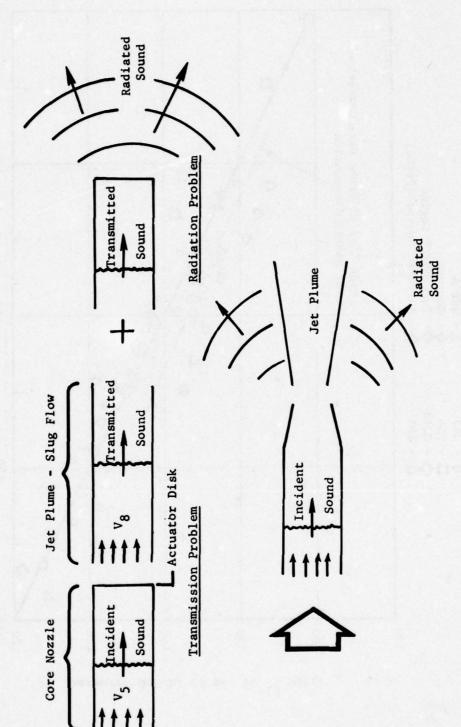


Figure 2.4-40 Schematic of Nozzle Transmission Problem Modeling

- Fan Speed = 4648 rpm
- Reading No. 74
- Immersion No. 3
- Acoustic Angle = 57.5°
- 213 ft. (65 m) Arc

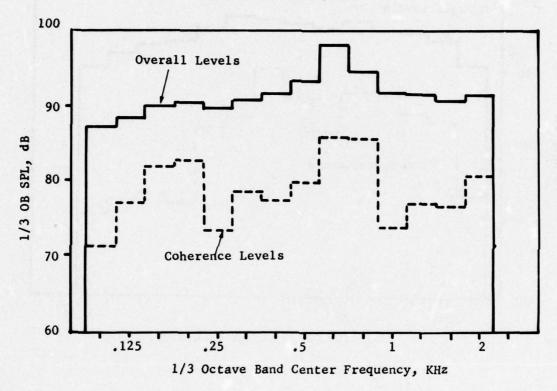


Figure 2.4-41 Turbofan Engine Probe-to-Farfield Coherence Spectra at 57.5° Acoustic Angle

- Fan Speed = 4648 rpm
- Reading No. 74
- Immersion No. 3
- Acoustic Angle = 97.5°
- 213 ft. (65 m) Arc

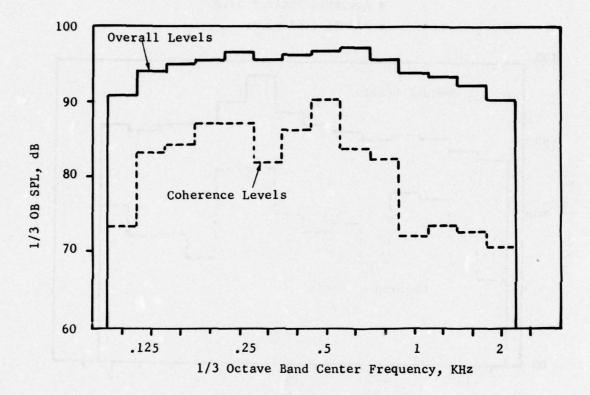


Figure 2.4-42 Turbofan Engine Probe-to-Farfield Coherence Spectra at 97.5° Acoustic Angle

- Fan Speed = 4648 rpm
- Reading No. 74
- Immersion No. 3
- Acoustic Angle = 107.5°
- 213 ft. (65 m) Arc

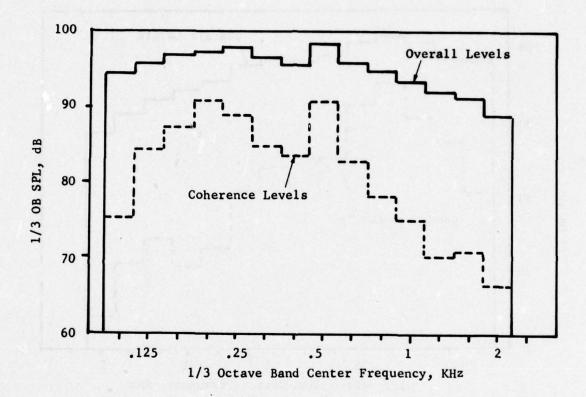


Figure 2.4-43 Turbofan Engine Probe-to-Farfield Coherence Spectra at 107.5° Acoustic Angle

- Fan Speed = 4648 rpm
- Reading No. 74
- Immersion No. 3
- Acoustic Angle = 117.5°
- 213 ft. (65 m) Arc

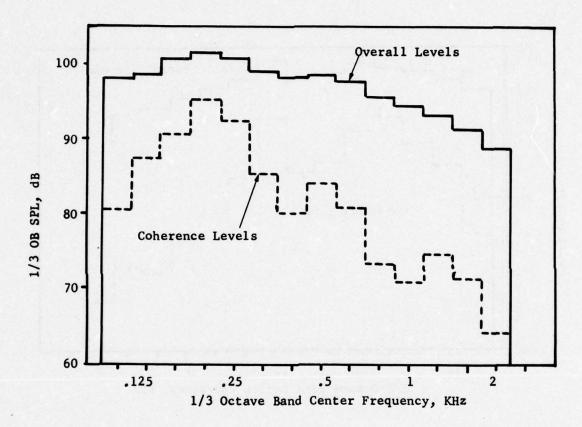


Figure 2.4-44 Turbofan Engine Probe-to-Farfield Coherence Spectra at 117.5° Acoustic Angle

- Fan Speed = 4648 rpm
- Reading No. 74
- Immersion No. 3
- Acoustic Angle = 127.5°
- 213 ft. (65 m) Arc

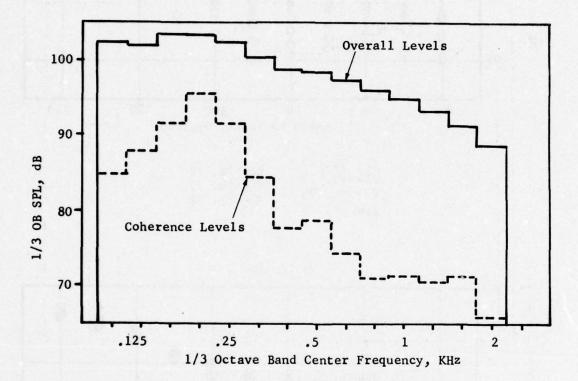
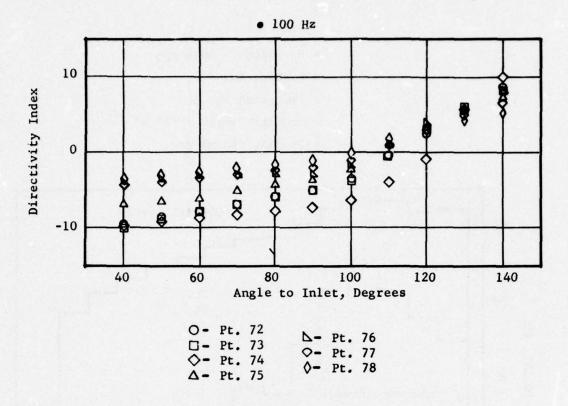


Figure 2.4-45. Turbofan Engine Probe-to-Farfield Coherence Spectra at 127.5° Acoustic Angle



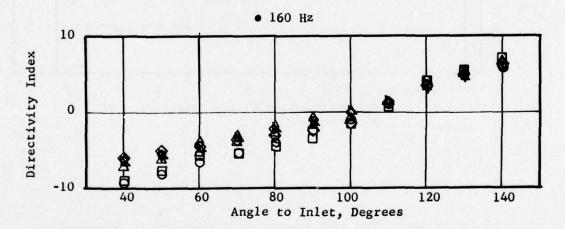
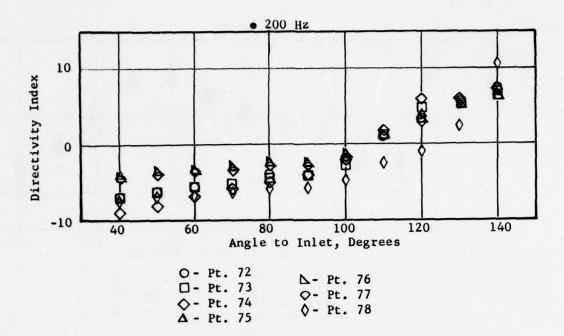


Figure 2.4-46 Turbofan Engine Core Noise Directivity Patterns at 100 and 160 Hz



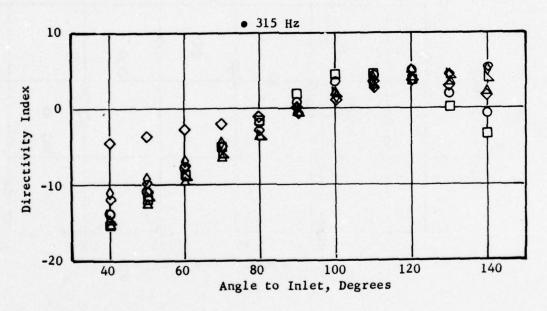


Figure 2.4-47 Turbofan Engine Farfield Core Noise Directivity Patterns at 200 and 315 Hz

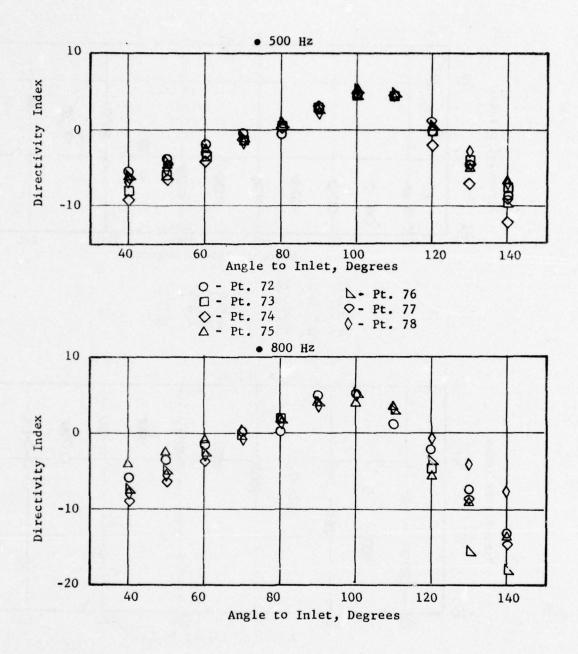


Figure 2.4-48 Turbofan Engine Farfield Core Noise Directivity Patterns at 500 and 800 Hz

2.5 EMISSIONS/NOISE RELATIONSHIPS

2.5.1 Objectives

The objective of this activity was to examine and evaluate emissions and noise data to establish the existence (if any) of emissions and noise relationships and the trade-offs involved. This required correlation of emission indices against performance parameters similar to those used for combustor noise correlation.

The configurations involved included the internal density/parametric tests (Section 2.2), where noise/emissions data were acquired concurrently, and the turboshaft and turbofan engine tests, for which emissions data were available. In addition, the results of the Experimental Clean Combustor Program (References 2.11) were also studied as these included noise and emissions levels for seven advanced low emissions combustor designs plus a standard (baseline) design. The D13 combustor used in the internal density/parametric tests was also included in this group.

2.5.2 Correlations for Emissions

The measured emissions levels of oxides of nitrogen (NO_X) , carbon monoxide (CO) and unburned hydrocarbons (HC) for the D13 double annular combustor used in Task I, corrected to standard (ISA) day takeoff conditions, are shown in Figures 2.5-1 through 2.5-3. Similar curves for turboshaft and turbofan combustors, referenced in Section 2.4, are shown in Figures 2.5-4 through 2.5-8. No emissions data were available for unburned hydrocarbons on the turboshaft engine. Correlations such as these are used to extrapolate measured emissions levels to actual engine operating conditions in compliance with EPA emissions requirements.

2.5.3 Noise/Emissions Comparisons

It has been found that noise and emissions both correlate with similar parameters, namely combustor inlet temperature and pressure, reference velocity and fuel/air ratio or temperature rise. Table 2.5-1 shows the qualitative impact on the various emission indices and noise level as each cycle parameter is varied individually. It would appear that trade-off studies could be conducted by varying each of the cycle parameters individually. These studies would be purely hypothetical since variations are impossible for a fixed engine cycle. For quantification purposes, two other approaches appear more desirable:

- Comparison of noise and emissions for standard and growth engine cycles.
- Evaluation of data from low-emissions and baseline combustors to determine the impact on noise of emissions reduction techniques.

Growth Cycles

Noise and emissions correlations have been derived for the D13 double annular combustor and those combustors used in the turboshaft and turbofan engines referenced in Section 2.4. The emissions correlations are shown in Figures 2.5-1 through 2.5-8. The noise correlation for the D13 combustor is shown in Figure 2.2-14. The turboshaft and turbofan core noise levels were found to correlate with the parameter given in Figure 2.4-22. Utilizing these correlations, noise and emissions levels were calculated for the D13, turboshaft and turbofan combustors for both standard and projected growth cycles applicable to engines on which these combustors are likely to be used. Typical results are shown in Table 2.5-2.

At takeoff power, combustor noise for the D13 is projected to increase 1.3 dB with a corresponding 14.4% increase in NO_X emissions for a 5.8% increase in thrust. At approach, combustor noise increases 1.4 dB with a 9% increase in the NO_X emissions and a 16% decrease in CO emissions. The relatively larger percentage changes seen for the NO_X emissions is attributed to the very high exhaust gas temperatures required to achieve the thrust increase.

The turboshaft and turbofan combustors produced similar results in terms of impact of growth on noise and emissions. At takeoff, both combustors are projected to have a 0.9 dB increase in combustor noise with an accompanying 7% increase in NO $_{\rm X}$ emissions. At approach, the combustor noise increases 0.7 dB with a 5 - 6% increase in NO $_{\rm X}$ emissions and a 8% decrease in CO emissions for a 9% growth in baseline thrust.

On an overall system noise basis, the above increases in combustor noise will result in negligible increases in flight noise levels at takeoff and approach for all three study engines since other noise sources, such as jet and/or turbomachinery, dominate the overall system noise. The increases in emissions levels at takeoff appear to be much more significant than the increase in combustor noise on an overall systems basis.

Impact of Low Emissions Techniques

A second approach to the problem of noise/emissions relationships is to consider the impact on noise of emission reduction techniques used in advanced combustors. Both emissions and noise measurements were taken on seven low emission configurations, including the D13 double annular combustor, and a standard production combustor under the Experimental Clean Combustor Program (References 2, 3, 4, 11). The major variations are shown in Figure 2.5-9 and detailed in Table 2.5-3. A comparison of the noise and emissions levels for the standard and D13 combustors is given in Table 2.5-4. The D13 low emissions combustor produced sigificant reductions in $NO_{\rm X}$ emissions at takeoff and approach power. This was found to be true for a range of ΔT 's set for the combustor. However, the noise increased at takeoff power relative to the standard CF6-50 production combustor. This increase in noise would not be predicted by the method outlined in Reference

10, since only gross cycle parameters are used, and these parameters would be the same for both combustors. A review of the D13 design indicates that the flow through the primary combustion zone was increased from 32% to 67% of the total core flow relative to the baseline. Therefore, the local velocity inside the combustor dome was considerably higher for the D13. This may explain why the D13 produced higher noise levels at takeoff inlet conditions. Using the current component correlation (see Figure 2.2-14) of V3.5, a 100% increase in local velocity would cause a 10.5 dB increase in noise. However, since the burn is somewhat leaner, the peak temperature produced is lower, and this would tend to produce lower noise levels. The net effect is that the D13 is approximately 5 dB higher than the baseline at the "take-off" inlet conditions. At approach inlet conditions, the noise levels from the two combustors are nearly equal. Since the air flow ratios (Wdome/Wtotal) were not available at this off-design condition, no assessment of the velocity effect could be made. Noise/emissions results from other combustors (References 4 and 11) are shown in Table 2.5-5. These data tend to support the D13 and CF6-50 comparison results. Table 2.5-5 indicates no definite trend between noise and emissions as a function of specific combustor design. However, the low emissions designs, in general, tended to have higher noise levels at takeoff inlet conditions than the baseline combustor. It is interesting to note that I-12 had virtually the same emission and noise levels as the CF6-50 combustor.

As evidenced by the results of the D13 and other low emissions combustor tests, the technique of increasing combustor dome flow, thus producing a lean burn condition resulting in lower peak temperatures and reaction time, to reduce NO_{X} emissions may result in an increase in combustor noise. It is believed that the critical parameter is the condition of the reactants in the primary combustion zone. The percentage of flow through the dome or the reference velocity is not always a reliable indicator of this, as is evidenced by the swirl-can combustors where a very large part of the dome air could sweep past the primary zone along the outer periphery. In contrast, all the D13 dome air is forced through the primary zone.

2.5.4 Summary and Conclusions

The combustor noise/emissions study produced no general quantitative relationship between noise and emissions. It was found, however, that for the combustors studied, several important trends could be identified:

- Emissions and noise can be correlated using the same cycle parameters.
- The advanced low emissions combustors studied indicate that those with the lowest emission levels also produced the highest noise level.
- For <u>typical engine</u> cycles, the change in combustor noise is relatively insignificant compared to the change in emission levels, and the impact on total system noise is minor.

4. For low emissions combustors studied, a decrease in NO_X levels at takeoff was accompanied by an increase in combustor noise. Although no conclusive data is available, it is believed that the noise increase was due to the higher flow rate through the primary combustion zone relative to the standard (base line) combustor. Hence, the emissions reduction technique of lean-burn-combustors, by increasing the local velocity through the primary combustion zone, (i.e., increased dome weight flow) is a potential cause of increased combustor noise.

Table 2.5-1 Combustor Noise/Emissions Trade-off

			Emissions	
Parameter	Noise	NOx	нс	СО
Reference Velocity	+	1	1	1
Inlet Pressure	†	1	+	+
Inlet Temperature		1	+	1

Symbols: Increase
Decrease

Table 2.5-2 Noise/Emissions Relationships for Turbofan/Turboshaft Growth Cycles

- Current Combustor
- 9% Increase in Baseline Thrust

	△PNL ⁽¹⁾	% Change in EI _{NO_x}	% Change in EI _{CO}	% Change in EI _{HC}
Takeoff				
Baseline	•		*	*
Growth	+0.9	+7.2	*	*
Approach				
Baseline	•	-	•	*
Growth	+0.7	+5.6	-7.8	*

- Advanced Combustor
- 5.8% Increase in Baseline Thrust

Takeoff				
Baseline	-	•	*	*
Growth	+1.3	+14.4	*	*
Approach				
Baseline	•	•	•	*
Growth	+1.4	+9.4	-16.0	*

^{*} Values Negligible

(1) 200 Ft. Sideline Reference

Table 2.5-3 Tabulation of Advanced Technology Combustor Configurations

Configu	uration	Туре	Number of Fuel Nozzles	% Core Weight Flow Thru Primary Combustion Zone
ØII	D13	Double Annular	60	67
	CF6-50	Single Annular	30	32
ØI	11-11	Double Annular	60	73
	11-12	Radial/Axial	90	82
	1-12	Swirl Can	90	76
	1-14	Swirl Can	90	82
	111-1	Swirl Can	60	85 .
	I-16	Swirl Can	72	85

Table 2.5-4 Noise/Emissions Relationships for Standard and D13 Combustor Designs

	EINOx	EIco	QAPWL, dB
Standard Combustor	35.5	0.5	155.0
D13	16.8	0.5	160.0

• Takeoff Power (1)

• Approach Power (1)

	EINOx	EIco	OAPWL, dB
Standard Combustor	10.4	1.6	155.5
D13	8.8	1.8	154.5

(1) Reference 4

(

Table 2.5-5 Noise/Emissions Relationships for Advanced Technology Combustor Designs

	Take	eoff	Approach			
Combustor Type	(1) OAPWL, dB	EI _{NO_x}	(1) OAPWL, dB	EI _{NO_x}		
Double Annular	155.3	7.2	150.4	6.9		
Double Annular	154.6	8.9	148.7	•		
Radial/Axial	156.8	8.6	150.2	6.4		
Swirl Can	155.5	11.6	148.5	1.0		
Swirl Can	150.8	13.0	149.3	4.7		
Single Annular	150.4	14.2	149.2	6.2		

⁽¹⁾ As Measured in Component Combustor Rig Test

⁽²⁾ Corrected to Following Conditions:

	T ₃ , ° R	P ₃ , PSIA	W ₃ , 1b./sec.	W _f /W _a
Takeoff	1477	70.0	36.3	.0231
Approach	1134	50.0	30.5	.0140

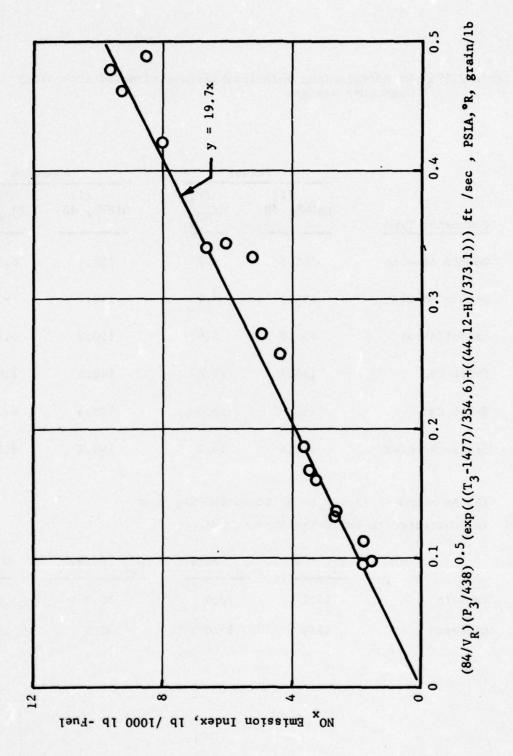


Figure 2.5-1 Effect of Inlet Conditions on $NO_{\mathbf{x}}$ Emissions, Double Annular Combustor

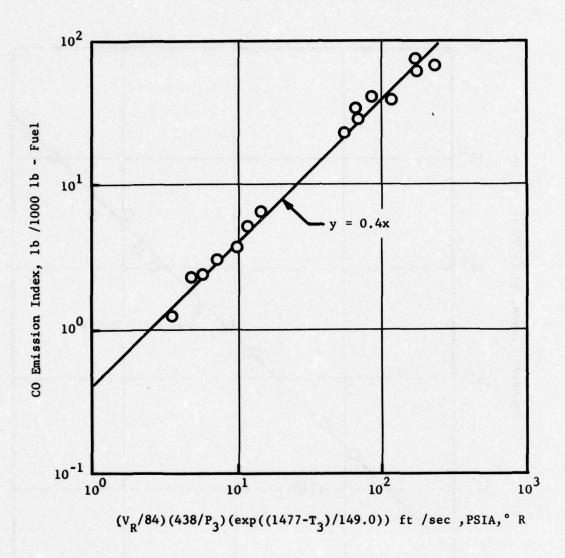


Figure 2.5-2 Effect of Inlet Conditions on CO Emissions, Double Annular Combustor

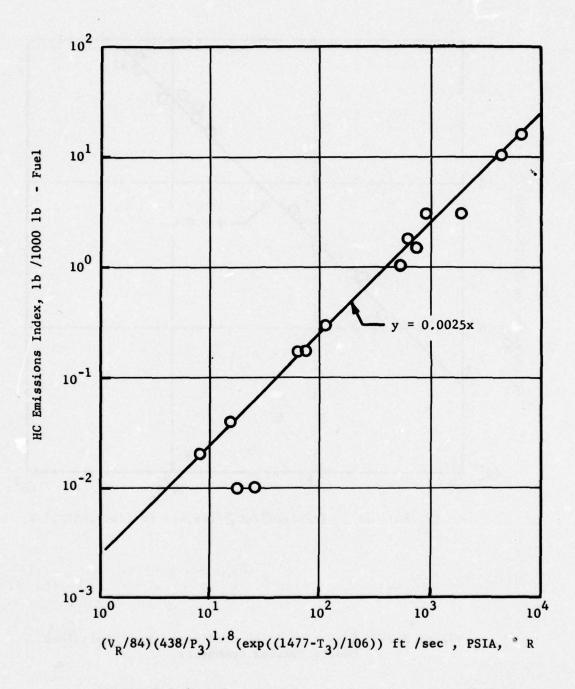


Figure 2.5-3 Effect of Inlet Conditions on HC Emissions, Double Annular Combustor

Figure 2.5-4 Effect of Inlet Conditions on $N_{\rm X}$ Emissions, Turbofan Engine

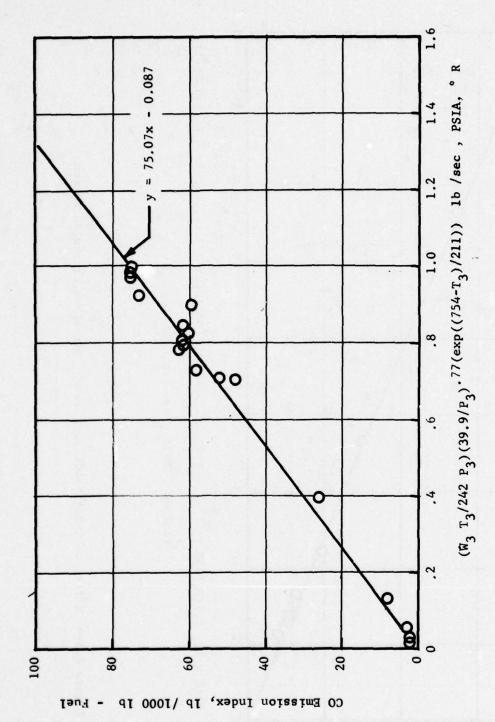
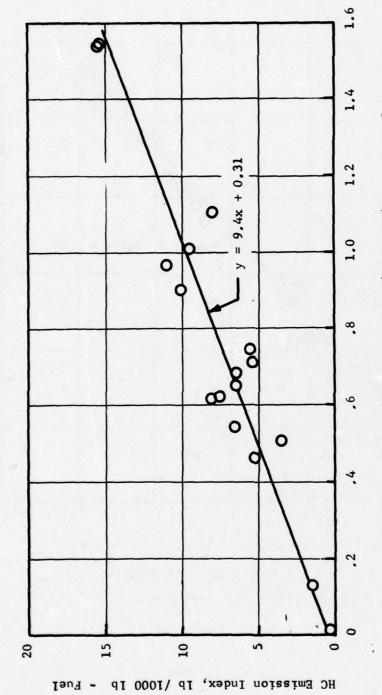


Figure 2,5-5 Effect of Inlet Conditions on CO Emissions, Turbofan Engine



 $(\mathfrak{M}_3 \ \text{T}_3/242 \ \text{P}_3)(39.9/\text{P}_3)(\exp((754-\text{T}_3)/85))$ lb /sec , PSIA, ° R

Figure 2.5-6 Effect of Inlet Conditions on HC Emissions, Turbofan Engine

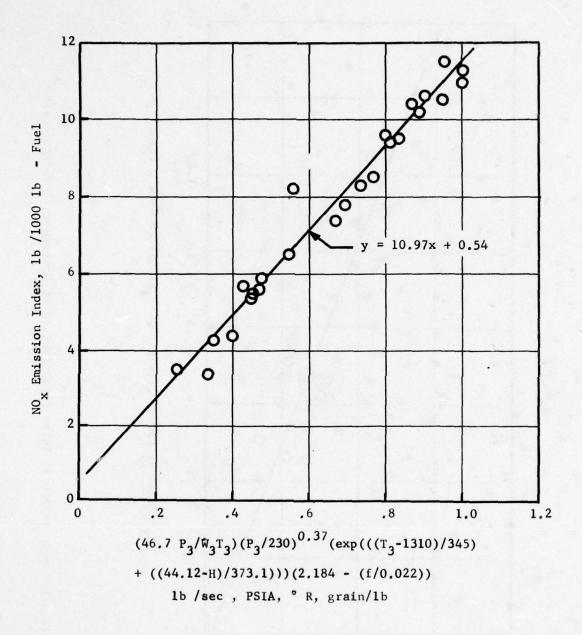


Figure 2.5-7 Effect of Inlet Conditions on $NO_{\mathbf{x}}$ Emission, Turboshaft Engine

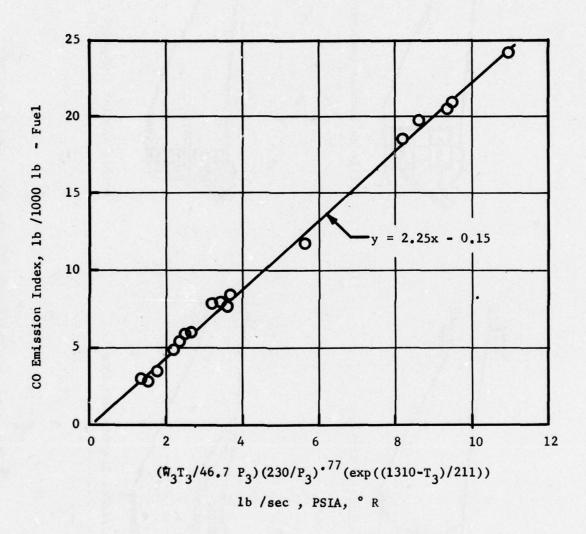


Figure 2.5-8 Effect of Inlet Conditions on CO Emissions, Turboshaft Engine

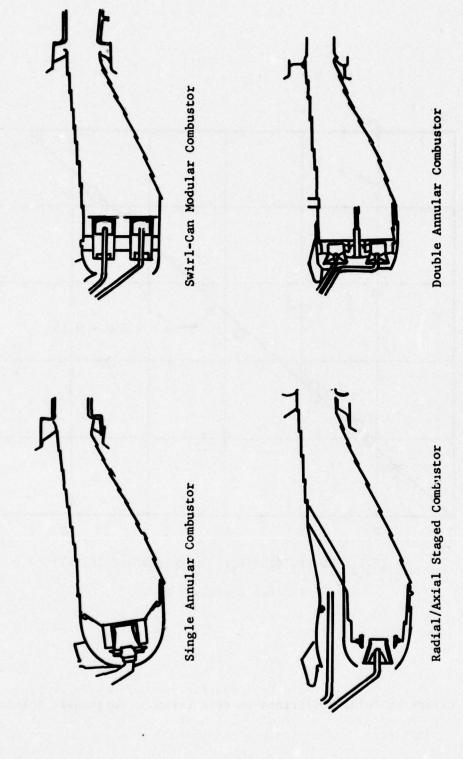


Figure 2.5-9 Schematics of Advanced Technology Combustors

2.6 PREDICTION UPDATE

The prediction update phase of this program brings together the salient results of each of the four tests discussed in Section 2.2-2.5. The objective here is to modify the core noise prediction technique, defined in Reference 10, consistent with the findings of this program and those available through open literature. Consequently, where quantitative results are available, they are evaluated and, where appropriate, incorporated into the core noise prediction technique.

2.6.1 Current Status

During the past few years, considerable work has been done, both experimental and analytical, in the area of core engine noise, specifically combustor noise. This volume of work has led to various prediction methods. Some of these are given in Table 2.6-1 (Reference 12). In addition, much work has been done in the analytical area by Strahle (Reference 13), Plett, et. al., (References 14,15), Hassan (Reference 16) and others. A large part of this work has been confined to combustion noise of open flames, but can combustor noise results are also reported. A recent paper by Mathews and Rekos (Reference 17) attempts to tie a refinement of Strahle's model to component and engine data as part of an FAA contract (FA75WA-3663).

The General Electric company undertook a detailed investigation of core engine noise under Contract FA72WA-3023. This program was completed in 1974 and added considerably to the understanding of core engine noise, including low frequency combustor noise. One major result of the combustor noise work done under this program was a simple, easy to use prediction technique for combustor noise from engines (Reference 10). The OAPWL is predicted using a semi-empirical correlation which initially yielded three separate lines for data from the three different engine types - turboshaft, turbojet and turbofan. However, when proper cognizance was accorded to the transmission loss through the turbine blade rows, the three lines were found to collapse into a unified line prediction (Reference 18). To complete the prediction, engine data were used to derive an empirical directivity and spectrum shape. This prediction technique has been substantiated by additional data, including those from a Garrett turboshaft (TPE 331-201), a Pratt and Whitney low bypass turbofan (JT8D-109 refan), and from several unidentified low and high bypass turbofan engines tested by The Boeing Company (Reference 18).

The problem with combustor noise prediction is the multitude of interacting elements involved (see Figure 2.6-1). After the noise is generated in the vicinity of the combustor, it must propagate through turbine blade rows, the terminating nozzle, and one or two jet streams before radiating to the farfield. Initially, only the first element was recognized and, not surprisingly, correlating lines varied from manufacturer to manufacturer and from engine to engine. As the different elements were properly added to the analysis, the varied correlations came closer together. The approach at General Electric has been to attack the problem simultaneously from two directions:

- Outside, looking in farfield data were analyzed and correlated into a prediction method - the unified line engine prediction. The various elements were recognized and included in the correlation parameters, but the extent of each was not separately identified.
- Inside, transmitting out the source levels at the combustor must be known, and the effect of turbine blade row and core nozzle transmission and propagation through the jet stream(s) imposed separately and sequentially to finally obtain farfield levels.

The first, "black box", approach provided a convenient but accurate systems tool. However, the second, "micro" or component investigation, is obviously necessary in order to define the impact of internal aero/mechanical configuration variations not recognized by the engine prediction method such as might be encountered for advanced, low emissions combustors, multi-element jet suppressors, etc.

2.6.2 Overall Power Levels

There exists two mechanisms through which the combustor can cause noise generation: directly due to the volumetric and pressure fluctuations associated with the combustion process, and indirectly due to the convection of turbulence and temperature non-uniformities inherent in the combustor through the large pressure gradients imposed by downstream turbine blade rows. The latter, also known as entropy noise, has been researched analytically and experimentally by several investigators (for example, References 19 and 20) and has failed to indicate generation of sufficient acoustically significant perturbations. In fact, study of this mechanism under Contract FA75WA-3663 (to Pratt and Whitney Aircraft) was curtailed when measurements yielded perturbations less than previously estimated. Some other investigations of entropy noise, however, are still underway using NASA funding (Contract NSG 3015). This program concentrated on direct combustor noise as the more viable mechanism of the two. Note that all the prediction methods shown in Table 2.6-1 result from consideration of the combustion process as the primary acoustic source.

Motsinger (Reference 21) argued that the noise generated could be represented as:

Acoustic Power = Thermal Power Input × Thermo-Acoustic Efficiency (2.6-1)

The thermal power input is given by heat release rate, \hat{Q} , while Knott (Reference 29) had shown that the thermoacoustic efficiency for atmospheric, non-premixed, turbulent combustion is directly proportional to the temperature rise, ΔT . Hence,

Acoustic Power = \dot{Q} $\Delta T = \dot{W} (T_4 - T_3)^2$ (2.6-2)

where \dot{W} is the air mass flow rate, T₃ is the inlet temperature and T₄ the exhaust temperature. Further, through consideration of engine data, Motsinger allowed that the effect of combustion at higher than atmospheric pressures and temperatures could be accounted by a (density)² term:

Acoustic Power
$$\propto \dot{W} (T_4 - T_3)^2 (\rho_3/\rho_0)^2$$
 (2.6-3)

where the subscripts o and 3 refer to ambient and combustor inlet conditions, respectively. This analysis was developed further under Contract FA72WA-3023 and culminated in the unified line correlation which included an allowance for the turbine attenuation factor:

OAPWL = 10
$$\log_{10} \left[\dot{w} \left(T_4 - T_3 \right)^2 \left(\rho_3 / \rho_0 \right)^2 \right] - 40 \log_{10} \left[T_4 - T_5 \right]_{\text{design}}$$
(2.6-4)

where:

OAPWL - acoustic power level, dB re 10-13 watt

W - air flow rate, 1b/sec.

T() - temperature, ° R

 (ρ_3/ρ_0) - density ratio, combustor inlet/ambient

[$(T_4 - T_5)_{\text{Design}}$] - temperaturé drop across the turbines at <u>design</u> point, ° R

The (T₄ - T₅) term representing the work extraction by the turbines was an outcome of a parametric exercise by Matta (Reference 23) of Bekofske's analysis for low frequency noise transmission through turbine blade rows. It must be emphasized, however, that the 40 log (T₄ - T₅) cannot be separated out and used as a predictor of the turbine attenuation. Since it combines all four elements shown in Figure 2.6-1, Equation (2.6-4) must be used as a whole. When this is done, it not only provides good agreement for GE data, but also for Garrett, Pratt and Whitney, and Boeing data (Reference 18). Further, recent work on a combustor noise prediction with the SAE A21 Jet Noise Subcommittee has revealed good agreement with Rolls Royce (turbofans, including RB211, and turboshaft) and Allison (turboshaft) data.

The parameter, developed by Motsinger, is similar to those arrived at independently by Ho and Tedrick (Reference 24) and Grande (Reference 9). Ho and Tedrick used dimensional analysis and atmospheric component (can) data to arrive at:

Acoustic Power
$$\sim \frac{P_4}{T_4} V_4 D_c (T_4 - T_3)^2 (1 + f)^2$$
 (2.6-5)

This corresponds closely to (2.6-2) since the fuel/air ratio f << 1 and P4 V4/T4 $D_C \sim \dot{W}/D_C$, where D_C is the combustor height.

Grande exploited the analysis of Arnold (Reference 25) and assumed stoichiometric combustion to obtain:

Acoustic Power
$$\sim W (T_4 - T_3)^2 (1+f) \left(\frac{L}{D_c}\right) \frac{\sqrt{T_4/T_0}}{T_0^2} \frac{1}{P_4^{3m}}$$
 (2.6-6)

where L is the combustor length and the exponent m is a small <u>fractional</u> number. The length to height ratio does not appear to vary significantly from combustor to combustor, and the main variables, once again, are W, $(T_4 - T_3)^2$.

Hence, there exists considerable justification for the unified line engine prediction method developed under Contract FA72WA-3023. Therefore, we proceed to the component prediction method, where the source noise and attenuation terms are considered separately.

There are two theories which attempt to construct the source noise generation through consideration of actual processes occurring. Both use conservation laws to form inhomogenous wave equations in which the fluctuating reaction rates due to a turbulent flame provide the forcing term. The theory of Chiu and Summerfield (see for example, Reference 15) is exact in retaining all the processes occurring. The theory and solution of Strahle (Reference 5) provides a considerable simplification by assumption of a velocity source as the prime contributor — thereby eliminating the pressure or explosive fluctuations from consideration — and by ignoring the space derivatives or convection terms. The Strahle theory yields the result that the acoustic perturbation is given by the volume integral of the time derivative of the heat release rate at retarded time, the integration being over the reacting volume $V_{\rm O}$:

$$p'(r,t) \sim \frac{\gamma - 1}{4\pi r^2 C_0^2} \int_{V_0} \frac{\partial \dot{Q}}{\partial t} dV \qquad (2.6-7)$$

The first term of the Chiu and Summerfield theory is similar except that it also includes the effect of propagation through the temperature differentials between the reaction zone and the surrounding fluid.

The volume integral of equation (2.6-7) can be converted into a surface integral:

$$p'(r,t) = \frac{\rho_0}{4\pi r} \int_{A_0} \frac{\partial \vec{u}}{\partial t} \cdot \hat{n} d\sigma \qquad (2.6-8)$$

The integrals cannot be evaluated because of insufficient knowledge of the turbulence structure in the reaction zone. However, scaling laws can be derived and Strahle and Shivshankara (Reference 13) suggest that the acoustic power for a combustor can is given by:

Acoustic Power,
$$P \sim A_{corr}$$
, $A_{can} < U_n^2 > \omega_c^2$ (2.6-9)

where

Acorr. - correlating area (for the fluctuating quantities)

Acan - can exit area

<U_n²> - velocity fluctuations, normal to the flame surface, due to differential heating

 $\omega_{\rm c}$ - characteristic frequency of the fluctuations

After some simplification, the authors arrive at:

$$P \sim A_{can} V_3^4 f^{2a} \left(\frac{H}{C_D T_3}\right)^2$$
 (2.6-10)

where

V3 - incoming velocity

a - constant varying from 0 (lean burn) to 1 (rich burn)

H - heating value of fuel

Cp - coefficient of specific heat at constant pressure

The fact that the exponent on the fuel term can vary has been independently verified by General Electric (see Figure 2.6-2, reproduced from Reference 3). One of the assumptions used by the authors is to define the characteristic frequency through dimensional analysis as a function of the incoming velocity, V₃, and the liner hole size, A_h,

$$\omega_{\rm c} \propto \frac{V_3}{\sqrt{A_{\rm corr.}}}$$
 (2.6-11a)

or

$$\omega_{\rm c} \propto \frac{V_3}{\sqrt{A_{\rm h} \, \text{Re}}}$$
 (2.6-11b)

where Re is the Reynolds number. If, on the other hand, it can be seen ω_{C} is invarient with flow, as has been observed on occasion, then equation (2.6-10) will reduce to

$$P \sim A_{can} V_3^2 f^{2a} \left(\frac{H}{C_p T_3}\right)^2$$
 (2.6-12)

Mathews and Rekos (Reference 17) have provided a somewhat different treatment of Strahle's basic equation to arrive at:

$$P \sim \frac{A_b^2}{N_f} P_3^2 \left(\frac{W_a^{\sqrt{T_3}}}{P_3^{A_b}}\right)^4 f^2 \left(\frac{H}{C_p T_3}\right)^2$$
 (2.6-13a)

$$\sim \frac{A_b^2}{N_f} \left(\frac{P_3}{T_3}\right)^2 V_3^4 f^2 \left(\frac{H}{C_p T_3}\right)^2$$
 (2.6-13b)

where

Ab - total burner area

Nf - number of fuel nozzles

Equations (2.6-10) and (2.6-13) are similar, since they both start with Strahle's basic formulation and use similar assumptions to derive the scaling laws. The big differences are the inverse dependency on the number of fuel nozzles used in the combustor, the area to the second power, and the inlet density terms.

The authors of Reference 17 combine equation (2.6-13) with a transmission loss model to obtain an OAPWL prediction method for both component and engine data. The transmission loss mechanisms considered are a combustor/duct coupling and the propagation through the turbines. The former is the ratio of the area over which the combustor noise pressure fluctuations are correlated at the combustor turbine interface to the total area. The authors suggest that 0.2 is a good value and hence

$$TL_{d} = 10 \log \frac{A_{corr}}{A_{exit}} = 7 dB$$
 (2.6-14)

The turbine loss is modeled by representing the turbines as a surface of discontinuity in characteristic impedance, ρc . Assuming a plane wave, the loss is obtained as a function of the ratio, F, of the upstream ρc to the turbine exhaust ρc :

$$TL_{turb} = 10 \log \left(\frac{(1+F)^2}{4F} \right) dB$$
 (2.6-15)

The model ignores the flow and the blade turning which, it is believed, is a serious omission. For typical engines, this relationship predicts turbine losses of 1 to 5 dB. This is <u>much</u> smaller than actually measured for turbines under NASA Contract NAS3-19435. Also, comparison of CF6 component and engine power levels indicates a combined nozzle and turbine loss of about 15 dB (Reference 18). On the other hand, the duct coupling transmission loss would appear to be double bookkeeping since the analysis already assumes that each of the N_f fuel nozzles functions as a totally uncorrelated source.

The duct-coupled component data, acquired under FA72WA-3023 (Reference 1), are compared to the proposed prediction method and are considerably higher than predicted (Figures 2.6-3 and 2.6-4). Clearly, a 7 dB combustor/duct coupling loss cannot be accommodated. Also, the data trends - noise versus correlating parameter - are different for the two combustors, and there are systematic differences between the varying flow rates.

The prediction method works a little better on General Electric engine data since the errors made in the two transmission loss models are self-compensating. Unfortunately, the data cannot be collapsed fully, as is shown in Figure 2.6-5. The turboshaft data, in particular, deviate considerably (10 to 12 dB) from the prediction line.

A brief summation is in order here. The analysis of Mathews and Rekos (Reference 17) provides a clever and innovative treatment of Strahle's basic combustor noise equation. The analysis yields an OAPWL prediction which appears to collapse Pratt and Whitney component and engine data. The authors necessarily have to make certain assumptions and simplifications about the combustion process, in order to arrive at a viable prediction method, and some of these are apparently violated by General Electric combustors. Also, some reservations must be expressed about the transmission loss models.

Grande (Reference 9) was the first to recognize that combustor noise is subject to transmission losses while propagating to the farfield. He postulates and approximates the losses due to the turbines and the exhaust nozzle as:

$$TL_{turb} = \left(\frac{T_4}{T_0}\right)^{N/2} \left(\frac{P_R}{N}\right)^{0.072(N-1)}$$
 (2.6-16)

and

$$TL_{nozzle} = (T_8/T_0)$$

where

N - number of turbine stages

PR - pressure ratio across the turbines

 T_A/T_O - temperature ratio across the turbines

 T_8/T_0 - temperature ratio across the exhaust nozzle

His analysis is based on the changes in specific impedance and Strouhal number, and for the turbine, recognizes the high Mach number existing at the exit from each stationary blade row.

Grande's transmission loss formulations are approximate. The loss through turbine blade rows is being investigated analytically and experimentally at General Electric under Contracts NAS3-19435 and 20027. One of the analytical models is described in Reference 3. The model indicates that the rotational speed is relatively unimportant; and, therefore, the results can be extended to the case of the exhaust nozzle which is simply an accelerating passage with no turning. Assuming that the sound is incident in the form of a plane wave, the transmission loss can be obtained as:

$$TL_{nozzle} = 10 \log \left\{ \frac{1}{4} \frac{\rho_{o} C_{o}}{\rho_{8} C_{8}} \left(\frac{C_{8}}{C_{o}} + \frac{\rho_{8}}{\rho_{o}} \right)^{2} \right\}$$
 (2.6-17)

where the subscripts 0 and 8 represent ambient and nozzle exit conditions, respectively. Using a perfect gas assumption and $\gamma = 1.4$, the equation further reduces to the following static temperature ratios:

$$TL_{nozzle} = 10 \log \left\{ \frac{1}{4} \left(\frac{T_{s8}}{T_o} \right)^2 \left(1 + \left(\frac{T_o}{T_{s8}} \right)^2 \right)^2 \right\}$$
 (2.6-18)

The current analytical model utilizes an actuator disk assumption. Therefore, all frequency dependence is lost. This effect becomes significant only when $(\omega a/C)$, where 'a' is a characteristic dimension, becomes very small. Hence, the frequency dependence is a factor only for multi-element exhaust as was explained earlier in Section 2.3. For the no flow case, it is well known (see, for example, Reference 6) that the transmission loss varies as

TL (
$$\omega$$
) \sim 10 log $\left(\frac{\omega a}{C}\right)^{-m}$ (2.6-19)

where m = 1 for planar elements

= 2 for circular elements

If it can be assumed that this loss can be superimposed on the nozzle loss defined by (2.6-17), then the <u>additional</u> transmission loss for multi-element nozzles beyond that for an equivalent conical nozzle can be defined by:

$$\Delta TL_{\text{nozzle}} = 10 \log \left(\frac{a_{\text{equiv.}}}{a_{\text{element}}} \right)^{\text{m}}$$
 (2.6-20)

It is apparent that while the analytical investigation of combustor noise is not sufficiently advanced to yield exact models for either the transmission losses or source noise, there is general agreement on some essential elements. For example, considering the source noise generation, the message is clear: the acoustic power generated by a combustor is a function of the flow rate, the thermal energy input, inlet conditions, and the burner area. However, the exact functional relationship remains to be resolved. Independent variation of these parameters is impossible in an engine, and thus component data must be used.

Let us start with a basic source noise prediction model:

$$P \sim A^{\alpha} V^{\beta} (T_4 - T_3)^{\gamma} P_3^{\delta} T_3^{\epsilon}$$
 (2.6-21)

The results of the D13 parametric test (Section 2.2) suggest that with V \equiv V_{Ref}, β = 3.5, γ = 1, δ = 1.5, ϵ = -1.5. Dimensional analysis can be used to show that the dimensionless groupings to be used here are (P/P₃ A/RT₃, (V_{Ref}//RT₃), and (T₄ - T₃)/T₃. Since the area term appears only in the acoustic power grouping, then α = 1. Using A = A_{Ref} (the area used to derive V_{Ref}) equation (2.6-21) gives:

$$P \sim A_{Ref} \left(\frac{P_3}{T_3}\right)^{1.5} V_{Ref}^{3.5} (T_4 - T_3)$$
 (2.6-22)

Note the close correspondence to the Strahle analytical scaling law which can be written as:

$$P \sim A_{Ref} \left(\frac{1}{T_3^2}\right) V_{Ref}^4 \left(T_4 - T_3\right)^{2a}$$
 (2.6-23)

The comparison of equations (2.6-22) and (2.6-23) would suggest a mean value of a=0.5 for the D13 component data. That brings up an interesting detail, one of potential significance to the next generation of low emission combustors. The current family of combustors utilize single fuel nozzles with approximately 30 to 35% of the total air participating in the primary

combustion due to constraints at the low (approach) power settings. The net result is a slightly rich primary zone at full power, while the approach power burn is slightly lean. According to Strahle, the value of the exponent "a" should then vary between 0 and 1 over the range of power settings. However, use of dual nozzle systems as in the Experimental Clean Combustor Program permits optimization of the primary zone over the entire operating region and, as discussed in the noise/emissions section, this means lean burn at all power settings. Hence there should, theoretically, be some reduction in the exponent on $(T_4 - T_3)$.

Unfortunately, as long as the conditions at the combustor exit are employed in the correlation, it is impossible to determine the condition (lean or rich) of the primary zone. This suggests the use of \underline{local} parameters such as the peak local velocity, V_L , which is defined by the peak temperature attained in the primary zone.

$$V_{L} = \frac{(k_{1} \dot{W}) R (T_{3} + \Delta T_{L})}{P_{3} A_{L}}$$
 (2.6-24)

where $(K_1 \ \dot{W})$ gives the amount of air participating in the primary combustion, (ΔT_L) is the local or peak temperature rise and is a function of the primary zone fuel/air ratio, and A_L is the local area. A reasonable assumption here might be to take K_1 as the ratio of the combustor dome flow to the total combustor flow and A_L as the area associated with the dome flow.

These local parameters were used in a relationship similar to equation (2.6-21) and the exponents determined for the D13 and Experimental Clean Combustor Program data through a multiple correlation routine. The results are shown in Figure 2.6-6. The D13 correlating line is given by

$$P \sim P_3 V_L^{1.5}$$
 (2.6-25)

Since V_L is a function of T_3 and the temperature rise, these terms do not appear explicitly in the correlation anymore. The data for the double annular, radial axial, and the baseline CF6-50 combustor are collapsed by this relationship. But the swirl-can combustor data form a separate grouping unto themselves. Table 2.5-3 shows that the value of K_1 used for these was around 0.8 or higher. A close examination of the swirl-can configurations reveals that a significant portion of the dome air enters at the outer periphery and sweeps past the primary zone without participation. Assuming that K_1 could be adjusted appropriately, the swirl-can data would move to the left, closer to the correlating line, as shown in Figure 2.6-6.

The detailed information required to avail of (2.6-25) as a prediction method is frequently impossible to determine. In an attempt to produce a more practical correlation, a local reference velocity was postulated based on inlet conditions only but still using the <u>local</u> area and participating air:

$$V_{L_{Ref}} = \frac{(K_1 \dot{W}) RT_3}{P_3 A_L}$$
 (2.6-26)

The corresponding correlation obtained is shown in Figure 2.6.-7 and is given by:

$$P \sim \frac{P_3}{T_3} V_{L_{Ref}}^{1.5} \Delta T_L$$
 (2.6-27)

Once again, good correlation is found, except for the swirl-can data for the same reason as before: a significant portion of the dome air bypasses the primary combustion zone.

There is little doubt that (2.6-25) or (2.6-27) produces more exact noise predictions, <u>if</u> all the local properties were known. Considering the problems in determining K_1 and the like, only equation (2.6-22) can provide a viable prediction method for source noise levels.

The D13 data all represent internal measurements made in the immediate vicinity of the combustor. Hence there is some question if these represent true sound levels which would be radiated to the farfield. Two sets of farfield acoustic data were acquired during Contract FA72WA-3023, using full scale annular combustor assemblies operating at atmospheric conditions (see Reference 1). These data were found to collapse fairly well using equation 2.6-22) as is shown in Figure 2.6-8. The somewhat large data scatter is due to the large off-design excursions in the combustor operation during the atmospheric tests. The correlating line is given by

OAPWL = 10 log
$$\left\{ A_{Ref} \left(\frac{P_3}{T_3} \right)^{1.5} V_{Ref}^{3.5} (T_4 - T_3) \right\} + Constant$$
 (2.6-28)

The agreement obtained is particularly important in that it indicates that (1) the noise generation by combustors exhausting to ambient conditions is representative of that obtained from combustors operating at elevated pressures, and (2) the data recorded during the D13 parametric tests, and during the preceding Experimental Clean Combustor Program (References 3 and 11) are valid acoustic measures. This added considerably to the data base that could be used in the noise/emissions study.

The component correlation was then used on the engine data available to General Electric. The results are shown in Figure 2.6-9. All the data collapsed on two lines: with the turboshaft engines all falling on one line 5 to 10 dB below the component data and the turbojet and turbofan engines on the other line some 15 to 20 dB below the component data. The two engine lines are parallel, but differ in slope from the component line. Because of the unknown effects of the turbine and nozzle transmission loss phenomena, it would be fruitless to carry the analysis any further at this

The state of the s

time. Work in the area of low frequency noise transmission through turbine blade rows is currently progressing under NASA Contracts NAS3-19435 and 20027.

The component (rig) and engine correlating parameters may appear to be quite different on the surface, when in fact due to the engine cycle operating constraint they are quite similar. Consider the two relationships:

Rig: OAPWL
$$\sim \left(\frac{P_3}{T_3}\right)^{1.5} V_{Ref}^{3.5} (T_4 - T_3) (A_{Ref})$$
 (2.6-29a)

Engine: OAPWL
$$\sim \dot{W} (T_4 - T_3)^2 (\rho_3/\rho_0)^2$$
 (2.6-29b)

Rearranging terms in the rig correlation:

$$OAPWL_{Rig} \sim \dot{W} (T_4 - T_3) V_{Ref}^{2.5} \rho_3^{0.5}$$
 (2.6-30a)

or
$$OAPWL_{Rig} \sim \dot{W} (T_4 - T_3) V_{Ref}^{2.5} (\rho_3^2/\rho_0^2) (\rho_0^2/\rho_3^{1.5})$$
 (2.6-30b)

It can be shown for a wide range of engines that $V_{Ref}^2 \ll (T_4 - T_3)$. Substituting into the above equation gives

$$OAPWL_{Rig} \sim \dot{W} (T_4 - T_3)^2 \left({}^{\rho}_{3} / {}^{\rho}_{o} \right)^2 \left(\frac{v_{Ref} {}^{\rho}_{o}^2}{{}^{\rho}_{3}^{1.5}} \right)$$
 (2.6-31)

$$\sim \text{OAPWL}_{\text{Engine}} + \frac{\sqrt{\text{VRef}} \rho_o^2}{\rho_3^{1.5}}$$

Over the normal operating range of an engine the last term does not vary considerably, especially when considering the unknown transmission loss effect. Hence the engine and rig correlation can be considered to be roughly equivalent.

The data acquired on the turboshaft and turbofan engines during this program (Section 2.4) was incorporated into the data base for the OAPWL correlation shown in Figure 2.4-39. Good agreement was obtained, reinforcing the general applicability of the unified line correlation. Further validation of the prediction method is being provided through the SAE A21 Jet Noise Subcommittee. Until work is completed on the turbine blade row

transmission investigation, the unified line correlation will remain the only viable power level predictor for engine combustor noise.

2.6.3 Spectrum Shape

The measured engine data taken under this contract suggests that core noise peaks between 315 and 500 Hz which is in agreement with previous measurements taken by GE (Reference 10) and others (References 5 & 9). Further, the peak frequency does not appear to shift significantly with engine size as indicated by comparison of the turboshaft and turbofan data taken under this contract, where both engines indicated a peak frequency of 315-400 Hz but differed significantly in combustor size. Note that the probe data are being used here for the turbofan engine for reasons explained earlier. Figure 2.4-37 shows the power level spectra measured on the turbofan engine test compared to the engine spectra from Reference 10 peaked at 315 Hz. The agreement is very good. Further, as shown in Section 2.4, Figures 2.4-4 thru -8, the turboshaft engine data also substantiates the low frequency end of the recommended spectrum shape when peaked at 400 Hz.

One anomaly is the combustor rig data (Section 2.2) which indicates a peak frequency occurring between 630 and 1000 Hz. These results, however, do not include the modifying effects of the turbine nozzle exit or refraction effects at the jet exhaust and were acquired with a very different end termination. Therefore it is difficult to assess the meaning of the higher peak frequency and the likelihood that low emission combustors when installed in engines will display the higher frequency spectrum.

Mathews and Rekos (Reference 17) proposed the peak frequency model for shown in Figure 2.6-10. The peak frequencies for the turboshaft and turbofan engines tested under this program are compared to the prediction line. The agreement with the CFM56 data is pretty good, however, the T700 is under predicted by one 1/3 octave band. Also, the component data acquired under FA72WA-3023 (Reference 1) are in disagreement with the prediction, as are the data from Engine A (Reference 18). While this model might work on Pratt and Whitney combustors, it cannot correlate data from GE combustors.

The general core noise spectrum shape recommended in Reference 10 has been substantiated by the engine data acquired under this program and others. Further the peak frequency appears to be 400 Hz, plus or minus one third octave band and this finding is also substantiated by others (Reference 9). It is therefore recommended that the current core noise spectrum shape, shown in Figure 2.6-11 be maintained without alteration, at least for conventional combustors. There is some indication that low emission combustors will peak at higher (630 to 1000 Hz) frequencies. A test of an engine incorporating such a combustor would be useful as the sound-separation probe could be utilized to extract the combustor noise spectrum.

2.6.4 Directivity

The results of the engine and scale model tests conducted under this program suggest that the current assumed core noise directivity, derived in Reference 1, may not apply at all frequencies. The mean directivities indicated by the engine tests are reproduced in Figure 2.6-12 thru 2.6-15 and compared to the scale model low frequency nozzle directivity test results at selected frequencies. The trends observed for the engine data are substantiated by the scale model data. The lower frequencies tend to have directivity patterns resembling jet noise while the higher frequency directivity field shapes are similar to those seen on previous single flow engine tests. Further, the directivity patterns appear to be independent of engine power setting. However, the frequencies do not scale with the nozzle diameters as would be suggested by some analyses (see Reference 26, for example). Instead, the scaling is more like $(d_{engine}/d_{model})^{\eta}$, where $\eta = 1/2$.

The agreement between the scale model and engine directivity pattern indicates that the convection/refraction effects imposed by the dual flow jet are an important factor. Therefore a change in the current directivity pattern, which is frequency independent, is recommended. Lack of a sufficient analytical modeling suggests using an empirical formulation based on the engine test results. Table 2.6-2 contains the recommended directivity indices as a function of frequency. It should be noted that these new indices apply only to dual flow systems. The current directivity patterns should be maintained for single flow systems until such time that a comprehensive set of directivity indices for a single flow engine can be measured utilizing the coherence technique or similar procedure.

2.6.5 Implementation of Prediction Methods

The prediction of combustor noise is separated into two categories: component and engine. The component prediction is based on the correlation derived from the parametric tests conducted under this program. (See Section 2.2). The overall power level calculation is made using

OAPWL =
$$10 \log [(P_3/T_3)^{1.5} V_{Ref}^{3.5} (T_4 - T_3) A_{Ref}] + 51.8 dB re: 10^{-13} watts$$

Where P₃ = combustor inlet total pressure ∿ psia

 T_3 = combustor inlet total temperature - $^{\circ}R$

T₄ = combustor exit total temperature - °R

 A_{Ref} = maximum combustor cross-sectional area \sim in.²

V_{Ref} = reference velocity defined as

$$V_{Ref} = \frac{W_3 RT_3}{P_3 A_{Ref}}$$

W₃ = total combustor air flow ∿ 1b/sec

The engine prediction is the same as that derived in Reference 18 with the exception of a new set of directivity indices. The overall power level is calculated by:

OAPWL =
$$10 \log [W_3 (T_4 - T_3)^2 (\rho_3/\rho_0)^2] -40 \log_{10} (T_4 - T_5)_{Design} + 171 dB re: 10^{-13} watts$$

where the nomenclature is described above and (T₄ - T₅)_{Design} is the total temperature drop across the high and low pressure turbines at the cycle design point. The power spectrum is then determined using the T64 spectrum shape shown in Table 2.6-3. From the 1/3 octave band power levels a space - averaged sound pressure level is calculated for any arc of interest. The far-field sound pressure levels are calculated by adding the appropriate directivity index, shown in Table 2.6-2, to the space averaged level. These sound pressure levels must then be adjusted for air attenuation and ground absorption effects for the appropriate arc radius. Figure 2.6-16 shows a flow chart for implementing this prediction procedure.

Table 2.6-1 Compilation of Parameters Used to Compute Low Frequency Core Noise

Author	Constant	Compute	Temperature	Pressure	Mass Flow Rate	Fuel Mixture	Velocity	Dimension
Ho/Tedrick	81	OAPWL	$\frac{\left(\mathrm{T_4-T_3}\right)^2}{\mathrm{T_4}}$	P4		(1+F) ²	۷4	o O
Motsinger	56.5	ОАРИТ	$\left[\frac{(T_4-T_3)T_0}{T_3}\right]^2$	(P ₃ /P ₀) ²	Œ			
Grande/Arnold	(1)	OAPWL	$\begin{bmatrix} (T_4 - T_3) \\ T_0 \end{bmatrix}^2 \frac{1}{T_3^3} $ (F)	(P ₄ /P ₀)	$(P_4/P_0) \begin{array}{ c c c c c c c c c c c c c c c c c c c$	(1+F)	$v_b^2 v_3$	DL/D ₄
Gerand, et al	(2)	OASPL(4)	τ_4^2	(P ₄ /P ₅) ²	$(P_4/P_5)^2$ $\frac{4\sqrt{T_4/T_0}}{3}$			193 - 193 -
Strahle	-	OAPWL		9 123 23		$\begin{bmatrix} \frac{F}{1+F} \end{bmatrix}^{0.41} \begin{bmatrix} v_3^{2.68} \\ v_1^{1.35} \end{bmatrix}$	$v_3^{2.68}$ $v_{bL}^{1.35}$	D _c .84

(2) (-15 for annular, -6 for can or can-annular)+5 dB (1) $205.5 + 10 \log(B_N B_T)$

Table 2.6-2 Recommended Core Noise Directivity Indices for Dual Flow Exhaust Systems

1/3 O.B Frequenc				Ang	le to	Inlet,	Degre	es			
Hz	40	50	60	70	80	90	100	110	120	130	140
50	-4.0	-3.8	-3.2	-3.0	-2.7	-2.0	-0.8	+0.8	+3.0	+5.0	+7.0
63	-4.0	-3.8	-3.2	-3.0	-2.7	-2.0	-0.8	+0.8	+3.0	+5.0	+7.0
80	-4.0	-3.8	-3.2	-3.0	-2.7	-2.0	-0.8	+0.8	+3.0	+5.0	+7.0
100	-4.0	-3.8	-3.2	-3.0	-2.7	-2.0	-0.8	+0.8	+3.0	+5.0	+7.0
125	-6.5	-5.8	-5.0	-4.0	-3.0	-1.5	0	+1.8	+4.0	+5.0	+5.0
160	-6.5	-5.8	-4.5	-3.5	-2.5	-1.5	0	+1.5	+3.5	+4.8	+6.0
200	-6.5	-5.8	-5.0	-4.5	-4.0	-3.0	-1.8	+1.0	+3.5	+5.5	+6.5
250-10K	-10.0	-8.5	-6.5	-4.5	-2.5	-0.5	+1.0	+2.5	+5.0	+4.5	+3.5

Table 2.6-3 Tabulation of Recommended Engine Core Noise Spectrum Shape

1/3 O.B. Frequency, Hz	SPL - Peak Frequency SPL, dB
50	-24.0
63	-20.0
80	-16.0
100	-13.0
125	-10.0
160	-7.0
200	-4.5
250	-2.5
315	-1.0
400	0
500	-1.0
630	-2.5
800	-4.5
1000	-7.0
1250	-10.0
1600	-13.0
2000	-16.0
2500	-20.0
3150	-24.0
4000	-27.5
5000	-31.5
6300	-36.0
8000	-40.0
10000	-45.0

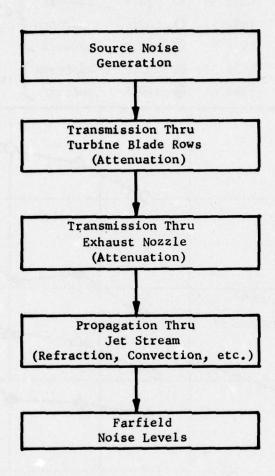


Figure 2.6-1 Flow Chart for Combustor Noise from Gas Turbine Engines

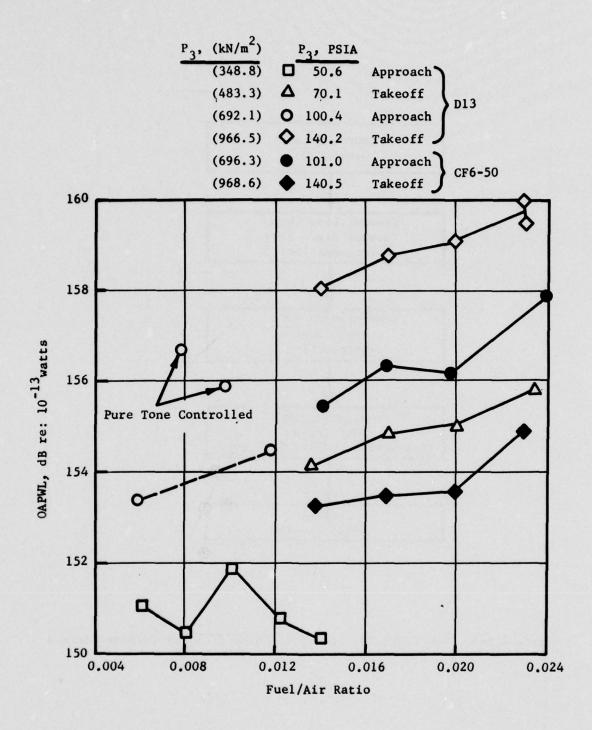


Figure 2.6-2 Effect of Fuel/Air Ratio on Overall Power Level

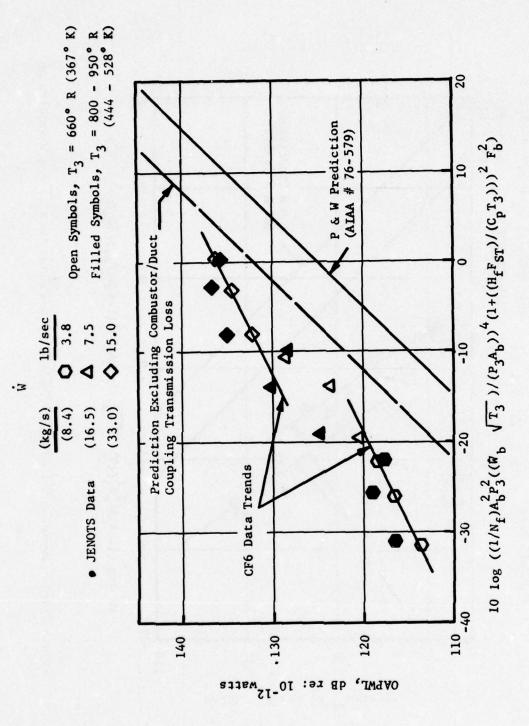


Figure 2.6-3 Comparison of CF6 Combustor Data to P & W Prediction

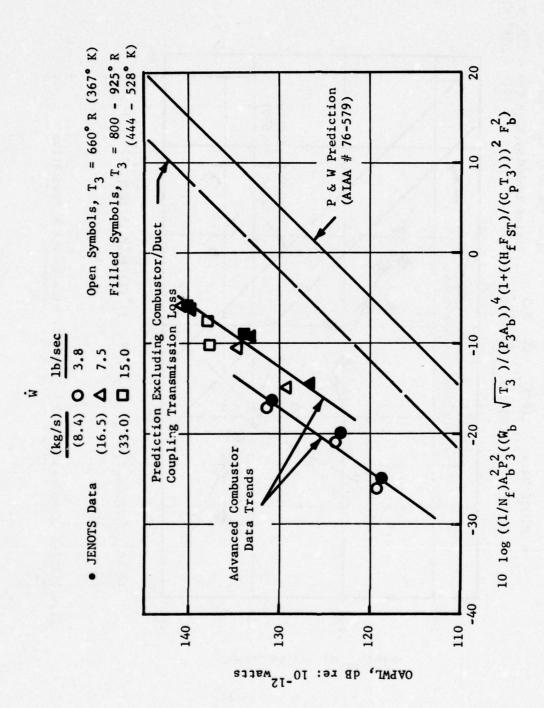


Figure 2.6-4 Comparison of Advanced Technology Combustor Data to P & W Prediction

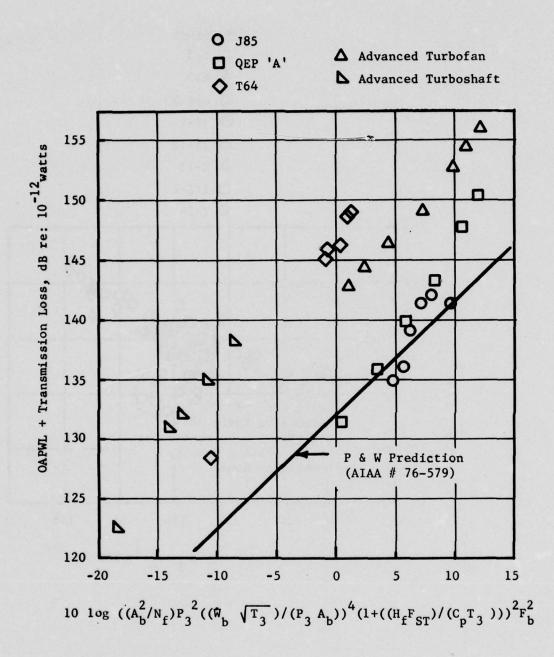


Figure 2.6-5 Measured Core Noise Levels vs. P & W Prediction

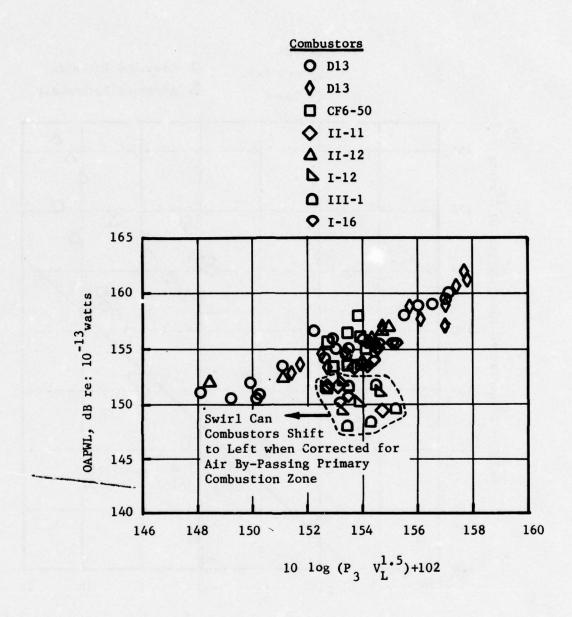


Figure 2.6-6 Combustor Noise Correlation based on Rig Data

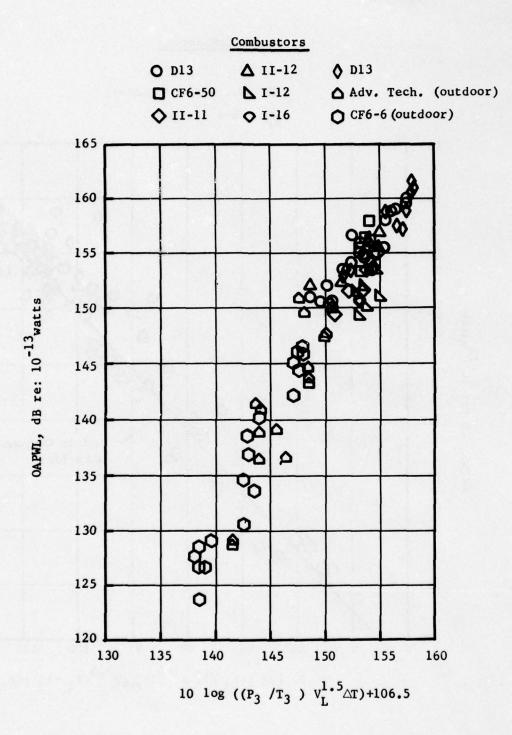


Figure 2.6-7 Combustor Noise Correlation based on Rig and Outdoor Data

Combustors

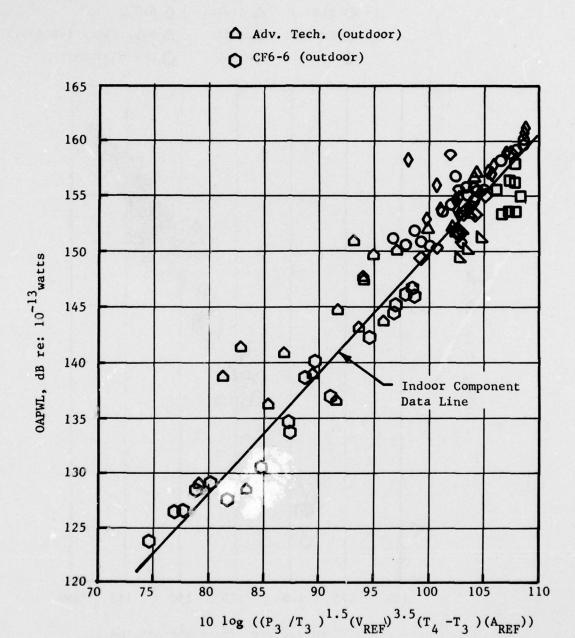


Figure 2.6-8 Combustor Noise Correlation based on Indoor and Outdoor Component Data

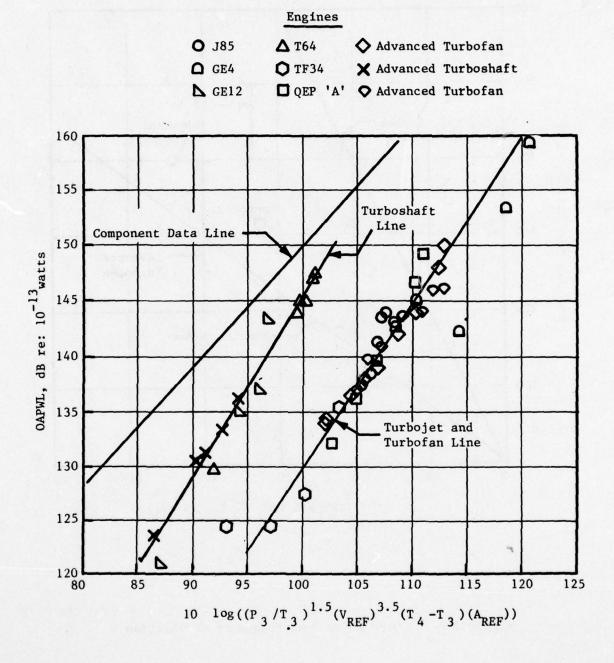


Figure 2.6-9 Measured Engine Core Noise Levels vs. Rig Correlation Parameter

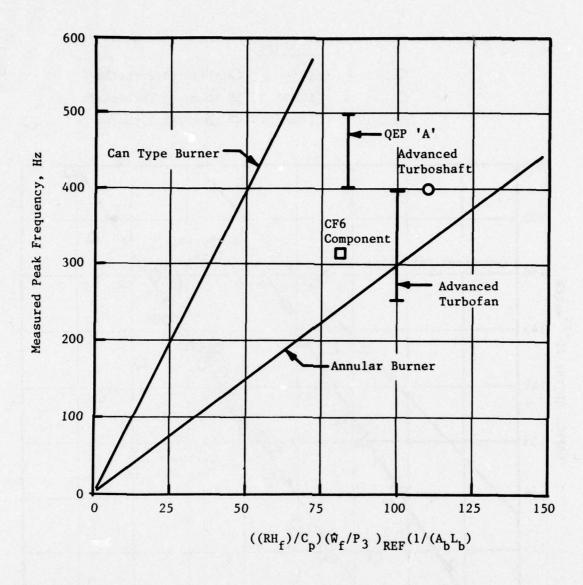


Figure 2.6-10 Core Noise Peak Frequency Correlation

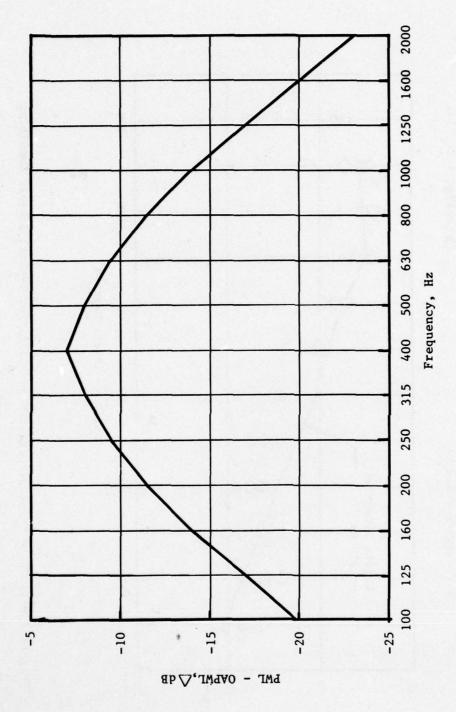


Figure 2.6-11 Recommended Core Noise Spectrum Shape

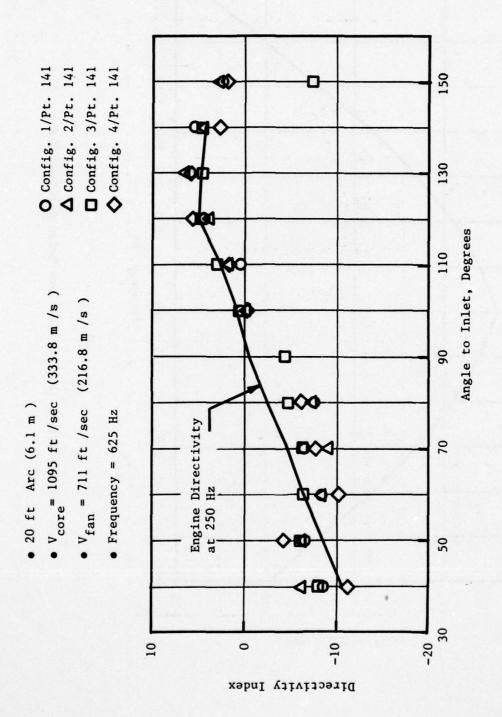
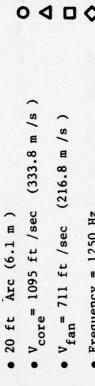


Figure 2.6-12 Core Noise Directivity at 625 Hz for Typical Takeoff Condition



10

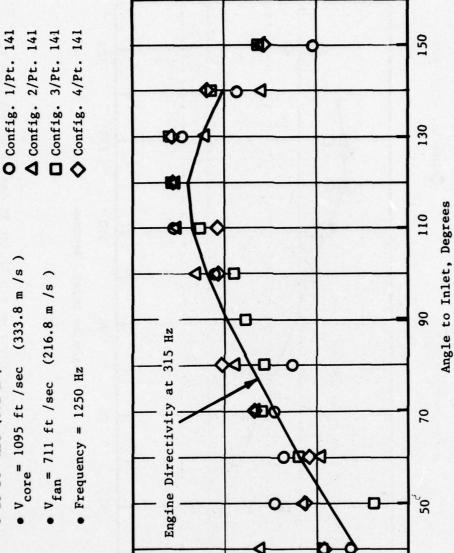


Figure 2.6-13 Core Noise Directivity at 1250 Hz for Typical Takeoff Condition

30 -20

0

-10

Directivity Index

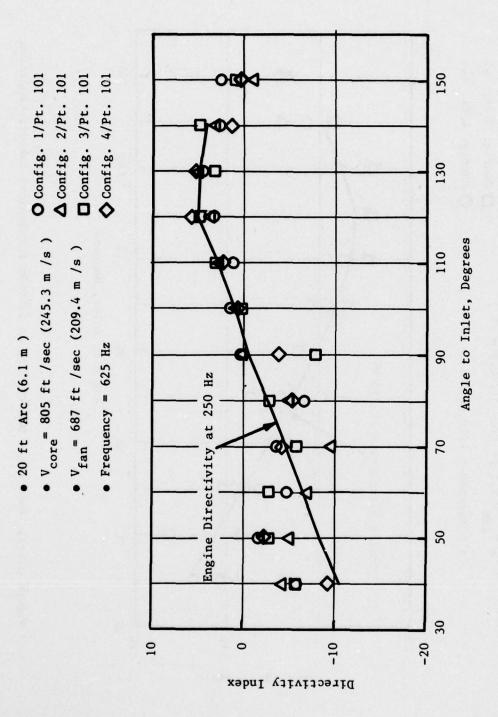


Figure 2.6-14 Core Noise Directivity at 625 Hz for Typical Approach Condition

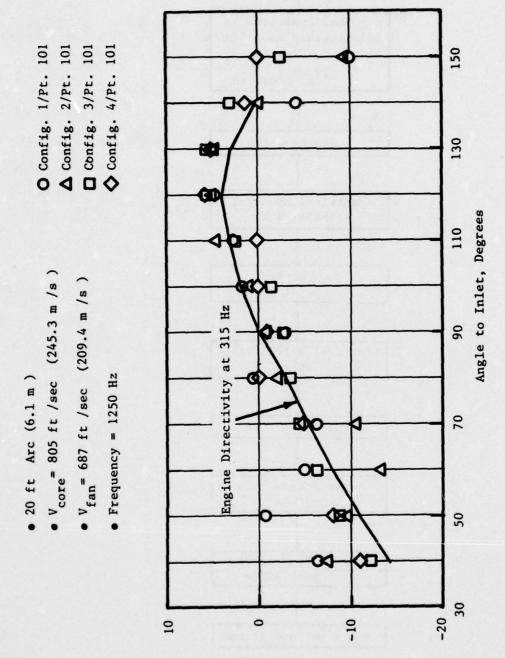


Figure 2.6-15 Core Noise Directivity at 1250 Hz for Typical Approach Condition

Directivity Index

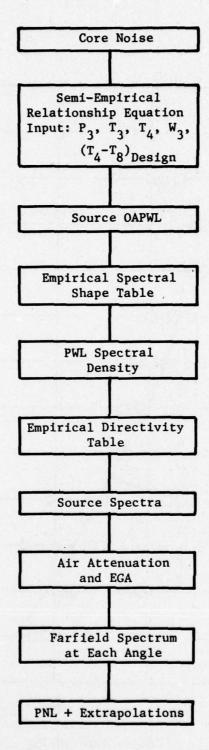


Figure 2.6-16 Flow Chart for Core Noise Prediction

SECTION 3.0

TURBINE NOISE

3.1 BACKGROUND

System studies (Reference 28) and analysis of existing data indicate that the turbine is and will remain a significant contributor to the farfield noise signature of the commercial aviation fleet. In order to enhance the understanding of turbine noise and identify methods for its reduction, the initial Core Engine Noise Control Program efforts (Reference 10) were directed, in part, towards the development of an analytical prediction procedure which would incorporate the effect of the pertinent aero-mechanical design details, such as the blade row spacing and vane lean. The value of an analytical procedure which has the potential of identifying means of source noise reduction is enhanced by the interest in energy-efficient noise suppression techniques.

This analytical procedure for turbine tone noise generation gave excellent results for the last stage of a three stage turbine (see Figure 3.1-1). However, the analysis yields the acoustic power level at the source and does not recognize the part played by downstream blade rows through which the noise must propagate. Comparison of predicted 'source' levels for upstream blade row tones with the actual levels measured downstream of the last stage indicated significant transmission loss occuring through the intervening blade rows. A controlled test to measure the actual attenuation experienced was obviously needed.

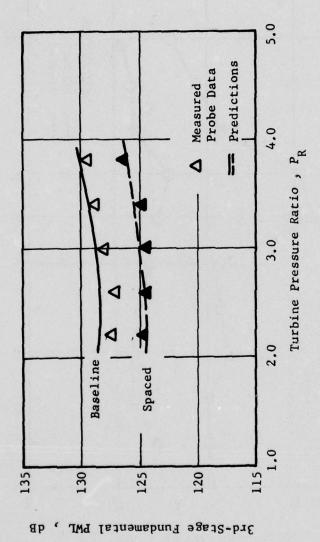
The major efforts thus far have been directed towards turbine discrete frequency noise. However, comparison of farfield noise spectra from engines with and without acoustic treatment in the core reveals substantial broadband noise contribution (Figure 3.1-2). Investigators have largely ignored this noise component partly due to problems in discerning and separating turbine broadband noise from fan and jet noise in the case of engine tests using farfield measurements, and partly due to the difficulty in separating sound and turbulence signals in the case of engine or component tests utilizing internal measurements. Recently, however, using correlation techniques, General Electric demonstrated the ability to extract true sound levels by rejecting the convected turbulence component. This technique was conveniently incorporated into the noise attenuation test mentioned in the preceding paragraph.

The Core Engine Noise Control Program also revealed that the passage of turbine tones through the exhaust jet stream turbulence resulted in scattering of the discrete frequency energy, mainly into adjacent sidebands. This broadening, or haystacking, of the tonal energy content (see Figure 3.1-3) suggested a means of noise "suppression" through reduction in the

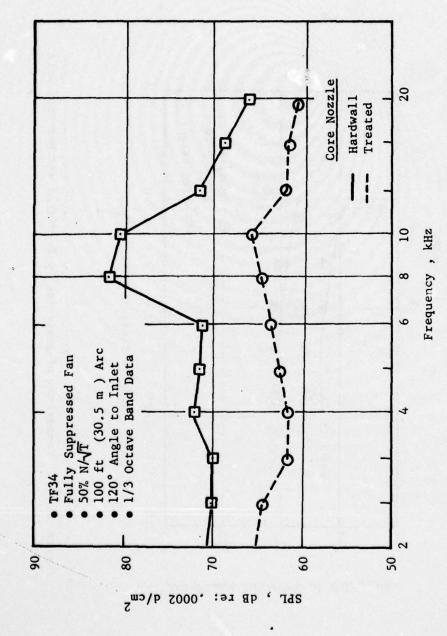
tone (PNLT) correction. A limited set of engine data yielded a first-cut prediction method in terms of the velocity of the outer jet stream. Analytical studies conducted under the same contract have identified significant parameters in this propagation phenomenon as turbulence, mixing zone thickness, tone frequency, velocity ratio, and intensity and micro-scale of turbulence. Unfortunately, the complexity of the mechanism precluded any quantification of the results in terms of convenient engine parameters. A parametric test series was thought to be necessary to complete the investigation.

This section describes the efforts directed towards extending the turbine noise technology in these three areas. Two test series were conducted:

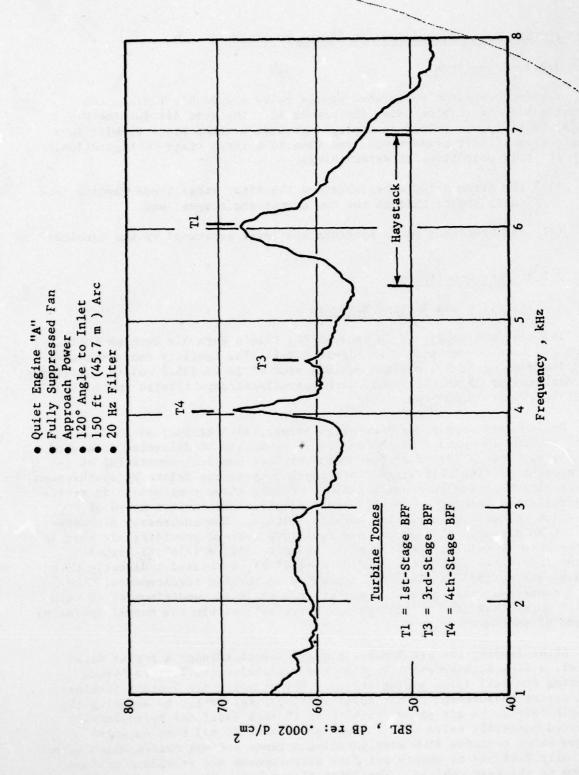
- (1) Turbine tests utilizing a three stage and a single stage configuration of a low pressure turbine rig.
- (2) Model tests of a dual flow arrangement with simulated turbine noise generation.



Comparison of Analytically Predicted and Measured Data. Figure 3.1-1

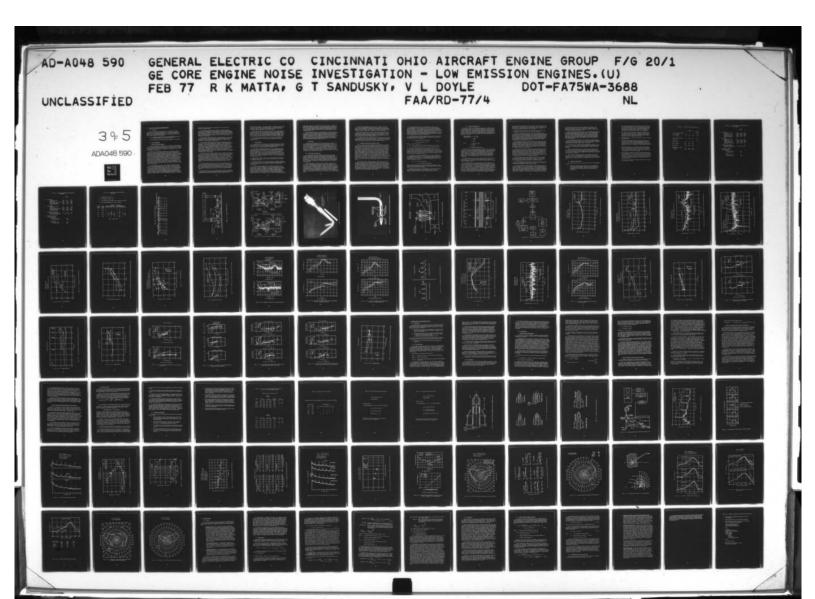


Engine Noise Suppression Achieved Using Core Treatment for the TF34Figure 3.1-2



Farfield Narrowband Spectrum Showing "Haystack"

Figure 3.1-3



3.2 TURBINE TONE ATTENUATION AND BROADBAND NOISE

3.2.1 Objectives

Turbine component tests have proved to be a valuable tool in the investigation of turbine noise (Reference 1). The Warm Air Turbine Rig (WATR) facility was therefore employed to test a three stage turbine in a single stage (first stage alone) and then in a three stage configuration, with the twin objectives of determining:

- (1) the attenuation experienced by the first stage blade passing tone as it passed through the two downstream stages, and
- (2) the broadband noise spectrum and level generated by the turbine.

3.2.2 Test Description

Facility and Turbine Hardware

The test was conducted in General Electric's Warm Air Turbine Facility, which is shown schematically in Figure 3.2-1. The facility can accommodate vehicles ranging from a minimum hub diameter of 14 in. (35.6 cm) to a maximum tip diameter of 32 in. (81.3 cm), with operational capabilities up to 15,000 HP (1186 kW) at 15,000 rpm.

Maximum air supply consists of 80 lb/sec (36.3 kg/sec) at 1560° R (866° K), and 150 psia (1034 kN/m² abs.). This air is delivered from the Central Air Supply System of the Component Test Complex, consisting of an arrangement of five multistage centrifugal compressors driven by synchronous motors through speed increasing gears. Staging these compressors in series or parallel or using them as exhaustors provides the various modes of operation normally required for turbine testing. The compressor discharge air can be directed through various auxiliary systems providing air that is filtered to ten micron particle size, dried to 530° R (216° K) dewpoint, heated indirectly with steam to 710° R (450° K), or heated indirectly with natural gas to 1560° R (866° K), depending on turbine requirements. The tests conducted under this program were run at inlet conditions of 40 psia (275.8 kN/m²) and 760° R (422° K) which are well within the normal operating ranges of the facility.

After leaving the air heater, the air passes through a porous metal filter, a flow straightening section and a circular arc Venturi before entering the cell inlet piping system. The circular arc Venturi provides an accurate measurement of the inlet airflow rate. Prior to entering the vehicle inlet, the air passes through an 18 inch (45.7 cm) hydraulically actuated butterfly valve used for emergency shutoff and then an inlet plenum which contains flow straightening screens and egg crates which were specially designed to smooth out flow disturbances and provide a uniform stream to the test vehicle. The inlet plenum bolts directly to the vehicle

forward frame and is located on a wheeled dolly for rapid removal for access to the vehicle inlet.

Air enters the first stage nozzle through a convergent bellmouth section. Turbine discharge air leaves through a constant annular passage and expands into a discharge plenum designed to provide a uniform circumferential pressure distribution. As the air exits the vehicle it is discharged into a large exhaust scroll. A 42 in. (107 cm) exhaust pipe leaves the exhaust scroll and ducts the discharge air back to the vacuum header in the Central Air Supply System.

The generated turbine horsepower is extracted by means of a high speed waterbrake coupled to the turbine shaft by flexible couplings and a short spool piece. This waterbrake design provides excellent speed stability throughout the entire turbine operating map.

For protection against overspeed and excessive temperature or vibrations, a two-level trip system is used. The level 1 trip is signaled by an overspeed. Level 2 trip is signaled by excessive bearing temperatures or vibrations, or critical support system temperatures or pressures. The turbine facility control console is located in the Test Cell Control Room. All necessary controls and critical turbine or facility monitoring instrumentation are strategically located to enable two man control of the entire test facility. This feature is a direct result of the utilization of analog closed-loop control circuits for setting and maintaining all prime speed, discharge pressure, and rotor net thrust; which can all be maintained automatically at pre-set values.

The selection of the Highly Loaded Fan Turbine (HLFT-IVA) was based on the turbine's capability of being operated as both a single and three-stage machine. This low pressure turbine (LPT) is a highly loaded design with a large number of blades in all three stages. It is part of an on-going research and development program at General Electric and as such, represents the advanced technology in fan turbine design. Figures 3.2-2 and 3.2-3 provide cross-sectional views of the single and three stage builds. Design characteristics for both builds of the low pressure turbine are shown in Table 3.2-1, along with some pertinent airfoil design details in Table 3.2-2.

The three-stage build consists of a set of 116 pre-swirl vanes with radial trailing edges which orient the flow into the first stage stator at about a 25° angle to simulate the conditions at the exit of an HP turbine. The average annulus area at the inlet measuring plane is 92 in. 2 (594 cm²). The turbine discharge area is 370 in. 2 (2387 cm²) in the constant annular section which is essentially the same as at the exit to the third stage rotor.

When the LP turbine is run as a single stage, the last two stages are removed and both inner and outer exhaust casings are replaced with different casings which form a smooth transition from first stage rotor exit to

turbine vehicle discharge. The exhaust annulus is straight and has an area of 187 in.^2 (1206 cm^2) at the measuring planes. The rotor exit area for the single stage is 161.7 in.^2 (1043 cm^2) which represents a 15% area contraction from the measurement to rotor exit plane.

The turbine vehicles are supported by forward and aft frame assemblies which mount directly into the air turbine facility. The forward frame assembly consists of a 10 strut frame and outer and inner flowpath casings. Each of the 10 struts contain leading edge instrumentation elements. Five struts contain five total pressure elements and five struts contain five total temperature elements located at centers of five equal annular areas.

The aft frame assembly consists of a 12 strut frame and outer and inner flowpath casings. The aft frame mounts directly to the facility discharge plenum.

Instrumentation

The performance of the HLFT-IVA has been mapped previously on an IR&D program, therefore, the only aerodynamic instrumentation required for this test series were total pressure and temperature rakes upstream and static rakes downstream in order to establish the operating point.

The acoustic instrumentation consisted of four casing-mounted transducers upstream and two casing-mounted and four probe-mounted transducers downstream (see Figures 3.2-2 and 3.2-3). The sensors were used in pairs with axial spacings of 1 in. (2.54 cm) between the paired transducers. Kulite transducers were used in each case and were exposed directly to the perturbations in order to preserve phase information for later correlation analysis. The resulting sound-separation probe constitutes a unique piece of hardware and is shown in Figures 3.2-4 and 3.2-5. The casing mounts are shown in Figure 3.2-6.

Figure 3.2-7 provides a layout of the instrumentation in the form of an unwrapped casing. The acoustic sensors were clustered at two diametrically opposite locations.

An on-line calibration of the Kulite systems was performed frequently during the course of the tests to determine changes in transducer sensitivity at operating temperature and to maximize the use of the tape recorder dynamic range.

The Kulite signals measured in the vehicle in the test cell were amplified prior to being transmitted to the recording equipment to ensure proper signal strength. A schematic illustrating the general setup of the acoustic data acquisition system for this program is shown in Figure 3.2-8. All the data were recorded on magnetic tape using a Sangamo Sabre IV 28 channel recorder having a dynamic range of 48 dB and a flat frequency response to 40 kHz. The data acquisition and recording system for these acoustic tests was set up in the A.C. mode to record the fluctuating pressure

measurements between 110 to 160 dB from the Kulite sensors. An end-to-end phase check calibration was made of the entire system while in the D.C. mode, which accounted for individual component sensitivities and responses (i.e., transducer, amplifier, tape recorder, and leadout cables). This ensured accurate recorded levels when the system was operated in the A.C. mode during a data run.

The coupling with the digital system performed two valuable functions: (1) accurate on-line auto-spectra could be obtained to monitor the acoustic performance and (2) the data were digitized and recorded on disks which improved the available dynamic range to about 70 dB. The latter was an important consideration for the broadband noise levels as some data indicate that the turbine tones can have as much as 60 dB signal-to-noise ratio, meaning that at least that much dynamic range is required to accommodate both the broadband and discrete frequency levels.

Test Matrices

Acoustic data were acquired at the test matrix points of Table 3.2-3. Inlet conditions were maintained at 40 psia (275.8 kN/m 2) and 760° R (422° K) and the speed ranged from 50% to 110% design value. The pressure ratio was varied from 1.6 to 2.5 for the single stage build and 2.0 to 5.2 for the three stage build. In each case, the test matrix provided a combination of 5 speeds and 4 pressure ratio settings. A total of 20 points were set on the single stage configuration, including 16 different test conditions and 4 repeats, and 19 on the three stage configuration, including 16 different test conditions and 3 repeats.

3.2.3 Data Reduction and Results

The turbine tone levels were obtained directly from auto-spectra. However, the broadband levels were determined through sound-separation in order to eliminate the influence of the turbulence pseudo-sound. The principle and process involved in sound-separation was explained previously in Section 2.4. Also, in the case of the broadband noise, the upstream sensors were used to check if the dominant acoustic levels were associated with the turbine or the facility. The former was found to be the case in every instance.

Typical auto-spectra for both builds are provided in Figures 3.2-9 and 3.2-10. Two spectra are shown in each figure. Both spectra of Figure 3.2-9 are from the wall-mounted sensors - K5 and K6 (see Figure 3.2-7), while Figure 3.2-10 provides a comparison between a wall- and a probe-mounted sensor (K6 and K9). There appears to be no significant difference between the sensors as far as the tone levels are concerned. However, the broadband levels below 10 kHz are significantly lower for the wall Kulite (Figure 3.2-10). This is almost entirely due to the differences in flow turbulence seen by the two sensors; the wall Kulites were shielded by the casing bountary layer.

Typical turbine broadband spectra are shown in Figures 3.2-11 and 3.2-12. The sound-separation indicates that the turbulence and acoustic perturbations are of about the same order of magnitude, in that, the acoustic levels lie 1 to 10 dB below the auto-spectrum. However, the acoustic signal dominates the OASPL, particularly at operation near the design point.

The single stage spectrum of Figure 3.2-11 clearly peaks at the blade passing tone. The spectrum of the three stage turbine also peaks at one of the blade passing tones, although the peak is not as pronounced. The peak tends to shift towards the BPF second harmonic at off-design points; this will be discussed at greater length in Section 3.2.5.

The broadband spectra were converted to 1/3 octave band levels and then to power levels, and are tabulated in Appendix C. The conversion from SPL to PWL included area and flow corrections as noted in Section 2.4. Tone power levels were computed similarly and are also included in Appendix C.

3.2.4 Analysis of Turbine Tone Attenuation Data

Figure 3.2-13 shows how the attenuation was determined for each speed line. The tone power levels were plotted as a function of the first stage pressure ratio. The tone level is controlled by the pressure ratio and turbine speed, and therefore this ensured a constant source level comparison. (It was assumed that the addition of the second stage nozzle contributed very little to the BPF power level at the source (see Reference 5) through the resultant rotor-nozzle interaction). The difference between the power level measured downstream of the single and three stage builds was then simply the attenuation due to the second and third stages. These attenuations are plotted as a function of the turbine speed and pressure ratio in Figure 3.2-14. The attenuation clearly increases with the speed except for one data point: 110% N/ \sqrt{T} , 2.0 P_p. The computed attenuations for the 70% speed points are very small. This suggests either that the mechanism involved behaves like a step function and has negligable effect below this speed, or that the additional noise source provided by the interaction of the first stage rotor with the second stage nozzle (RIN2) contributes to the BPF power level.

The attenuation of low frequency noise by turbine blade rows was accounted for by a work extraction term (Reference 6). Therefore, the tone attenuations were plotted as a function of the temperature drop through the two stages responsible for the attenuation. The results are shown in Figure 3.2-16. The attenuation does appear to increase with ΔT near the design pressure ratio. However the trend is reversed for small ΔT , perhaps due to the increasing incidence at these extreme off-design points. The analysis of low frequency noise through turbine blade rows (Reference 6) indicates that incidence will be a factor beyond a certain range.

The dominating parameter here is undoubtedly the turbine speed - causing increases in attenuation of 10 to 20 dB over the operating range (50 to $110\% \ N/\sqrt{T}$). It can be argued that this is an acoustic baffling effect attributable to the physical obstructions presented by each rotating blade row, since the frequencies of interest here are such that the propagating sound "recognizes" the individual airfoils and flow passages. In contrast, the attenuation of low frequency (combustor) noise is a consequence of the impedance and flow Mach number change across each blade row, and the effect of wheel speed is negligible (Reference 7).

The attenuation was correlated against the wheel speed, work extraction and incidence angle using a multiple regression analysis and an index of determination of 0.85 was obtained with

$$\Delta = 98.9 \log_{10} [\%N/\sqrt{T}] + 13.4 \log_{10} (\Delta T) + 5.6 \log_{10} [|i+7.5|] - 217.5$$
(3.2-1)

where \triangle = PWL attenuation, dB

(AT) = total temperature drop through the second and third stages, ° R

i = incidence angle into the tip of the second stage rotor, deg.

The values used in the regression analysis are given in Table 3.2-4.

It should be cautioned that this correlation is strictly valid only over the range of speeds used here. Extrapolations to very low speeds, for example, could yield negative values, which is impossible. Also, it should be realized that the \triangle computed using (3.2-1) is a conservative (low) estimate in that the noise contribution from the second interaction (RIN2), has not been factored in as was explained earlier.

The influence of the speed is derived from two different effects and they are apparently additive. First, an increase in speed corresponds to an increase in the tone frequency. Using dimensional analysis, this can be represented by (t/λ) where t is the blade pitch (passage width) and λ the acoustic wavelength. Note that

$$2\pi(t/\lambda) = 2\pi \frac{ft}{c}$$
 - Strouhal number
= kt - Wave number representation

Second, for a given frequency, the physical obstruction presented by the rotating blades increases with speed. The proper representation is through $(U_{\rm T}/c)$ or $M_{\rm T}$, the blade tip Mach number.

Therefore, for a given ΔT , the attenuation is a function of (kt, M_T). These two combined produce about a 100 log(rpm) effect. The explicit dependence on the two must be extracted through a parametric test.

3.2.5 Turbine Broadband Noise

Figure 3.2-17 shows two broadband noise signals for the single stage build at design speed; one at the "design" pressure ratio and the other at a far off-design point. The design point spectrum has a pronounced peak at the BPF, while the off-design spectrum is fairly flat. This is typical of the entire speed range. The effect becomes somewhat more obvious when the broadband spectra are reduced to 1/3 octave band values, normalized with respect to the BPF level and plotted against a Strouhal number based on the blade pitch and speed:

$$\frac{\text{frequency x pitch}}{\text{wheel speed}} = f \times \frac{\pi D}{B} \times \frac{60}{\pi DN}$$
$$= f \times \frac{60}{BN}$$

where:

B = number of blades

D = diameter

= f/BPF

N = rpm

BPF = blade passing frequency

Typical results are shown in Figures 3.2-18 and 3.2-19. The noise can be seen to peak at the blade passing frequency (BPF) at settings near the design point. However, at extreme off-design operation, the spectrum tends toward a peak in the region of the second harmonic of the BPF. These conditions generally correspond to high incidence angles, which would result in skewed viscous wakes (Figure 3.2-20) containing higher harmonic energy content. This suggests that in turbines not only the discrete frequency, but also the broadband noise is controlled by viscous wake interaction.

It would appear then, that acoustic energy shifts from the BPF to the second harmonic with increasing incidence angle and would explain the observed change in spectral shape from takeoff to approach power for Quiet Engine "C" (Figure 3.2-21).

The pronounced peak of the single stage build is not repeated in the broadband noise spectra for the three stage build (see Figures 3.2-17 and 3.2-22) as there are no less than five viscous wake interactions contributing to the measured noise: the spectral overlap obfuscating the individual trends. Hence the shift to a flatter spectrum with off design operation is not as obvious as in the case of the single stage turbine. The spectrum for a multi-stage turbine should peak at the BPF of the stage that is dominant. Since the dominant stage is a combined function of the pressure ratio, which determines the source levels, and speed, which determines the attenuation, the peak shifts with operating point. Generally, the peak

occurs at the first stage BPF at low pressure ratios and speeds, and at the last stage BPF at high pressure ratios and speeds. This is consistent with the fact that the pressure ratio for the succeeding stages increases at a proportionally faster rate than for the first stage.

Normalized 1/3 octave band spectra are shown in Figure 3.2-23, with (a) defining the speed effect and (b) the pressure ratio effect.

Figure 3.2-24 provides a spectral overlay for the single and three stage builds at the turbine design point. The three stage build was actually quieter by some 12 to 15 dB even though first stage is doing the same work in both cases. The reason, no doubt, lies in the large noise attenuation due to the turbine blade rows. The attenuation due to each additional stage more than offsets the additional noise source introduced and the net effect is a significantly quieter turbine. This makes a good case for front-loaded turbines over uniformly loaded ones.

The broadband noise power levels were computed and correlated against pertinent performance parameters. The results for the single stage build are shown in Figures 3.2-25 through 3.2-28. In general, the pressure ratio provided the most consistent trends (Figure 3.2-25), the noise increasing at about a 40 log (pressure ratio) rate at constant speed. This figure also shows the noise to be a minimum at design speed - with small increases with change in speed in either direction.

Figure 3.2-26 provides the correlation with blade relative Mach number. Use of the value at the tip or at the hub, where the Mach number is the highest, produces exactly the same trends. There is an increasing trend with relative velocity for the two lowest pressure ratios (1.6 and 1.9). However, the most prominent feature at the two higher pressure ratios (2.2 and 2.5) is the pronounced dip in noise at the design speed point. It is not clear if this can be attributed to the turbine or to the facility, that is whether this was a source or a propagation phenomenon.

The correlations with tip speed (Figure 3.2-27) and rotor incidence angle (Figure 3.2-28) yield trends remarkably similar to the preceding. Note that the incidence angle correlation is analagous to one with the rotor turning angle since the exit angle is relatively invarient.

The corresponding three stage build results are, as in the case of the spectral shape, confused by the multitude of contributing sources and the absence of clear domination by any individual stage.

The correlations with the first stage and turbine pressure ratios are shown in Figure 3.2-29. On an overall basis, there is a small increase in noise with pressure ratio at constant speed. On an individual speed line basis, the noise versus pressure ratio line for each speed becomes increasingly flatter going from 70% N/ \sqrt{T} to 110% N/ \sqrt{T} . This could be a reflection of the change in relative contribution by the three stages to the overall spectrum. For example, at 70% speed the tone attenuation results indicate

relatively small attenuation of the first stage noise (~70% dB). The attenuation increases to over 30 dB at 110% speed. Hence the relative contributions from each stage can be expected to change with speed, as is illustrated schematically in Figure 3.2-30.

The same slope variation with speed line is discernible in the relative Mach number correlations provided in Figure 3.2-31. It is interesting to note that when the relative velocity into the first stage rotor is used, the 110, 100, 90, and 70% speeds separate out into different lines going from left to right. When the relative velocity into the second or third stage rotors is used, the 110, 100, and 90% lines almost merge together, while the 70% speed line stands alone and shifts to the left relative to the other speed lines.

The corresponding relative velocity correlations at constant turbine pressure ratio are shown in Figure 3.2-32. The only consistent relationship is provided by the relative velocity into the first stage rotor - the noise increases with both turbine pressure ratio and velocity.

The correlation with blade tip speed is examplified by Figure 3.2-33. Except for the lowest $P_{\rm R}$, there is some indication that the noise decreases with speed. The correlation with incidence angle is confused and is not shown here.

The common denominator between the single and three stage results is the relative velocity into the first stage rotor and the pressure ratio. For the three stage build the first stage and turbine pressure ratio yield similar results. In general, the broadband PWL increases with both pressure ratio and relative velocity.

However, since the single stage correlations suggest that relative velocity, tip speed, or turning angle (or incidence) can be used interchangeably, in the case of domination by any individual stage, the data may be correlated by a pressure ratio term in combination with any of the other three.

3.2.6 Summary and Conclusions

The significant results from the HLFT-IVA turbine tests are summarized below.

 Comparison of the downstream noise levels for the single and three stage results indicates significant insertion loss due to the second and third stages. Both the discrete frequency and broadband noise levels associated with the first stage were attenuated.

- The tone levels showed that the insertion loss was a function of the speed, work extraction, and the incidence angles associated with the second and third stages. The speed was the most dominant parameter, perhaps because it included the incident tone frequency and baffling tip speed effects. The insertion loss varied from 5 dB at 50% speed to over 30 dB at 110% speed.
- The reduction of the first stage noise by the second and third stages more than compensated for the additional noise sources associated with these two stages. Consequently, the three build was quieter than the single stage build with the first stage operating at the same condition in each case.
- Sound-separation was successfully employed to extract the turbine broadband levels.
- The single stage broadband noise spectral results showed a pronounced peak at the BPF near design operating points, with a large shift in energy to the BPF second harmonic region at off-design conditions. The resultant flattening of the spectrum for off-design conditions is consistent with observations from engine data.
- The three stage spectral results did not show any pronounced peaks, possibly because of the multiplicity of the contributing sources and attenuating blade rows. Small peaks could be discerned at one of the three BPF's at most points, but there was no clear domination by any individual stage.
- The broadband noise OAPWL was found to correlate with pressure ratio and relative velocity into the first stage rotor, generally increasing with both. The three stage noise data correlated with both the pressure ratio for the first stage and for the turbine. In the case of the single stage build, the relative velocity, the tip speed, and blade turning angle (or incidence) proved to be analogous parameters.
- The single stage results also suggest that deviation from design point could be a parameter.

Table 3.2-1 HLFT-IVA Design Characteristics

	1	Stage 2	3	Overal1
Wt. Flow Function, $\frac{W\sqrt{T}}{P}$	_	-	1	32.08
Loading, $\frac{gJ\Delta H}{\Sigma U_p^2}$	3.52	3.12	1.60	2.70
Pressure Ratio (Total)	1.73	1.81	1.41	4.72
Speed, N/\sqrt{T}	• • -	_	-	152
Nozzles Vanes	100	144	140	- -
Rotor Buckets	206	190	160	1 -
Radius Ratio	0.811	0.735	0.663	-
Tip Diameter at Stage Exit (in) (cm)	25 (63.5)	27.2 (69.1)	28.8 (78.2)	

Table 3.2-2 HLFT-IVA Pesign Details (Pitch-line)
• FPS Units

			Stage	
		1	2,	3
•	Stator Vane			
	Stagger Angle (deg)	31.5	25	17.5
	Chord (in)	1.280	0.890	0.986
	Blade-to-Blade Pitch	0.943	0.507	0.534
	Camber Angle (deg)	89.8	110.4	99.8
	T _{max} /Axial Chord (%)	14.06	9.17	7.63
	Rotor Blade			
	Stagger Angle (deg)	16	14	13
	Chord (in)	0.565	0.644	0.676
	Blade-to-Blade Pitch	0.345	0.390	0.470
	Camber Angle (deg)	112.5	110.3	83.6
	T _{max} /Axial Chord (Pct)	11.10	12.04	9.91
	Blade-Row Axial Spacing			
	Vane-Blade Spacing (in)	0.29	0.34	0.32
	Blade-Vane Spacing (in)	0.3	33 0.:	36
•	Flow Area at Acoustic			
	Measuring Sections			
	3-Stage Rig			
	Inlet Area (in ²)		92	
	Exit Area (in ²)		370	
	1-Stage Rig			
	Inlet Area (in ²)		92	
	Exit Area (in ²)		187	

Table 3.2-2 HLFT-IVA Design Details (Pitch-line)

• MKS Units

		S	tage		
		1	2	3	
•	Stator Vane				
	Stage Angle (deg)	31.5	25	17.5	
	Chord (cm)	3.85	2.26	2.50	
	Blade-to-Blade Pitch (cm)	2.35	1.29	1.36	
	Camber Angle (deg)	89.8	110.4	99.8	
	T _{max} /Axial Chord (%)	14.06	9.17	7.63	
•	Rotor Blade				
	Stagger Angle (deg)	16	14	13	
	Chord (cm)	1.44	1.64	1.72	
	Blade-to-Blade Pitch (cm)	0.88	0.99	1.19	
	Camber Angle (deg)	112.5	110.3	83.6	
	T _{max} /Axial Chord (%)	11.10	12.04	9.91	
•	Blade-Row Axial Spacing				
	Vane-Blade Spacing (cm)	0.74	0.86	0.81	
	Blade-Vane Spacing (cm)	0.84	0.91		
•	Flow Area at Acoustic				
	Measuring Sections				
	3-Stage Build				
	Inlet Area (cm ²)		594		
	Exit Area (cm ²)		2387		
	1-Stage Build				
	Inlet Area (cm ²)		594		
	Exit Area (cm ²)		1206		

Table 3.2-3 Low Pressure Turbine Test Matrix (HLFT-IVA)

- Design Speed, $N/\sqrt{T} = 152.2$
- Flow Function, $W/\sqrt{T/P} = 32.0$
- Inlet Absolute Total Pressure P_o = 40 psia (275.8 kN/m²)
- Inlet Total Temperature, T_o = 760° R (422°K)

				Press	ure Ra	tio (P	To/PS2)	
% Design	Speed	Sin	gle Sta	age Bu	ild	Thre	ee Stag	ge Bui	1d
Speed	(rpm)	1.6	1.9	2.2	2.5	2.0	3.0	4.0	5.2
50	2098	x	-	-	-	x	-	-	-
70	2937	x	x	x	-	x	x	x	-
90	3776	x	x	X	x	x	X	x	x
100	4196	x	X	X	X	x	x	x	X
110	4615	x	x	x	x	x	X	x	x

Repeat Points

Table 3.2-4 Tone Attenuation Parameters

									2nd Sto	Doto	- 44	Indidana A.	110
ZN/VT		APWL (dB)	dB)			(AT),	(AT), (R)		ליווח מרא	1, (deg.)	eg.)	in org. notor ith incluence angle	ng re
					-Turbi	ne Pre	SSIITO	urbine Pressure Ratio					
	2.0	3.0	3.0 4.0 5.2 2.0 3.0 4.0 5.2	5.2	2.0	3.0	4:0	5.2	2.0 3.0 4.0 5.2	3.0	4:0	5.2	
02	5.0	5		1	- 42 81 107	81	107	1	12 -3 +1 +4	Ŧ	Ŧ	7	
06	6.5	2.0	2.0 2.5 9.5 45 86 117 142	9.5	45	98	1117		-34 -15 -7 -4.5	-15	-1	-4.5	
100	16.0	9.0	9.0 8.0 13.0 48	13.0	84	92	92 115 145	145	-45.5 -21 -14 -10	-21	-14	-10	
110	14.0	14.0	14.0 19.0 25.0 51 90 117 144	25.0	51	8	117		-61.5 -40 -21 -16	-40	-21	-16	

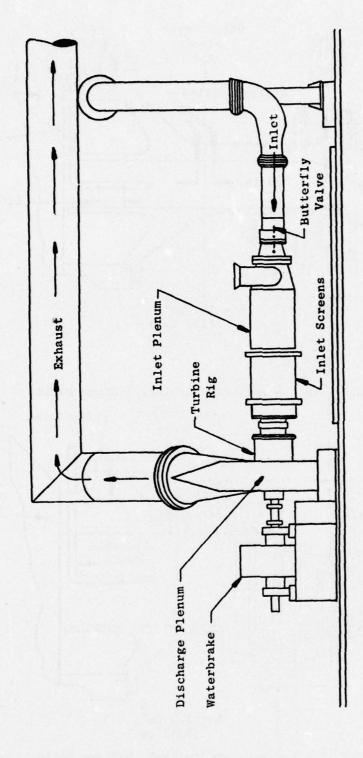


Figure 3.2-1 Warm Air Turbine Facility

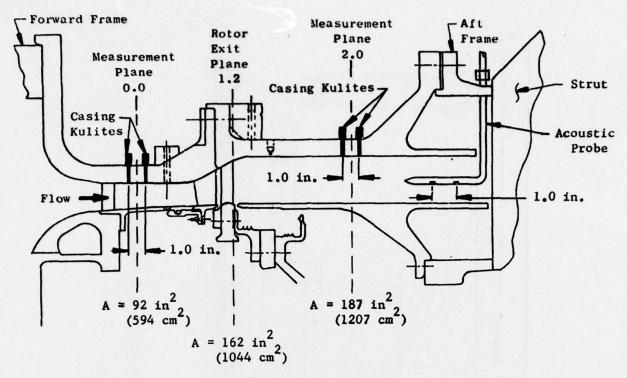


Figure 3.2-2 HLFT-IVA Low Pressure Turbine, 1-Stage Build

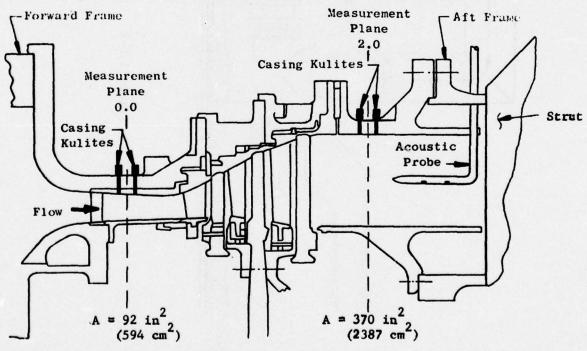


Figure 3.2-3 HLFT-IVA Low Pressure Turbine, 3-Stage Build

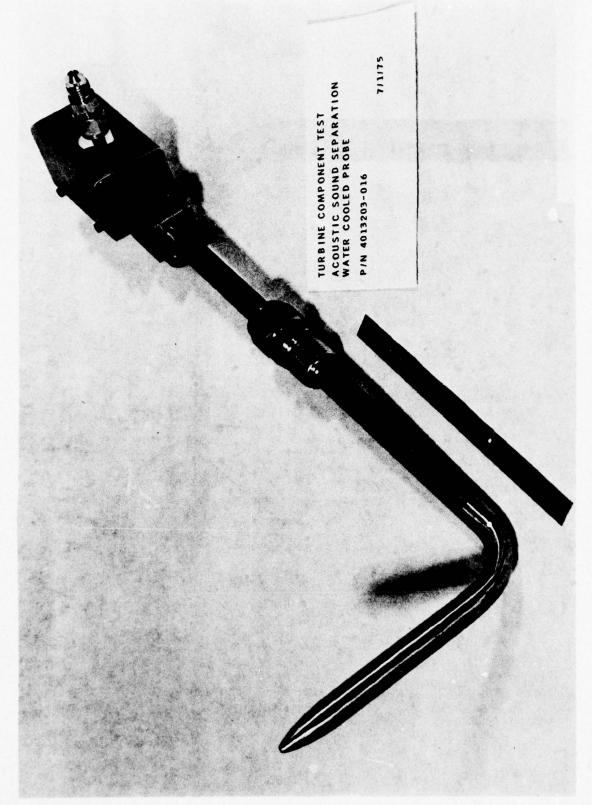
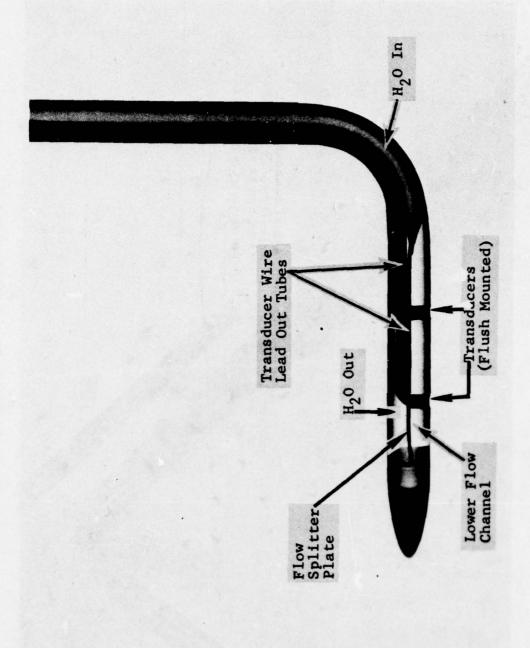


Figure 3.2-4 Water-cooled Sound Separation Probe



X-Ray Photograph of Water-Cooled Sound Separation Probe Figure 3.2-5

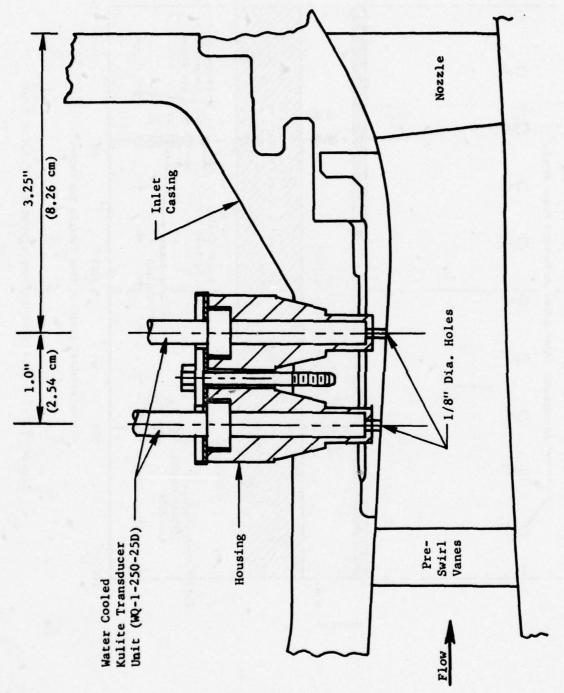


Figure 3.2-6 Inlet Kulite Mounting for HLFT-IVA

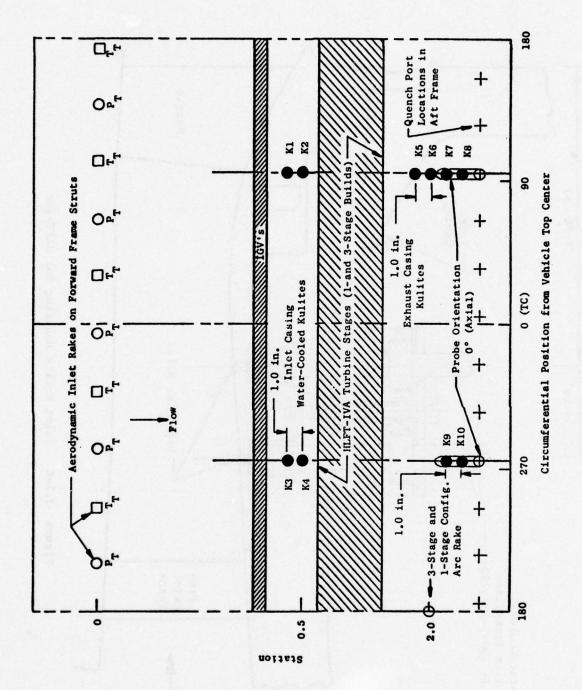


Figure 3.2-7 Instrumentation Layout for Turbine Test

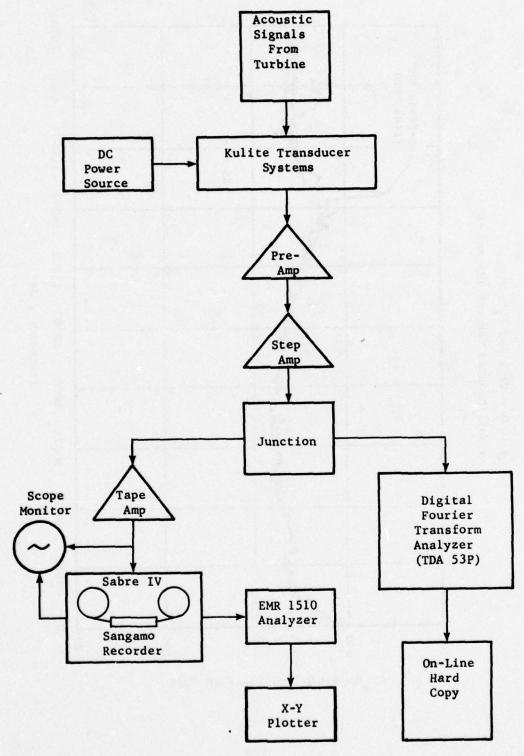


Figure 3.2-8 Acoustic Data Acquisition System



• 100% N/ \sqrt{T} , 1.9 P_R



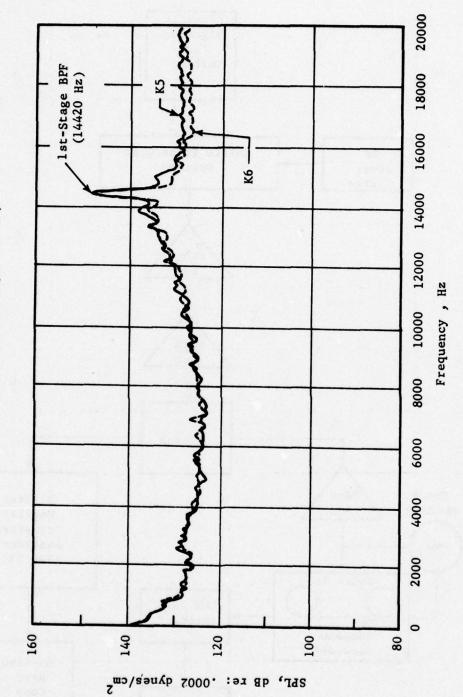
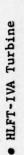


Figure 3.2-9 Autospectra for Single Stage Configuration



• 100% N/ \sqrt{T} , 5.2 P_R



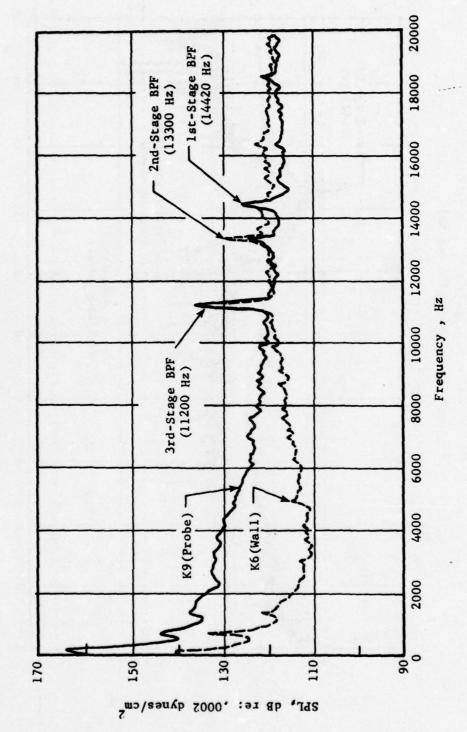
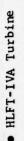
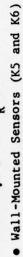


Figure 3.2-10 Autospectra for Three Stage Configuration



^{• 100%} N/ \sqrt{T} , 2.2 P_R



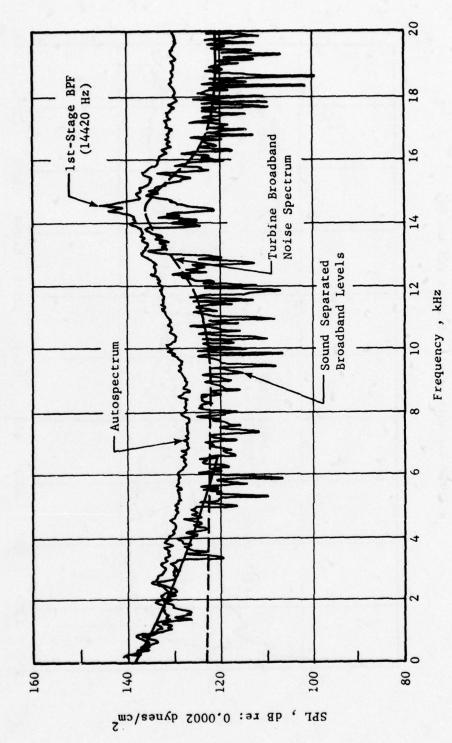


Figure 3.2-11 Downstream Broadband Noise for Single Stage Configuration

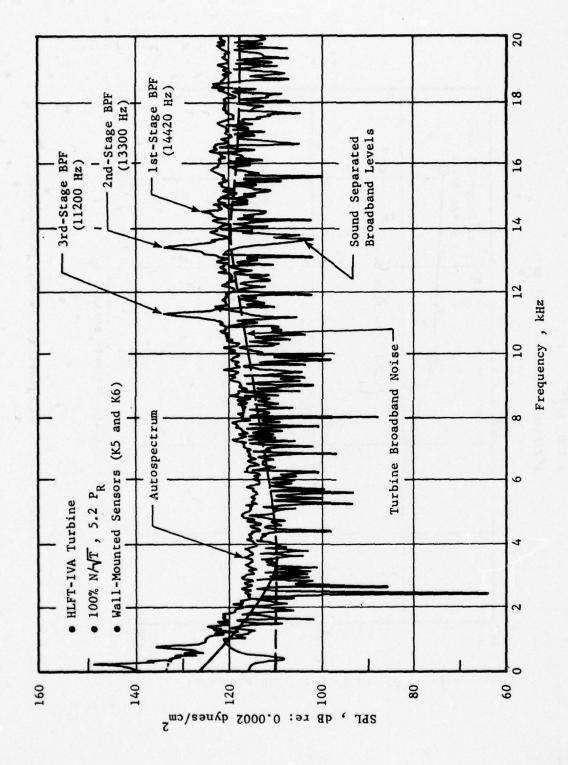


Figure 3.2-12 Downstream Broadband Noise for Three Stage Turbine







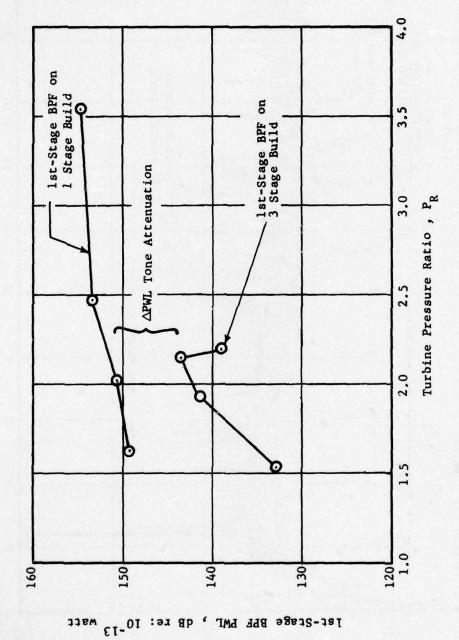


Figure 3.2-13 Determination of Tone Attenuation

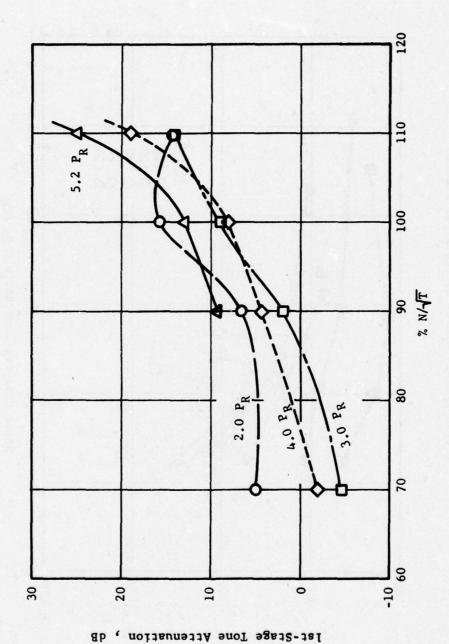


Figure 3.2-14 Tone Attenuation as a Function of Turbine Speed and Pressure Ratio



- Solid Symbols Denote Single Stage
- Open Symbols Denote 1st-Stage of 3 Stage

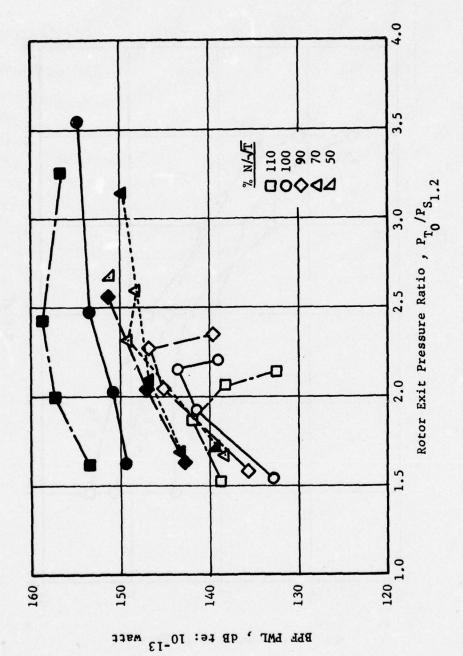


Figure 3.2-15 Tone PWL Data Trends

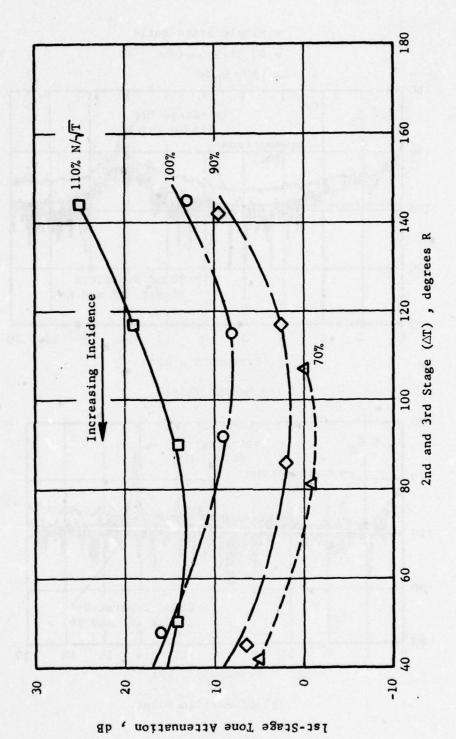
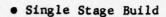
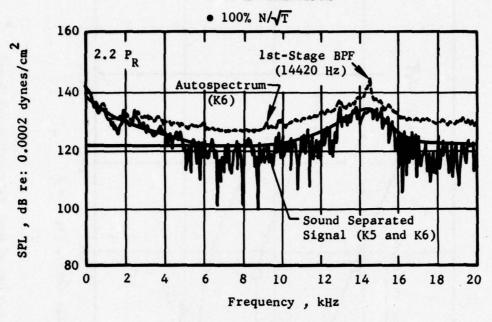
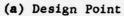


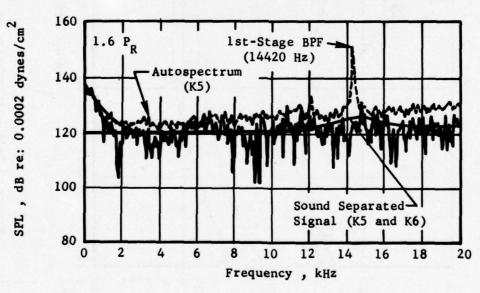
Figure 3.2-16 Attenuation as a Function of Work Extraction and Speed



• 40 Hz Bandwidth



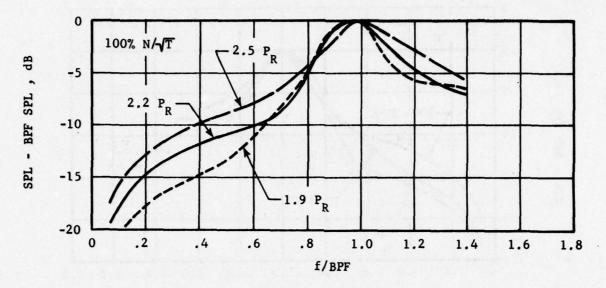




(b) Off-Design Point

Figure 3.2-17 Broadband Noise Spectra for Single Stage Build

- Single Stage Build
- 1/3-Octave Band Data



(a) Design Point

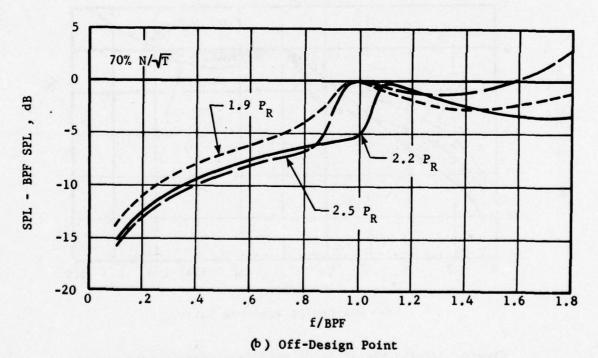
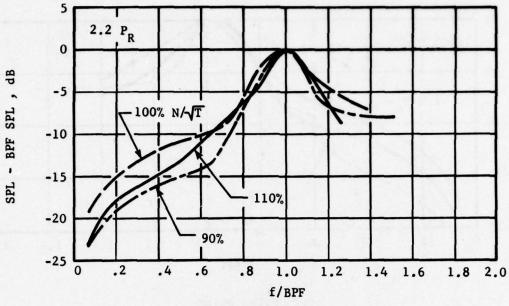


Figure 3.2-18 Variation of Broadband Noise Spectrum with Pressure Ratio for the Single Stage Build

- Single Stage Build
- One Third Octave Band Data



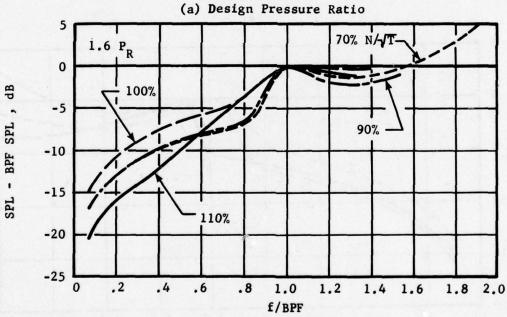


Figure 3.2-19 Variation of Broadband Noise Spectrum with Speed for the Single Stage Build

(b) Off-Design Pressure Ratio

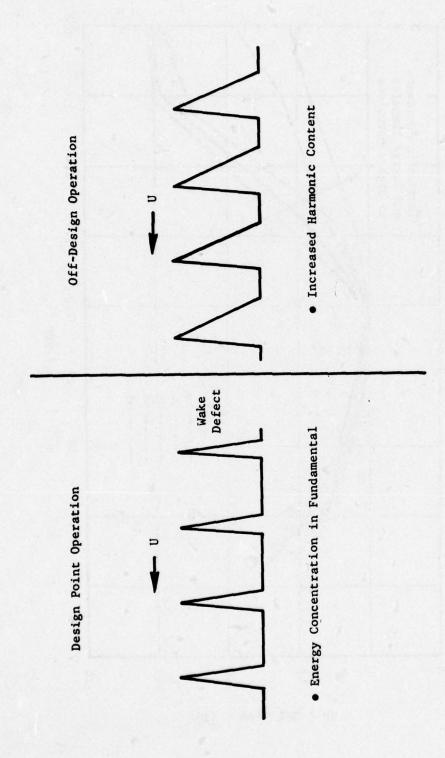


Figure 3.2-20 Viscous Wake Variation with Operating Point



- 150 ft (45.7 m) Arc
 - 120° Angle to Inlet

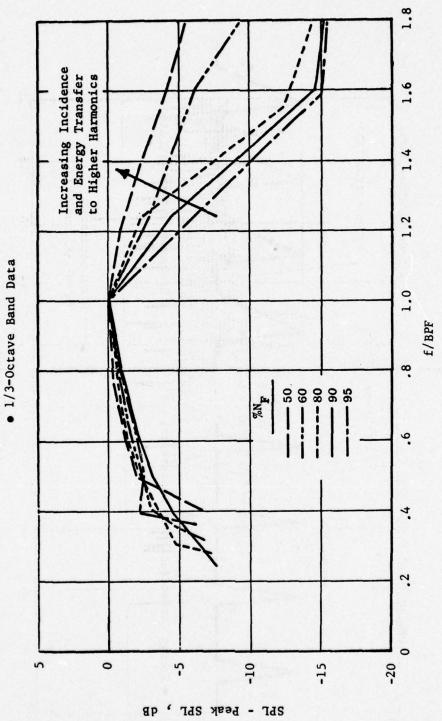
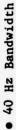
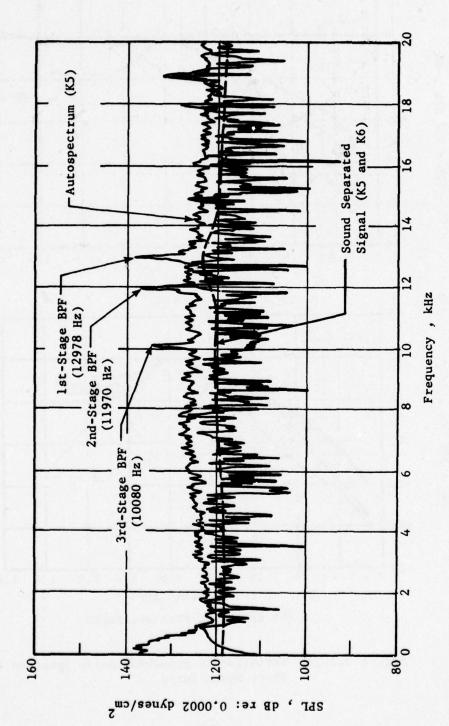


Figure 3.2-21 Variation in Turbine Broadband Noise Spectrum with Power Setting

• Three Stage Build

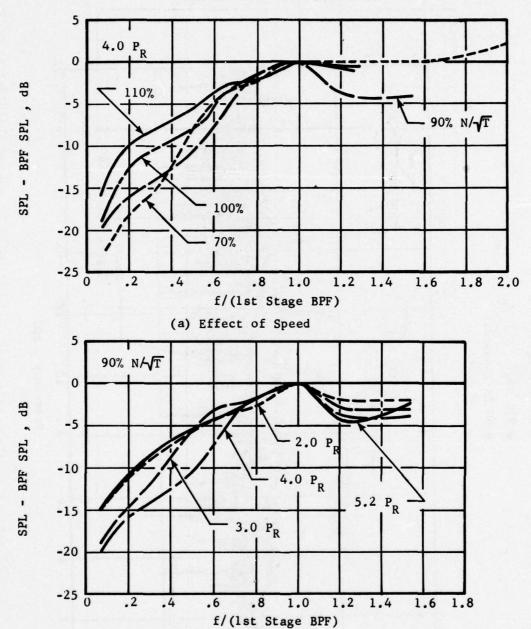
^{• 90%} N/√T , 2.0 P_R





Three Stage Build Broadband Signal at Off-Design Points Figure 3.2-22

- Three Stage Build
- One-Third Octave Band Data



(b) Effect of Pressure Ratio

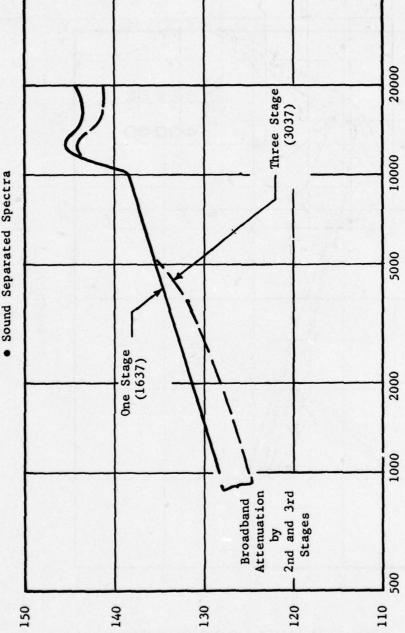
Figure 3.2-23 Variation in Broadband Noise Spectrum for Three Stage Build



T/N %06 .

• 1/3 Octave Band Data



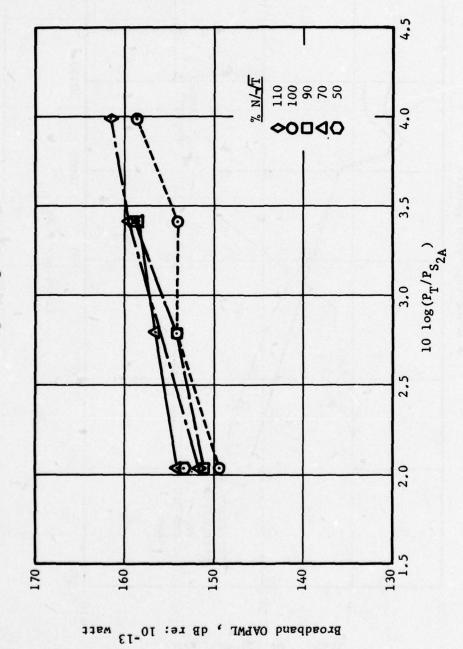


Broadband Noise Attenuation by Second and Third Stages Figure 3.2-24

Frequency , Hz

50000

PWL , dB re: 10-13 watt



Single Stage Build Broadband Noise Correlation with Stage Pressure Ratio Figure 3.2-25

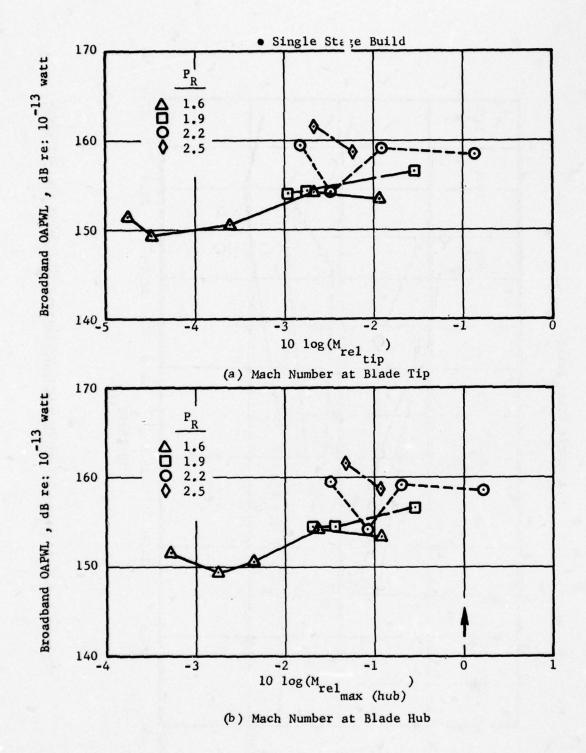


Figure 3.2-26 Single Stage Build Broadband Noise Correlation with Blade Relative Mach Number

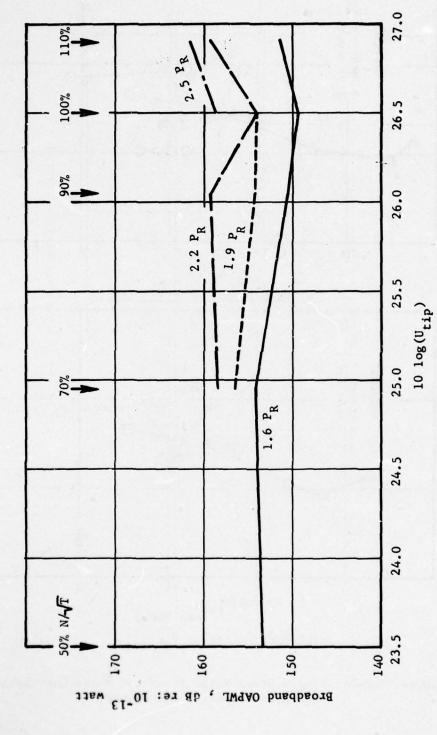


Figure 3.2-27 Single Stage Build Broadband Noise Correlation with Tip Speed

43.

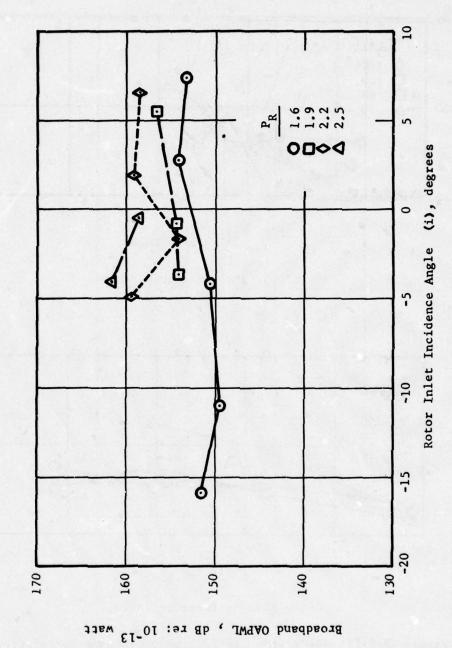
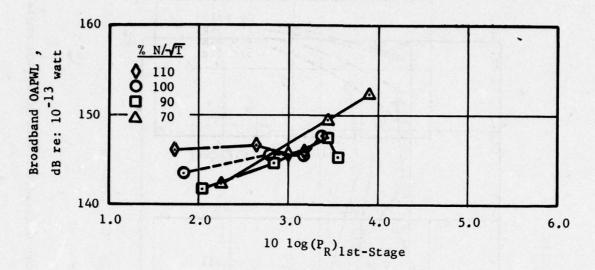
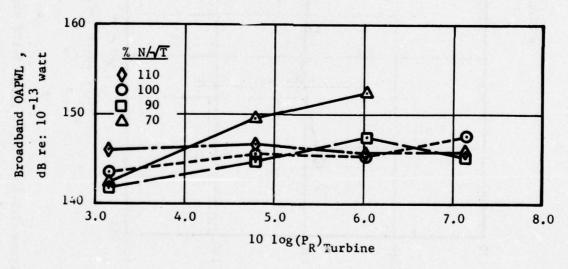


Figure 3.2-28 Single Stage Build Broadband Noise Correlation with Incidence Angle

• Three Stage Build



(a) 1st-Stage Pressure Ratio



(b) Turbine Pressure Ratio

Figure 3.2-29 Three Stage Build Broadband Noise Correlation with Pressure Ratio

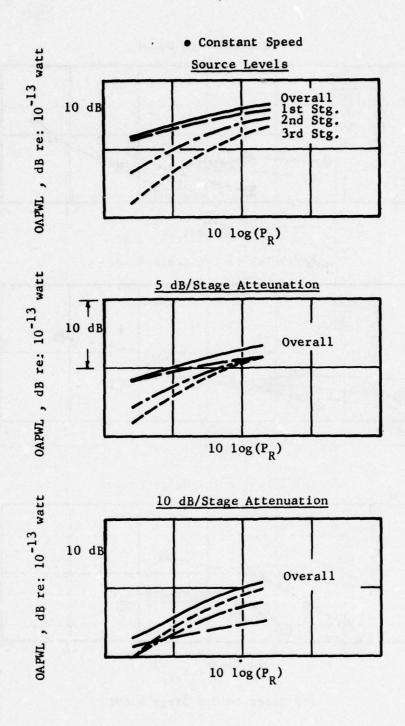


Figure 3.2-30 Schematic of Changes in Overall Noise Trend due to Varying Blade Row Attenuation

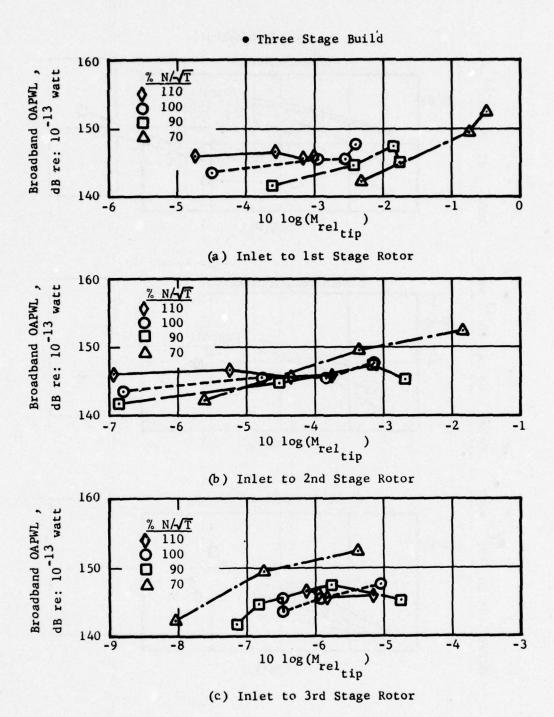


Figure 3.2-31 Three Stage Build Broadband Noise Correlation with Relative Mach Number (at Constant Speed)

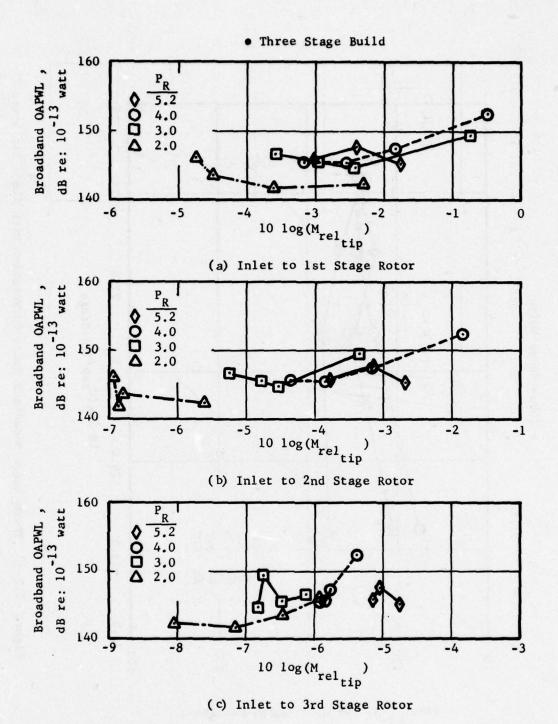


Figure 3.2-32 Three Stage Build Broadband Noise Correlation with Relative Mach Number (at Constant Pressure Ratio)

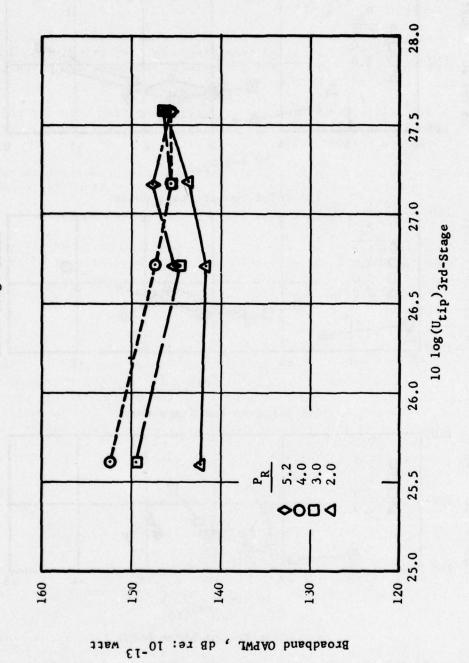


Figure 3.2-33 Three Stage Broadband Noise Correlation with Blade Tip Speed

3.3 TURBINE TONE/JET STREAM INTERACTION TESTS

3.3.1 Objectives

A parametric study of the analytical model for turbine tone scattering by jet stream turbulence identified tone frequency, jet velocities, and turbulence properties as significant parameters (Reference 29). The objectives of these model tests were to:

- (1) Parametrically exercise the tone frequency, fan velocity and jet velocity to individually define the effects of frequency, velocity, and velocity ratio.
- (2) Vary and establish the effect of turbulence properties through:
 - (a) Change in the axial position of the outer (fan) jet exhaust relative to the inner (core) exhaust.
 - (b) Use of turbulence generators placed on the cowls.

Since farfield information was to be obtained simultaneously at all angles, a third objective could be accomplished without much additional effort:

(3) Indicate the effect of the above variations on turbine tone directivity.

3.3.2 Test Description

The testing was accomplished concurrently with the Low Frequency Noise Directivity Tests described in Section 2.3. A description of the facility is included in that section. The siren used to simulate the combustor noise was also used to simulate turbine noise. The frequency range of interest here was much higher (greater than 3.15 kHz) and therefore a rotor with 60 slots was required instead of the one with 20 slots used for combustor noise.

The testing was accomplished in three series:

Task I - Parametric survey of jet velocities and tone frequency.

Task II - Exhaust Plane variation.

Task III - Additional Turbulence generation using vortex rings immersed in the flow.

The parametric tests were conducted using a short fan duct (Figure 3.3-1) representative of the CF6 geometry. The fan exhaust plane is roughly one fan diameter (L/D-1) upstream of the core exhaust plane. The relative exhaust plane location tests used this and three other geometries, namely a long fan duct (L/D-0.5), coplanar exhausts (L/D-0) and extended fan exhaust (L/D-0.5), in addition to the short fan duct. All four configurations are

shown in Figure 3.3-2. Additional turbulence generation was through vortex rings on both the fan and core shrouds, as shown in Figure 3.3-3. Detailed dimensions can be found in Section 2.3. The value of D was approximately 10 in. (25.4 cm).

A master test matrix was established after consideration of approach and take-off velocity settings for current high bypass turbofan engine cycles (Table 3.3-1). This matrix is shown in Table 3.3-2 and was constructed to encompass the operating line for the engines of Table 3.3-1. Eleven dual flow combinations were selected, ranging over velocity ratios of 0.6 to 1.15. In addition, no flow, fan flow only, and core flow only settings were used. The entire matrix was utilized for the Parametric Survey (Task I) tests.

The matrices for Tasks II and III are shown in Tables 3.3-3 and 3.3-4. The former consisted of the frequency survey at the "mean" approach power point, namely $V_{\rm core}$ = 800 fps (244 m/s) and $V_{\rm fan}$ = 680 fps (207 m/s). The Task III matrix consisted of a velocity ratio variation at $V_{\rm core}$ = 800 fps (244 m/s), one on either side of the approach power point, with a frequency survey at each of the three velocity ratios.

The frequency survey consisted of setting siren fundamental points of 3.15, 4.0, and 5.0 kHz. The associated higher harmonics gave tones at 6.3, 8.0, 9.45, 10.0, 12.0, and 15.0 kHz.

Farfield data were acquired with the same microphones and system described in Section 2.3. The microphones were elevated to 16 ft (4.9 m) and placed on a 40 ft (12.2 m) arc. Ground reflections do not represent a problem for the frequencies of interest here and therefore flush mounting on the ground was not required. Thirteen farfield angles from 40° through 160° at 10° increments were covered.

Some data were acquired on the levels inside the core using a wave-guide probe and B&K microphone. The system is shown schematically in Figure 3.3-4. The siren levels at the source were monitored using a Kulite transducer immediately downstream of the siren exit port.

The data were recorded using the same tape system described in Section 2.3. Approximately 2 minutes of data were acquired at each siren setting.

3.3.3 Test Results

A farfield spectrum for a no-flow point is shown in Figure 3.3-5. The siren was nominally set at 4 kHz and the fundamental tone is clearly visible, along with harmonics at 8, 12, 16, and 20 kHz. The 4th and 5th harmonics were not always discernible for the dual flow points and hence only the first three tones were utilized in the analysis.

The spectrum of Figure 3.3-5 was obtained using analog data reduction. This type of data reduction processes a continuous 12.8 second sample from the tape. On the other hand, digital processing of the data enabled spot sampling of the entire two minute tape segment. This is believed to be inherently more accurate, particularly for tone data. Hence the vast majority of the data were processed digitally. A second advantage of the digital processing was that a smaller band width (10 Hz) could be utilized. This yielded a 6 dB improvement in signal/noise ratio over the analog processing.

3.3.4 Data Analysis

Characteristics of Haystacking

It is helpful to briefly review the turbulence scattering mechanism and the general characteristics associated with "haystacking" before discussing the test results.

"Haystacking" can be attributed to turbulence scattering of turbine tones by inhomogeneities in the exhaust jet mixing regions. Using a simplified analytical model, it has been shown in (Reference 1) that as a coherent (discrete frequency) signal propagates through a region of turbulence, part of the incident acoustic energy is redistributed into a scattered wave by the turbulence cells. The change of inhomogeneities in time, as seen by the incident wave, produces a change in the frequency of the scattered wave and results in a broadening that can be inferred from the form of the time autocorrelation functions of the amplitude and phase fluctuations. In particular, the frequency spread is determined by the correlation time of the turbulence eddies. The amplitude transformation is a strong function of the correlation length, of the eddies, and the turbulence intensity.

In the period since this modulation mechanism was first suggested by General Electric (during the Core Engine Noise Control Program) several investigators have indicated their apparent corroboration (References 18, 23, and 29).

The analytical model splits the farfield signal into two distinct parts:

- (a) the unaffected, or residual, portion of the initial wave;
- (b) the scattered or modulated wave.

The residual portion consists of the surviving discrete frequency signal. The scattered wave, however, reflects the turbulence spectrum and consists of a "haystack" of noise, the peak frequency of which exhibits a Doppler shift due to the fact that the scattering cells are in motion. When the scattered wave contains less acoustic energy than the residual tone, a discrete frequency spike is seen capping the haystack (somewhat obscuring the

Doppler shift of the haystack). When the scattered wave contains more energy than the residual tone, there is no visible tone content, and the haystack peak frequency shift can be observed quite clearly (the peak moving to higher frequencies as the observation angle, measured from the inlet, increases—see Figure 3.2-6).

The initial (or residual) tone content was unfortunately very much in dominence all throughout the tests and the haystacking effect therefore at times difficult to define. However the model test spectra shown in Figure 3.2-7 clearly reveal both components for that particular setting. The scattered wave can be observed shifting in frequency with the farfield angle as would be expected.

While these spectra establish that the siren tones were subjected to turbulence scattering, the magnitude of the effect was much lower than expected.

To get some idea of the magnitude of the interaction effect, the tone levels for the zero flow and fan flow only were compared. The parametric test results indicated that both the fan velocity and velocity ratio were important determinants of the scattering (as will be shown later). Hence, the maximum interaction for a given fan velocity would be encountered for "zero" core flow. Actually, the siren flow always produced a core flow, roughly 100 fps (30.5 m/s). Figure 3.3-8 gives the tone power levels for the short fan duct configuration at these two conditions. The circles provide the PWL's for the "no flow" case and the triangles the levels with no core flow but with V_{fan} = 680 fps (207 m/s). The difference between the two should be the maximum tone scattering encountered for Vfan = 680 fps (207 m/s). This difference is plotted against the frequency at the bottom of the figure. It appears that the amplitude loss increases as (frequency)2, as would be expected from analysis, only above 9 kHz. Below this, one observes only about 2 dB per frequency doubling instead of the 6 dB predicted by the analysis. Because the onset of the scattering effect was somehow delayed in the spectrum, the max interaction loss at 15 kHz, for example, is 6 dB. If the scattering had begun at 3.15 kHz, as was expected, the max interaction loss would have been 14 dB!

The reason scattering was expected to start at 3.15 kHz was because the turbulence eddy size in the fan stream reaches roughly $(\lambda/4)$ for a 3.0 kHz tone at the approach setting $(V_{fan} = 680 \text{ fps})$. The turbulence eddy size, l_c , is computed using:

$$1_c = 0.4b/(1 + 0.38M_{fan})$$
 (3.3-1)
and From Reference 29
 $b/D = 0.21 [(Z/D) - 0.2]$ (3.3-2)

where b is the shear layer thickness, Z the axial location downstream of the nozzle exit plane, D the fan nozzle diameter and M the jet Mach number. Using D = 10 (25.4 cm) inches; $Z/D \sim 2$ - that is, the tone propagates out into the fan shear layer about one fan diameter downstream of the core nozzle exit; and V_{fan} = 680 fps (207 m/s):

 $1_c \sim 1.25$ inches (3.18 cm)

b ~ 3.8 inches (9.65 cm)

Therefore, $1_c \sim \lambda/4$ for 3 kHz.

Instead, the scattering phenomena appears only after the turbulence eddies approach wavelength size. That is, the effects become discernible only when at least a complete cycle is subjected to scattering. The $\lambda/4$ limit shows when an acoustic signal will "recognize" an eddy as an obstruction. Apparently, recognition is not enough. A full cycle of disruption is the limiting criterion.

The relatively small amount of scattering coupled with the data scatter inherent in the use of tones in outdoor testing made it difficult to establish trends in certain cases.

The analytical model essentially postulates acoustic energy conservation as there is no absorption mechanism involved. Energy loss has been noted for sound transmission in a turbulent medium (Reference 35) but the loss was limited to frequencies below 2000 Hz. In an effort to verify the energy conservation for high frequency noise transmission, "source noise" data were acquired inside the core nozzle using a wave-guide probe. Figure 3.3-9 compares the interior sound pressure levels with the corresponding farfield levels for the different tones. The nominal difference between the two spectra is due to the different areas, specific impedance and air attenuation. The exact difference varies considerably from tone to tone apparently because of the presence of a reflected wave in the core nozzle. Hence the probe data proved to be less than valuable. It is recommended that sound-separation probes be utilized for duct measurements of all kinds since these probes can distinguish between forward and backward travelling waves.

Effect of Frequency and Velocity on Scattering

The parametric survey tests were dedicated to quantification of the dependence on the tone frequency, core velocity, and fan velocity.

Figure 3.3-10 demonstrates that the haystacking increases with frequency; all other variables being held constant. Propagation of a tone through jet stream turbulence results in an energy transfer from the discrete incident tone frequency to adjacent frequencies in the form of the scattered wave. Hence, as discussed in the analysis, the farfield spectrum

will contain two signals: an incident wave manifested as a discrete frequency spike and a scattered wave consisting of a hump roughly centered (for certain observation angles) at the tone frequency. Assuming energy is essentially conserved during the scattering process and the loss in the discrete frequency tone amplitude is paralleled by a corresponding increase in the haystack size. A convenient measure of the scattered wave energy is then provided by the slope of the hump. Figure 3.3-10 shows that this slope is roughly doubled going from 8 to 16 kHz. Therefore, the interaction effect is given by 20 log (frequency) as used in the existing prediction method. Figure 3.3-8 indicated the same result based on the drop, δ , in the tone amplitude. It can be observed that the dependence below 8 to 9 kHz was much less. The break point is when the incident wavelength approaches or is smaller than the turbulent eddy size.

The determination of velocity effects was made on the basis of tone power level rather than SPL at any given angle in order to eliminate the effect of refraction and convection by the jet streams.

Figure 3.3-11 shows the effect of the fan velocity on the power level (PWL) for the 4.0 and 8.0 kHz tones. The scattering is given by the drop in this discrete frequency PWL. In general, the scattering is seen to increase with the fan velocity. The energy transfer suffered by any tone is a function of the turbulence encountered in both shear layers. Normally, the turbulence seen by the tone in the outer shear is dominant and the scattering well defined by the parameters describing the outer mixing region alone. However, the $V_{\rm core}$ = 500 fps setting for the 8 kHz tone shows a small initial increase in PWL with increase in fan velocity. This result is typical of the results for the other tone frequencies and is apparently a consequence of the fact that the shear between the fan and core streams decreases with increasing fan velocity when the core velocity is held constant (with $V_{\rm fan} < V_{\rm core}$). For $V_{\rm core}$ = 500 fps the fan velocities involved are so low that the $|V_{\rm core} - V_{\rm fan}|$ effect is able to reverse the trend.

Change in core velocity obviously effect the radiated PWL - apparently increasing with velocity. This must be taken into account when comparing data sets at different core settings.

A multiple regression analysis was conducted using V_{fan} and $|V_{core} - V_{fan}|$ as the independent parameters and the following average fit was obtained using all the tone sets:

Scattered PWL \approx 10 log(V_{fan}/c) + 10 log [1 + $|V_{core}-V_{fan}|/c$] $^{2/3}$ (3.3-3) c = ambient acoustic velocity

Note that $[1 + |V_{core}-V_{fan}|]$ is very similar to the velocity ratio. The velocity ratio would involve a V_{fan} term in the denominator which would require a compensating increase in dependency on the first term (V_{fan}/c) to the 5/3 power.

Including the frequency dependence gives:

Scattered PWL = $10 \log (V_{fan}/c) [1 + |V_{core} - V_{fan}|/c]^{2/3} (f_o^2)$ (3.3-4)

Effect of Varying Fan Shroud Length on Scattering

Theoretically, the greater the distance between core and fan exhaust planes, the greater the haystacking because of increasing fan stream shear layer thickness seen by the turbine tones. Hence, the short fan duct should result in the most tone modulation and the coplanar configuration the least. The extended fan duct was an unknown quantity.

Narrowband spectra for the four configurations are compared in Figure 3.3-12 at the 130° angle. This figure shows the farfield 40 ft (12 m) arc signature using a 3.15 kHz siren fundamental. Similar results are available for 4.0 and 5.0 siren fundamentals, giving a total of 14 tones for each configuration. The 130° angle was selected for the comparison because the Doppler shift imposed on the haystack causes it to shift out from under the "incident" tone and thereby makes it readily discernible. From observation of the haystack, or the absence thereof, it is apparent that both the coplanar and extended shroud result in very much reduced tone scattering. For example, the siren fifth harmonics still retain their tone identity for the coplanar and extended shroud configurations, while they are lost in classic haystacks for the short and long fan shroud configurations. If anything, the extended fan shroud reduces haystacking even more than the coplanar configuration, which was somewhat unexpected. The reduction may be due to the fact that the fan and core streams in the extended duct configuration meet at lower Mach numbers than would be the case for fully expanded flows.

Since the energy in the haystacks is derived from the incident tones, a corresponding loss (or gain) in tone amplitude should be noted for each configuration. As in Task I, the amplitude comparison was made on a power level (PWL) basis in order to accommodate directivity variations. Unfortunately, due to the delayed onset (above 9 kHz) of turbulence scattering, the amplitude change involved was fairly small and not immediately apparent (see Figure 3.3-13).

Engine data were used in FA72WA-3023 to show, that reducing the relative distance between fan and core exhaust planes resulted in reduced haystacking (Figure 3.3-14). The same data also showed that this effect could be approximated by 20 log (1 + L/D) where L is the distance between fan and exhaust planes and D) the fan exhaust diameter. However, the turbulence scattering analysis (see Reference 29) suggests that the fan diameter may not be necessary as a non-dimensionalizing parameter. This is obviously a critical point.

Four configurations were tested: L/D=1, 0.5, 0, -0.5. If the effect were defined by 20 log (1+L/D), then the difference between the L/D of 1 (short fan shroud) and 0 (coplanar shrouds) would be 6 dB on the tone levels. On the other hand, since D was 6 ft for Quiet Engine 'C', then the engine data would equally well support 20 log (1+L/6). In the model tests L was about 0.9 ft, in which case the difference in tone levels for the two configurations would be about 1.2 dB. Considering the data scatter band $(\pm 1.5 \text{ dB})$, which is very good for tones in outdoor testing), the latter would result in negligible difference in the tone levels for the different configurations.

The data, several of which have been verified by repeat points, in fact indicate there is little difference in the tone levels (Figure 3.3-10), even though the haystacking in the form of frequency broadening is visibly reduced at the base by reducing L (Figure 3.3-12). This task then supports the contention that it is the absolute value of L that is important rather than L/D.

Effect of Additional Turbulence Generation on Scattering

Figure 3.3-15 presents two typical results in the form of directivity plots for the 5 and 8 kHz tones. At this velocity setting there is very little effect on the 5 kHz tone. However, the 8 kHz tone is significantly reduced at the peak angles (100 to 120°). Frequencies lower than 5 kHz tend to follow the 5 kHz trend, and those above, the 8 kHz trend.

On a power level basis, the results are provided in Figure 3.3-16. For 6300 Hz and higher tones, both turbulence generators result in power level reductions of 3 to 8 dB. However, below 5000 Hz the turbulence generators appear most effective at the lowest fan velocity (560 fps), giving 2 to 5 dB reduction over the baseline configuration. By the time the fan jet velocity is increased to the value of the core jet velocity (800 fps), at most 1 dB reduction is observed, and in fact the core shroud turbulence generator gives a tone increase of almost 6 dB at 4000 Hz. This last could be linked to the appearance of ring-induced tones at 1000 Hz and higher harmonics, including 4000 Hz.

In a brief summation, the turbulence generators effectively decrease the tone power level for 6300 Hz and above. Below this frequency, the generators are effective at low fan stream velocities only, the reduction being negligible when the fan stream velocity becomes equal to the core stream velocity. Both generators produce the same effect.

It could be hypothesized that the size of the turbulence eddies produced by the vortex rings varies with the flow velocities. The eddy size produced at the lower velocities could then be more conductive towards scattering of the lower frequencies. The higher frequencies would not be effected as greatly since the wavelengths are much smaller.

Directivity Effects

The short, long and coplanar fan shroud configurations produced similar directivities and are discussed below. The directivity patterns associated with the extended fan shroud were unique to that configuration and will be discussed separately at the end of this section.

Figure 3.3-17 provides the change in directivity going from "no flow", to fan only, to dual flow for the 3.15 kHz tone. The "no flow" directivity is shown separately on the left hand side and exhibits lobes similar to those one might expect from a piston in an infinite baffle (see Figure 3.3-18). The piston involved here is actually annular and the sound pressure in the farfield can be approximated by (refer to Figure 3.3-18(a)):

$$P^{-(j\rho_0 ck/2\pi r)U_0}e^{j(\omega t-kr)}$$
 $a_1^{\int_{\sigma d\sigma}^{a_2}}$ $\int_{e^{jk\sigma sin\theta sin\psi}d\psi}^{2\pi}$

or

$$P = (\rho_0^{ck/2\pi r})U_0^2 \left[J_1(ka_2^{sin\theta})/ka_2^{sin\theta} - (a_1/a_2)^2 (J_1(ka_1^{sin\theta}/ka_1^{sin\theta})) \right]$$

for $a_1/a_2 << 1$ this results in the directivities shown in Figure 3.3-18(b). Initially, for very low frequencies the angular distribution resembles that of a simple source since for $(kasin\theta) < 1$

$$2J_1(kasin\theta)/kasin\theta \sim 1 - (kasin\theta)^2/8 + \dots$$

The infinite baffle assumption is obviously violated by the fan flow. However, even then a lobed pattern is still visible for the fan flow only case shown in Figure 3.3-17. Also apparent is a shadow angle extending through 130° and an increase in the forward quadrant. It would seem that there is a shift in acoustic energy from the aft to the front, a throw-back which can be attributed to refraction effects. Unfortunately, existing refraction theories are somewhat defficient in this area.

Turning on the core flow has a very large effect on the directivity. Only one major lobe remains, peaking around 100 to 130°, and the shadow angle increases. The core flow alters the nozzle radiation characteristics from those of the piston in the wall model. The increasing shadow angle is a consequence undoubtedly of the refraction by the core jet. Also, a drop in source power level is indicated by the farfield data and confirmed by probe measurements in the core nozzle.

The dual flow directivity pattern shown in Figure 3.3-17 is representative of the patterns observed for other frequencies and velocity settings.

The effect of frequency is small but well-defined. The peak angle shifts towards the sideline inversely with frequency, as is shown in Figure 3.3-19. The major impact appears in the angles forward of 120° where the fall-off tends to increase with frequency. There is also a similar change

at $140 - 160^{\circ}$, but this is of little consequence in the case of an aircraft flyover.

The effect of velocity ratio at constant core velocity and constant fan velocity is illustrated in Figure 3.3-20 and there are no discernible trends.

The effect of power setting corresponds to a combined change in frequency and velocity ratio. Assuming the cycle for Engine "C", the difference between the approach and take-off settings is shown in Figure 3.3-21, and appears to be negligible.

Turbulence generators could effect the directivity since the additional scattering is concentrated at the peak angles. However, since the tone energy is scattered mainly into sidebands, the effect on a 1/3-octave band directivity will be negligible until the haystack spills over into adjacent 1/3 octave bands.

One of the most striking results from this test series was the appearance of a second lobe near 90° for the directivity in the case of the extended fan shroud configuration. The directivity observed for the other configurations showed only one peak (near 120°) for dual flow points. Typical comparisons are provided in Figures 3.3-22 and 3.3-23. The second lobe is apparent at all four frequencies shown in the figures. Simultaneously, there is a drop in the levels at the conventional peak angle.

3.3.5 Summary and Conclusions

The turbine tone/jet stream model tests provided the following significant results:

- The tests produced all the salient characteristics associated with haystacking in engines, including the appearance of a haystack (scattered wave) exhibiting a peak frequency shift with observation angle.
- $\begin{array}{lll} \bullet & \text{Both shear layers were found to contribute to the scattering.} \\ & \text{The outer layer through V_{fan} and the inner layer through} \\ & |V_{core}\text{-}V_{fan}| \,. \end{array}$ The scattering increased with both.
- The dependence of the tone amplitude loss and frequency spread on the incident tone frequency was explicitly extracted and shown to be f_0^2 .
- The scattering mechanism was found to be significant only for wavelengths of the order of or smaller than the turbulence eddy size. As a result, the amplitude loss was much smaller than expected.

- The haystacking, in the form of frequency modulation, was reduced by the coplanar and extended configurations. The extent of the reduction noted for the former was somewhat unexpected. Correponding amplitude modulation was hard to discern, partly as a result of data scatter and partly due to lower tone amplitude loss than expected.
- The variation of the fan exhaust plane showed that the important parameter was the absolute value of the distance (L) between the fan and core exhaust planes and not the number of nozzle diameters (L/D). The scaling dimension is therefore (L + constant), not D.
- The turbulence generators effectively decreased the tone PWL for model frequencies of 6.3 kHz and above. Below this, the effectiveness was limited to low fan velocities and/or low velocity ratios. The impact was concentrated near the nominal peak angles (100 to 120°).
- In general, for dual flow points, the tones were observed to peak at 120° and fall-off in both directions. Slight variations were noted with tone frequency.
- The extended fan shroud introduced a second lobe near 90°, while reducing the level of the primary lobe at 120°.

Table 3.3-1 Typical Velocities and Exhaust Temperatures for Current Technology High Bypass Engines

• Mean Area Ratio (fan/core) = 3.0

Takeoff

Engine	v _{core}		V _{fan}		Velocity	Tcore	
area areas	fps	(m/s)	fps	(m/s)	Ratio	•R	(°K)
CF6-6	790	(241)	660	(201)	0.84		-
CF6-50	800	(244)	690	(210)	0.86	1300	(722)
TF34	520	(158)	515	(157)	0.99	-	-
QEP 'A'	640	(195)	510	(155)	0.79	-	-
QEP 'C'	460	(140)	520	(159)	1.13	-	11111

Approach

Engine	V		V _{fan}		Velocity	Tcore	
	fps	<u>(m/s)</u>	fps	(m/s)	Ratio	• R	(°K)
CF6-6	1330	(405)	930	(284)	0.70	-	-
CF6-50	1550	(472)	1030	(314)	0.66	1500	(833)
TF34	920	(280)	715	(218)	0.78	-	-
QEP 'A'	1180	(360)	790	(241)	0.67	-	-
QEP 'C'	870	(265)	840	(256)	0.96	-	-

Table 3.3-2 Parametric Survey Test Matrix

Frequency Survey: Siren Fundamentals at 3.15, 4.0, 5.0 kHz + Harmonics

Core Velocity			Velocity Ratio				
fps	(m/s)	0	0.6	0.7	0.85	1.0	1.15
0	(0)	x					x
500	(152)			x	х	x	x
800	(244)	x		x	х	x	x
1200	(366)		x	x	x		

Table 3.3-3 Exhaust Plane Variation Test Matirx

• T_{fan}= Ambient

Frequency Survey:

Siren Fundamentals at 3.15, 4.0, 5.0 kHz + Harmonics

 $V_{core} = 800 \text{ fps } (244 \text{ m/s})$

 $V_{fan} = 680 \text{ fps } (207 \text{ m/s})$

Velocity Ratio = 0.85

The frequency survey was conducted at this setting for each of the four configurations.

Table 3.3-4 Turbulence Effects Test Matrix

- T_{core}= 1400 ° R (778 ° K)
- T_{fan}= Ambient

Frequency Survey:

Siren Fundamentals at 3.15, 4.0, 5.0 kHz + Harmonics

 $V_{core} = 800 \text{ fps } (244 \text{ m/s})$

V_{fan} = 560, 680, 800 fps (171, 207, 244 m/s)

Velocity Ratios = 0.70, 0.85, 1.00

The frequency survey was conducted at each of the three velocity settings for both configurations.

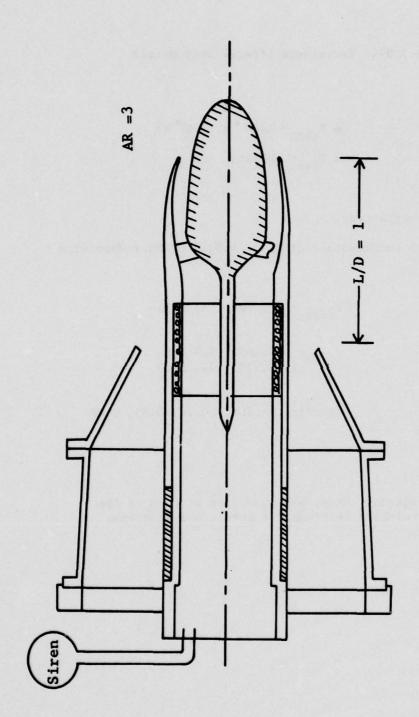


Figure 3.3-1 High Bypass Nozzle Configuration Used for Parametric Survey

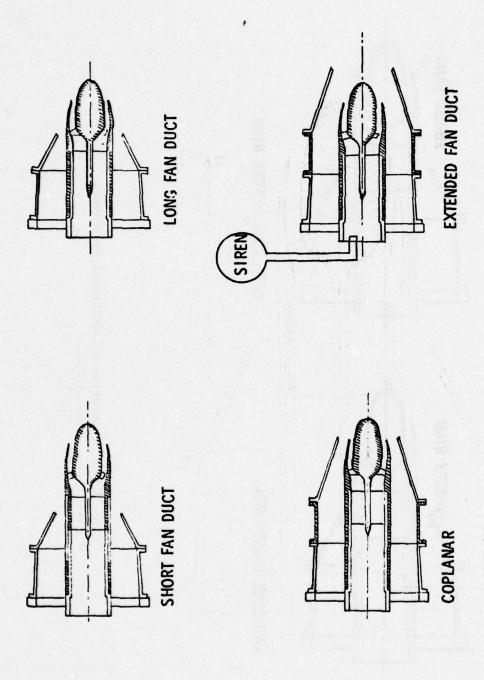


Figure 3.3-2 Variation of Fan Nozzle Exhaust Plane

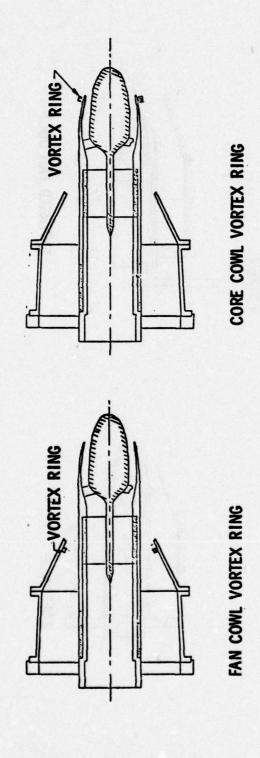


Figure 3.3-3 Generation of Additional Turbulence

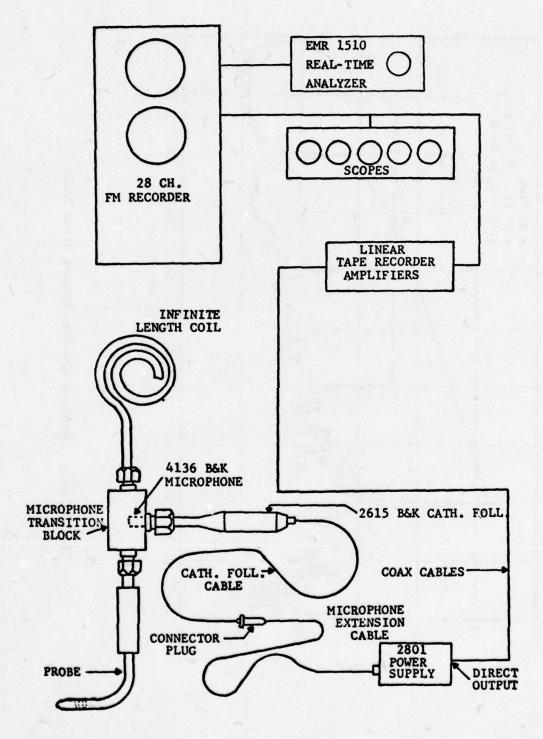


Figure 3.3-4 Waveguide Probe Used to Measure Core Nozzle Levels

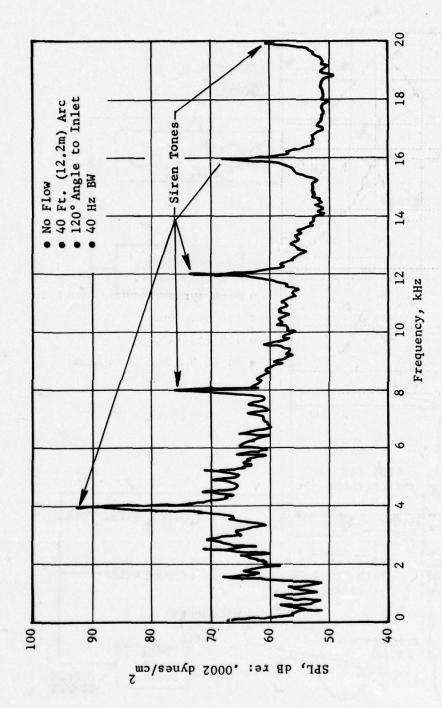


Figure 3.3-5 Farfield Spectrum Showing Siren Tones

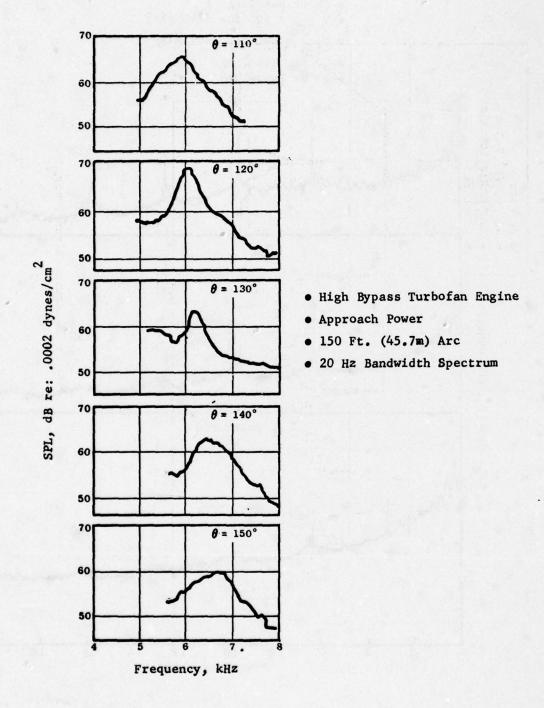


Figure 3.3-6 Haystack Peak Frequency Shift with Observer Angle

- Short Fan Duct
- V_{core} = 800 fps (244 m/s) V_{fan} = 680 fps (207 m/s)
- 40 Ft. (12m) Arc 10 Hz Bandwidth

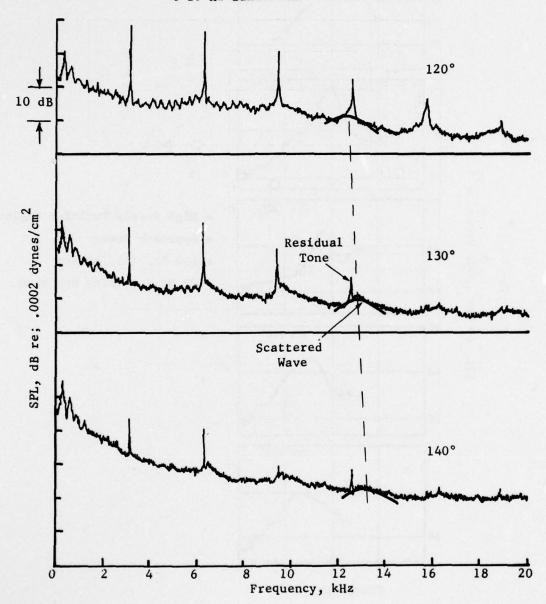
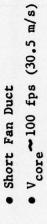
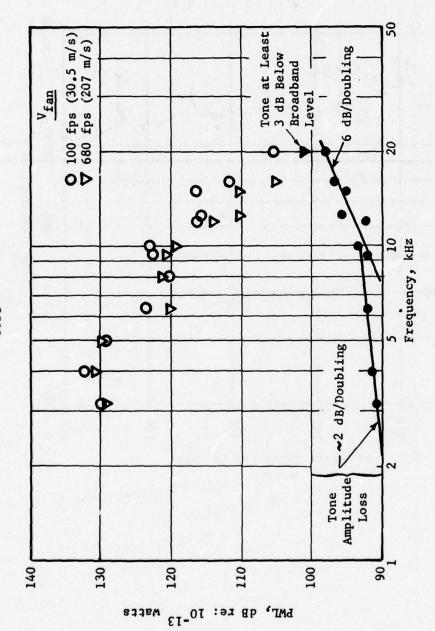


Figure 3.3-7 Haystack Frequency Shift with Angle





Maximum Amplitude Loss Expected for 680 fps (207 m/s) Fan Velocity Figure 3.3-8

Figure 3.3-9 Comparison of Duct and Farfield Siren Levels

• Short Fan Duct • $v_{core} = 100 \text{ fps } (30.5 \text{ m/s})$

• $V_{fan} = 680 \text{ fps } (207 \text{ m/s})$

• 40 Ft. (12m) Arc • 120° Angle to Inlet • 40 Hz Bandwidth

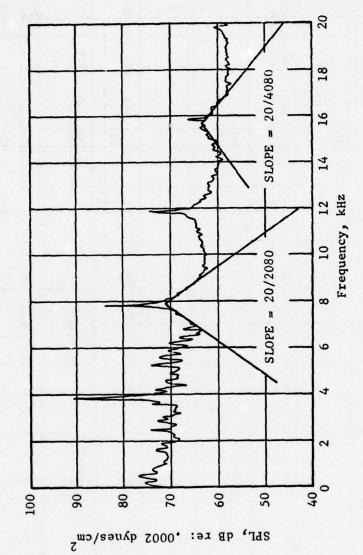


Figure 3.3-10 Increased Haystacking with Tone Frequency

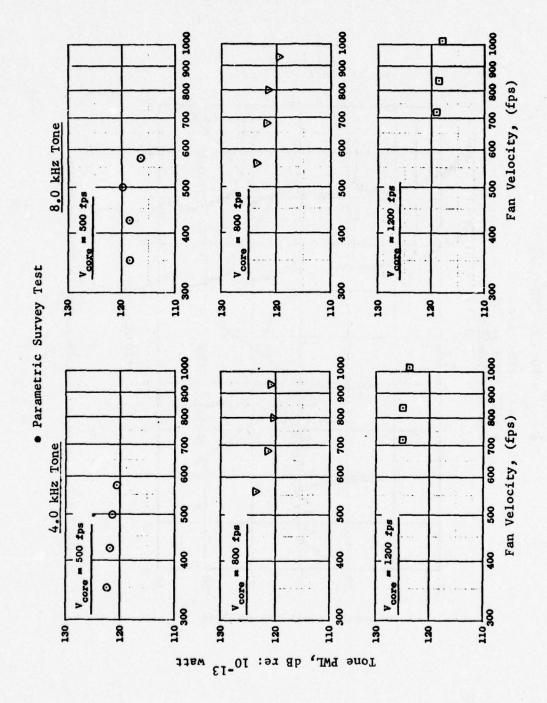


Figure 3.3-11 Variation of Tone PWL With Fan Velocity

- V_{core} = 800 fps (244 m/s)
- $V_{fan} = 680 \text{ fps } (207 \text{ m/s})$
- 3.15 kHz Fundamental
- 40 Ft. (12m) Arc
- 130° Angle to Inlet

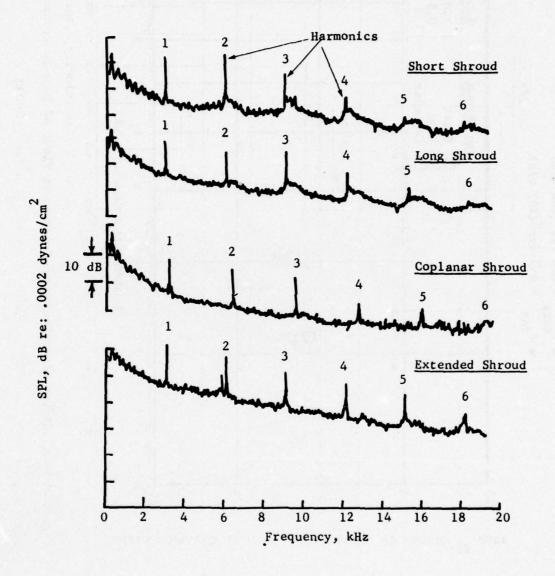
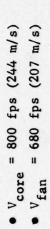


Figure 3.3-12 Effect of Fan Shroud Length on 3.15 kHz Siren Tones



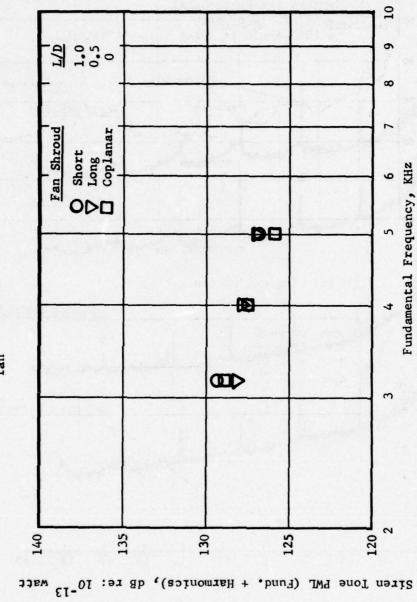
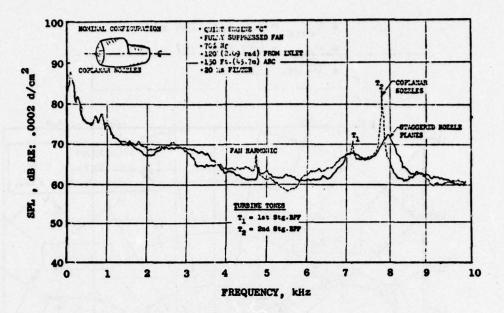
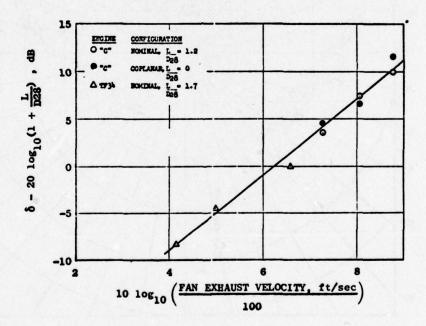


Figure 3.3-13 Effect of Variation of Fan Exhaust Plane of Tone Power Levels



(a) Engine Spectra



(b) Effect of Exhaust Plane Spacing

Figure 3.3-14 Engine Data Showing Effect of Relative Distance Between Fan and Core Nozzle Exhaust Planes

- V_{core} = 800 fps (244 m/s) • V_{fan} = 680 fps (207 m/s)
- 40 Ft. (12m) Arc

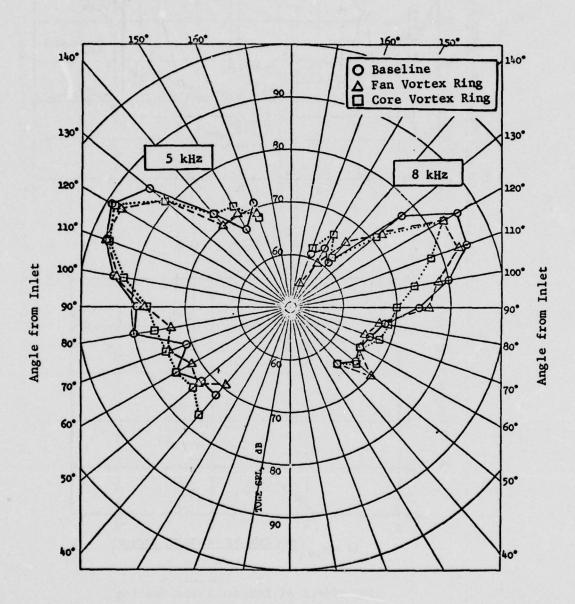


Figure 3.3-15 Effect of Turbulence Generators on Tone Directivities

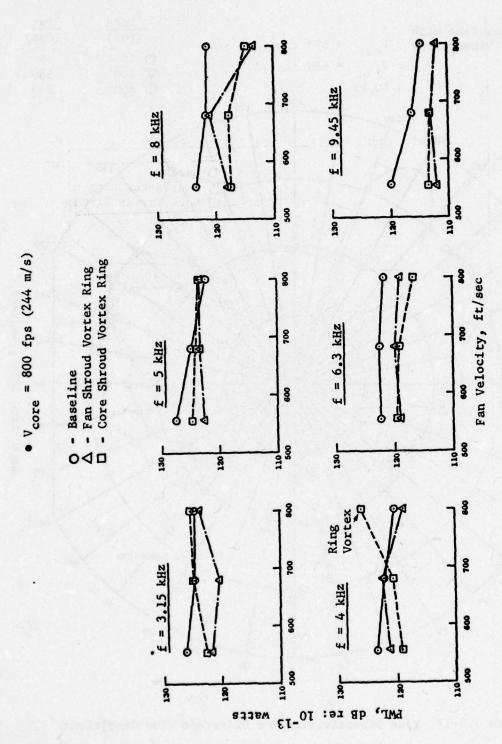


Figure 3.3-16 Effect of Turbulence Generators on Tone Power Level

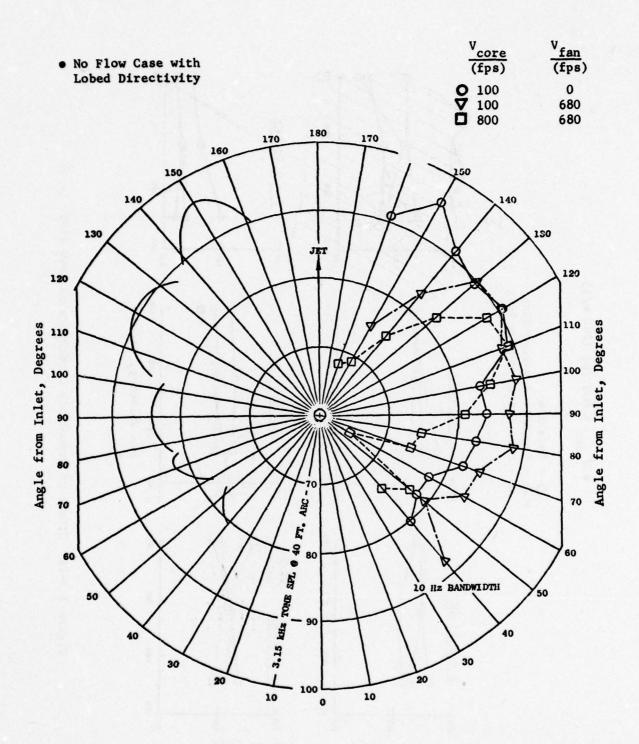
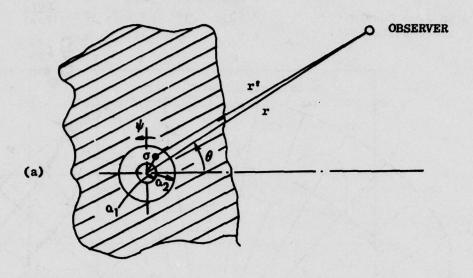


Figure 3.3-17 Tone Directivities for Different Flow Conditions



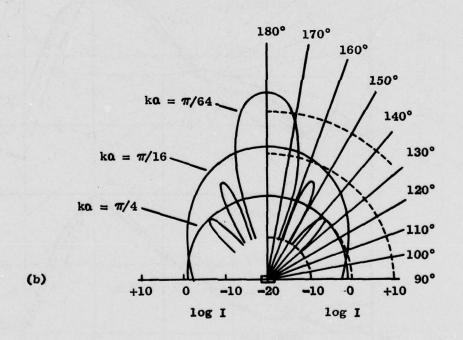
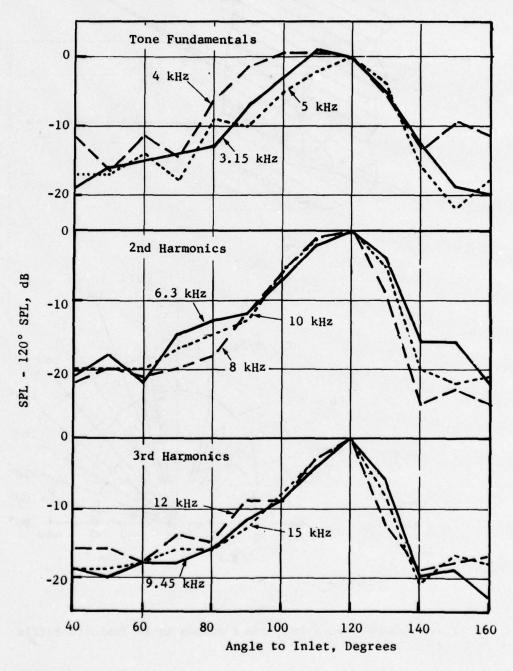


Figure 3.3-18 Radiation from a Piston in an Infinite Baffle

- Short Fan Shroud
- V_{fan} = 680 fps (207 m/s) V_{core} = 800 fps (244 m/s)



Directivity Change with Tone Frequency Figure 3.3-19

- Short Fan Shroud
- $f_0 = 3.15 \text{ kHz}$

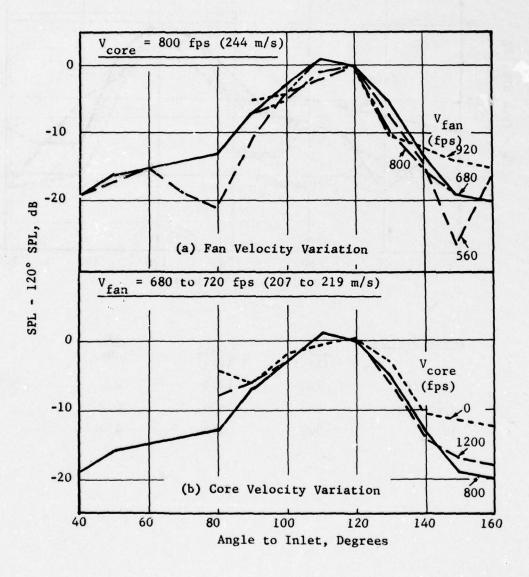
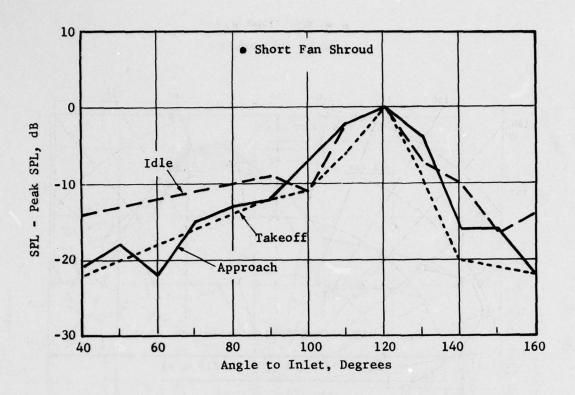


Figure 3.3-20 Directivity Change with Velocity and Velocity Ratio



Power Setting	V _{fan} (fps)	V _{core} (fps)	BPF (kHz)
Takeoff	720	1200	10.0
Approach	680	800	6.3
Idle	500	500	4.0

Figure 3.3-21 Directivity Change with Power Setting.

- 40 Ft. (12m) Arc
- 10 Hz Narrowbands

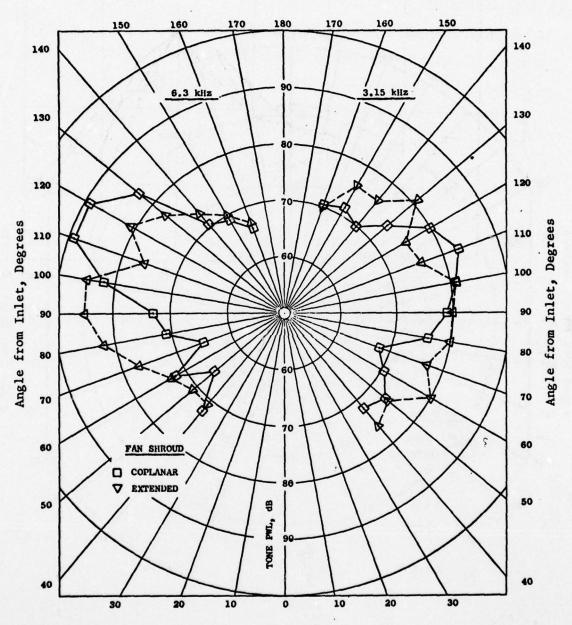


Figure 3.3-22 Comparison of Tone Directivities from Extended and Short Fan Shroud Configurations

- 40 Ft. (12m) Arc
- 10 Hz Narrowbands

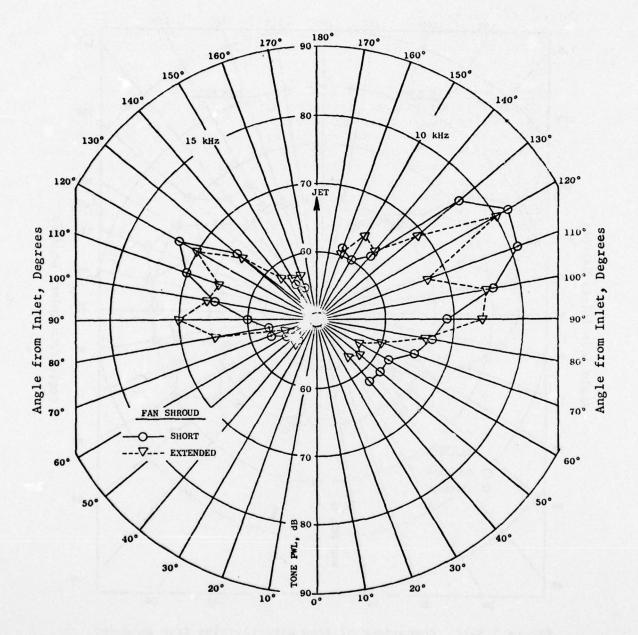


Figure 3.3-23 Change in Tone Directivity with Extended Fan Shroud

3.4 PREDICTION UPDATE

3.4.1 Status

Three different prediction methods were formulated in FA72WA-3023 in order to fully accommodate the varying requirements of different investigators and the amount of information available for the turbine (Reference 10):

- 1. Analytical Method - The viscous wake interaction mechanism responsible for discrete frequency noise generation in turbines was modeled analytically and a prediction provided for the tone PWL at the source. Radial and circumferential modal information was included. Subsequently, the analysis was extended to include the case of leaned or curvilinear vanes (Reference 29). A great deal of interstage performance data, including full knowledge of the velocity triangles at hub, pitch and tip, is required to exercise the method. However, the method makes it possible to predict the effect of aero-mechanical configuration changes such as number of blades, solidity, blade thickness, spacing, etc. on the noise generation. It is especially valuable when source noise reduction is sought. The accuracy of this method was demonstrated by comparison with the noise generation by the last stage. No meaningful comparison was possible with the internal stages because of the unknown of attenuation by the intervening turbine blade rows.
- Preliminary Design Method A semi-empirical correlation was derived using engine data and overall cycle parameters such as might be available at the very early design stage. The farfield noise signature of the turbine as a whole was provided as a function of the low pressure turbine pressure ratio, tip speed, and exit area.
- 3. Comprehensive Method A second semi-empirical correlation was derived using engine data but taking cognizance of the individual turbine stages. Spectral and directivity information was developed for the turbine OASPL and tone SPL, such that a complete turbine noise spectrum could be predicted for each angle. The correlating parameters included the pressure ratio, tip speed, blade relative Mach number, and exit area for the dominant stage.

The effect of scattering by the jet stream turbulence on the tones was entered separately through an empirical correlation of available engine data which gave both a drop in the discrete frequency acoustic energy and a spread into the adjoining sidebands. An analytical modeling of this turbine tone/ jet stream interaction indicated several parameters of pertinence, the effect of which could be separated out only through controlled model tests.

The identification of turbulence scattering as the mechanism responsible for haystacking and the dependence of turbine noise generation on the pressure ratio (a work term) in addition to the velocity provided significant advancements in the state of art for turbine noise prediction which at that time was represented by Smith and Bushell (Reference 30), Peart and Dunn (Reference 31), etc. Mathews and Peracchio (Reference 32) independently came to the same conclusions at about the same time. Their paper deals only with turbine discrete noise and associated haystacking and unfortunately does not provide the absolute numbers which would permit their prediction method to be utilized or assessed by others.

To reiterate the status briefly, the three prediction methods of FA72WA-3023 provide a framework encompassing the varying spectrum of needs, from that of the preliminary design engineer who knows only the turbine work requirements, speed and size; to the acoustic engineer seeking to evaluate the impact of internal aero-mechanical configuration changes. Both discrete frequency and broadband noise are addressed. Such a range is obviously beyond the scope of any one prediction method - either currently available or that which can be envisaged. This program preserves the framework, but seeks to enhance the working range and accuracy of the three methods.

3.4.2 Noise Levels

The analytical prediction program gives a tone PWL at the source. The transmission loss through intervening blade rows and the exhaust nozzle must be computed and accounted for in order to obtain the energy radiated.

The turbine tests of Section 3.2 demonstrated that turbine tones are subject to large transmission losses on propagation through turbine blade rows. The test data indicated that the insertion loss due to the second and third stages of the three stage HLFT-IVA could be represented by:

$$\Delta = 98.9 \log (N/\sqrt{T}) + 13.4 \log (\Delta T) + 5.6 \log (|i+7.5|)$$

$$- 217.5 \qquad (3.4-1)$$

The speed term actually defined the effect of tone frequency, blade pitch, and blade tip speed:

$$\Delta_{N} = fn \left(\frac{ft}{c}, \frac{U_{T}}{c}\right) \tag{3.4-2}$$

The problem remains to separate out the two dependencies.

Most existing analyses of noise transmission cannot be applied here either because they limit themselves to "no flow" situations or to flat plate models which are somewhat unrepresentative of turbine flows, for example, Reference 33 and 34.

The results of the parallel combustor noise transmission tests (NAS3-19435) indicated a clear frequency dependence for tones above 1200 Hz, as is shown in Figure 3.4-1. This figure provides the transmission loss through the turbine at design point for siren tones inserted upstream of the turbine. The frequency dependence followed, in general, a fourth power law. Assuming that these results can be extrapolated to the case of turbine tones, the blade row attenuation can be represented by:

$$\Delta(f) = 58.9 \log \left(\frac{U_T}{c}\right) + 40 \log \left(\frac{ft}{c}\right) + 13.4 \log_{10} (\Delta T) + 5.6 \log \left(|i+7.5|\right) + 11.5$$
 (3.4-3)

As was explained in Section 3.2, this correlation is strictly valid only for the range of speeds used in the data base.

Alternately, the attenuation can be estimated using Figure 3.2-16 along with the assumption that the second and third stages contributed equally to this transmission loss. An interesting example of such an application is provided in Figure 3.4-2. The acoustic power levels for the second stage BPF were analytically predicted and the source levels compared to the data. The good agreement between the data, which were measured downstream of the third stage, and the predicted source levels suggests that the attenuation due to the last stage was small. The dashed line shows the predicted levels if it were assumed that the third stage was responsible for half the attenuation plotted in Figure 3.2-16. Obviously then, either the measured attenuations were due in large part to the second stage, or the analytical prediction method under-estimates the noise generation due to interior stages. At this time, neither possibility can be precluded. However, the data correlations used in the comprehensive prediction method outlined below support the limited attenuation due to the last stage hypothesis as data are included for both last and second-to-last stage blade passing frequencies.

The power level for the HLFT IVA second stage BPF was analytically predicted, the attenuation computed using (3.4-3), and compared with the measured levels. Reasonable agreement was obtained as to the trends with pressure ratio, as shown in Figure 3.4-2. The difference in absolute levels is being examined.

The comprehensive prediction method for farfield turbine requires use of the <u>dominant</u> stage. A preliminary determination of this can be made by predicting BPF power level for each stage and then applying equation (3.4-3) to determine the effect of the intervening downstream stages.

The noise levels can be found using the following relationship (see Figure 3.4-3):

Peak OASPL = 8.75 log
$$\left(\frac{\Delta T}{T}\right)_{stage}$$
 + 20 log $\left(\frac{V_{rel}}{c}\right)$ + 5 log (25/ ℓ) + 1 log A + 102.9 (3.4-4)

Peak SPL = 20 log
$$\left(\frac{\Delta T}{T}\right)_{\text{stage}}$$
 - 20 log (U_T) + 10 log (25/£)
+ 10 log A + 161.5 (3.4-5)

Peak OASPL = combined broadband and discrete frequency OASPL at 120° and 200 ft (61 m) sideline in dB re 0.0002 dynes/cm².

where Peak SPL = SPL of 1/3 octave band containing BPF at 120° and 200 ft (61 m) sideline. The SPL does not include air or extra ground attenuation as these are strong functions of the tone frequency.

$$\left(\frac{\Delta T}{T}\right)_{\text{stage}} = 1 - \left(\frac{1}{P_{R_{\text{Stage}}}}\right)^{\frac{\gamma-1}{\gamma}}$$

PR_{stage} = dominant stage total-to-static pressure ratio

Vrel = tip blade relative velocity at inlet to the rotor, fps

U_T = blade tip speed of dominant stage, fps

c = mean acoustic velocity, fps

(s/l) = ratio of axial spacing to upstream airfoil chord

A = turbine exit area, ft²

γ = ratio of specific heats, ~1.4

These correlations were derived using turbine noise spectra extracted from farfield engine data. The extraction process is described in Reference 10. The correlation parameters are in agreement with the results of the turbine tests conducted in this program and during FA72WA-3023, in that the significant parameters consist of the pressure ratio along with either relative velocity, for broadband noise, or tip speed, for tones.

Frequently, $V_{\rm rel}$ and $P_{\rm Rstage}$ are not readily available, as for example, at the preliminary design stage or at off-design operating points. Correlations were obtained using fundamental performance parameters (see Figure 3.4-4) and approximate turbine noise estimates may be made using the following expressions which define the correlating lines:

Peak OASPL = 40 log
$$\left(\frac{\Delta T}{T}\right)_{\text{turbine}}$$
 - 20 log U_T + 10 log A + 164 (3.4-6)
Peak SPL = 40 log $\left(\frac{\Delta T}{T}\right)_{\text{turbine}}$ - 20 log U_T + 10 log A + 165 (3.4-7)

where Peak OASPL = overall sound pressure level at 120° and 200 ft sideline, dB re 0.0002 dynes/cm²

Peak SPL = SPL at 120° and 200 ft (61 m) sideline of 1/3 octave band containing the dominant BPF. As explained before, air attenuation and EGA must be computed separately and subtracted.

$$\left(\frac{\Delta T}{T}\right)_{\text{turbine}} = 1 - \left(\frac{1}{P_R}\right)^{\frac{\gamma-1}{\gamma}}$$

 P_R = turbine total-to-static pressure ratio, P_{T_0}/P_{S_2}

U_T = blade tip speed of last stage, fps

A = core nozzle exit area, ft²

Y = ratio of specific heats ~ 1.4

3.4.3 Broadband Noise Spectrum

A brief recapitulation of the HLFT IVA turbine test results is in order here. The single stage build provided a broadband noise spectrum with a pronounced peak at the BPF near design operating points. A large shift in energy to the vicinity of the second harmonic occurred at far off-design points, with a resultant flattening of the spectrum. The three stage build did not provide any pronounced peaks, possibly because of the multiplicity of the contributing sources and attenuating blade rows. Only minor peaks were discernible at the BPF's.

This suggests that jet engines with one or even two low pressure turbine stages will be characterized by a more peaked turbine broadband noise spectrum than engines utilizing multi-stage low pressure turbines. Also, the former class of engines will exhibit a spectral shift with power setting. Engine "C" falls into the first category since it employs a two stage low pressure turbine, with both BPF's generally falling into the same 1/3 octave band. The CF6-50 and TF34, on the other hand, use four stage low pressure turbines, with the BPF's occurring in different 1/3 octave bands. The extracted turbine noise broadband spectra are very different, as can be seen from Figure 3.4-5. The spectral shift with power setting for the two stage turbine is obvious [-5(a)]. On the other hand, the spectra associated with the four stage turbines are essentially similar over an operating range of 40 to 80% design speed [-5(b)]. It is recommended that the spectra of Figure 3.4-5(a) be utilized for prediction of the noise generated by engines incorporating single and two stage low pressure turbines and for multi-stage configurations in which all the BPF's fall into the same 1/3 octave band. The spectrum of Figure 3.4-5(b) is recommended for multi-stage turbines in which the tones fall into several frequency bands. Note that data along a polar arc were used to define the spectra at several aft-quadrant angles and it was found that the peak angle spectra provided a reasonable representation of the spectra at the other angles. A different spectral set would have to be provided for each angle if the definition had been on a sideline basis.

3.4.4 Directivity

The directivity to be used for the turbine noise OASPL, which includes both discrete frequency and broadband noise content, was determined from high bypass turbofan engine data (see Reference 10). A small difference was found between the approach and take-off power values as can be seen from Figure 3.4-6. The peak angle was 120° from inlet in both cases.

The discrete frequency noise was also found to peak at 120° for these high bypass turbofan engines. However, the fall-off from the peak angle was faster, as is evident from Figure 3.4-7 in which the solid line provides the mean of the data from Engine "C" and TF34 at approach power. The solid line is the directivity for a 1/3 octave band containing a turbine tone. However, the tone itself decays at an even faster rate, as can be verified by using narrowband data. Engine "C" 20 Hz bandwidth data corresponding to the 1/3 octave band directivity are shown in the same figure. These data can be seen to be in a very good agreement with the narrowband data from the model tests of Section 3.3. Therefore, it is obvious that the 1/3 octave band levels for angles other than 90 to 120° are controlled by the turbine broadband noise and not the tone. This, of course, is consistent with the flatter directivities of Figure 3.4-6 for the turbine OASPL. It is not clear why high frequency discrete frequency and broadband noise exhibit different directivities, but the reason may lie in the modal content. If it can be argued that the high frequency broadband noise consists of a large number of modes due to the random nature of its source, then an analytical case can be made for a flat farfield directivity.

Both the model and engine tone data indicate that the effect of tone frequency and velocity ratio is small, even on a narrowband basis. For example, the model data frequency effect at approach power is summarized in Figure 3.4-8. The peak angle for frequencies below 4.0 kHz shifted to between 110 and 120°. For frequencies above 6.3 kHz, the peak always occurred at 120°. In general, turbine tones occur at 6.3 kHz or above due to the large number of airfoils used. Figure 3.4-7 suggests that the 1/3 octave band directivity forward of 120° would also be effected.

The effect of power setting, which involves a simultaneous change in velocities, velocity ratio and tone frequency, is summarized in Figure 3.4-9. The main difference was increased fall-off rate aft of 90°. The impact on the 1/3 octave band directivities would probably be minimal, except perhaps at 110°, where the level could decrease by as much as 3 dB.

Finally, it is recalled that extending the fan shroud more than half a diameter beyond the core nozzle could introduce a second peak at 90°, accompanied by a drop in the 120° peak. The relative magnitude of the two peaks was found to be a function of the tone frequency. The 90° lobe was found to increase with frequency relative to the 120° lobe, with the break point (equal peaks) occurring around 6.3 to 8 kHz.

3.4.5 Turbine Tone/Jet Stream Interaction

The prediction method of References 10 and 29 has already been discussed in Section 3.3. Briefly, the method consists of defining the incident tone amplitude loss, δ , and the slope m, of the haystack (see Figure 3.4-10) using engine data correlations. The results of the model tests described in Section 3.3 indicate that the correlation for δ can be recast as:

$$\delta = 10 \log \left\{ \left(\frac{V_{fan}}{c} \right) \left[1 + \left| V_{core} - V_{fan} \right| / c \right]^{2/3} \right\} + 20 \log (f_0)$$

$$+ 20 \log (1 + L/6) - 68.7 \qquad (3.4-8)$$

where & = drop in 20 Hz narrowband SPL at 120°, dB

Vfan = fan velocity, Vcore = core velocity, fps

c = acoustic velocity, fps

L = distance between fan and core nozzle exhaust planes, ft

fo = incident tone frequency, Hz.

Equation (3.4-8) is valid only for wavelengths of the order of and smaller than the eddy size. Equations (2) and (3) from Reference 29 (see Section 3.3.4) can be utilized to express this limit as $(f_0L/c) \ge 12$.

Another limitation on equation (3.4-8) is a positive L: fan nozzle upstream of the core nozzle. The model test results demonstrated that the scattering for an extended plane configuration was of the same order as that of a coplanar configuration. Hence it is recommended that L=0 be used for extended fan shrouds.

The effect of flight can be included through consideration of the effect on the outer shear layer. The thickness will be reduced by a factor $(1-\zeta/1+\zeta)$ where ζ is the ratio of the flight velocity to the fan jet velocity (see Reference 29). The impact is analogous to a change in L and, therefore, consists of adding a 20log term to equation (3.4-8):

$$\delta = 10 \log \left\{ \left(\frac{V_{fan}}{c} \right) \left[1 + \left| V_{core} - V_{fan} \right| / c \right]^{2/3} \right\} + 20 \log (f_o)$$

$$+ 20 \log (1 + L/6) + 20 \log \left(\frac{1 - \zeta}{1 + \zeta} \right) - 68.7 \quad (3.4-9)$$

The scattered energy is transferred to the tone sidebands and becomes significant only in the case of spill-over into adjacent 1/3 octave bands coupled with a relatively low broadband floor. The analysis of the phenomenon and engine data both show that the frequency spread is proportional to the amplitude loss, δ . The relationship derived from engine data in Reference 10 can therefore be utilized here (see Figure 3.4-11):

$$10 \log (1/m) = 0.85\delta + 8.4$$
 (3.4-10)

where m = slope of haystack sides on a 20 Hz bandwidth spectrum.

Also, the scattered wave (or haystack) will exhibit a peak frequency shift due to the motion of the scattering eddies. In Reference 29, it was shown that the peak frequency, f, could be computed using the classical Doppler relationship:

$$\frac{f}{f_0} = [1 - M_t \cos (\Psi - 30)]^{-1}$$
 (3.4-11)

where

f = peak frequency of scattered wave.

 M_t = (phase velocity of eddies/c) = 0.65 M_{fan}

ψ = angle from jet axis, degrees.

The foregoing procedure will provide the tone scattering and haystack formation for an isolated turbine tone. When two or more tones occur in close proximity, an enlarged haystack occurs, as is illustrated in Figure 3.4-12. Such a multiple tone haystack occurs, for example, in the case of the JT9D (Reference 32). The associated spectrum should not be confused with the turbine broadband noise spectrum, as has apparently been done by the authors of Reference 36.

The turbine noise prediction methods of Section 3.4.2 provide both an OASPL and a tone SPL. The <u>latter</u> includes the haystack energy content and this energy should be redistributed into adjacent 1/3 octave bands if so indicated by the haystack spillover computed by the prediction method. Otherwise, the turbine noise prediction methods assume that the tone and associated haystack are contained within the same 1/3 octave band and the spectrum is defined accordingly.

3.4.6 Implementation of Prediction Methods

Three different prediction methods have been provided to accommodate varying needs and the information available to the user.

- 1. Analytical Prediction of Turbine Discrete Frequency Noise capability includes evaluation of aero-mechanical configuration changes such as blade number, solidity, axial spacing, vane lean, etc. on the tone power level. Implementation requires knowledge of the blade geometry and the stage aerodynamics. The scope of the analysis and the input required are given in Table 3.4-1. A computer program, the coding, a logical flow chart, and an input sheet are given in Reference 29. The output consists of the duct modes and the acoustic power level. The attenuation due to downstream blade rows can be computed using equation (3.4-3).
- Preliminary Design Method provides quick, approximate turbine noise levels in the farfield. Based on engine data correlations, the method requires the low pressure turbine pressure ratio, blade tip speed, tone frequency, and exit area as inputs. The turbine noise OASPL, which includes both discrete frequency and broadband content, at the peak angle (120° for high bypass turbofan engines) is computed using equation (3.4-6). The SPL for the 1/3 octave band containing the "dominant" stage BPF is obtained using equation (3.4-7) and the corresponding air attenuation and EGA. The dominant stage normally consists of either the last or second-to-last stage. The SPL is logarithmically subtracted from the OASPL and the resultant "broadband" OASPL is distributed according to the spectra of Figure 3.4-5. The process is repeated at the other angles with the OASPL being determined through the directivities of Figure 3.4-6 and the tone SPL through the 1/3 octave band directivity in Figure 3.4-7.

The tone SPL is attributed in its entirety to the 1/3 octave band containing the BPF of interest unless exercise of equations (3.4-9) through (3.4-11) shows the associated haystack spilling over into the adjacent 1/3 octave bands. It is recalled, once again, that the haystack spectrum is distinct from the broadband noise spectrum, and that they must be computed separately and added together to obtain the turbine noise spectrum.

3. Comprehensive Method - provides a complete turbine noise spectrum through consideration of the stage parameters rather than the overall turbine performance. It is, for this reason, inherently more accurate than the Preliminary Design Method. The computational method is similar to the preceding and is outlined in the flow chart of Figure 3.4-13. The input required is the stage pressure ratio, inlet relative Mach number at the rotor tip, tip speed, tone frequency, blade row spacing/chord ratio, and the stage exit area. The peak angle OASPL and BPF 1/3 octave band SPL are calculated using equations (3.4-4) and (3.4-5). The spectrum, directivity, and haystacking are determined as in the Preliminary Design Method.

The two semiempirical methods were derived using data from high bypass turbofan engines. Subsequently, it was found that the methods would also provide reasonable prediction of the turbine noise from turbojet engines (see Figure 3.4-4 which includes J85 data). However, the peak angle must first be shifted to 110° - high bypass turbofan engine turbine noise generally peaks at 120°.

Table 3.4-1. Analytical Computation of Turbine Tone, Power Level.

- Noise Generation Mechanisms are Similar to Those for Fan/Compressor
- 2. Viscous Wake Interaction is the Dominant Mechanism
- Modified Analytical Model Developed for Fan/Compressor Noise to Accommodate Turbine Blading:
 - Thick, Highly Cambered Blades
 - Trailing Edge Thickness
 - Favorable Pressure Gradients
- 4. Input
 - Pressure
 - Blade Relative Velocity
 - Number of Vanes and Blades
 - Turbine Size
 - Axial Spacing
 - Blade Geometry
 - Chord
 - Solidity
 - Aspect Ratio
 - Trailing Edge Thickness
- 5. Output
 - Tone PWL at Source
- 6. Apply Blade Row Attenuation Per Stage
 -Tone PWL at Turbine Exit

GENERAL ELECTRIC CO CINCINNATI OHIO AIRCRAFT ENGINE GROUP F/G 20/1 GE CORE ENGINE NOISE INVESTIGATION - LOW EMISSION ENGINES.(U) FEB 77 R K MATTA, G T SANDUSKY, V L DOYLE DOT-FA75WA-3688 AD-A048 590 FAA/RD-77/4 UNCLASSIFIED NL 495 ADA048 590 - YEARS C

- Simple Stage High Pressure Turbine
- Data Normalized to 1400°R (783°K)
- Averaged Values from Coherent Spectra
- $P_R = 2.14$, $N/\sqrt{T} = 100\%$

Data

O- 1400°R (783°K)

Δ- 810°R (450°K)

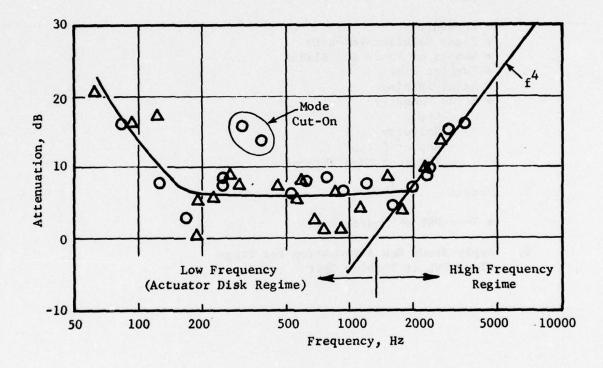


Figure 3.4-1 Determination of Tone Frequency Dependence from Combustor Noise Transmission Results

- ILFT-IVA Turbine
- 3-Stage Configuration
- 2nd-Stage BPF
- N/√T = 90%

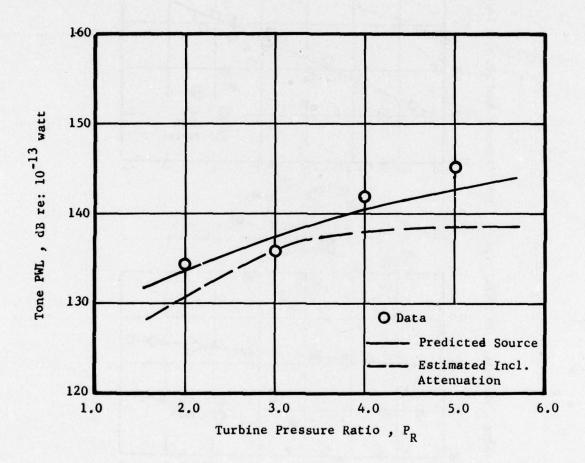
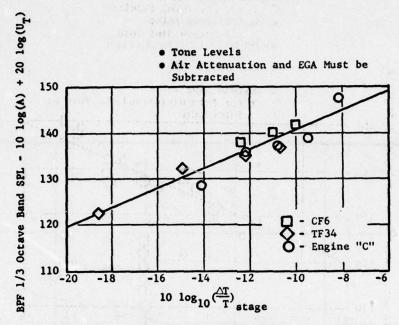


Figure 3.4-2 Comparison of Analytically Predicted and Measured Noise for an Upstream Turbine Stage

- 200 Ft. (61m) Sideline 120° from Inlet
- 1/3 Octave Band Data



- Broadband Plus Tone Levels
- Air Attenuation and EGA are

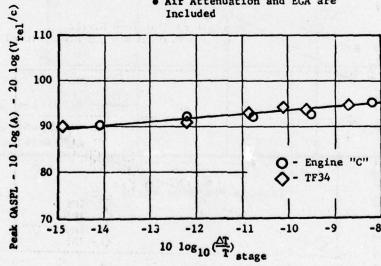
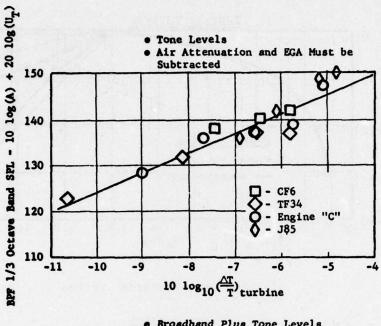
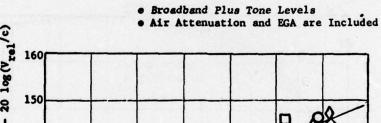


Figure 3.4-3 Noise Level Correlation for Comprehensive Prediction Use

- 200 Ft. (61m) Sideline
 120° from Inlet
 1/3 Octave Band Data





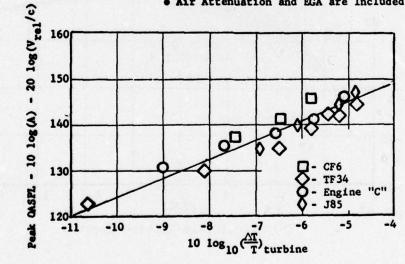
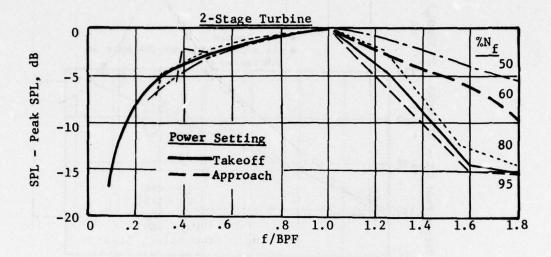


Figure 3.4-4 Noise Level Correlation for Preliminary Design Use.

- 150 Ft. (45.7m) Arc 120° from Inlet
- 1/3 Octave Band Levels



(a) Two Stage Turbine Spectra

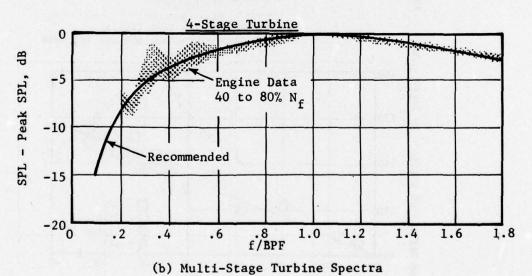
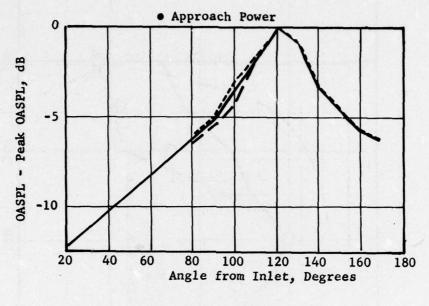


Figure 3.4-5 Turbine Broadband Noise Spectra.

- 150 Ft. (45.7m) Arc
- 1/3 Octave Band Data



---- Engine "C" ---- TF34 ---- Recommended

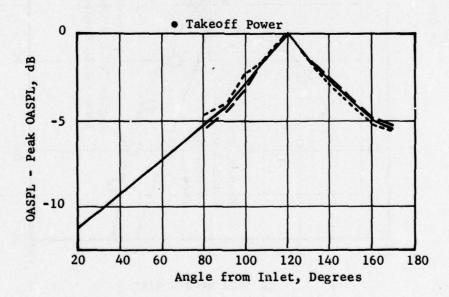


Figure 3.4-6 Directivity for Turbine Noise OASPL





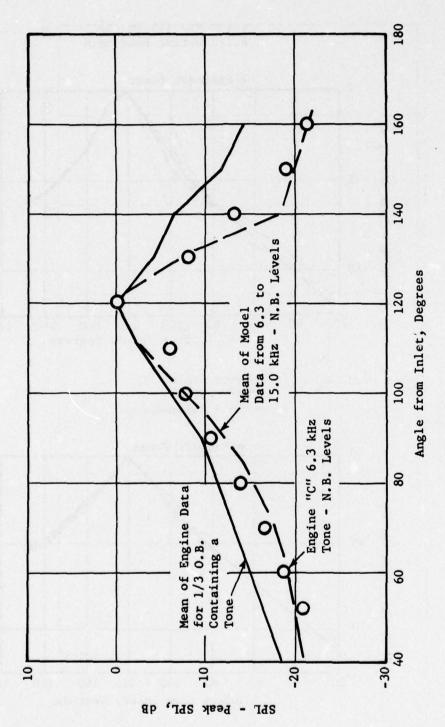
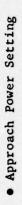


Figure 3.4-7 Effect of Bandwidth on Tone Directivity



• Arc Data

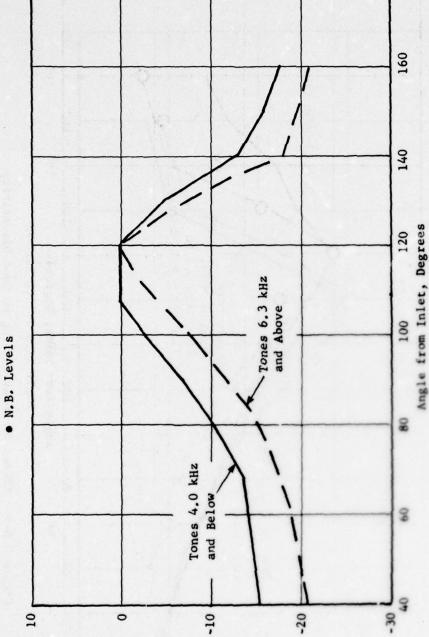
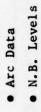


Figure 3.4-6 Effect of Frequency on Tone Directivity

180

SPL - Peak SPL, dB



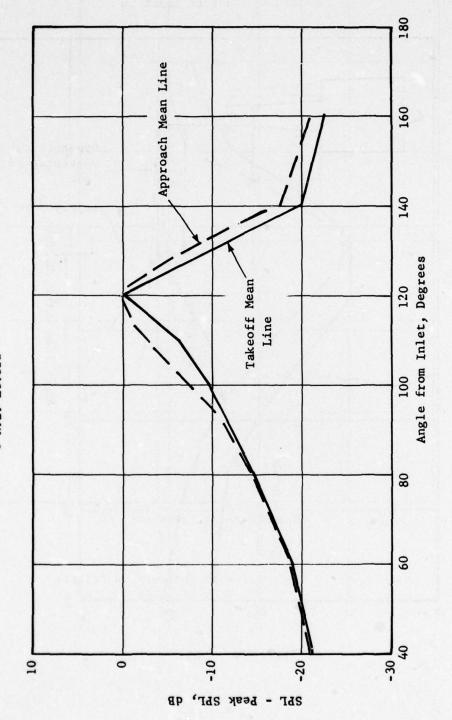
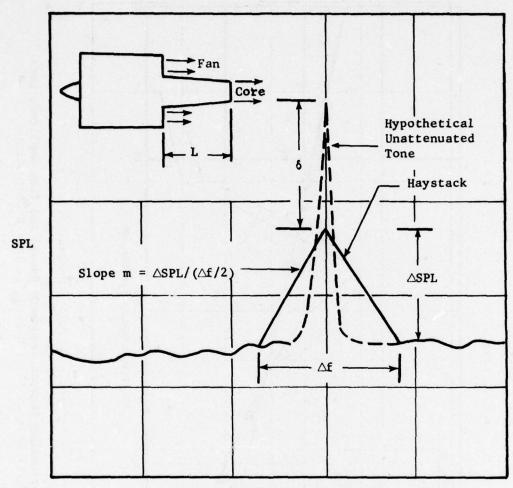


Figure 3.4-9 Effect of Power Setting on Tone Directivity

• 20 Hz Bandwidth Spectrum



Blade Passing Frequency, Hz

Figure 3.4-10 Definition of Interaction Effects

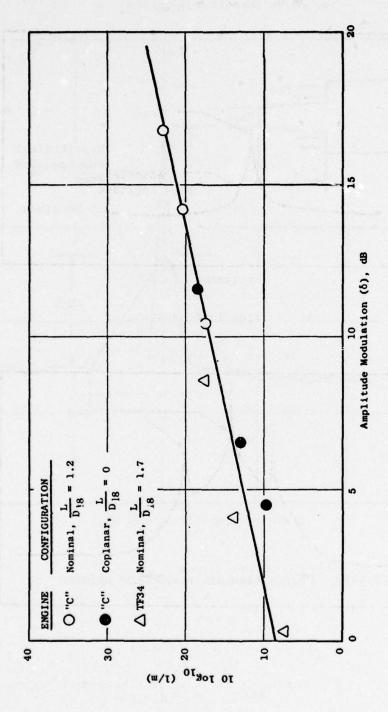
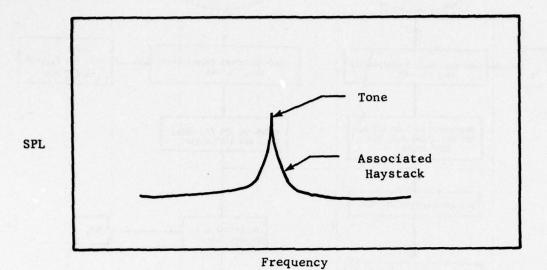
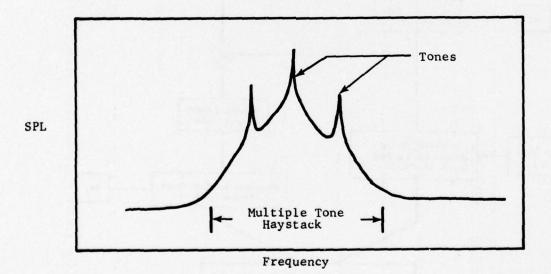


Figure 3.4-11 Relationship between Frequency Spread and Tone Amplitude Loss

- Turbine Noise
- Narrowband Spectra



(A) Isolated Tone Haystack



(B) Multiple Tone Haystack

Figure 3.4-12 Schematic of Haystack Enhancement due to Multiple Tone Contribution

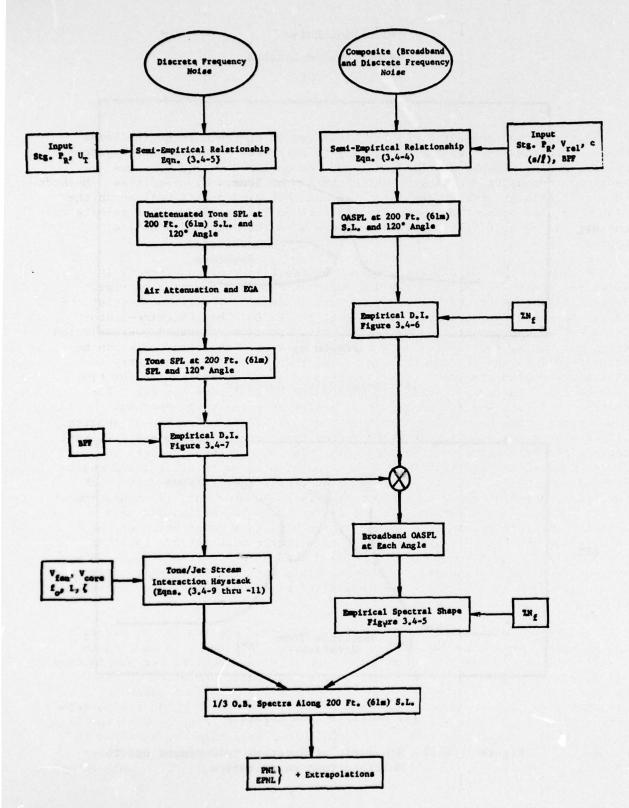


Figure 3.4-13. Flow Chart for Comprehensive Turbine Noise Prediction Procedure.

SECTION 4.0

SYSTEMS STUDY

An important and extremely practical result of the Core Engine Noise Control Programs is that the capability to carry out aircraft noise systems studies has been substantially enhanced. As outlined in the previous sections, combustor and turbine noise can now be accurately predicted. Methods for prediction of high bypass jet noise and that due to obstructions in the flow were also presented in the Final Report on FA72WA-3023. This permits the evaluation of flight system noise in a more thorough and detailed manner.

A plot of the noise event produced by the flight of an aircraft is shown in Figure 4-1 as the perceived noise in PNL as a function of time. From this tone-corrected PNL event one can calculate by well known relationships the effective perceived noise level in EPNdB. This PNL-time-history is of course the result of a series of noise spectrums averaged over selected time increments, and plotted as a function of time. The time scale can be translated into angles from the engine inlet when the flight geometry and aircraft velocity are known. The spectrum measured at each angle (or time increment) is the sum of the spectra produced by the noise sources. For example in Figure 4-2 a typical systems-noise-spectrum at an approach power setting has been decomposed into the most important component spectra. Different sources, out of the four plotted here, control or impact different regions of the systems spectrum and this "mix" of component spectra is, for a given engine and airframe, a function of both power setting and angle from the engine inlet. It is apparent therefore, that if a prediction of the flight noise of a new engine/aircraft is to be made, or, if an assessment of the impact of each component noise source is to be carried out on a measured aircraft system noise event, in both cases a description of the major noise sources is required. This description must include spectrum characteristics as a function of far-field angles and power setting. This type of detailed systems study is now possible with the level of combustor, turbine, and jet noise predictive capability produced by the Core Engine Programs.

This very detailed accounting of all component spectra in the aircraft noise-event-time-history is very time consuming. Although, it is used in selected systems studies, a simple approach is often required for preliminary assessments and large scale studies covering extensive variation of the parameters. This approach is based on the fact that for most subsonic aircraft, the EPNL is effectively controlled by the peak PNL and the duration correction. If a change is made in any combination of noise components the change in the peak PNL usually affects the EPNdB more than the duration change. A simplified systems study approach has been developed by concentrating on the change in the peak PNL components, and handling the resulting

duration changes as a second order effect. An example of the results of this technique is shown in Figure 4-3, where the major noise components have been assessed in terms of PNdB at the maximum angles in both the forward and aft quadrants. These component PNL's were determined using the prediction capability developed under the Core Engine Program. The effects of forward aircraft speed are included as well as the important atmospheric propagation efforts. The case shown in Figure 4-3 is for a typical high-bypass ratio turbofan powered aircraft with a treated nacelle, at the takeoff altitude and power setting of today's widebody aircraft. Similarly in Figure 4-4 the approach case is shown. At the right of each figure is the EPNL value determined from the peak PNL's and appropriate duration corrections. Regardless of whether these figures represent an existing engine/aircraft or whether it is the prediction of a new aircraft system, the capability to accurately construct data like that on Figures 4-3 and 4-4 permit systems-noise-studies to be conducted with the following results.

- It leads to concentration of development activity on the most "important" noise sources. In the examples used one would conclude that if significant takeoff noise reduction is to be achieved the jet and aft radiated fan noise must be reduced. Similarly at approach, the major contributor is aft fan noise with the turbine generated noise becoming important for larger noise reduction goals.
- It provides the impact of a given level of component noise reduction on the system EPNdB. Although "major sources" are usually apparent, the secondary sources in a given "component-mix" also contribute and these contributions prevent the system EPNdB reduction from being as large as a given component PNL reduction. Incorrect assessment of the secondary sources often leads to less-than-anticipated EPNL reductions for a major component suppression. A corollary of this is that accurate component prediction capability also permits the correct assessment of engine measured component suppression, either static and/or flight. A component noise reduction feature which fails to perform as expected on an engine or aircraft test can be the result of poor design, or the masking effect of another noise source. Test results can be properly interpreted in this case if reliable noise component prediction capability is in hand.
- The evaluation of EPNdB changes produced by cycle or design modifications due to engine "growth" can be done with confidence. Modifications to aircraft engines which increase and/or improve performance are continually being studied and implemented, and the impact on noise must be accurately evaluated.
- "Lower-noise" engine designs which have minimum impact to the engine/aircraft system can be determined. If for example a system noise reduction of 2 EPNdB is needed at approach, the component PNL's of Figure 4-4 indicate that various combinations

of aft fan noise, forward fan noise, and aft radiated turbine noise reduction could meet the required systems noise reduction goal. In fact there are an infinite number of noise reduction combinations for these three components which give the required suppression. Without accurate component prediction methods, the only feasible approach is to over-design, i.e. reduce all three components by a generous amount. This insures success but often unnecessarily penalizes the engine in terms of weight, performance and cost. With component prediction capability a design can be selected based on a system trade study. The acoustic portion of such a study is illustrated in Figure 4-5 where for simplicity one of the variables, i.e. forward fan noise reduction, is held constant, and the system EPNdB change is shown as a function of combinations of aft fan and turbine noise reduction (in component PNL), plotted in a "carpet plot." The dashed line which represents a constant 2 EPNdB system reduction, shows that aft fan reduction from 2 to 10 PNdB is required in conjunction with turbine reduction of 0 to 8 PNdB. The "balance" between these component suppressions can be selected now, based on the economic impact of various suppression approaches.

• The combustor and turbine prediction techniques which have been developed provide some insight into source mechanisms and resulting important variables which result in novel noise reduction approaches. The definition of source characteristics and transmission phenomenon involved in combustion and turbine noise which has been generated on this program have provided insight into these physical processes and naturally result in the identification of unique opportunities to affect noise reduction of these components.

The foregoing comments list general systems noise study advantages resulting from the technology produced under the Core Engine Program. There are also, some specific results related to the turbine and combustor noise sources that are illustrated with noise studies of future engine systems.

The noise components of one of these future engines are shown in Figures 4-6 and 4-7 at takeoff and approach respectively. This engine is typical of an energy-efficient turbofan with a bypass ratio of 7.5, in a long duct mixed flow nacelle. Typical values of aircraft gross weight, takeoff attitude, approach power setting, and aircraft velocities, have been used in making these estimates and these are tabulated on the figures. Similarly Figures 4-8 and 4-9 show the noise components of a typical high-bypass ratio (β^{\approx} 12) turbofan which might power a short takeoff and landing (STOL) aircraft of the future. An acoustic design criteria of 95 EPNdB for a 500 foot sideline distance has been assumed as a possible STOL aircraft noise criteria. A study of these noise components (and the previously shown "current-engine" components) from a systems viewpoint leads to the following conclusions about turbine and combustor noise.

- Turbine noise is an important noise component at approach power, for both current and future turbofan engines. The noise components shown on Figure 4-4 for a current high bypass ratio turbofan in a treated nacelle has been reduced by about 5 PNdB due to acoustic treatment. If additional system noise reduction is desired the turbine noise should be reduced still further in order to provide a balanced system design. Future engines, as shown in Figure 4-7 will emphasize the need for turbine noise reduction for two reasons; 1) the other major sources have been reduced as a result of improved suppression performance and a higher bypass ratio, mixed flow exhaust system and 2) turbine noise has tended to increase because of higher loading per stage. Mixer nozzles on the core also reduce the area available for treatment. These factors result in a turbine noise reduction requirement of 7 PNdB in order to meet a stringent study-noise goal. As indicated with the shaded areas on Figure 4-7 the required turbine noise reduction will need both suppressor (2 PNdB) and source noise (5 PNdB) reduction features. It is obvious that accurate turbine prediction techniques, as provided under this current Core Noise Program, are mandatory, if a correct and early assessment of the impact of turbine noise on the system noise requirements is to be feasible.
- Unsuppressed turbine noise is also shown to be important in assessing STOL engine acoustics in Figure 4-8. It is the highest aft radiated noise component at approach and a contributor to the system noise level at takeoff. In both cases, suppression, indicated by the shaded area, would be necessary to achieve the system noise goals.
- This present work has provided insight into the mechanism of turbine noise generation and transmission so that the effects of stage loading, wheel speed, and blade number can be assessed for future designs. The effects of the jet mixing layer in scattering turbines tones have been described which enables an accurate accounting for this "haystacking" phenomenon in static and flight tests, and with various nozzle geometries.
- The combustion noise shown as a component in these systems studies is not a major contributor for most current fan engines or for the energy efficient turbofan whose components are shown in Figure 4-6 and 4-7. It is important, however, in these systems to have a reliable combustion noise assessment in order to accomplish the results in a systems noise study discussed earlier in this section. There is a specific advantage not previously mentioned which comes about from this combustion noise prediction capability, in the area of jet noise i.e., determination of jet noise relative velocity effects. Since the combustion and jet noise spectra shapes are very similar it has been difficult in the past to determine the change in jet noise which comes about as a result of forward motion. When "unexpected" relative velocity effects were detected from test

results, it has been convenient to suspect combustion noise as a contaminating noise floor. With the combustion noise prediction capability developed under this program in hand, jet relative velocity effects can be determined experimently with confidence.

- There are engine systems on which the combustion noise does become a major noise component. The STOL engine noise components shown in Figures 4-8 and 4-9 illustrate such an engine. The impact of unsuppressed combustion noise at takeoff and approach in this case demanded a suppressor system as indicated by the cross-hatched areas. Although not specifically studied, it is anticipated that turboshaft and duct burning turbofans may also have significant combustion noise.
- Finally the capability to determine the change in combustion noise due to low emissions combustor designs is important and has been discussed in a previous section.

In summary, the turbine and combustion noise investigations carried out under this program have made a substantial impact on the ability to carry out meaningful systems noise studies. Major component sources can now be accurately determined and engine acoustic systems designs can now be developed which minimize the cost, weight, and performance penalties associated with noise reduction features.

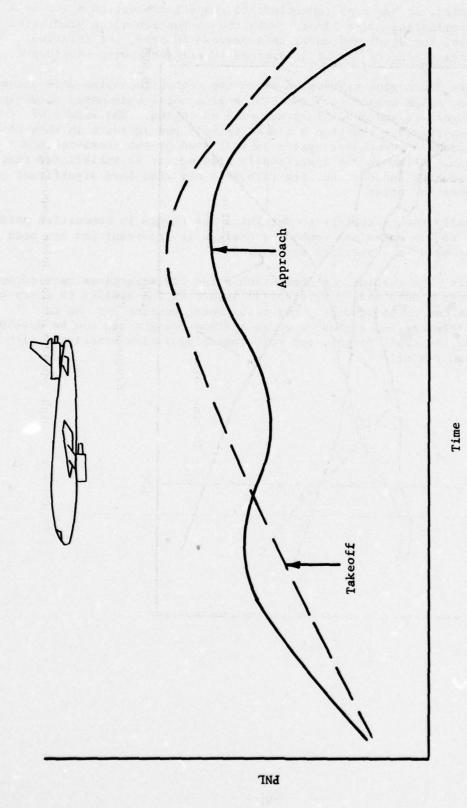


Figure 4-1 Flight Noise Characteristics

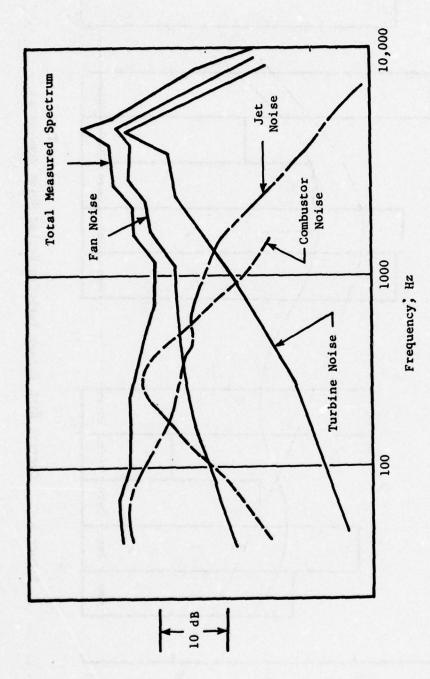


Figure 4-2 High Bypass Turbofan Noise Components



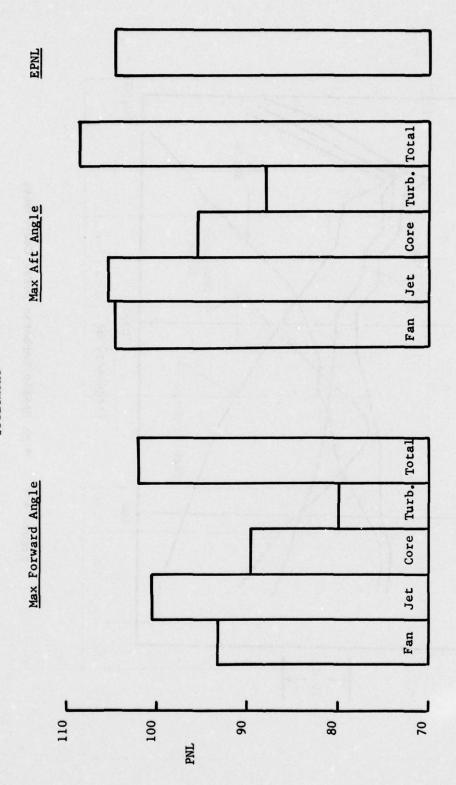


Figure 4-3 Current High Bypass Turbofan Engine Noise Components

 Approach Power
 Levels Include Nacelle Treatment

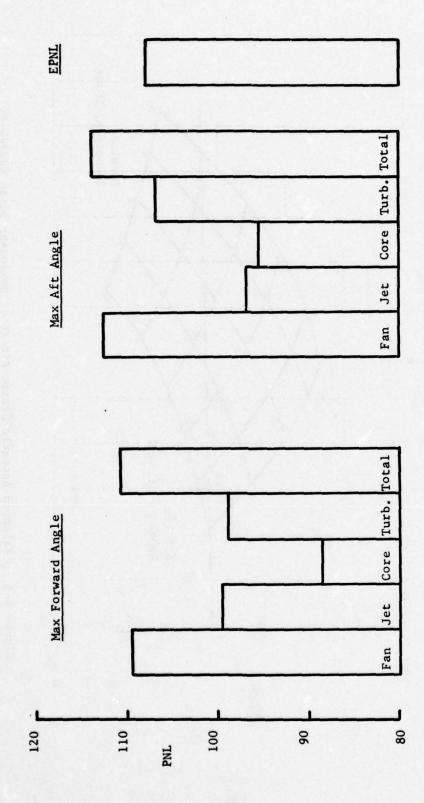
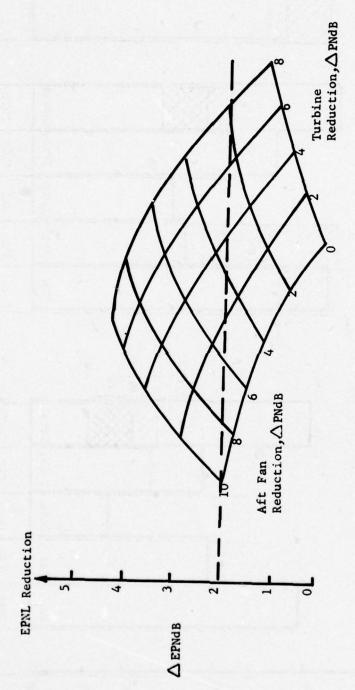


Figure 4-4 Current High Bypass Turbofan Engine Noise Components



Balanced Acoustic Design Effect of Component Noise Trade-off Figure 4-5

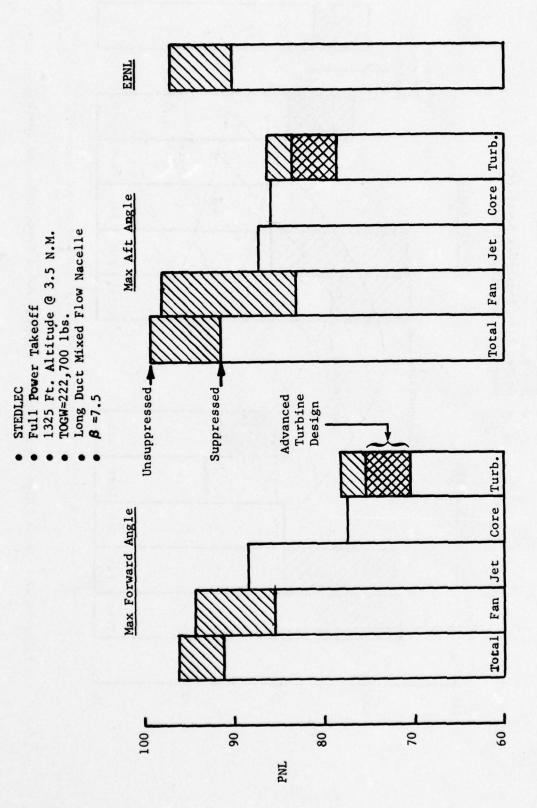
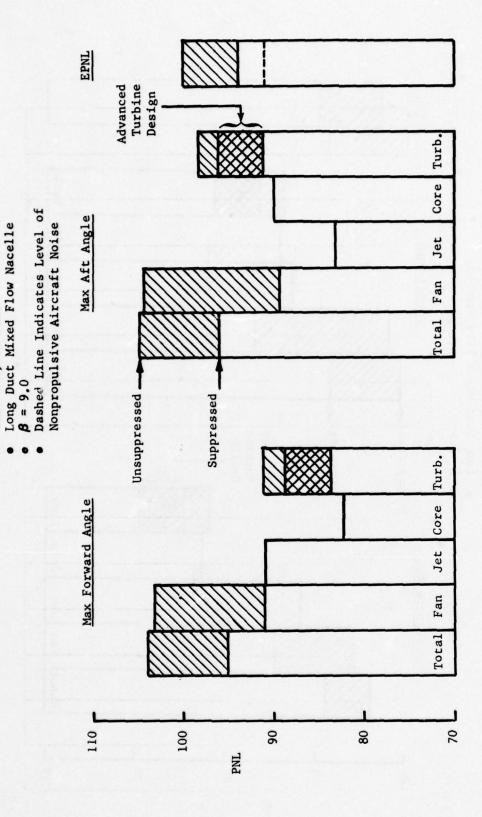


Figure 4-6 Future High Bypass Turbofan Engine Noise Components



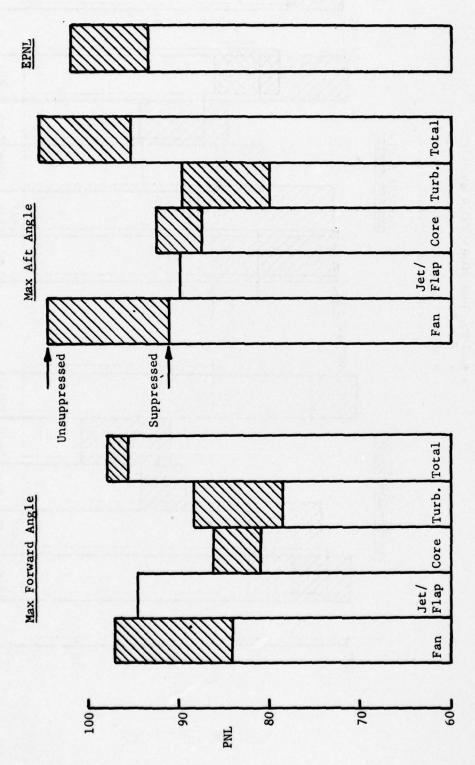
Approach Power - 40% Thrust TOGW=222,700 lbs.

STEDLEC

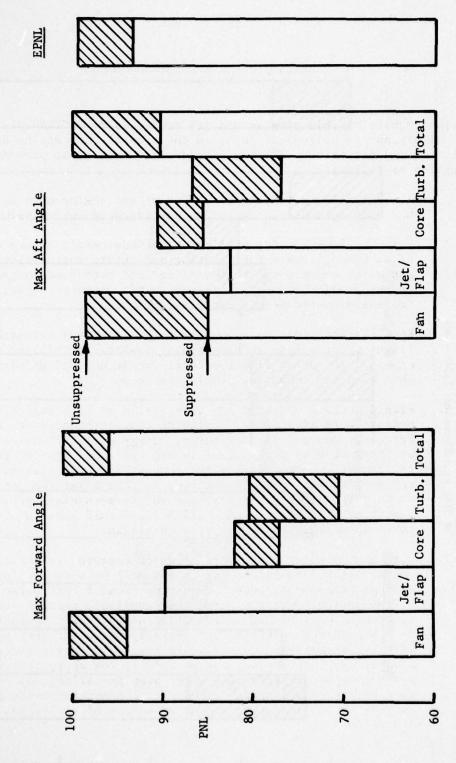
Future High Bypass Turbofan Engine Noise Components (Approach) Figure 4-7



• 500 Ft. Sidelina (150.4 m)



Future High Bypass Turbofan Engine Noise Components for STOL Application Figure 4 -8



Future High Bypass Turbofan Engine Noise Components for STOL Application Figure 4-9

SECTION 5.0

CONCLUSIONS AND RECOMMENDATIONS

The results of this program and its predecessor, FA72WA-3023, have provided significant technological gains in the area of core engine noise source prediction and reduction. The benefits derived from these programs may be summarized as follows:

- 1. A substantial data base of component and engine core noise data has been accumulated including new advanced low emissions combustors.
- 2. The core engine noise prediction methods permit accurate prediction of component levels for existing and future engine systems. Major and minor sources can be identified and resources concentrated on the problem areas in a cost-effective manner. Also, there is increased confidence in cycle selection.
- 3. Knowledge of individual component levels allows estimation of flight effects through comparison of static and flight data. For example, jet noise flight effects can be determined with confidence only when the combustor levels are known.
- 4. Viable methods of obtaining suppression of core engine.noise components were identified, including compact suppressors for low frequency noise. In particular, energy efficient noise reduction at the source is desirable leaned vanes and spacing for turbines, lowered reference velocity for combustors, exploitation of turbine and nozzle blade row attenuation, 24 lobe mixer for jet noise and so on. The understanding of the source mechanisms attained as a result of this program and FA72WA-3023 could lead to other new and novel approaches to obtaining suppression.
- Core engine noise components of major concern are turbine and combustor noise. Turbine noise is and will be a factor for CTOL systems at approach power, requiring about 5 PNdB noise suppression at the source, over and above that available through acoustic treatment for advanced, fuel efficient engines. Combustor noise is a significant contributor generally where jet and fan noise levels are depressed. This would include configurations utilizing mixers, very high bypass cycles (STOL), low approach power settings, and turboshaft engines with quiet prop installations. In addition, duct burners could present a potential combustor noise problem due to lack of turbine attenuation or because of excitation of duct resonances.

- 6. Current techniques of reducing emissions by increasing reactant velocity through the primary combustion zone will increase combustor noise. However the impact on the system noise levels is negligible for current CTOL engines. Also, growth cycles will have a much greater impact on the emissions than on noise.
- 7. Diagnostic tools were developed: (1) sound-separation using internal sensors was demonstrated for both high and low frequency noise, (2) coherence was used to produce farfield combustor noise spectra, and (3) probe-acquired internal measurements in the vicinity of the combustor were shown to be representative of farfield noise levels.
- 8. The stage has been set for further improvement in the engine noise prediction methods by recognition of all the individual elements involved: source noise generation, transmission losses, and radiation effects.

These two programs have provided many answers; but as is usual, they have also raised many questions. Several promising leads have been generated which need to be pursued. The following recommendations for further work address the immdediate needs identified by this program.

- Identify viable means of obtaining turbine source noise reduction.
 This will impact both current and future CTOL systems. The systems study has high-lighted this requirement.
- Continue the elemental approach to turbine and combustor noise study whereby noise production at the source, transmission, radiation, and propagation (including inflight) effects are considered separately. The turbine and combustor tests conducted under this program have demonstrated the value of such an approach. There is considerable potential for exploitation of the different elements to obtain farfield noise reduction, e.g., through blade row attenuation.

There are some specific items which merit further investigation:

- The core noise radiation by an engine incorporating one of the super low emission combustors, such as tested in the High Density Parametric Tests, should be determined. There are questions as to the spectrum and power-level. The sound-separation probe would provide the ideal diagnostic tool.
- The suppressive effect of the exhaust nozzle on low frequency noise should be analyzed in greater detail. Models have been proposed for both the "transmission" (accelerating flow) and "radiation" problems (for characteristic length << sound wavelength). These should be refined and validated.

- The dependence of turbine noise attenuation by blade rows on the frequency, tip speed, and other parameters should be verified parametrically through analytically modeling and controlled tests.
- The viscous wake interaction model for discrete frequency noise generation should be extended to predict broadband noise as suggested by the results of the turbine tests.
- The mechanism responsible for the two lobed directivity for the extended fan shroud model tests should be clarified. It could be of significance to flyover noise levels.

REFERENCES

- Kazin, S.B. and Matta, R.K., et al., "Core Engine Noise Control Program Vol. II, "Report No. FAA-RD-74-125, II, August 1974.
- Gleason, C.C., Rogers, D.W., Bahr, D.W., "Experimental Clean Combustor Program - Phase II Final Report," Report No. NASA CR-134971, August 1976.
- Emmerling, J.J. and Bekofske, K.L., "Experimental Clean Combustor Program - Noise Measurement Addendum - Phase II Final Report," Report No. NAS CR-135045, January 1976.
- Emmerling, J.J., "Experimental Clean Combustor Program Noise Measurement Addendum Phase I Final Report," Report No. NAS CR-134853, July 1975.
- 5. Strahle, W.C. and Shivashankara, B.N., "Combustion Generated Noise in Gas Turbine Combustors," ASME paper 75-GT-27.
- Levine, H. and Schwinger, J., "On the Radiation of Sound From an Unflanged Circular Pipe," Physical Review, Vol. 73, No. 4, pg. 383-406, February 1948.
- 7. Bilwakesh, K.R., et al, "Supersonic Jet Exhaust Noise Investigation Final Report," Report AFAPL-TR, July 1976.
- 8. Clapper, W.S., et al, "High Velocity Jet Source Noise Location and Reduction Task IV," to be published.
- 9. Grande, E., "Core Engine Noise," AIAA Paper No. 73-1026.
- Kazin, S.B. and Matta, R.K., et al., "Core Engine Noise Control Program Vol. III," Report No. FAA-RD-74-125, III, August 1974.
- 11. Bahr, D.W. and Gleason, C.C., "Experimental Clean Combustor Program Phase I Final Report," Report No. NASA CR-134737, June 1975.
- 12. Motsinger, R.E. and Emmerling, J.J., "Review of Theory and Methods for Combustion Noise Prediction," AIAA Paper No. 75-541.
- 13. Strahle, W.C., "The Convergence of Theory and Experiment on Direct Combustion Generated Noise," AIAA Paper No. 75-522.
- 14. Plett, E.G. and Leshner, M.D., "Combustion Intensity and Distribution Relation to Noise Generation," AIAA Paper No. 75-524.
- Chiu, A.A., Plett, E.G., and Summerfield, M., "Noise Generation by Ducted Combustion Systems," AIAA Paper No. 73-1024.

REFERENCES

- 16. Hassan, H.A., "On the Origin of Combustion Generated Noise," Internal memo written at North Carolina State University, Department of Mechanical and Aerospace Engineering.
- Mathews, D.C. and Rekos, N.F., "Direct Combustion Generated Noise in Turbopropulsion Systems - Prediction and Measurement," AIAA Paper No. 76-579.
- Kazin, S.B., Matta, R.K., and Emmerling, J.J., "Core Engine Noise Control Program Vol. III Supplement I," Report No. FAA-RD-74-25, March 1976.
- 19. Marble, F.E., "Acoustic Disturbance from Gas Nonuniformities Convected Through a Nozzle," Proc. Interagency Symposium of Univ. Research in Transportation Noise, II, pp. 547-561, 1973.
- Cumpsty, N.A., and Marble, F.E., "The Generation of Noise by Fluctuations in Gas Temperature into a Turbine," University of Cambridge Report No. CUED/A TURBO/TR57, 1974.
- 21. Motsinger, R.E., "Prediction of Engine Combustor Noise and Correlation with T64 Engine Low Frequency Noise," General Electric Co. Report No. R72AEG313, 1972.
- 22. Knott, P.R. "Noise Generated by Turbulent Non-Premixed Flames," AIAA Paper No. 71-732.
- 23. Doyle, V.L. and Matta, R.K., "A Program for Measuring the Noise Transfer Functions Through Aircraft Engine Turbines," NASA Contract No. NAS3-19435, Final Report, to be Published.
- 24. Ho, P.Y. and Tedrick, R.N., "Combustion Noise Prediction Techniques for Small Gas Turbine Engines," Internoise 72 Proceedings, October 1972.
- 25. Arnold, J.S., "Generation of Combustion Noise," J. Acoust. Soc. Am., Vol. 14, January 1972.
- Mani, R., "Refraction of Exhaust Duct Waveguide Modes by Exhaust Jets," Quarterly Appl. Math., 30, 4, pp. 501-520, January 1973.
- Sofrin, I.G. and Riloff, N., R., "Experimental Clean Combustor Program - Noise Study," NASA CR-135106, September 1976.
- 28. Neitzel, R.E., Hirschkron, R. and Johnston, R.P., "Study of Turbofan Engines Designed for Low Energy Consumption," NASA CR135053, August 1976.

REFERENCES

- Matta, R.K., and Mingler, P.R., "Core Engine Noise Control Program, Vol. II, Supplement I, "Report No. FAA-RD-74-125, II-I, July 1976.
- 30. Smith, M.J.T. and Bushell, K.W.; "Turbine Noise Its Significance in the Civil Aircraft Noise Program," ASME Paper No. 69-WA/GT-12, 1969.
- 31. Dunn, D.G. and Peart, N.A.; "Aircraft Noise Source and Contour Estimation," NASA CR-114649, July 1973.
- 32. Mathews, D.C., and Peracchio, A.A., "Progress in Core Engine and Turbine Noise Technology," AIAA Paper No. 74-948, August 1974.
- 33. Kaji, S. and Olazaki, T., "Study on Plane Sound Waves Passing Through a Compressor Blade Row, " Paper #F-5-1 at the 6th International Congress on Acoustics, Tokyo, Japan, August 21-28, 1968.
- 34. Mani, R. and Horvay, G.; "Sound Transmission Through Blade Rows," Report No. 69-C-104, General Electric R&D Center, Schenectady, N.Y., February 1969.
- 35. Takaku, I. and Horiuchi, T., "Attenuation of Low-Frequency Sound in a Turbulent Duct," J. Acoust. Soc. Am., Vol. 58, No. 4, October 1975.
- 36. Mathews, D.C., Nagel, R.T., and Kester, J.D., "Review of Theory and Methods for Turbine Noise Prediction," AIAA Paper No. 75-540, March 1975

APPENDIX A

Internal Density Combustor

Test Data

Table A-1 Combustor Rig Test Data SPL's

Rdg. Point	764		765	S	766	9	767	7	763	3	762	2
Probe Frequency	u*	D**	Ω	Q	Ð	Q	Ð	Q	Þ	Q	p	۵
31.5	125.5	131.8	127.0	140.0	127.0	137.8	127.5	136.0	130.0	136.3	129.8	130.8
07	126.4	131.3		136.0	-	136.8		133.8	131.1	135.8		134.8
20	123.6		126.9	134.2	126.9	131.5		133.2	131,4		131.6	
63	121.6		125.1	129.6	124.4	130.9		131.4	131.1		129.6	134.9
8	122.3		123.5	128.6	122.8	129.6	125.5	128.9	131.3		130.0	132.9
100	125.1			131.8		130.0		128.3			132.4	132.3
125	125.3		128.3	129.8	128.5	128.8	129.8	129.5			132.0	131.8
160	126.8		126.0	129.1	125.0	128.9	127.5	130.1	134.5	136.6	133.3	134.6
200	128,5		129.5	130.1	129.5	130.5	132.0	130.8	136.2		134.5	136.0
250	137.1		127.8	129.9	127.3	130.4	130.1	132.1	139.8	140.9	138.8	139.1
315	159.9		133.2	131.8	133.2	132.0	135.2	133.8		146.5	147.2	144.3
400	159.2	152.9	139.9	136.6	140.2	136.6	141.7	138.1	148.9	146.4	149.2	147.1
200	140.7	131.4	142.7	137.1	142.5	136.9	143.7		147.7		147.5	142.6
630	145.8	133.5	144.3	139.0	145.8	140.7	144.8	140.2	149.8	144.5	149.8	144.5
800	141.7	133.7	146.0	•	147.7	143.2	148.0	144.2	149.7		150.2	146.9
1000	139.9	130.6	145.1	142.1	144.6		147,1	143.6	147.6		147.1	143.6
1250	132.9		143.6		144.1		145.1	144.2	142.1		141.1	143.4
1600	133.2	127.2	136.4		136.4	138.9		141.7	142.7		142.2	141.4
2000	130.5	•	136.0		136.5	138.0	137.8	140.0	140.3		139.5	138,5
2500	129.5		136.3	136.5	135.8	136.5	138.0	139.5	137.5	137.3	137.8	136.5
3150	126.9		130.9	136.8	131.9		133.7	140.0	134.7		133.4	137.5
4000	123.8		128.1	135.5	129.1	-	.*	139.5			131.3	135.8
2000	122.6	119.2	125.3	134.4	126.6	135.1	127.8	138.4	128.8		128.3	133.4
6300	122.7		122.0	130.6	122.5	133.1	123.5	134.9	127.0	131.1	125.7	130.6
8000	128.8	122.3	121.6	130.9	120.6	133.9		136.4	129.1	•	127.6	7
10,000	132.5	•	122.8	136.3	122.3	131.3	123.5	132.8	132.0	134.8	131.8	133.3
OASPL.	162.7	156.1	152.4	151.0	153.1	151 2	154.0	152 7	157 4	155.0	157 1 . 15% 6	157. 6

Table A-2 Combustor Rig Test Data SPL's

754 761 11 12	n a n	.3 129.5 129.6	129.1 131.5	130.6 131.7	129.9 133.9	129.5 132.1	130.4 133.3	134.8 132.3	131.8 135.1	136.0 135.0	.1 134.3 138.4 153.3	139.9 140.5	146.9 141.9	148.0 143.4	149.0	152.2 147.4	151.6 147.9	150.6 148.2	144.7 145.4	144.8 144.8	144.8	141.2 145.0	139.6 146.3	136.3 146.9	131.5	9 126.8 138.6	8 128.8 136.8	1 7 3 1 5 7 3 1
751 10	a D	127.5	127.1	128.4	128.6	127.5	128.6	132.8	130.3	134.5	136.9 132.3 136.1	138.2	145.2	146.5		150.2	150.1	8.4 149.4 146.2	142.4	142.5	142.5	138.7	136.8		128.5	_	80	157 1 157 1 155 3
752	Þ		129.9	130.9	130.6	130.8	131.1	134.0	132.0	0 136.0	9 135.1	8 140.2	9 146.2	9 148.0	2 149.0	.4 151.7	152.5	150.9	145.4	144.5	144.8	140.7	138.1	135.8	130.0	126.1 1	126.8 1	0 851
753 8	Q D	129.5 129	130.4 132.8	-		130,3 131,1					131.6 133.	-	2	1				146.4 143.7										155.5 154.3
Rdg. Point	Probe Frequency	31.5	9	20	63	8	100	125	160	200	250	315	007	200	630	800	1000	1250	1600	2000	2500	3150	4000	2000	6300	8000	10,000	OACDI

Table A-3 Combustor Rig Test Data SPL's

1			11
9	Δ	137.8 137.5 139.2 140.1 138.3 140.1 140.1 141.8 144.6 144.6 144.6 144.6 151.9 151.9 151.9 151.0 153.0 153.0	
756	Þ	139.3 138.1 138.1 138.6 140.3 140.3 141.7 141.7 143.7 151.0 151.0 151.0 151.0 151.0 151.0 151.0 151.0 151.0 151.0 151.0	
2	Q	138.5 138.5 138.5 143.9 142.6 141.0 141.3 143.9 144.9 145.8 148.9 154.9 154.9 154.9 154.9 154.9 154.9 154.9 154.9 154.9 154.9 154.9 154.9 154.9 154.9 156.4 166.3	
755	D	140.0 133.9 139.9 141.0 141.0 142.2 140.1 152.2 156.9 156.9 156.9 156.9 156.9 156.9 156.9 156.9 153.3 133.3	
8	Q	137.0 139.0 144.1 142.6 140.0 141.0 146.4 152.9 153.6 153.6 153.7 154.7	
758	n	138.8 137.4 137.4 137.9 139.0 142.3 142.2 157.2 157.2 157.6 157.0	
7	Q	136.0 137.5 138.5 140.4 137.8 139.3 144.9 145.1 152.1 152.1 152.1 152.1 152.1 150.2 146.8 146.8 146.8 146.5 146.5 139.3	
25.21	Ω	137.5 133.6 135.1 135.6 137.3 137.3 141.5 141.7 145.6 160.0	
	D	133.3 136.0 137.2 138.6 135.8 137.2 136.6 142.1 149.0 149.0 149.0 149.0 140.3 144.8 145.0 142.4 137.1	
760	n	135.0 133.9 133.9 133.9 133.1 135.1 136.8 136.8 136.8 147.9 147.0 144.5 144.5 144.5 130.2 131.1 131.1	
6	D	135.8 138.7 141.4 140.9 139.3 139.3 144.8 147.9 153.6 153.6 153.6 153.6 153.1 153.1 153.1 153.1 147.3 147.3 147.3 147.3	
759	D	137.0 134.6 136.1 138.0 138.5 140.8 142.2 142.2 145.1 155.0 155.0 150.0 147.3 147.3 147.3 147.3 147.3 147.3	
Rdg. Point	Probe Frequency	31.5 40 50 63 100 100 100 100 100 100 100 10	

APPENDIX B

Low Frequency Noise Directivity Data

Table B-1

Low Frequency Core Noise Directivity Test Data

- 20 Ft. (6.1m) Arc
- 1 Hz Bandwidth
- Tone SPL's

Angle to inlet			Ton	e frequ	ency - 1	lz			
(degrees)	125	400	625	250	800	1250	375	1200	1875
40	78.7	(79.0)	82.3	77.9	(80.8)	76.3	(79.8)	(78.0)	(76.8
50	(79.0)	(80.0)	80.0	(80.0)	78.0	(79.0)	(80.7)	(78.3)	(78.8
60	(80.7)	(85.6)	80.4	(80.5)	(81.0)	76.2	(80.8)	(78.5)	(77.7
70	(81.2)	84.0	88.1	(81.7)	(81.5)	(79.3)	(81.0)	(78.5)	78.4
80	(81.0)	86.0	88.1	(83.0)	85.2	82.9	(82.5)	(80.0)	79.8
90	(82.7)	85.0	91.2	(83.7)	85.3	81.8	84.6	(80.8)	83.6
100	(83.6)	88.0	88.5	(85.3)	86.9	87.1	(85.0)	81.8	83.8
110	(83.7)	90.3	92.9	(88.0)	90.1	92.0	(88.5)	84.6	88.1
120	87.3	94.5	94.3	(90.2)	93.5	94.4	(89.8)	87.8	88.0
130	90.0	100.2	96.0	(93.4)	94.2	95.6	(92.8)	84.4	(87.3
140	95.3	106.5	(98.0)	(98.2)	(95.7)	97.7	(98.6)	95.7	87.2
150	96.2	107.3	97.2	(101.5)	(97.3)	96.30	(100.7)	91.0	86.8
160									

NOTE: Values within parenthesis denote the broadband floor level — tone was not discernible.

- 20 Ft. (6.1m) Arc
- 1 Hz Bandwidth
- Tone SPL's

Conf	iguratio	on1	No. 1			Rea	ding No.	151	
	v18 =	821	_ft/sec	(_250	_ m/sec)	T18 = 628	°R (349	_ °K)
	v8 =	1106	ft/sec	(337	m/sec)	T8 = 1407	°R (782	°K)

Angle to			Ton	e freque	ency - I	lz			
inlet (degrees)	125	400	625	250	800	1250	375	1200	1875
40	77.8	76.9	86.0	(76.7)	73.7	75.4	(77.0)	(75.0)	(73.0
50	79.3	75.7	88.5	76.0	73.7	81.4	(78.0)	75.1	(73.7
60	(78.8)	80.1	81.5	80.4	78.9	80.2	(78.7)	74.8	(74.6
70	(78.8)	(79.8)	87.5	82.7	77.9	78.4	(79:0)	75.5	74.4
80	78.6	83.7	87.5	81.3	78.8	85.1	(80.0)	75.0	75.9
90	83.3	83.4	93.3	83.6	80.1	85.4	(81.0)	74.7	(78.4
100	81.8	82.8	93.0	88.0	(82.6)	87.8	(82.5)	83.5	76.9
110	83.9	82.7	93.3	90.1	84.6	91.0	(85.5)	85.3	75.1
120	87.6	(88.0)	96.6	94.0	85.8	88.4	(87.3)	85.7	77.1
130	90.4	(90.0)	99.2	95.2	88.4	87.6	(90.0)	(85.0)	(81.0
140	95.5	(91.7)	98,1	96.3	(90.0)	(86.5)	(92.0)	(87.0)	(81.9
150	97.6	(92.5)	93.5	99.5	(91.3)	(84.0)	(93.7)	(84.8)	(80.6
160									

Table B-3
Low Frequency Core Noise Directivity Test Data

- 20 Ft. (6.1m) Arc
- 1 Hz Bandwidth
- Tone SPL's

Configuration	No	. 1	-				Read	ing No.	141	<u>4</u> -10
v18 = _	717	ft/sec	(219	m/sec)	T18 =	637	°R (_	354	_ °K)
v8 =	1088	ft/sec	(332	m/sec)	T8 = _	1382	_°R (768	°K)

Angle to inlet			Tone	freque	ency - I	łz			
(degrees)	125	400	625	250	800	1250	375	1200	1875
40	77.4	72.8	86.0	72.8	68.9	75.8	(71.0)	70.8	72.0
50	78.6	(73.0)	88.0	74.9	71.9	84.0	(72.0)	70.6	68.4
60	75.8	74.9	86.0	80.6	77.4	83.0	(73.5)	73.3	65.7
70	75.8	(74.0)	88.0	77.6	73.8	84.0	(74.0)	71.8	73.7
80	76.8	80.1	87.0	79.3	77.7	82.0	(75.5)	75.7	78.4
90	79.6		94.0	84.3		87.5	(79.0)		78.3
100	82.1	81.3	95.0	85.0	81.0	90.5	(78.0)	81.4	80.3
110	82.3	77.7	95.0	87.8	83.0	95.0	(80.0)	81.3	80.3
120	87.6	79.7	99.0	90.3	83.1	95.0	(83.0)	83.8	82.3
130	88.7	81.7	100.5	92.8	81.9	94.0	82.7	80.8	79.7
140	93.0	85.7	100.0	93.4	85.6	88.0	(0.88)	76.7	(75.0
150	95.4	(90.0)	97.0	97.0	86.6	79.8	87.7	(78.0)	(74.0
160									

Table B-4
Low Frequency Core Noise Directivity Test Data

- 20 Ft. (6.1m) Arc
- 1 Hz Bandwidth
- Tone SPL's

Angle to inlet			Ton	e freque	ncy -	Hz			
(degrees)	125	400	625	250	800	1250	375	1200	1875
40	77.3	69.9	86.0	(69.0)	77.0	75.0	(70.0)	(66.0)	69.1
50	79.0	(70.0)	88.0	(71.0)	76.3	74.3	(71.0)	(67.0)	69.6
60	75.7	72.8	85.0	(72.5)	77.3	75.4	(71.0)	(68.0)	67.0
70	76.7	(73.0)	89.0	(73.0)	79.5	78.0	(73.0)	(68.0)	75.8
80	79.0	77.3	87.0	(75.0)	80.5	81.0	(74.0)	(69.0)	75.8
90	82.4	78.3	94.0	(76.0)	83.0	79.5	(75.0)	(69.0)	75.0
100	83.3	80.3	94.0	77.0	81.3	84.0	(77.0)	70.4	78.3
110	83.0	82.7	94.0	(79.0)	83.4	. 86.0	(77.0)	(72.0)	78.8
120	86.8	85.0	95.0	(80.0)	76.0	, 79.6	(79.0)	73.0	79.1
130	88.3	85.4	97.5	(82.0)	82.7	* 82.8	(82.0)	(75.0)	77.7
140	88.7	87.3	96.0	(85.0)	82.3	76.0	(84.0)	(76.0)	(72.0
150	91.9	(86.0)	95.0	(86.5)	81.8	(75.0)	(85.5)	(74.0)	(71.0
160									

Table B-5
Low Frequency Core Noise Directivity Test Data

- 20 Ft. (6.1m) Arc
- 1 Hz Bandwidth
- Tone SPL's

Configuration	No. 1	Reading No. 101
V18 = 604	ft/sec (<u>184</u> m/sec) $T18 = 637$ °R (354 °K)
v8 = <u>801</u>	ft/sec (244 m/sec) $T8 = 1305$ °R (725 °K)

Angle to inlet			Ton	e freque	ency - 1	Hz			
(degrees)	125	400	625	250	800	1250	375	1200	1875
40	76.8	76.0	86.8	68.8	78.0	80.0	61.1	(63.8)	72.0
50	79.8	73.5	91.0	74.7	81.0	85.6	68.2	(66.0)	73.8
60	75.8	79.0	87.9	76.0	81.0	81.5	69.8	(66.5)	73.0
70	76.3	73.2	89.0	76.5	80.0	80.0	68.4	(67.0)	79.0
80	80.6	81.4	86.0	72.0	84.0	86.8	71.1	(66.2)	74.0
90	82.7	81.1	93.0	79.0	88.0	83.4	75.0	(68.3)	79.8
100	82.0	84.0	94.2	81.0	86.1	88.0	71.6	(68.8)	82.8
110	84.5	83.3	93.9	81.0	87.8	89.0	77.0	(70.7)	81.7
120	85.1	84.6	96.0	80.0	86.5	91.0	78.6	(71.2)	86.6
130	88.0	85.5	97.3	.84.8	87.8	91.2	79.3	(72.9)	80.
140	91.2	90.0	95.3	86.1	86.1	82.2	81.1	(72.9)	71.
150	91.5	89.3	95.2	87.6	88.0	76.3	80.2	(71.9)	70.
160									

Table B-6
Low Frequency Core Noise Directivity Test Data

- 20 Ft. (6.1m) Arc
- 1 Hz Bandwidth
- Tone SPL's

Conf	iguration	No. 1			Read	ling No.	51
	V18 = 482	_ft/sec (_147_	_ m/sec)	T18 =	669	_°R (372	°K)
	v8 = 500	_ft/sec (152	_ m/sec)	T8 = _	884	_°R (491	_ °K)

Angle to inlet			Tone	freque	ncy - I	lz			
(degrees)	125	400	625	250	800	1250	375	1200	1875
40	73.0	73.0	74.0	77.0	84.0	79.5	64.6	73.0	68.4
50	75.0	82.5	82.5	81.0	86.0	75.5	62.9	79.5	69.1
60	76.5	65.6	84.0	81.5	85.5	80.0	69.4	76.0	80.5
70	75.0	78.0	83.0	82.0	85.5	78.5	74.0	74.5	75.3
80	77.0	84.5	86.0	82.0	84.0	80.0	74.0	77.0	78.5
90	78.0	88.5	85.0	83.0	86.0	80.5	72.4	72.5	72.3
100	69.7	85.5	86.0	84.5	87.0	84.0	75.5	76.0	67.7
110	80.0	88.0	89.0	88.0	89.0	86.0	73.4	78.0	76.9
120	80.5	89.0	89.0	87.0	90.0	89.0	71.9	83.5	82.0
130	79.5	89.0	89.0	88.5	89.5	88.5	74.1	86.5	82.0
140	83.5	92.0	86.0	89.0	92.0	85.0	74.0	83.0	71.0
150	84.5	92.5	86.5	88.0	92.0	64.4	73.7	75.0	72.0
160		10 1							

Table B-7
Low Frequency Core Noise Directivity Test Data

- 20 Ft. (6.1m) Arc
- 1 Hz Bandwidth
- Tone SPL's

Configuration No. 2						Rea	ding No.	191	Side
	V18 =	912	_ ft/sec	(278	_ m/sec)	T18 = 659	°R (366	_ °K)
	v8 = _	1491	_ft/sec	(455	_ m/sec)	T8 = 1399	°R (777	°K)

Angle to inlet		Tone frequency - Hz												
(degrees)	125	400	625	250	800	1250	375	1200	1875					
40	81.7	80.9	87.1	(81.0)	87.3	88.8	(83.0)	86.7	75.2					
50	79.0	84.1	89.5	77.7	86.7	88.5	(80.0)	82.3	(77.0					
60	(80.0)	80.0	84.7	81.8	80.0	89.5	(80.0)	78.5	77.9					
70	(81.0)	81.4	86.4	(81.0)	(81.0)	92.0	79.7	84.7	(79.0					
80	(82.0)	86.3	89.0	79.2	85.3	88.8	(82.0)	86.0	(77.0					
90														
100	84.8	87.8	95.0	(86.0)	(85.0)	90.3	(86.0)	84.0	(83.0					
110	82.7	91.3	95.8	(88.0)	93.0	88.1	85.7	85.8	81.7					
120	88.8	91.9	98.8	89.0	93.7	(86.0)	(90.0)	(87.0)	86.9					
130	92.8	95.8	100.8	91.7	93.8	86.7	(94.0)	(89.0)	86.0					
140	98.7	99.8	101.7	97.0	(96.0)	(91.0)	(98.0)	(92.0)	(87.0					
150	102.3	101.0	96.7	102.0	(97.0)	(91.0)	(101.0)	(91.0)	(86.0					
160														

Table B-8

Low Frequency Core Noise Directivity Test Data

- 20 Ft. (6.1m) Arc
- 1 Hz Bandwidth
- Tone SPL's

Configuration No. 2							Read	ing No.	151		
31	V18 =	826	_ft/sec	(278	m/sec)	T18 =	659	_°R (366	_ °K)
	v8 = _	1096	_ft/sec	(334	m/sec)	т8 = _	1397	_°R (776	_ °K)

Angle to inlet		Tone frequency - Hz												
(degrees)	125	400	625	250	800	1250	375	1200	1875					
40	81.8	83.3	92.0	(79.6)	77.7	77.8	(31.7)	(79.0)	80.0					
50	76.0	79.3	91.8	(78.0)	(78.8)	76.3	(79.9)	(75.4)	77.0					
60	78.3	79.8	88.0	(80.0)	81.1	76.3	(80.0)	(74.0)	76.3					
70	80.1	80.3	90.2	(81.2)	79.9	78.1	(80.0)	(75.5)	78.9					
80	(80.0)	84.7	91.6	(82.0)	81.7	80.7	(81.0)	73.7	82.3					
90														
100	83.8	86.1	97.0	(86.0)	84.9	87.0	(85.0)	(79.8)	86.4					
110	86.3	88.3	98.2	(88.0)	86.8	89.8	(88.0)	(82.6)	87.1					
120	88.8	91.7	101.0	(90.0)	88.7	92.2	(88.3)	81.0	89.0					
130	90.3	96.3	103.0	(91.0)	90.7	89.5	(90.0)	(84.6)	83.3					
140	92.8	98.0	100.1	(94.5)	88.0	84.8	(94.0)	(85.5)	80.0					
150	96.8	94.0	97.3	(98.0)	(90.2)	82.0	(94.9)	(84.3)	(79.0					
160														

Table B-9
Low Frequency Core Noise Directivity Test Data

- 20 Ft. (6.1m) Arc
- 1 Hz Bandwidth
- Tone SPL's

Configuration	·	No. 2				Readi	ng No.	141	_
v18 = _	727	ft/sec	(222	m/sec)	T18 = _	655	_°R (364	_ °K)
v8 =	1110	ft/sec	(338	m/sec)	T8 =	1396	_°R (776	_ °K)

Angle to inlet			Tor	e frequ	ency -	Hz			
(degrees)	125	400	625	250	800	1250	375	1200	1875
40	85.3	(78.3)	90.0	(77.0)	(78.7)	81.4	(80.0)	(74.0)	81.8
50	79:6	(76.0)	90.0	(76.0)	(75.5)	76.8	(76.8)	(70.8)	77.3
60	77.6	(79.2)	87.5	(78.0)	76.9	74.7	(79.0)	(71.3)	76.0
70	79.3	(77.0)	87.0	(78.0)	78.6	81.7	(77.0)	(71.0)	75.8
80	78.8	84.0	88.7	(80.0)	78.7	84.0	(79.7)	76.0	81.2
90									
100	37.1	86.3	96.0	81.0	79.4	88.3	(83.0)	78.1	85.7
110	86.7	88.3	98.0	82.1	85.9	90.4	80.7	84.1	89.0
120	91.4	90.5	100.0	(86.0)	84.6	90.6	(87.2)	85.2	91.2
130	94.2	94.3	102.7	(90.0)	87.8	87.3	(89.2)	80.4	83.3
140	97.2	96.0	100.6	91.0	85.4	81.2	(92.0)	(82.0)	77.8
150	100.0	92.9	99.0	92.4	(86.8)	(81.6)	(93.7)	(81.0)	(75.0)
160									

Table B-10

Low Frequency Core Noise Directivity Test Data

- 20 Ft. (6.1m) Arc
- 1 Hz Bandwidth
- Tone SPL's

Con	figuratio	n N	0.2				111	_		
	V18 =	708	_ft/sec	(216	_ m/sec)	T18 =	656	_°R (364	_ °K)
	v8 = _	819	_ft/sec	(250	_ m/sec)	T8 = _	1424	_°R (791	_ °K)

Angle to inlet		Tone frequency - Hz												
(degrees)	125	400	625	250	800	1250	375	1200	1875					
40	81.9	77.0	90.5	81.4	78.1	75.1	(78.0)	72.0	(70.0					
50	79.3	80.4	89.5	81.4	75.1	69.9	(75.0)	67.9	(68.0					
60	76.3	73.7	87.5	83.8	75.3	69.0	(76.0)	71.8	(69.0					
70	74.0	75.8	86.5	84.8	75.7	76.3	(76.0)	67.2	(69.0					
80	76.0	84.6	87.5	84.0	82.0	82.0	(77.0)	71.9	(71.0					
90	80.6	85.6	93.5	84.7	83.0	82.5	(79.0)	75.7	70.4					
100	76.7	86.0	94.5	88.4	82.0	86.0	(79.0)	78.4	74.0					
110	79.5	87.0	95.5	90.3	84.8	90.0	(81.0)	76.3	75.3					
120	85.7	87.7	96.5	91.8	85.3	90.0	(83.0)	79.3	78.7					
130	87.7	89.4	99.0	90.7	87.4	88.0	(84.0)	73.2	72.2					
140	90.7	90 6	96.0	93.4	87.8	83.6	(87.0)	(79.0)	(74.0					
150	93.1	88.8	92.4	95.4	85.3	73.9	(87.0)	(76.0)	(73.5)					
160														

Table B-11
Low Frequency Core Noise Directivity Test Data

- 20 Ft. (6.1m) Arc
- 1 Hz Bandwidth
- Tone SPL's

Configuration	n	No. 2					Read	ing No	101	
V18 =	708	_ft/sec	_	216	m/sec)	T18 =	653	°R (362	_ °K)
v8 = _	824	_ft/sec	(_	251	m/sec)	T8 = _	1446	_°R (803	_ °K)

Angle to inlet			Tor	e frequ	ency - F	z			
(degrees)	125	400	625	250	800	1250	375	1200	1875
40	80.8	79.7	89.8	(75.0)	78.5	79.0	(73.8)	70.1	68.8
50	78.6	78.4	89.0	(76.0)	75.5	76.8	(73.0)	68.3	(70.8
60	79.0	(73.0)	87.1	(75.7)	(70.0)	73.1	(74.8)	(67.1)	(69.0
70	80.3	74.8	84.5	(78.1)	(77.0)	75.8	(74.0)	(68.0)	(69.4
80	78.9	82.5	89.0	(77.0)	80.0	84.4	(75.0)	(70.0)	71.3
90	80.0	85.0	94.3	(79.0)	78.1	85.6	(77.5)	(72.0)	(72.7
100	80.7	87.0	95.0	80.1	79.1	87.5	(79.0)	77.4	(75.0
110	81.8	86.6	97.0	83.7	82.7	91.0	(80.5)	81.0	79.5
120	86.6	89.0	97.8	81.8	85.0	91.5	(80.5)	80.1	84.0
130	87.1	89.7	99.2	82.0	86.4	91.1	(82.5)	80.5	79.5
140	89.5	87.5	97.3	(87.0)	83.0	86.2	(83.6)	(74.8)	(72.7
150	92.8	86.7	93.0	(89.0)	82.2	77.0	(85.5)	(73.7)	(72.2
160									

Table B-12

Low Frequency Core Noise Directivity Test Data

- 20 Ft. (6.1m) Arc
- 1 Hz Bandwidth
- Tone SPL's

Conf	iguratio	n N	0. 2				Reading No.					
	V18 =	489	_ft/sec	_	149	m/sec)	T18 =	644	°R	(358	°K)
	v8 = _	474	_ft/sec	(_	144	m/sec)	T8 = _	1014	_°R	(563	°K)

Angle to inlet			Ton	e freque	ncy - 1	Hz			
(degrees)	125	400	625	250	800	1250	375	1200	1875
40	78.4	86.5	78.0	(70.0)	92.5	79.0	(70.0)	68.1	74.6
50	78.0	82.0	77.0	(71.0)	86.5	81.0	(68.0)	75.0	74.0
60	75.3	84.5	72.4	67.7	86.0	79.0	(68.5)	73.0	71.6
70	75.4	83.5	76.5	74.3	88.0	78.0	67.0	73.0	72.8
80	79.5	87.5	77.5	69.2	89.0	78.5	(69.0)	73.5	73.3
90	80.5	89.0	80.0	74.8	89.0	79.0	67.7	75.0	71.3
100	78.0	88.5	81.0	76.6	89.5	82.0	69.7	77.0	77.8
110	80.4	88.0	82.5	78.3	94.0	86.5	71.9	80.5	79.0
120	82.0	87.0	84.0	77.0	91.5	89.0	70.2	83.0	82.0
130	83.4	87.5	85.5	80.3	93.5	89.0	(75.5)	82.0	82.0
140	86.0	90.0	83.0	81.3	92.0	87.5	(76.0)	83.0	66.8
150	85.8	88.0	80.5	84.4	93.0	72.3	(76.0)	69.0	66.0
160	16.303								

Table B-13

Low Frequency Core Noise Directivity Test Data

- 20 Ft. (6.1m) Arc
- 1 Hz Bandwidth
- Tone SPL's

Coni	Configuration No. 3 V18 = 891 ft/sec (Read	ing No.	191	HE-no
	V18 =	891	_ft/sec	ر	272	_ m/sec)	T18 =	641	_°R (356	_ °K)
	v8 = _	1481	_ft/sec	(451	_ m/sec)	T8 = _	1410	_°R (783	_ °K)

Angle to inlet		Tone frequency - Hz											
(degrees)	125	400	625	250	800	1250	375	1200	1875				
40	(82.0)	83.8	82.1	77.8	(81.0)	81.6	(82.5)	(79.2)	84.0				
50	79.6	(81.8)	(83.0)	(81.6)	(81.8)	79.4	(80.3)	(79.2)	83.5				
60	(77.7)	(82.0)	86.0	(81.5)	(81.8)	(78.4)	(81.2)	(80.0)	86.1				
70	(79.2)	(82.2)	89.0	(82.4)	(83.0)	81.9	(84.0)	(80.5)	84.7				
80	(80.0)	86.6	(83.0)	(81.8)	80.6	86.0	(84.0)	(81.4)	87.7				
90	(82.3)	(84.0)	90.0	(82.7)	84.6	83.4	(85.5)	(80.8)	85.2				
100	(81.0)	85.1	92.4	(85.0)	(87.0)	(83.8)	(87.0)	86.9	85.8				
110	86.8	(89.0)	98.0	86.0	86.4	89.7	87.0	88.9	(87.0				
120	91.2	93.9	100.0	89.2	87.2	88.7	(92.1)	89.7	(88.0				
130	96.3	97.3	98.9	96.7	95.1	90.3	(98.6)	93.4	(90.0				
140	100.5	107.2	103.5	99.0	(100.0)	97.6	98.9	(98.3)	(91.8				
150	103.2	109.0	109.1	104.4	(102.8)	102.9	(105.0)	96.2	93.0				
160	101.9	109.5	109.6	(105.2)	97.0	104.30	106.5)	99.7	88.2				

Table B-14

Low Frequency Core Noise Directivity Test Data

- 20 Ft. (6.1m) Arc
- 1 Hz Bandwidth
- Tone SPL's

Con	figuratio	n		Reading No151							
	v18 =	823	_ft/sec	C	251	m/sec)	T18 =	638	_°R (354	_ °K)
	v8 = _	1112	_ft/sec	(339	_ m/sec)	T8 = _	1406	_°R (781	_ °K)

Angle to inlet			Tone	frequer	cy - H	z			
(degrees)	125	400	625	250	800	1250	375	1200	1875
40	82.0	85.0	88.5	(76.7)	84.0	77.9	(77.0)	75.4	89.3
50	82.3	84.0	89.9	(77.5)	82.6	83.6	(78.0)	77.1	90.1
60	(77.0)	79.6	90.0	(78.5)	87.4	79.2	76.8	79.6	89.3
70	(76.5)	81.8	89.3	77.3	85.6	87.5	(78.8)	81.4	93.0
80	80.6	87.2	90.8	(79.0)	83.8	83.4	75.7	79.0	96.0
90	85.5	90.8	90.4	(80.0)	85.2	87.0	(80.0)	78.2	98.7
100	75.9	92.0	96.0	(81.5)	87.4	89.0	(81.6)	83.0	98.0
110	87.4	94.5	99.0	83.8	88.4	91.0	(84.3)	89.8	100.0
120	91.0	97.5	101.0	86.9	92.3	92.0	(86.0)	93.2	97.0
130	95.4	95.2	100.6	92.7	90.0	92.5	(89.0)	92.3	95.0
140	100.0	95.6	101.0	96.6	87.7	87.7	(91.7)	90.3	77.7
150	102.7	97.6	(92.5)	98.4	92.7	84.8	(96.8)	85.2	85.8
160	101.1	101.6	97.1	97.0	91.1	(80.8)	(97.5)	80.9	83.4

Table B-15
Low Frequency Core Noise Directivity Test Data

- 20 Ft. (6.1m) Arc
- 1 Hz Bandwidth
- Tone SPL's

Angle to inlet			Ton	e freque	ency -	Hz		
(degrees)	125	400	625	250	800	1250 375	1200	1875
40	84.7	79.6	87.3	(74.0)	79.2	77.4 (75.0)	74.7	81.6
50	83.0	83.3	89.3	77.0	78.0	71.8 (75.7)	76.3	86.1
60	(75.0)	79.6	89.0	(76.8)	75.7	80.0 (76.3)	81.0	83.1
70	(74.0)	83.7	89.0	(79.0)	78.8	84.0 (75.6)	84.8	87.8
80	81.5	87.5	90.6	80.2	78.4	83.8 (77.3)	80.5	88.3
90	85.5	89.0	91.0	80.7	84.7	85.7 (79.0)	79.4	91.0
100	85.0	91.0	96.0	(80.0)	84.3	87.0 (80.4)	84.4	92.0
110	86.5	92.3	98.4	87.3	86.9	90.7 (83.0)	88.7	93.4
120	93.7	94.4	100.2	86.9	90.2	93.8 (85.0)	92.0	92.0
130	97.0	91.4	100.0	89.6	90.0	94.0 89.5	90.4	90.3
140	100.0	94.2	100.1	97.4	89.8	89.6 (92.0)	89.2	(79.9
150	103.0	95.6	88.0	99.6	91.4	84.4 (94.6)	82.8	(78.3
160	102.0	97.5	94.0	98.9	90.5	80.1 (94.6)	78.6	(74.6

Table B-16
Low Frequency Core Noise Directivity Test Data

- 20 Ft. (6.1m) Arc
- 1 Hz Bandwidth
- Tone SPL's

Angle to inlet			Ton	e freque	ency -	Hz			
(degrees)	125	400	625	250	800	1250	375	1200	1875
40	75.3	83.0	90.0	(67.0)	74.0	69.9	(70.0)	76.5	78.0
50	74.3	85.0	92.5	70.9	77.4	70.0	70.8	71.3	79.5
60	76.8	84.0	92.0	72.6	78.0	71.0	70.0	80.0	77.4
70	75.0	84.5	92.0	71.0	77.4	73.3	70.0	80.0	80.0
80	76.3	86.5	94.5	73.8	79.5	75.4	68.7	79.5	83.0
90	81.5	89.5	93.0	84.5	81.0	80.0	(74.0)	79.0	83.0
100	81.4	90.0	97.5	76.8	85.0	82.0	74.0	82.0	86.0
110	78.2	91.5	99.0	78.8	81.0	84.0	74.9	85.0	87.0
120	84.5	94.5	101.0	80.8	88.0	87.5	77.5	88.0	89.0
130	87.5	93.0	98.0	81.8	90.0	87.0	(80.0)	84.5	85.0
140	88.8	93.5	101.0	(82.5)	90.0	85.0	78.7	82.0	76.0
150	94.0	90.0	95.5	(84.0)	90.0	80.0	(82.0)	78.4	74.6
160	92.4	86.0	87.0	(83.0)	86.0	74.6	(81.0)	75.0	67.4

Table B-17
Low Frequency Core Noise Directivity Test Data

- 20 Ft. (6.1m) Arc
- 1 Hz Bandwidth
- Tone SPL's

Config	guration	n <u>N</u>	0. 3				Read	ing No.	101	_
	v18 =	589	ft/sec	(_180	_ m/sec)	T18 =	638	_°R (354	_ °K)
	v8 = _	773	ft/sec	(236	_ m/sec)	T8 = _	1415	_°R (786	_ °K)

Angle to inlet			Tor	ne freque	ency -	Hz			
(degrees)	125	400	625	250	800	1250	375	1200	1875
40	77.0	84.0	.90.0	72.0	75.0	70.4	77.7	73.0	77.0
50	79.0	86.0	93.0	75.0	79.0	73.7	(69.5)	68.1	79.0
60	77.0	83.0	93.0	71.3	79.0	76.0	(70.1)	76.0	80.0
70	74.3	85.0	90.0	76.3	77.0	78.0	(69.0)	77.0	80.0
80	75.4	88.0	93.0	78.6	80.0	79.0	(70.0)	78.0	80.0
90	80.5	90.0	88.0	81.0	82.5	79.7	70.7	78.3	84.4
100	78.3	91.0	96.0	79.0	85.0	81.0	(74.0)	80.0	83.0
110	78.3	87.0	99.0	82.3	83.0	85.0	(75.0)	83.0	87.0
120	84.0	96.0	100.7	84.7	89.0	88.0	(76.8)	87.0	87.0
130	87.0	94.0	99.0	84.0	91.0	88.0	77.7	83.0	82.0
140	91.0	94.0	100.7	84.2	90.8	85.5	76.9	80.0	79.4
150	93.4	91.0	96.8	84.3	91.0	80.0	(80.0)	71.8	77.7
160	91.2	88.2	78.8	(83.0)	87.4	72.2	(78.8)	68.6	81.2

Table B-18

Low Frequency Core Noise Directivity Test Data

- 20 Ft. (6.1m) Arc
- 1 Hz Bandwidth
- Tone SPL's

Conf	iguratio	n	No. 3	_			Read	ing No.	51	_
	V18 =	518	_ft/sec	158	_ m/sec)	T18 =	632	_°R (351	_ °K)
, ia	v8 = _	496	_ft/sec	(151	_ m/sec)	T8 = _	974	_°R (541	_ °K)

Angle to inlet			Ton	e frequ	ency -	Hz			
(degrees)	125	400	625	250	800	1250	375	1200	1875
40	75.5	73.5	74.0	81.0	84.0	77.0	64.6	75.5	69.1
50	77.0	73.0	73.0	82.5	87.0	69.0	1.9	74.5	67.6
60	76.5	77.0	76.5	79.5	85.0	78.0 (6	4.0)	79.5	(69.0
70	76.0	67.1	76.0	83.0	86.0	80.0	6.6	80.0	(68.5
80	78.0	80.0	64.0	83.0	86.0	82.0	0.0	79.0	(68.0
90	80.0	83.0	76.5	86.0	89.0	82.0	9.4	79.0	70.9
100	78.5	77.5	76.0	86.0	90.0	84.0	4.4	84.0	68.9
110	81.0	82.0	73.3	89.5	90.0	87.5	0.7	84.0	75.1
120	81.0	87.0	79.0	89.0	92.5	87.5	1.7	87.5	81.0
130	82.5	84.0	82.0	89.0	91.0	88.0 7	1.3	87.0	79.0
140	85.5	89.0	88.0	90.0	93.0	86.0 7	4.9	86.0	76.5
150	84.5	88.5	79.5	90.5	94.5	78.0 7	4.7	81.0	73.0
160	83.0	88.5	85.0	85.5	89.0	79.5 6	9.9	79.5	74.0

- 20 Ft. (6.1m) Arc
- 1 Hz Bandwidth
- Tone SPL's

Angle to inlet			Ton	e frequ	ency -	Hz			
(degrees)	125	400	625	250	800	1250	375	1200	1875
40	80.8	(78.0)	86.3	79.8	(82.0)	(77.0)	80.0	(77.0)	76.9
50	(78.0)	89.0	89.0	(80.0)	79.7	88.0	(79.0)	(77.0)	80.3
60	80.8	80.8	84.7	77.7	(80.0)	79.8	77.7	76.4	81.3
70	79.9	82.0	90.0	(80.0)	(80.0)	83.1	(81.0)	79.0	80.3
80	81.6	84.8	86.4	(81.0)	81.9	81.8	79.7	(80.0)	86.4
90	(81.0)	83.5	87.1	(83.0)	(82.5)	83.8	81.7	(81.5)	88.7
100	83.8	90.6	95.0	86.8	(86.0)	90.0	81.1	(84.0)	92.4
110	84.9	90.3	94.8	86.9	(88.0)	93.4	(88.0)	89.7	92.7
120	90.9	96.0	100.0	93.7	88.7	93.4	86.1	92.3	93.7
130	96.6	102.3	92.2	96.6	(95.0)	92.0	91.2	90.9	87.7
140	95.3	100.3	91.8	93.8	86.1	(89.0)	(95.0)	85.7	79.4
150	102.1	110.0	104.6	104.8	101.9	101.1	102.9	94.7	(91.0
160									

- 20 Ft. (6.1m) Arc
- 1 Hz Bandwidth
- Tone SPL's

Configuration	1	No. 4					Reading No. 151				
V18 = _	817	ft/sec	_	249	m/sec)	T18 =	639	_°R (355	_ °K)	
v8 =	1093	ft/sec	(_	333	m/sec)	T8 = _	1389	_°R (772	°K)	

Angle to inlet			Tone	freque	ency - l	lz			
(degrees)	125	400	625	250	800	1250	375	1200	1875
40	79.7	69.2	87.5	71.9	83.4	80.0	71.7	78.4	72.3
50	79.3	84.0	94.0	73.5	83.8	82.5	(73.0)	76.0	77.5
60	84.0	76.6	87.0	72.7	81.4	80.0	71.7	77.6	84.0
70	82.3	80.9	88.5	76.8	81.1	91.0	73.9	85.0	84.5
8G	79.7	87.0	91.0	77.4	81.1	92.5	(76.0)	86.5	81.8
90	78.8	88.5	94.5	75.7	83.4	93.0	78.0	87.5	89.0
100	87.0	92.0	98.0	81.6	87.4	94.0	(79.5)	89.0	92.0
110	87.4	91.4	98.5	85.3	84.3	94.0	(81.0)	90.0	90.0
120	90.0	95.0	103.0	90.6	84.0	98.0	85.0	93.0	89.4
130	95.5	95.3	103.0	90.3	88.3	98.5	87.0	92.4	83.9
140	94.0	93.0	98.5	89.3	82.0	95.0	82.7	88.8	75.3
150	100.3	91.7	98.4	99.7	88.0	89.4	89.7	(84.0)	75.2
160									

Table B-21
Low Frequency Core Noise Directivity Test Data

- 20 Ft. (6.1m) Arc
- 1 Hz Bandwidth
- Tone SPL's

Angle to inlet			Ton	e freque	ency -	Hz			
(degrees)	125	400	625	250	800	1250	375	1200	1875
40	78.0	74.7	85.0	71.0	85.0	83.5	73.8	79.0	72.1
50	78.4	84.0	92.0	71.0	84.0	85.5	(71.0)	80.0	79.4
60	83.0	66.7	86.0	(73.0)	75.8	85.0	69.7	78.0	83.0
70	82.0	78.7	88.5	73.9	84.5	91.0	74.0	86.5	82.0
80	79.0	87.0	90.0	72.7	79.0	94.5	73.9	88.5	84.0
90	81.0			77.8	-		77.8	-	-
100	85.5	91.5	96.0	78.0	87.0	95.0	79.0	89.0	90.0
110	88.0	92.0	98.0	84.1	86.3	95.0	77.7	92.5	86.4
120	91.0	95.0	102.0	90.5	91.0	100.0	83.9	94.5	84.5
130	95.5	96.5	102.0	93.3	90.3	100.0	83.7	94.0	79.4
140	93.5	94.0	99.0	89.1	85.6	96.0	82.7	92.0	70.9
150	101.0	91.0	98.0	99.6	89.3	90.0	87.7	89.4	75.8
160									

Table B-22

Low Frequency Core Noise Directivity Test Data

- 20 Ft. (6.lm) Arc
- 1 Hz Bandwidth
- Tone SPL's

Conf	iguration	No. 4		Reading No. 111				
	v18 = 671	ft/sec (_205 m/s	sec) T18 =	648	_°R (360	°K)	
	v8 = 788	ft/sec (240 m/s	sec) T8 = _	1408	_°R (782	°K)	

Angle to inlet			Ton	e freque	ency - I	-lz			
(degrees)	125	400	625	250	800	1250	375	1200	1875
40	77.3	77.5	86.0	82.0	83.0	77.0	(67.0)	75.0	68.6
50	74.6	86.5	92.5	84.0	82.0	79.0	(68.5)	68.4	66.4
60	76.6			83.5	_	_	67.9		
70	77.6	85.0	91.0	84.0	81.0	83.0	67.7	77.0	74.3
80	81.5	88.5	91.0	84.5	79.5	88.0	68.7	79.0	73.5
90	77.7	89.5	92.5	87.0	84.0	86.0	73.0	77.0	77:0
100	77.3	90.0	96.0	87.0	86.0	88.5	72.9	75.0	76.1
110	81.6	90.5	97.0	90.0	86.5	88.0	72.7	79.5	79.6
120	81.1	93.0	101.5	93.0	90.0	92.5	74.7	84.0	83.0
130	86.8	93.0	100.0	92.5	92.0	93.5	(78.5)	81.4	81.0
140	84.0	89.5	97.0	89.0	88.0	89.5	73.2	77.1	73.0
150	93.4	89.4	95.0	96.0	90.0	87.0	(81.5)	(73.0)	66.9
160									

Table B-23

Low Frequency Core Noise Directivity Test Data

- 20 Ft. (6.1m) Arc
- 1 Hz Bandwidth
- Tone SPL's

Configuration	Figuration No. 4					Reading No. 101					
v18 =	599	ft/sec	(183	m/sec)	т18 =	660	°R (367	_ °K)	
v8 =	786	ft/sec	(240	m/sec)	T8 = _	1390	_°R (772	_ °K)	

Angle to inlet			Ton	e freque	ncy - I	łz			
(degrees)	125	400	625	250	800	1250	375	1200	1875
40	77.8	81.6	85.0	74.5	86.0	78.0	70.3	74.1	70.4
50	79.0	86.2	92.0	72.8	85.7	81.0	67.3	67.8	66.0
60									
70	80.0	84.0	90.0	76.9	85.0	84.0	67.4	76.5	76.3
80	78.0	88.4	89.0	77.3	82.0	88.7	71.3	78.0	(71.3)
90	81.3	91.0	90.5	79.4	86.0	88.0	73.3	78.0	80.0
100	84.0	91.3	95.0	81.1	87.5	89.0	73.4	75.5	80.2
110	81.5	91.5	96.6	83.4	89.0	89.0	71.9	80.7	83.0
120	85.0	93.7	100.0	84.4	90.6	94.6	77.2	82.0	85.0
130	89.8	95.0	99.6	85.3	92.6	94.4	(78.0)	84.0	82.8
140	86.5	91.5	95.7	82.0	89.4	90.3	(78.0)	79.7	74.4
150	95.0	90.3	94.8	(84.4)	94.0	89.0	(80.0)	77.4	76.0
160									

Table B-24
Low Frequency Core Noise Directivity Test Data

- 20 Ft. (6.1m) Arc
- 1 Hz Bandwidth
- Tone SPL's

Angle to inlet			Tone	freque	ency - 1	Hz			
(degrees)	125	400	625	250	800	1250	375	1200	1875
40	75.0	73.0	78.5	74.5	86.0	80.0	72.0	74.0	75.5
50	77.5	84.5	84.5	79.0	85.0	82.0	73.5		73.5
60	-	_	_	-	_		<u>.</u>		
70	77.5	82.0	83.0	80.0	85.5	84.5	72.4	76.0	78.5
80	78.5	86.0	83.0	80,5	81.0	86.5	74.0	77.0	78.0
90	79.0	88.0	81.0	82.0	84.0	84.0	75.0	78.0	82.0
100	76.5	87.5	84.0	83.0	87.0	88.0	78.0	75.0	82,5
110	81.5	89.0	85.5	85.5	87.0	86.0	75.4	79.5	83.5
120	81.5	90.0	89.0	86.5	89.0	90.0	77.4	81.0	82.5
130	82.5	91.0	86.5	86.0	88.5	90.0	76.3	82.0	85.0
140	82.0	90.0	83.5	84.0	84.5	86.5	73.5	78.5	78.0
150	86.0	91.5	82.0-	88.5	90.0	76.5	74.3	76.0	78.5
160	140416								

Table B-25
Low Frequency Core Noise Directivity Test Data

- 20 Ft. (6.1m) Arc
- 1 Hz Bandwidth
- · Tone SPL's

Angle to inlet			Tone	frequer	ncy -	Hz			
(degrees)	125	400	625	250	800	1250	375	1200	1875
40	78.9	(77.0)	86.4	74.8	74.6	79.0	(79.0)	75.8	(73.0)
50	74.8	(76.5)	88.8	77.4	74.3	84.6	77.0	(74.0)	72.6
60	(75.0)	77.3	89.4	(76.0)	76.2	79.0	(78.0)	78.5	(74.0)
70	(75.0)	80.1	84.5	77.0	76.9	87.2	(77.0)	78.4	(77.0)
80	(78.0)	79.3	89.6	(80.0)	77.8	89.0	(78.7)	81.7	(77.8)
90	83.0	83.0	89.8	79.0	85.0	90.0	(80.0)	87.0	(78.0)
100	82.4	82.9	95.5	78.8	84.1	93.2	(82.0)	86.7	(79.0)
110	82.8	86.4	97.5	82.0	86.7	95.0	(84.0)	88.0	81.1
120	89.2	(85.6)	100.7	(85.0)	88.4	96.7	(85.4)	94.3	82.4
130	91.3	(89.0)	102.3	(90.0)	88.8	94.0	(88.3)	88.9	84.8
140	93.6	(94.0)	103.2	(92.6)	(90.5)	(88.0)	(94.0)	(88.0)	(84.0)
150	98.1	(97.8)	98.9	(97.0)	(91.0)	87.6	(97.8)	(86.8)	(83.0)
160	95.8	(100.0)	97.9	(100.0)	(90.4)	(85.0)	(100.0)	(85.3)	(81.0)

Table B-26
Low Frequency Core Noise Directivity Test Data

- 20 Ft. (6.1m) Arc
- 1 Hz Bandwidth
- Tone SPL's

Angle to inlet		SIE	Ton	e freque	ency -	Hz			1
(degrees)	125	400	625	250	800	1250	375	1200	1875
40	80.6	77.0	85.0	81.7	76.7	74.4	(70.0)	(66.0)	66.8
50	80.0	71.1	86.0	85.0	81.6	80.8	(70.0)	66.6	(67.0)
60	76.3	83.4	89.7	85.5	77.1	72.8	(70.0)	67.4	(68.0)
70	75.4	81.9	83.8	83.5	77.5	82.5	(71.0)	(68.3)	70.0
80	80.7	79.9	85.4	86.0	80.2	81.9	(72.0)	73.1	70.0
90	85.5	86.3	89.0	87.0	84.6	83.0	(74.0)	75.8	(72.0)
100	85.0	88.2	92.0	90.0	85.5	87.7	(75.5)	77.3	79.8
110	85.7	88.4	95.0	92.0	87.0	91.0	(77.0)	77.8	77.5
120	90.1	90.0	97.2	94.7	90.0	91.8	(79.5)	83.3	80.9
130	91.0	91.3	97.7	95.7	.92.6	90.4	(81.0)	79.6	80.8
140	93.8	92.4	98.0	97.8	86.9	86.2	(85.2)	81.9	(76.4)
150	96.8	91.6	90.2	100.5	88.4	85.2	(88.3)	(78.4)	(75.0)
160	94.8	89.9	86.1	99.1	86.4	79.3	(89.0)	(77.0)	73.5

Table B-27
Low Frequency Core Noise Directivity Test Data

- 20 Ft. (6.1m) Arc
- 1 Hz Bandwidth
- Tone SPL's

Angle to inlet			Tone	freque	ncy - I	łz			
(degrees)	125	400	625	250	800	1250	375	1200	1875
40	79.6	78.0	84.5	67.8	68.1	70.8	(68.0)	67.6	66.1
50	80.4	67.1	86.3	(70.0)	72.7	80.5	(68.0)	(64.0)	72.4
60	79.0	82.6	88.0	(70.0)	73.0	70.4	(68.0)	69.7	73.0
70	76.4	82.8	85.2	(69.6)	68.0	76.6	(69.0)	(65.5)	78.8
80	81.5	83.6	83.8	(70.0)	74.0	79.8	(70.0)	71.7	74.4
90	85.5	85.8	89.3	73.8	78.4	79.2	(74.0)	76.3	78.4
100	84.0	88.0	93.0	75.0	79.2	84.0	(73.0)	77.1	71.8
110	87.0	88.6	94.2	77.8	80.8	87.3	(75.0)	77.3	77.3
120	90.2	89.2	97.5	77.8	83.4	91.0	(77.0)	84.0	82.0
130	92.0	90.0	97.8	(81.0)	85.0	92.2	(79.0)	85.0	79.3
140	95.0	94.0	98.0	(83.0)	82.4	89.8	(83.0)	80.4	(73.4)
150	97.0	90.5	92.0	(86.4)	81.3	88.0	(85.0)	78.6	73.7
160	95.0	91.4	86.5	(88.0)	79.4	85.8	(86.0)	77.7	(70.0

Table B-28
Low Frequency Core Noise Directivity Test Data

- 20 Ft. (6.1m) Arc
- 1 Hz Bandwidth
- Tone SPL's

Angle to inlet			Ton	e frequ	ency -	Hz			l bay
(degrees)	125	400	625	250	800	1250	375	1200	1875
40	77.8	77.3	80.0	75.3	79.0	68.3	(66.0)	(62.0)	66.6
50	78.8	70.7	85.0	74.0	82.2	68.3	67.0	(62.0)	65.1
60	77.2	82.0	86.0	72.8	79.8	67.5	67.6	(62.5)	68.4
70	76.3	80.0	81.6	74.0	80.0	68.7	(66.7)	(64.0)	66.6
80	79.3	81.0	81.8	74.0	81.5	70.7	(68.0)	(64.2)	70.0
90	80.0	85.0	81.5	80.0	85.5	70.7	71.5	(66.0)	71.4
100	81.8	86.0	88.0	79.3	85.8	79.2	74.4	67.4	74.1
110	83.0	86.8	90.0	84.0	87.0	78.0	74.9	70.8	76.0
120	87.3	88.4	91.7	85.0	90.0	80.3	77.8	73.9	77.0
130	89.4	89.0	91.0	87.0	92.2	79.1	79.1	72.8	77.0
140	91.0	92.4	92.4	86.9	87.2	76.4	80.4	(73.0)	(79.5)
150	92.2	91.0	86.6	88.8	90.0	78.2	(81.0)	(71.3)	73.9
160	89.6	91.0	79.8	84.7	87.7	75.0	(82.0)	(70.0)	69.1

Table B-29
Low Frequency Core Noise Directivity Test Data

- 20 Ft. (6.1m) Arc
- 1 Hz Bandwidth
- Tone SPL's

Angle to inlet (degrees)	Tone frequency - Hz									
	125	400	625	250	800	1250	375	1200	1875	
40	77.3	81.0	83.7	76.3	79.8	62.5	68.5	(58.4)	68.4	
50	78.7	73.0	85.9	78.0	82.0	76.8	72.1	62.7	62.8	
60	76.5	84.0	88.5	78.0	81.0	66.8	71.3	61.0	(62.6)	
70	76.5	83.3	84.3	79.0	81.2	72.0	68.1	(60.4)	(64.3	
80	79.9	85.0	85.0	75.5	82.7	74.7	66.8	62.3	(64.3)	
90	82.7	87.3	87.4	82.4	87.8	76.8	73.5	(62.0)	70.6	
100	82.7	88.0	90.7	83.0	86.0	80.0	74.2	66.1	77.5	
110	83.8	88.7	92.2	85.0	89.0	82.4	76.0	71.4	77.3	
120	85.6	88.1	94.7	87.0	90.3	86.3	78.0	72.1	76.0	
130	87.8	88.9	94.0	89.3	91.7	86.4	80.3	73.2	79.0	
140	90.0	92.7	95.7	89.2	88.4	86.3	79.7	72.7	69.2	
150	90.0	92.1	90.0	90.7	91.0	83.0	80.8	69.1	75.2	
160	88.8	92.8	86.6	86.3	87.4	77.6	78.8	(65.5)	71.4	

Table B-30
Low Frequency Core Noise Directivity Test Data

- 20 Ft. (6.1m) Arc
- 1 Hz Bandwidth
- Tone SPL's

Configuration No. 5						Reading No. 51				
	v18 =	489	_ft/sec	(_149	m/sec)	T18 =	621	°R (345	_ °K)
	v8 = _	482	ft/sec	(147	m/sec)	т8 = _	986	_°R (548	_ °K)

Angle to inlet (degrees)		Tone frequency - Hz									
	125	400	625	250	800	1250	375	1200	1875		
40	75.0	83.3	72.3	72,4	77.3	68.3	67.0	63.0	(56.0)		
50	77.0	76.3	69.8	75.0	78.5	72.2	68.4	65.8	61.4		
60	76.5	85.4	70.2	74.0	76.0	65.3	70.0	60.7	(59.0)		
70	75.7	86.0	74.4	74.5	78.0	74.0	67.6	61.3	(61.5)		
80	77.7	87.4	73.0	72.5	79.3	67.3	65.4	69.0	62.8		
90	80.0	89.0	75.0	78.0	83.5	71.5	71.9	74.0	69.1		
100	80.0	90.0	76.0	79.0	83.0	75.0	72.5	74.0	64.1		
110	80.2	90.0	73.9	80.0	86.0	78.7	74.0	75.3	74.1		
120	80.8	89.8	83.2	81.3	86.8	80.0	75.5	80.6	73.9		
130	82.7	90.0	84.3	82.7	89.0	80.8	77.2	81.5	75.4		
140	84.8	93.7	86.0	81.6	86.0	82.2	75.7	81.2	75.8		
150	84.0	94.2	79.9	-83.7	89.8	73.8	77.0	76.6	68.4		
160	82.1	94.3	79.5	81.0	85.4	77.7	75.4	80.0	70.4		

APPENDIX C

Turbine Noise Test Data

Table C-1. HLFT IVA 1-Stage Build Turbine Tone Levels.

				dB	dB
	Test	Hz	dB	Tone	Duct
%n/√T	Pt	BPF	SPL	PWL	OAPWL
110	2546	15845	173.0	176.6	176.7
	2246		176.0	178.8	178.8
	1946		175.5	177.3	177.3
	1646		163.0	163.6	163.6
100	2542	14420	171.0	174.8	174.8
	2242		170.5	173.4	173.4
	1942		169.0	170.9	170.9
	1642		168.5	169.2	169.2
90	2237	12978	174.0	177.0	177.0
	1937		165.0	167.0	167.0
	1637		162.0	162.8	162.8
70	2229	10094	166.5	169.8	169.8
	1929		160.5	162.8	162.8
	1629		162.0	163.1	163.1
50	1621	7210	158.0	159.4	159.4

Table C-2. HLFT IVA 3-Stage Build Turbine Tone Levels.

		Hz		dB	dB
	Test	1st Stage	dB	Tone	Duct
%N/√T	Pt	BPF	SPL	PWL	OAPWL
110	5246	15845	134.3	142.9	142.9
	4046		140.8	148.0	148.1
	3046		145.8	151.9	151.9
	2046		144.3	148.7	148.7
100	5242	14420	140.3	149.0	149.0
	4042		146.3	153.5	153.5
	3042		145.3	151.3	151.3
	2042		138.6	142.8	142.8
80	5237	12978	140.8	149.5	149.5
	4037		149.3	156.6	156.6
	3037		149.3	155.0	155.0
	2037		141.3	145.6	145.6
70	4029	10094	150.8	158.1	158.1
	3029		153.3	159.0	159.0
	2029		144.3	148.3	148.3
50	3021	7210	155.5	161.2	161.2
				4	

Table C-3. HLFT IVA 1-Stage Build Turbine Broadband PWL's.

		110% N/√T		
Point	2546	2246	1646	
Frequency, (Hz)	PWL, dB	PWL, dB	PWL, dB	
1000	154.2	154.4	146.2	
1250	155.2	155.4	147.2	
1600	156.2	156.4	148.2	
2000	157.2	157.4	149.2	
2500	158.2	158.4	150.2	
3150	159.2	159.4	151.2	
4000	160.2	160.4	152.2	
5000	161.2	161.4	153.2	
6300	162.2	162.4	155.2	
8000	164.2	164.4	157.2	
10000	168.2	167.4	160.2	
12500	173.2	170.4	163.2	
16000	180.2	177.4	167.2	
20000	167.2	168.4	166.2	
Duct OAPWL	181.7	179.5	171.6	
		100% N/s	∕ T	
Point	2542	2242	1942	1642
Frequency, (Hz)	PWL, dB	PWL, dB	PWL, dB	PWL, dB
1000	157.4	151.9	149.5	148.3
1250	158.4	152.9	150.5	149.3
1600	159.4	153.9	151.5	150.3
2000	160.4	154.9	152.5	151.3
2500	161.4	155.9	153.5	152.3
3150	162.4	156.9	154.5	153.3
4000	163.4	157.9	155.5	154.3
5000	164.4	158.9	156.5	155.3
6300	165.4	159.9	157.5	156.3
8000	166.4	160.9	159.5	157.3
10000	168.4	162.4	163.5	158.3
12500	172.4	169.5	170.5	161.3
16000	173.4	168.5	167.5	163.3
20000	169.4	164.5	165.5	163.3
Duct OAPWL	178.7	174.1	174.1	169.4

Table C-3. HLFT IVA 1-Stage Build Turbine Broadband PWL's. (Concluded)

		90% N/√T		
Point	2237	1937	1637	
Frequency, (Hz)	PWL, dB	PWL, dB	PWL, dB	
1000	152.0	151 0	140 4	
1000	153.8	151.8	148.4	
1250	154.8	152.8	149.4	0000
1600	155.8	153.8	150.4	
2000	156.8	154.8	151.4	
2500	157.8	155.8	152.4	
3150	158.8	156.8	153.4	
4000	159.8	157.8	154.4	
5000	160.8	158.8	155.4	
6300	161.8	159.8	156.4	
8000	162.8	160.8	157.4	
10000	168.8	163.8	158.4	
12500	176.8	170.8	165.4	
16000	169.8	163.8	163.4	
20000	168.8	166.8	164.4	
Duct OAPWL	179.1	174.3	170.6	
		70% N/√T		50%N/√T
Point	2229	1929	1629	1621
Frequency, (Hz)	PWL, dB	PWL, dB	PWL, dB	PWL, db
1000	157.9	155.8	148.7	154.0
1250	158.9	156.8	149.7	155.0
1600	159,9	157.8	150.7	156.0
2000	160.9	158.8	151.7	157.0
2500	161.9	159.8	152.7	158.0
3150	162.9	160.8	153.7	159.0
4000	163.9	161.8	154.7	160.0
5000	164.9	162.8	155.7	161.0
6300	165.9	163.8	156.7	162.0
8000	166.9	164.8	157.7	163.0
10000	167.9	169.8	164.7	163.0
12500	172.9	167.8	163.7	166.0
16000	170.9	167.8	164.7	166.0
20000	170.9	169.8	171.7	165.0
Duct OAPWL	178.5	176.6	174.1	173.4

Table C-4. HLFT IVA 3-Stage Build Turbine Broadband PWL's.

		110% N/√T		
Point	5246	4046	3046	2046
Frequency, (Hz)	PWL, dB	PWL, dB	PWL, dB	PWL, dB
1000	139.0	138.7	150.0	143.0
1250	140.0	140.0	141.0	144.2
1600	141.0	141.2	142.2	145.4
2000	142.0	142.4	143.3	146.6
2500	143.0	143.7	144.4	147.8
3150	144.1	144.7	145.5	148.5
4000	145.3	145.7	146.7	149.3
5000	146.8	146.7	147.8	150.3
6300	148.5	147.7	149.5	151.3
8000	151.0	149.2	151.0	152.3
10000	153.0	151.7	153.0	152.8
12500	155.0	152.7	154.5	152.3
16000	154.0	154.7	155.5	150.8
20000	150.0	153.7	151.0	147.8
Duct OAPWL	160.9	160.7	161.7	161.1
		100% N/√T		
Point	5242	4042	3042	2042
Frequency, (Hz)	PWL, dB	PWL, dB	PWL, dB	PWL, dB
1000	136.0	135.6	139.4	140.6
1250	137.0	136.8	140.4	141.7
1600	138.0	138.1	141.4	142.9
2000	139.0	139.5	142.4	144.0
2500	140.1	140.8	143.4	145.4
3150	141.0	142.4	144.4	146.6
4000	142.5	143.3	145.4	147.4
5000	143.5	144.8	146.4	148.3
6300	146.0	145.6	147.9	148.6
8000	149.0	147.6	149.4	149.1
10000	153.0	151.6	152.9	150.1
12500	157.0	153.6	153.4	148.1
16000	157.5	154.1	152.4	148.6
20000	156.0	154.6	153.4	147.6
Duct OAPWL	162.7	160.5	160.6	158.6

Table C-4. HLFT IVA 3-Stage Build Turbine Broadband PWL's. (Concluded)

8700 L. O.		90% N/√T		3110
Point	5237	4037	3037	2037
Frequency, (Hz)	PWL, dB	PWL, dB	PWL, dB	PWL, dB
1000	139.1	137.7	135.1	135.7
1250	140.1	138.7	136.1	136.7
1600	141.1	139.7	137.1	137.7
2000	142.1	140.7	138.1	138.7
2500	143.1	141.7	139.1	139.7
3150	144.6	142.7	140.6	140.7
4000	145.9	143.7	142.1	141.7
5000	147.1	144.7	145.1	143.2
6300	148.6	146.7	148.1	144.7
8000	150.1	150.7	151.1	146.7
10000	152.1	155.7	152.1	147.7
12500	154.1	157.7	154.1	150.7
16000	149.6	153.7	151.1	148.7
20000	152.1	153.7	151.1	148.7
Duct OAPWL	160.2	162.4	159.8	156.8
		70% N/√T		
Point	4029	3029	2029	
Frequency, (Hz)	PWL, dB	PWL, dB	PWL, dB	
1000	137.7	135.1	131.4	
1250	138.7	136.1	132.4	
1600	138.7	137.1	133.4	
2000	141.2	138.6	134.9	
2500	142.7	140.1	135.9	
3150	144.2	143.1	137.4	
4000	146.7	147.1	138.9	
5000	151.7	150.6	140.9	
6300	155.7	152.6	144.4	
8000	157.2	155.1	149.4	
10000	159.7	156.1	151.4	
12500	159.7	155.1	148.9	
16000	159.7	155.1	149.4	
20000	161.7	160.1	148.4	
Duct OAPWL	167.4	164.5	157.2	

APPENDIX D

Turbine Tone/Jet Stream Interaction Data

Table D-1
Interaction Effects - Parametric Test Data

- 40 Ft. (12.2m) Arc
- 40 Hz Bandwidth
- Tone SPL's

V18 = 10 ft/sec (3 m/sec); T18 = 494
$$^{\circ}$$
R (274 $^{\circ}$ K)
V8 = 0 ft/sec (0 m/sec); T8 = 491 $^{\circ}$ R (272 $^{\circ}$ K)

Angle From			1	one F	requency	- KHz		No. of the last	
Inlet		Funda	mental		2nd Har	monic	31	d Harmon	nic
(degrees)	3.15	4.0	5.0	6.3	8.0	10.0	9.45	12.0	15.0
40	80.3	89.4	77.1	73.5	67.3	69.9	76	64.9	56.9
50	78.1	37.5	85	79.9	70.2	72	74.9	67.2	60.1
60	78.1	88.8	85	73.7	68.6	78.7	73.5	67	55.1
70	82	87.9	83.2	74.2	74.4	70.3	78.1	67.4	57.8
80	83	90.2	85	73.1	70.7	77	79.9	65	62.7
90	84.2	88.7	87.9	77.2	77.6	74.5	79.5	69.9	63
100	83.6	89.3	89.4	82.1	76	80	80	74.2	63.9
110	89	90.3	90.7	82.3	80.1	84.7	81.9	73.6	74.9
120	90.8	93	88.3	79.4	76.5	77.5	82.2	74	74.4
130	89.8	93.6	86	82.8	77.4	77.1	83.5	76.5	71.7
140	91	92.2	88.9	81.5	81.6	74.6	81	76.9	67.3
150	95.9	89.1	81.6	87.1	84	81.2	81	77.9	78
160	91.1	88	87.1	87.1	82.3	88.9	81.7	77.4	81.1
PWL	130.1	132.4	129.2	123.3	120.4	122.9	123.1	116.7	116.8

Table D-1

Interaction Effects - Parametric Test Data (continued)

- 40 Ft. (12.2m) Arc
- 10 Hz Bandwidth
- . Tone SPL's

Configuration: Short Fan Shroud

V18 = $\frac{675}{\text{ft/sec}}$ ft/sec ($\frac{206}{\text{m/sec}}$); T18 = $\frac{635}{\text{c}}$ °R ($\frac{352}{\text{c}}$ °K) V8 = $\frac{96}{\text{ft/sec}}$ ($\frac{29}{\text{m/sec}}$); T8 = $\frac{570}{\text{c}}$ °R ($\frac{316}{\text{c}}$ °K)

Angle From			ann at s	Tone F	requency	- KHz				
Inlet		Fundamental			2nd Harmonic			3rd Harmonic		
(degrees)	3.15	4.0	5.0	6.3	8.0	10.0	9.45	12.0	15.0	
40										
50										
60										
70										
80	85.8	87.0	77.2	70.0	71.5	69.0	69.6	63.0	59.3	
90	84.7	86.8	84.0	72.0	73.2	72.0	71.6	64.0	61.8	
100	88.4	88.0	86.0	78.0	77.0	76.0	74.8	69.5	(66.0)	
110	90.0	90.0	87.4	80.3	82.3	74.6	79.0	69.2	65.0	
120	90.2	90.7	90.0	81.3	79.0	74.0	79.9	72.0	64.8	
130	87.3	83.6	86.0	80.0	83.8	74.0	72.2	66.8	63.9	
140	80.0	81.0	78.0	70.0	67.4	63.3	62.2	62.1	55.8	
150										
160										
PWL	127.9	128.3	125 8	118 2	119.5	114 1	116.3	109.3	105.4	

Table D-1

Interaction Effects - Parametric Test Data (continued)

- 40 Ft. (12.2m) Arc
- 10 Hz Bandwidth
- . Tone SPL's

V18 =
$$705$$
 ft/sec (215 m/sec); T18 = 631 °R (350 °K)
V8 = 1186 ft/sec (391 m/sec); T8 = 1409 °R (782 °K)

Angle From				Tone F	requency	- KHz		and the second	1.583 95.4	
Inlet	Tient.	Fundamental			2nd Harmonic			3rd Harmonic		
(degrees)	3.15	4.0	5.0	6.3	8.0	10.0	9.45	12.0	15.0	
40										
50										
60										
70										
80										
90	84	84	79	77	70	69	66	70	(64)	
100	87	86	85	76	73	70	73	73	(67)	
110	91	87	89	82	80	75	75	72	(68)	
120	90	87	91	85	85	81	79	74	65	
130	84	83	85	77	74	72	71	67	(60)	
140	76	73	74	66	64	61	(60)	61	(53)	
150	73	71	70	65	61	60	(58)	60	55	
160										
PWL	127.1	125	126.2	120.2	119	115.7	114.4	113	107.7	

Table D-1

Interaction Effects - Parametric Test Data (continued)

- 40 Ft. (12.2m) Arc
- o 10 Hz Bandwidth
- Tone SPL's

V18 = 837 ft/sec (255 m/sec); T18 = 635
$$^{\circ}$$
R (352 $^{\circ}$ K)
V8 = 1200 ft/sec (366 m/sec); T8 = 1406 $^{\circ}$ R (781 $^{\circ}$ K)

Angle From				Cone Fr	equency	- KHz				
Inlet		Fundamental			2nd Harmonic			3rd Harmonic		
(degrees)	3.15	4.0	`5.0	6.3	8.0	10.0	9.4	12.0	15.0	
40										
50										
60										
70										
80										
90	85	84	80	76	70	(68)	68	71	(64)	
100	87	87	85	77	75	70	72	74	(68)	
110	92	86	88	84	81	73	75	73	(68)	
120	88	87	90	86	84	75	80	72	(67)	
130	82	82	82	75	72	68	69	67	(61)	
140	(76)	75	72	(68)	(65)	(61)	(62)	64	(56)	
150	(74)	72	69	(66)	(61)	(60)	(60)	63	(56)	
160	71	69	69	66	(60)	(58)	(60)	62	(54)	
PWL	127.2	125	125.3	121	118.6	111.9	114.7	113.2	(110.5)	

Table D-1
Interaction Effects - Parametric Test Data (continued)

- 40 Ft. (12.2m) Arc
- o 10 Hz Bandwidth
- Tone SPL's

V18 = 1018 ft/sec (310 m/sec); T18 = 632 °R (351 °K) V8 = 1209 ft/sec (368 m/sec); T8 = 1400 °R (777 °K)

Angle From				Tone Fi	requency	- KHz			4.5 g 1 A
Inlet (degrees)		Funda	mental		2nd Har	monic	3rd Harmonic		
	3.15	4.0	5.0	6.3	8.0	10.0	9.45	12.0	15.0
40	(72)	74	73	71	(66)	(65)	(66)	(65)	(62)
50	(75)	74	74	(70)	(68)	(67)	(67)	(66)	(64)
60	(74)	74	74	(70)	(67)	(67)	(66)	(65)	(62)
70	76	80	74	(70)	(70)	(67)	(67)	(66)	(63)
80	(77)	80	75	75	(70)	(68)	(67)	(67)	(65)
90	82	85	77	76	(72)	70	(71)	(70)	(66)
100	84	87	84	78	75	(70)	74	(72)	(70)
110	87	90	86	81	81	(72)	76	73	(70)
120	85	86	89	86	83	74	80	(72)	(66)
130	(82)	81	(79)	(75)	(72)	(70)	(71)	(69)	(65)
140	(80)	(79)	(75)	(73)	(70)	(67)	(70)	(66)	(62)
150	(77)	(75)	(75)	(70)	(67)	(65)	(66)	(64)	(60)
160	.(76)	(74)	(72)	(70)	(65)	(62)	(63)	(63)	(57)
PWL	123.7	126	124	120.6	118.5	(111,6)	(115.0)	(112.9)	(112)

Table D-1
Interaction Effects - Parametric Test Data (continued)

- 49 Ft. (12.2m) Arc
- 10 Hz Bandwidth
- Tone SPL's

Angle From				Tone Fr	requency	- KHz		ano a "	algar	
Inlet (degrees)	i bafa	Funda	amental	91 00	2nd Harmonic			3rd Harmonic		
	3.15	4.0	5.0	6.3	8.0	10.0	9.45	12.0	15.0	
40	72	75	72.6	64.7	60.8	61.5	61.4	61.9	52.3	
50	74	72.8	75.8	68.5	63.2	62.3	61.9	63.2	55	
60	76.1	68.2	72.5	64.1	63.1	(59.1)	61.4	61.1	52.7	
70	72.5	70.3	78.7	69	63.8	(62.3)	65.7	62.9	55.2	
80	70.2	80.2	78.7	74.3	66.6	64.8	64	64.5	58.1	
90	80	84.2	81.9	72	71.3	69	72.1	68.1	60.9	
100	87.1	85.3	88.2	79	78	72.1	77.1	70	65.1	
110	89	87,	89.6	80.1	84	74.5	81	76	70.8	
120	90.7	81.4	90.9	84.5	89.1	82.5	84	81.6	76.2	
130	84.2	79.2	88.2	83.5	83	77.1	80.4	73	66.2	
140	76.8	71.9	75.1	71	64.9	61.2	62.5	62.1	55	
150	65.3	73	70.5	66.5	62.5	59.6	61.3	61.2	57.1	
160	74	70.1	73.7	65.5	60.2	62.3	58.9	60.9	56.7	
PWL	126.2	123.5	127.5	122.2	123.4	118.2	120	116.8	112.6	

Table D-1

Interaction Effects - Parametric Test Data (continued)

- 40 Ft. (12.2m) Arc
- 10 Hz Bandwidth
- Tone SPL's

V18 = $\frac{673}{1}$ ft/sec ($\frac{205}{1}$ m/sec); T18 = $\frac{638}{1}$ R ($\frac{354}{1}$ K) V8 = $\frac{802}{1}$ ft/sec ($\frac{244}{1}$ m/sec); T8 = $\frac{1416}{1}$ R ($\frac{786}{1}$ K)

Angle From				Ione Fr	equency	- KHz			
Inlet	E 53	Funda	mental		2nd Har	monic	31	d Harmon	nic
(degrees)	3.15	4.0	5.0	6.3	8.0	10.0	9.45	12.0	15.0
40	69	72	72	66	64	62	62	63	54
50	72	67	72	69	66	62	61	63	(54)
60	73	72.	75	65	65	62	63	61	55
70	74	69	71	72	66	65	63	65	57
80	75	77	80	74	68	67	65	64	57
90	81	82	79	75	74	69	69	70	60
100	85	84	84	90	80	76	72	70	65
110	89	84	87	85	85	81	77	76	70
120	88	83.5	89	87	86	82	81	79	73
130	83	78	85	83	77	77	75	67	65
140	75	70	73	71	(61)	62	61	60	(52)
150	69	74	67	71	63	60	62	61	56
160	68	72	71	65	61	61	58	62	55
PM.	124.8	122.2	124.9	122.8	121.8	118.6	116.3	115.2	110.5

Table D-1

Interaction Effects - Parametric Test Data (continued)

- 40 Ft. (12.2m) Arc
- 10 Hz Bandwidth
- Tone SPL's

Configuration: Short Fan Shroud

V18 = $\frac{780 \text{ ft/sec}}{100 \text{ ft/sec}} = \frac{238 \text{ m/sec}}{100 \text{ m/sec}}; \quad \text{T18} = \frac{632 \text{ o}}{100 \text{ R}} = \frac{631 \text{ o}}{100 \text{ c}} = \frac{631 \text{$

Angle From				rone Fr	equency	- KHz			45,984	
Inlet		Funda	mental		2nd Har	monic	3	rd Harmo	nic	
(degrees)	3.15	4.0	5.0	6.3	8.0	10.0	9.45	12.0	15.0	
40										
50										
60										
70										
80										
90	82	75	82.8	74	75	68.3	69	65	59.8	
100	84	81	82.0	76	79	76.6	70	67	64.0	
110	88	86	82.3	85	85	81.4	75	74	67.6	
120	89	79	81.9	87	85	78.0	80	77	69.5	
130	80	76	79.8	79	75	71.7	70	67	60.2	
140	74	(70)	71.7	70	(64)	61.2	63	61	(54.0	
150	70	69	68.0	67	62	62.0	(60)	60	(56.0	
160	69	70	-	67	64	-	(58)	60	111-	
PWL	124.8	120.3	122.2	121.9	121.4	117	114.8	112.9	107.9	

Table D-1 Interaction Effects - Parametric Test Data (continued)

- 40 Ft. (12.2m) Arc
- 10 Hz Bandwidth
- e Tone SPL's

V18 = $920 \text{ ft/sec} (280 \text{ m/sec}); T18 = 634 ^{\circ}R (352 ^{\circ}K)$ V8 = 823 ft/sec (251 m/sec); T8 = $1396 ^{\circ} \text{R}$ ($775 ^{\circ} \text{K}$)

Angle From				Cone F	requency	- KHz		2009	3 - 3 - 3
Inlet	10.0	Funda	mental		2nd Har	monic	3r	rd Harmonic	
(degrees)	3.15	4.0	5.0	6.3	8.0	10.0	9.45	12.0	15.0
40									
50									
60									
70									
80									
90	84	80	79	74	70	(69)	70	(65)	(60)
100	85	84	84	79	76	73	71	(66)	(63)
110	90	80	87	85	83	77	75	73	67
120	89	82	89	85	84	78	79	76	70
130	79	76	82	77	72	69	70	(66)	(62)
140	(77)	75	(72)	(71)	(66)	(64)	(65)	(64)	(58)
150	(75)	(74)	72	70	(65)	(63)	(64)	(62)	(57)
160									
PWL	126	120.8	124.4	121.2	119.5	114.8	114.6	112.1	109.7

Table D-1

Interaction Effects - Parametric Test Data (continued)

- 40 Ft. (12.2m) Arc
- 40 Hz Bandwidth
- Tone SPL's

V18 = $\frac{22 \text{ ft/sec}}{1 \text{ m/sec}}$; T18 = $\frac{735}{1 \text{ N}}$ ($\frac{408}{1 \text{ N}}$) V8 = $\frac{786}{1 \text{ ft/sec}}$ ($\frac{240}{1 \text{ m/sec}}$); T8 = $\frac{1401}{1 \text{ N}}$ ($\frac{778}{1 \text{ N}}$)

Angle From			NF - v	one Fr	equency	- KHz		Bann	
Inlet	144	Funda	mental		2nd Har	monic	3r	d Harmon	ic
(degrees)	3.15	4.0	5.0	6.3	8.0	10.0	9.45	12.0	15.0
40	77.7	69.8	72.5	68.1	60.1	58.5	58.7	57	54
50	78	73.4	77.6	69	61.6	61.1	63.1	61.6	54.9
60	76.1	80.5	72.1	69.4	60.3	66.1	63	60.1	54
70	74.1	79	78.9	71.2	64.1	66.1	74.4	63	55.3
80	73.8	72.3	66.8	73.7	62.8	72	65	65	57.1
90	79	86.8	81.3	72.5	68	70.1	70.8	66.4	60.2
100	87	81.1	79.2	77.7	76	70.1	75.9	71.8	63.9
110	91.5	77.3	80	83.9	82.1	81.1	82.3	75.1	68.1
120	92.2	79.9	84.9	87.9	85.1	82.2	85.2	77.7	75.7
130	86.8	76.8	87.9	87.7	80.8	78	82.5	72.5	74.1
140	83.6	78	82.9	81.6	73.9	69.5	72.5	67.5	64.3
150	76.9	76.8	76	74.9	70.7	64.6	67.4	65	63.3
160	72.9	73.4	73.5	69.9	64.7	63	61.1	60.1	57.3
PWL	127.8	122.1	123.2	123.8	120.2	118.4	121	114.3	113.9

Table D-1

Interaction Effects - Parametric Test Data (continued)

- 40 Ft. (12.2m) Arc
- 40 Hz Bandwidth
- Tone SPL's

Configuration: Short Fan Shroud

V18 = 346 ft/sec (105 m/sec); T18 = 638 °R (354 °K) V8 = 520 ft/sec (158 m/sec); T8 = 1402 °R (778 °K)

Angle From				Ione Fr	equency	/ - KHz		-1 - 149	
Inlet	A GAT	Funda	mental		2nd Har	monic	3r	d Harmon	ic .
(degrees)	3.15	4.0	5.0	6.3	8.0	10.0	9.45	12.0	15.0
40					,				
50									
60									
70									
80									
90	'80	81	81	82.1	72.1	67.5	63.6	63.7	56.8
100	84.9	76.7	77.3	82.3	80	75.5	68	69.4	58,.8
110	88.8	82.9	77.5	80.3	78.9	76.9	67	71.6	66.6
120	90	87	81.8	84.1	82.1	78	75.1	78.2	66.9
130	86.2	81.3	83.7	84.7	78.6	76	76.5	76.1	64.7
140	78.9	78.6	83	74.5	66	65.6	66	61.6	56.1
150	72.6	68	75	67.1	62	61	61.8	59.9	55.9
160	74.5	71	73.7	66.7	63.5	60.7	61.1	60.8	57.1
PWL	125.7	122.3	121.2	122.5	118.5	115.3	111.8	113.9	111.7

Table D-1
Interaction Effects - Parametric Test Data (continued)

- 40 Ft. (12.2m) Arc
- 40 Hz Bandwidth
- . Tone SPL's

V18 = 428 ft/sec (130 m/sec); T18 = 637 °R (354 °K) V8 = 523 ft/sec (159 m/sec); T8 = 1414 °R (785 °K)

Angle From	-			Ione Fr	equency	- KHz			
Inlet		Funda	mental		2nd Har	monic	3r	d Harmon	ic
(degrees)	3.15	4.0	5.0	6.3	8.0	10.0	9.45	12.0	15.0
40	73	76.2	73.9	71.8	61.1	64.5	56	58.8	56.1
50	78.5	70.5	69.8	73.9	69.7	66.6	60.5	61.9	54
60	72.3	73.6	72.6	73	68.8	65.8	62.8	62	51.3
70	77.1	76	77.6	76.8	69	69.4	62.5	60.6	53.1
80	80	76	74.8	77.9	66.9	65.2	66.2	63.8	51.7
90	83.7	80.9	77.1	83	74.1	71.9	64.3	62	56
100	86.7	77	75.9	82.1	79	78.5	70	69.5	58.8
110	90.3	82.1	79.6	84.9	77.3	74.4	71.3	69	65.5
120	91.2	86.3	81.1	84.7	83	77.2	77.5	78	66.6
130	88.1	80.9	83.1	85.1	76.9	78.7	80	76.8	66
140	80.3	78.5	80.2	76.5	63	64.7	65.1	62	54.3
150	71.9	67	71.5	69.1	64.6	65.1	67.2	61.8	57
160	68.6	68.8	76	67.5	65.7	63.7	61.8	59.9	56.4
PWL	127.5	121.8	120.2	123.6	118.6	116.8	115.1	114.4	112.5

Table D-1
Interaction Effects - Parametric Test Data (continued)

- 40 Ft. (12.2m) Arc
- 40 Hz Bandwidth
- Tone SPL's

V18 = 500 ft/sec (152 m/sec); T18 = 641 °R (356 °K) V8 = 532 ft/sec (162 m/sec); T8 = 1431 °R (795 °K)

Angle From				Ione Fi	requenc	y - KHz			A place
Inlet		Funda	mental		2nd Ha	rmonic	3r	d Harmon	nic
(degrees)	3.15	4.0	5.0	6.3	8.0	10.0	9.45	12.0	15.0
40									
50									
60									
70									
80									
90	81.8	77.1	76.1	78.4	72.5	71.6	62.1	62.8	55.8
100	86	75	81	81.1	80.3	75.1	71.1	67.4	60.2
110	89.3	84	85.2	83	78.6	74.9	74.8	73.9	66.1
120	90.5	86.1	87.1	86.8	83.8	81.8	79.6	77.1	69.6
130	86	79	85.4	85.1	80.8	81.2	80	77.1	65
140	80	75.8	77.1	71.9	65	65.8	64.3	63.2	55.8
150	67.2	69.6	73.1	70.1	64.9	63.7	64.2	62.7	58.2
160	70.6	71.8	78.6	69.8	62	63.9	60	62.4	55.8
PWL	126.6	121.3	123.3	123.1	119.9	118.3	116.1	114.5	113.6

Table D-1

Interaction Effects - Parametric Test Data (concluded)

- 40 Ft. (12.2m) Arc
- 40 Hz Bandwidth
- Tone SPL's

V18 = 559 ft/sec (170 m/sec); T18 = 634 °R (352 °K) V8 = 536 ft/sec (163 m/sec); T8 = 1422 °R (790 °K)

Angle From				Tone Fr	equency	- KHz			
Inlet		Funda	mental		2nd Har	monic	31	d Harmon	nic
(degrees)	3.15	4.0	5.0	6.3	8.0	10.0	9.45	12.0	15.0
40	71.5	73.1	70.8	72.5	61.3	60.3	57.2	56.8	54.1
50	72.2	75.1	69.5	72.8	64.9	62.2	60.2	58	54.6
60	72.7	78.1	73.7	67.1	66.4	61.3	61.9	56.7	53
70	77	74.8	73.8	74	67	65.6	64	58.7	54.8
80	75.4	70	79.2	78.6	65.8	66.6	64.9	58.1	54.9
90	81.1	78.7	76.7	78.1	69.3	63.3	65	63.1	57.2
100	83.7	84.1	77.3	79	75.6	71.6	68.6	68	58.4
110	88	87.5	84	81	76.4	71.8	73.2	72.1	65.1
120	88.8	84.6	84.5	84.8	80.6	78.7	78.4	76	65
130	83.1	77.5	84.8	82.4	76.1	78.2	78.2	71.1	(58)
140	75.1	70.6	71.3	68.9	62.8	(60.8)	61.3	60	60
150	65.2	69.7	67.3	66.3	60	61.2	63.9	59	61.1
160	69.3	69.2	72	65	61	60	59.2	60.1	57.7
PWL	124.7	123.1	122	121.4	116.4	115.2	114.9	112.3	111.3

Table D-2

Interaction Effects - Exhaust Plane Variation Test Data

- 40 Ft. (12.2m) Arc
- 10 Hz Bandwidth
- Tone SPL's

Configuration: Long Fan Shroud

V18 = 686 ft/sec (209 m/sec); T18 = 639 °R (355 °K) V8 = 810 ft/sec (247 m/sec); T8 = 1378 °R (765 °K)

Angle From				Tone Fr	requency	- KHz				
Inlet		Funda	mental		2nd Har	monic	3r	d Harmon	ic	
(degrees)	3.15	4.0	5.0	6.3	8.0	10.0	9.45	12.0	15.0	
40										
50										
60										
70				13						
80	75.0	80.0	73.6	72.7	68.6	62.4	63.2	60.3	57.7	
90	79.2	84.7	79.0	77.5	69.2	68.3	67.8	65.0	62.0	
100	79.6	88.5	82.4	80.4	74.1	72.0	71.9	68.4	67.7	
110	79.3	90.0	89.7	85.0	79.5	77.0	77.3	71.0	69.0	
120	75.0	88.0	90.1	86.9	84.0	83.8	84.6	77.3	71.3	
130	78.3	80.0	82.0	74.0	74.0	72.5	73.8	62.5	59.6	
140	72.2	74.5	71.8	68.0	66.0	(63.0)	(64.5)	(62.0)	(62.2)	
150										
160										
PWL	117.9	126.3	125.2	121.9	118.0	117.2	117.9	111.7	108.4	

Table D-3

Interaction Effects - Exhaust Plane Variation Test Data

- 40 Ft. (12.2m) Arc
- e 10 Hz Bandwidth
- Tone SPL's

Configuration: Coplanar Fan Shroud

V18 = $\frac{695}{\text{ft/sec}}$ ($\frac{212}{\text{m/sec}}$); T18 = $\frac{636}{\text{c}}$ ($\frac{353}{\text{c}}$) V8 = $\frac{799}{\text{ft/sec}}$ ($\frac{244}{\text{m/sec}}$); T8 = $\frac{1400}{\text{c}}$ ($\frac{777}{\text{c}}$)

Angle From				Tone F	requency	- KHz			
Inlet		Funda	mental		2nd Har	monic	31	d Harmon	nic
(degrees)	3.15	4.0	5.0	6.3	8.0	10.0	9.45	12.0	15.0
40									
50									
60									
70									
80	k								
90	79.4	78.0	75.0	71.6	73.0	66.0	67.0	60.4	57.0
100	81.0	87.5	79.0	82.0	76.0	70.0	69.0	67.0	61.0
110	83.0	88.0	87.0	89.3	82.0	77.5	77.0	75.0	65.0
120	80.0	84.0	89.0	89.0	86.0	80.0	82.0	76.0	68.0
130	74.0	78.0	83.0	81.0	75.0	71.0	72.7	65.0	63.5
140	70.0	71.0	70.5	66.0	62.0	60.0	60.0	59.4	(54.0)
150	68.0	69.0	68.5	64.0	60.0	58.0	58.0	57.4	52.0
160	67.0	68.0	67.5	63.0	59.0	57.0	57.0	56.4	51.0
PWL	119.7	123.8	123.5	124.6	120.1	114.8	115.9	111.7	104.7

Table D-4

Interaction Effects - Exhaust Plane Variation Test Data

- 40 Ft. (12.2m) Arc
- 10 Hz Bandwidth
- Tone SPL's

Configuration: Extended Fan Shroud

V18 = 680 ft/sec (207 m/sec); T18 = $643 \, ^{\circ}\text{R}$ ($357 \, ^{\circ}\text{K}$) V8 = $794 \, \text{ft/sec}$ ($242 \, \text{m/sec}$); T8 = $940 \, ^{\circ}\text{R}$ ($522 \, ^{\circ}\text{K}$)

Angle From				Ione Fr	equency	- KHz			
Inlet		Funda	mental		2nd Har	monic	3r	d Harmon	ic
(degrees)	3.15	4.0	5.0	6.3	8.0	10.0	9.45	12.0	15.0
40	76.0	72.0	72.0	71.0	68.0	57.0	64.0	56.0	55.0
50	74.0	75.0	72.0	71.0	67.0	58.0	66.0	58.0	54.0
60	80.0	74.0	72.0	73.0	71.0	57.0	64.0	56.0	52.0
70	77.0	75.0	77.0	77.0	71.0	60.0	69.0	62.0	55.0
80	80.0	76.0	77.0	82.0	76.0	66.0	75.0	67.0	65.0
90	80.0	82.0	79.0	85.0	80.0	74.0	79.0	75.0	70.0
100	81.0	84.0	82.0	85.0	78.0	75.0	80.0	72.0	66.0
110	76.0	86.0	85.0	76.0	30.0	67.0	68.0	69.0	65.0
120	75.0	86.0	87.0	81.0	35.0	75.0	71.0	71.0	70.0
130	81.0	88.0	81.0	77.0	80.0	69.0	70.0	69.0	64.0
140	76.0	82.0	79.0	73.0	75.0	63.0	66.0	61.0	58.0
150	76.0	78.0	76.0	70.0	71.0	64.0	66.0	59.0	57.0
160	70.0	75.0	70.0	67.0	66.0	60.0	62.0	59.0	57.0
PWL	120.3	124.8	123.2	122.7	121.3	113 5	117.3	113.0	109.8

Table D- 5

Interaction Effects - Turbulence Effects Test Data

- 40 Ft. (12.2m) Arc
- 5 Hz Bandwidth
- Tone SPL's

Configuration: Fan Cowl Vortex Ring

V18 =
$$550$$
 ft/sec (168 m/sec); T18 = 632 °R (351 °K)
V8 = 778 ft/sec (237 m/sec); T8 = 1394 °R (774 °K)

Angle From				Tone Fr	equency	- KHz			
Inlet		Funda	mental		2nd Har	monic	3	rd Harmon	ic
(degrees)	3.15	4.0	5.0	6.3	8.0	10.0	9.45	12.0	15.0
40									
50									
60	P. Car								
70									
80									
90	77.0	80.3	78.3	69.2	67.7	66.6	65.6		
100	80.0	83.7	80.8	75.7	74.0	68.4	69.0		
110	85.7	82.7	85.0	81.5	80.4	73.7	70.8		
120	86.0	83.3	86.6	84.0	83.3	77.0	77.5		
130	79.8	77.7	82.4	78.7	76.9	70.4	70.9		
140	71.0	70.4	71.3	65.0	63.0	59.0	(57.0)		
150									
160	4.94								
PWL	121.8	121.4	122.7	119.0	117.9	112.3	112.0		

Table D- 5
Interaction Effects - Turbulence Effects Test Data (continued)

- 40 Ft. (12.2m) Arc
- 10 Hz Bandwidth
- Tone SPL's

Configuration: Fan Cowl Vortex Ring

V18 = $\frac{685}{1}$ ft/sec ($\frac{209}{1}$ m/sec); T18 = $\frac{648}{1}$ R ($\frac{360}{1}$ K) V8 = $\frac{805}{1}$ ft/sec ($\frac{245}{1}$ m/sec); T8 = $\frac{1408}{1}$ R ($\frac{382}{1}$ K)

Angle From		Tone Frequency - KHz									
Inlet (degrees)	Fundamental			A.S.	2nd Har	monic	3rd Harmonic				
	3.15	4.0	5.0	6.3	8.0	10.0	9.45	12.0	15.0		
40	72.0	72.7	69.3	67.0	64.4	54.0	58.0	56.0	53.0		
50	71.0	71.5	72.7	67.0	70.0	58.8	60.5	58.0	55.0		
60	70.5	69.3	71.5	66.6	65.0	58.2	60.1	60.0	57.0		
70	71.7	73.4	74.6	70.0	65.0	59.3	61.0	62.0	59.0		
80	74.0	76.0	74.5	72.3	77.0	66.7	66.1	64.0	(61.0)		
90	76.3	81.0	78.5	74.1	79.2	71.6	(70.0)	(69.0)	(68.0)		
100	81.4	86.4	84.5	79.0	81.5	73.8	73.6	71.3	(68.0)		
110	84.7	84.0	86.0	85.0	86.2	79.0	76.2	76.0	68.0		
120	85.0	82.2	87.0	84.6	86.0	81.0	79.0	76.7	69.7		
130	77.0	77.8	84.3	77.0	76.6	73.0	70.7	67.8	(65.0)		
140	73.7	72.0	71.7	67.6	72.0	62.5	62.0	62.5	59.8		
150	68.0	70.5	70.4	62.0	59.7	55.0	58.4	60.5	57.8		
160	66.0	70.6	69.0	65.5	55.0	52.5	56.0	58.5	55.8		
PWL	121.0	122.2	123.5	120:7	122.6	116.4	114.4	113.3	108.8		

Table D- 5

Interaction Effects - Turbulence Effects Test Data (concluded)

- 40 Ft. (12.2m) Arc
- 5 Hz Bandwidth
- Tone SPL's

Configuration: Fan Cowl Vortex Ring

V18 = 795 ft/sec (242 m/sec); T18 =
$$639$$
 °R (355 °K)
V8 = 800 ft/sec (244 m/sec); T8 = 1396 °R (775 °K)

Angle From	Tone Frequency - KHz									
Inlet (degrees)	1.6	Fundamental			2nd Harmonic			3rd Harmonic		
	3.15	4.0	5.0	6.3	8.0	10.0	9.45	12.0	15.0	
40										
50	168									
60										
70										
80										
90	77.5	78.0	75.5	73.6	(73.5)	(69.7)	(69.6)			
100	82.4	83.0	82.5	76.3	(76.0)	(70.0)	70.0			
110	87.3	80.8	85.5	83.6	(74.0)	(70.0)	72.0			
120	88.5	79.0	86.7	82.0	(72.0)	(70.6)	76.7			
130	79.0	73.7	79.6	76.7	(71.0)	(67.6)	68.2			
140	73.0	70.8	69.6	(68.0)	(68.4)	(62.8)	(64.5)			
150										
160										
PWL	123 0	118 0	123 2	110.0	113.5	110.1	112 1			

AD-A048 590

GENERAL ELECTRIC CO CINCINNATI OHIO AIRCRAFT ENGINE GROUP F/G 20/1 GE CORE ENGINE NOISE INVESTIGATION - LOW EMISSION ENGINES.(U) FEB 77 R K MATTA, G T SANDUSKY, V L DOYLE DOT-FA75WA-3688 FAA/RD-77/4 NL

UNCLASSIFIED

5 ° 5 ADAO48 590







END DATE FILMED 2 -78

Table D-6

Interaction Effects - Turbulence Effects Test Data

- 40 Ft. (12.2m) Arc
- 10 Hz Bandwidth
- Tone SPL's

Configuration: Core Cowl Vortex Ring

V18 = 571 ft/sec (174 m/sec); T18 = 651 °R (361 °K) V8 = 790 ft/sec (241 m/sec); T8 = 1402 °R (778 °K)

Angle From	Tone Frequency - KHz										
Inlet (degrees)		Fundamental			2nd Har	monic	31	rd Harmonic			
	3.15	4.0	5.0	6.3	8.0	10.0	9.45	12.0	15.0		
40											
50											
60											
70											
80	77.0	78.4	77.5	69.5	69.7	68.0	68.0	66.0	(59.0)		
90	79.4	74.0	77.0	71.5	70.6	71.0	69.0	69.3	64.0		
100	82.5	80.0	82.0	75.0	76.0	74.0	72.0	70.3	(68.0)		
110	86.0	81.0	87.5	84.0	80.4	75.0	73.7	71.0	66.0		
120	86.0	80.3	90.0	83.0	82.5	79.4	78.4	75.0	66.0		
130	79.0	79.0	83.0	78.0	73.6	70.0	70.0	(69.5)	(67.0)		
140	72.5	70.0	71.5	65.0	62.0	61.0	(60.3)	65.0	58.0		
150											
160											
PWL	122.5	119.1	124.7	119.4	117.6	114.6	113.5	111.8	107.1		

Table D-6

Interaction Effects - Turbulence Effects Test Data (continued)

- 40 Ft. (12.2m) Arc
- 10 Hz Bandwidth
- Tone SPL's

Configuration: Core Cowl Vortex Ring

V18 = 683 ft/sec (208 m/sec); T18 = 649 °R (360 °K) V8 = 785 ft/sec (239 m/sec); T8 = 1394 °R (774 °K)

Angle From Inlet (degrees)	Tone Frequency - KHz									
	Fundamental				2nd Harmonic			3rd Harmonic		
	3.15	4.0	5.0	6.3	8.0	10.0	9.45	12.0	15.0	
40	73.5	77.0	74.0	68.0	64.0	62.7	64.5	61.6	54.4	
50	76.0	75.0	74.0	68.0	66.5	65.0	64.5	61.6	56.4	
60	73.0	75.0	75.0	68.0	65.5	64.0	64.5	63.6	58.4	
70	78.0	79.0	75.0	69.0	68.0	66.0	66.0	65.6	60.4	
80	(80.0)	78.5	77.7	74.2	(70.0)	70.0	(68.4)	(67.6)	(62.4	
90	82.1	79.0	78.3	73.6	73.0	72.0	(70.3)	(68.5)	(64.0	
100	84.0	82.0	83.0	76.3	75.0	73.8	73.8	69.8	(65.0	
110	89.0	83.0	87.3	82.0	79.9	73.8	74.2	70.3	(66.0	
120	89.8	82.0	89.0	85.5	84.0	74.5	76.0	71.0	(67.0	
130	(82.4)	80.0	84.0	75.5	74.5	72.0	(69.0)	68.3	(64.0	
140	(76.0)	75.0	83.7	(67.0)	65.5	63.8	(63.0)	64.0	59.0	
150	71.0	70.5	72.0	64.0	66.0	63.0	60.0	61.0	57.0	
160	71.0	70.3	68.0	64.0	62.0	60.0	58.8	60.0	56.0	
PWL	125.4	121.3	124.7	119.9	118.4	113.3	113.2	110.5	106.7	

Table D-6

Interaction Effects - Turbulence Effects Test Data (concluded)

- 40 Ft. (12.2m) Arc
- 10 Hz Bandwidth
- Tone SPL's

Configuration: Core Cowl Vortex Ring

V18 = 806 ft/sec (246 m/sec); T18 = 696 $^{\circ}$ R (386 $^{\circ}$ K) V8 = 795 ft/sec (242 m/sec); T8 = 1416 $^{\circ}$ R (786 $^{\circ}$ K)

Angle From	Tone Frequency - KHz									
Inlet (degrees)	Fundamental				2nd Har	monic	3rd Harmonic			
	3.15	4.0	5.0	6.3	8.0	10.0	9.45	12.0	15.0	
40										
50										
60										
70										
80										
90	(82.0)	81.0	(78.0)	(74.0)	(72.3)	(70.5)	(70.0)	(70.0)	(65.0)	
100	85.0	88.0	83.0	(75.0)	(73.0)	(71.0)	(70.6)	(68.0)	67.0	
110	88.0	87.8	86.4	78.7	76.2	70.3	(71.7)	(69.0)	(67.0)	
120	87.8	82.6	86.0	79.8	77.0	70.6	(72.0)	(69.0)	(67.0)	
130	(84.0)	81.8	77.0	(75.0)	(73.6)	69.5	(70.0)	(70.0)	(65.0)	
140	(80.0)	88.0	77.0	(70.0)	(67.5)	66.0	(65.0)	65.8	(60.0)	
150	76.0	84.0	74.0	67.0	65.5	67.0	63.0	63.8	59.0	
160	75.0	83.0	74.0	67.0	65.0	65.0	62.0	62.8	58.0	
PWL	125.2	126.0	123.4	116.8	114.8	110.8	111.6	110.2	107.9	